

2013

# Polymer Microsystems for the Enrichment of Circulating Tumor Cells and their Clinical Demonstration

Joyce W. Kamande

*Louisiana State University and Agricultural and Mechanical College, joykamande@gmail.com*

Follow this and additional works at: [https://digitalcommons.lsu.edu/gradschool\\_dissertations](https://digitalcommons.lsu.edu/gradschool_dissertations)



Part of the [Chemistry Commons](#)

---

## Recommended Citation

Kamande, Joyce W., "Polymer Microsystems for the Enrichment of Circulating Tumor Cells and their Clinical Demonstration" (2013). *LSU Doctoral Dissertations*. 2652.

[https://digitalcommons.lsu.edu/gradschool\\_dissertations/2652](https://digitalcommons.lsu.edu/gradschool_dissertations/2652)

This Dissertation is brought to you for free and open access by the Graduate School at LSU Digital Commons. It has been accepted for inclusion in LSU Doctoral Dissertations by an authorized graduate school editor of LSU Digital Commons. For more information, please contact [gradetd@lsu.edu](mailto:gradetd@lsu.edu).

POLYMER MICROSYSTEMS FOR THE  
ENRICHMENT OF CIRCULATING TUMOR CELLS  
AND THEIR CLINICAL DEMONSTRATION

A Dissertation

Submitted to the Graduate Faculty of the  
Louisiana State University and  
Agricultural and Mechanical College  
in partial fulfillment of the  
requirements for the degree of  
Doctor of Philosophy

in

The Department of Chemistry

by  
Joyce W. Kamande  
B.S., University of Nairobi, 2007  
December 2013

To my Father in heaven, the Holy Spirit and my savior Jesus Christ for standing by me through the tough times and the good times.... you are awesome!!! (Jeremiah 29:11)

I dedicate this work to my loving parents, Mrs. Winny Wamaitha Kamande, and Peter Ng'ang'a Kamande my siblings; David Ng'ang'a Kamande, Esther Gathoni Chiama, and Mary Waithira Musyimi for their unwavering support and prayers.

I also wish to dedicate this work to the Carpenter family, Ms Marilyn Carpenter, Mr. Glen Carpenter, Mrs Jenny Carpenter, Ms Alaina Carpenter and Ms Terri Carpenter. Words cannot fully describe the hospitality and kindness that you have shown to me throughout my graduate school career.

## **ACKNOWLEDGEMENTS**

My sincere gratitude goes to my research advisor, Prof. Steven A. Soper whose great enthusiasm and passion for research in science has inspired and motivated me throughout my graduate school career. Without his supervision and constant help, this dissertation would not have been possible. I would also like to thank my committee members, Prof. William Crowe, Prof. Kermit Murray, Prof. William Doerrler and Prof. Randy Duran for their ideas, suggestions and advice regarding my dissertation project.

Also, I would like to thank the Soper Research group, past and present members for their friendship and exchange of ideas that helped me attain my project goals. A special thank you goes to Jason Emory, for his tutelage and helpful discussions at the very start of my lab studies. My sincere appreciation goes to Dr. Udara Dharmasiri, Dr. Makgorzata Witek and Dr. Mateusz Hupert for their role as research mentors.

I would also like to thank UNC collaborators, Dr. Jen Jen Yeh for the pancreatic cancer study; and Dr. Peter Voorhees for the multiple myeloma study. Both have been instrumental in attaining clinical samples and proving the clinical utility of the polymer microfluidic devices developed in our group.

Finally, I wish to thank the LSU chemistry department especially Prof. Gilman and all the ladies in the administrative office namely; Genell Bodoïn, Norma James, Kelly Pitre and Deborah Carter, for their support in facilitating my process of graduation especially after having moved to UNC.

## TABLE OF CONTENTS

ACKNOWLEDGEMENTS.....	iii
LIST OF TABLES.....	vii
LIST OF FIGURES.....	viii
LIST OF SCHEMES.....	xix
ABBREVIATIONS.....	xx
ABSTRACT.....	xxiii
CHAPTER 1. MATERIALS AND MICROFLUIDICS: ENABLING THE CLINICAL UTILITY OF CIRCULATING TUMOR CELLS.....	1
1.1 Introduction.....	1
1.2 Substrates Commonly Used by Microfluidics for CTC Enrichment.....	9
1.2.1 Silicon and Glass Materials for CTC Enrichment Microfluidic Devices ...	9
1.2.2 Polymer Substrates for Microfluidic Devices used for CTC Enrichment	12
1.2.3 Magnetic Materials for CTC Enrichment using Microfluidic Devices .....	19
1.3 Biological and Physical Properties for CTC Enrichment.....	24
1.3.1 Microfluidics for CTC Enrichment Based on Biological Properties.....	24
1.3.2 Microfluidics for CTC Enrichment Based on Physical Properties.....	44
1.4 Beyond Enumeration of CTCs .....	51
1.4.1 Phenotypic Characterization of CTCs.....	51
1.4.2 Genotype Characterization of CTCs selected by Microfluidics.....	53
1.4.3 Drug Targeting and Response Monitoring from Microfluidically Selected CTCs .....	55
1.4.4 Culture of Viable CTCs Isolated from CTC Enrichment Microdevices ..	57
1.5 References .....	61
CHAPTER 2. MODULAR MICROSYSTEM FOR THE ISOLATION, ENUMERATION AND PHENOTYPING OF CIRCULATING TUMOR CELLS: MANAGING PATIENTS WITH PANCREATIC CANCER .....	80
2.1 Introduction.....	80
2.2 Experimental .....	86
2.2.1 Materials .....	86
2.2.2 Fabrication of Microfluidic Modules .....	87
2.2.3 HT-CTC Selection Module .....	87
2.2.4 Evaluation of Flow Uniformity in HT-CTC Selection Bed.....	91
2.2.5 Impedance Module.....	91
2.2.6 Staining and Imaging Module.....	92
2.2.7 Cell Culture.....	94
2.2.8 Patient Samples .....	94
2.2.9 Patient-derived Xenograft (PDX) Models .....	95

2.2.10	Staining Procedure .....	95
2.2.11	HT-CTC Module Operation .....	96
2.2.12	Operation of the Integrated System and Data Collection and Analysis .....	97
2.3	Results and Discussion .....	98
2.3.1	HT-CTC Module .....	98
2.3.2	Optimization of anti-EpCAM Antibody Concentration .....	103
2.3.3	Effect of CTC Selection Bed Length on Recovery .....	105
2.3.4	Impedance Sensor Module .....	106
2.3.5	Staining and Imaging Module .....	108
2.3.6	Correlation of Impedance Responses with Imaging Data .....	111
2.3.7	Preclinical Studies Using PDX Models .....	113
2.3.8	Clinical Studies in Metastatic and Local Resectable PDAC Patients ..	114
2.4	Conclusion .....	120
2.5	References .....	122
CHAPTER 3.	MOLECULAR PROFILING OF ENRICHED LOW-ABUNDANCE CIRCULATING TUMOR CELLS (CTCS) USING A HIGH-THROUGHPUT MICROFLUIDIC SYSTEM.....	128
3.1	Introduction.....	128
3.2	Experimental .....	132
3.2.1	Materials and Reagents .....	132
3.2.2	Cell Culture and Imaging.....	133
3.2.3	Fabrication of Microsampling Unit .....	133
3.2.4	Antibody Immobilization .....	135
3.2.5	SW620 Cell Capture, Release and Enumeration Using the HTMSU ..	136
3.2.6	DNA Extraction .....	138
3.2.7	PCRs, LDRs and CE .....	138
3.3	Results and Discussion .....	140
3.3.1	PCRs/LDRs/CE .....	140
3.4	Conclusion.....	145
3.5	References .....	145
CHAPTER 4.	ISOLATION AND CHARACTERIZATION OF CIRCULATING MULTIPLE MYELOMA CELLS (CMMCS) USING A POLYMER MICROFLUIDIC DEVICE.....	150
4.1	Introduction.....	150
4.2	Experimental .....	154
4.2.1	Fabrication of the CMMC Selection Device .....	154
4.2.2	Materials .....	157
4.2.3	Cell Culture.....	158
4.2.4	Flow Cytometry: RPMI-8226 Surface Antigen Characterization.....	158
4.2.5	Clinical Samples .....	159
4.2.6	CMMC Selection Device Operation.....	159
4.2.7	On-chip Immunostaining of Phenotypic Cell Surface Antigens and Light Chain Cytoplasmic Immunoglobulins ( $\lambda$ light chains and $\kappa$ light chains) .....	160

4.2.8 Impedance Sensing .....	161
4.2.9 <i>KRAS</i> Mutational Analysis of CMMCs .....	162
4.3 Results and Discussion .....	165
4.3.1 Flow Cytometry Phenotype Characterization of RPMI-8226 as a Model Cell Line for CMMC .....	165
4.3.2 RPMI-8226 Cell Translational Velocity Optimization for Capture on the CMMC Selection Device .....	166
4.3.3 On-chip Phenotype and Clonal Identification of RPMI-8226 Cells and CMMCs from Clinical Samples .....	171
4.3.4 CMMCs in SMM and Active MM Clinical Samples .....	176
4.3.5 <i>KRAS</i> Mutational Analysis of Isolated CMMCs (PCR/LDR/CE) .....	178
4.4 Conclusion .....	184
4.5 References .....	184
CHAPTER 5.    FUTURE STUDIES: DEVELOPMENT OF A MODULAR WORKSTATION FOR CTC GENOTYPING.....	191
5.1 Background .....	191
5.2 Enrichment of Invasive and Epithelial Phenotype CTCs from Whole Blood using Serially Arranged Modules Positioned on a Fluidic Motherboard .....	195
5.2.1 Bi-functional Linkers.....	195
5.2.2 Nanotextured Surfaces.....	197
5.2.3 Seprase and EpCAM.....	200
5.3 Generation of an Addressable 2-Dimensional (2D) Cell Array for Immunophenotyping via Fluorescence Imaging.....	201
5.3.1 Dual Electrode Pair Impedance Sensor .....	201
5.3.2 2D Cell Array.....	203
5.4 Integration of Fluidic Modules for Continuous Molecular Processing of CTCs even at the Single-Cell Level.....	207
5.4.1 PCR/LDR/FRET Assay for the Detection of <i>KRAS</i> Point Mutations ....	207
5.5 Optical Read Out Module.....	209
5.5.1 Characterization and Clinical Application of the Modular Work Station .....	211
5.6 References .....	213
APPENDIX : PERMISSIONS.....	221
VITA .....	252

## LIST OF TABLES

Table 1.1 Various polymer materials used in CTC enrichment devices.....	18
Table 1.2 Clinical performance metrics of CTC enrichment devices for various cancers .....	60
Table 2.1 Average number of CTCs, leukocytes and double-stained cells selected using the HT CTC selection module depicted in Figure 2.2 for two different PDAC pathologies and healthy donors. For this data, the selected cells were stained within the selection module and not released from the surface using trypsin. The cells were stained with DAPI (nucleus), cytokeratins and CD45. Each row of the data set corresponds to a different patient analyzed, which was performed in triplicate (blood sample, split into three equal volumes and run on three different HT-CTC modules). The number shown represents the mean for each patient.....	118
Table 4.1 <i>KRAS</i> PCR primer sequences .....	163
Table 4.2 <i>KRAS</i> LDR primer sequences .....	164
Table 4.3 <i>KRAS</i> mutational analysis on clinical samples .....	183



## LIST OF FIGURES

Figure 1.1 CTCs escape immune surveillance and result in metastatic malignancy. (Reproduced from Elshimali *et al.* [16] with permission).....2

Figure 1.2 Enrichment of circulating tumor cells (CTCs) from the peripheral blood of cancer patients is based on physical or biological properties of CTCs. (A) Physical properties include size (membrane filter devices), deformability (microfluidic system in a chip), density (Ficoll centrifugation), and electric charge (dielectrophoresis). (B) Biological properties include expression of cell surface markers and invasive capacity. Cell surface markers include an epithelial cell adhesion molecule (EpCAM) for positive selection and CD45 for negative selection; anti-EpCAM or anti-CD45 antibodies conjugated with magnetic beads, used to enrich CTCs in a magnetic field; and anti-EpCAM antibodies on microposts or columns of nanobeads. Invasive capacity refers to adherence and invasion of fluorescent matrix. Abbreviations: glyco A, glycophorin A (a 131-amino-acid protein present at the extracellular surface of the human red blood cell); CAM, cell adhesion matrix; fluo-CAM, fluorescent cell adhesion matrix; RBC, red blood cells. (Reproduced from Alix-Panabières *et al.* [38] with permission) .....5

Figure 1.3 (A) SEM image of a silicon microsieve filter with uniform honeycomb pore structures fabricated using silicon on insulator technology (SOI), (B) SEM image of the backside of the microsieve membrane showing the supporting rings. The dimension of the silicon microsieve and membrane area is 7.5 mm and 5 mm in diameter, respectively. (C) Composite fluorescent images of enriched MCF-7 cells (red and blue) and leukocytes (green and blue) stained with fluorescent labeled antibodies against membrane antigens EpCAM (red) and leukocyte marker CD45 (green). All nuclei were stained with DAPI. Scale bar: 30  $\mu\text{m}$  (20 $\times$ ). (Reproduced from Lim *et al.* [49]with permission)..... 11

Figure 1.4 (A) Kern micromilling machine (MMP) is a computer numerically controlled (CNC) milling machine that is used to pattern microstructures on metal mold inserts using very small milling bits (down to 25  $\mu\text{m}$  diameter) rotated at very high speeds in the range of 40,000 – 200,000 rpm. Mold inserts can then be used as masters for the production of microstructures on polymer substrates (B) Hex03 hot embossing equipment capable of molding polymer parts containing features with micro- and nano-dimensions including high aspect ratios (>10 : 1) through a combination of heat and pressure. It is commonly used to produce polymer microfluidic chips for biomedical applications. .... 14

Figure 1.5 (A) Principle of magnetic self-assembly. A hexagonal array of magnetic ink is patterned at the bottom of a microfluidic channel. Beads coated with an antibody are injected in the channel. Beads are submitted to Brownian motion. The application of an external vertical magnetic field induces the formation of a regular array of bead columns

localized on top of the ink dots. (B) Two levels PDMS integrated microchip. Channels were filled with colored water. Delivery and separation channels for the cells appear in yellow. Inlets ports appear in orange. The separation channel is the longer vertical branch. The area bearing magnetic posts is marked by the dotted white box. Channels in the upper PDMS layer, controlling the opening and closing of the inlet channels, appear in blue. The green wire is a thermocouple for in situ control of the temperature in the system. (Scale bar: 0.5 cm.) (C) Magnetically assembled array of columns of 4.5  $\mu\text{m}$  beads coated with anti-CD19 mAb (specifically retaining Raji B-Lymphocytes). Typical column shapes are shown in the insets. (Scale bar: 80  $\mu\text{m}$ .) (D) Optical micrograph of the columns after the passage of 1,000 Jurkat cells. No cell can be seen. (Scale bar: 80  $\mu\text{m}$ .) (E) After the passage of 400 Raji cells, numerous ones are captured and rosetted on the columns. (Scale bar: 80  $\mu\text{m}$ .) (Reproduced from Saliba *et.al* [122] with permission from the Proceedings of the National Academy of Sciences of the United States of America (*PNAS*)).....23

Figure 1.6 Box plots presenting count of CTCs and WBCs selected in UV-PMMA (5 PDX (Patient Derived Xenograft models)) and UV-COC (4 PDX) chip from mice blood samples. Data are normalized to 1 mL. Lower and upper edges of box show 25th and 75th percentiles, respectively. Solid line in box represents median, and solid diamond represents mean. Error bars show maximum and minimum values. (Reproduced from Jackson *et al.* [30] with permission from the Royal Society of Chemistry) .....30

Figure 1.7 (A) The HB-Chip consists of a microfluidic array of channels with a single inlet and exit. Inset illustrates the uniform blood flow through the device. (B) Cartoon illustrating the cell-surface interactions in the HB-Chip, and (C) a traditional flat-walled microfluidic device. (D) Micrograph of spiked cancer cells captured on the HB-Chip, representative of capture cell viability (LIVE/DEAD). (Scale bar: 40  $\mu\text{m}$ ). (E) Micrograph of spiked cells captured on the herringbone chip and subsequently cultured on the device for 21 d. (F) On-chip FISH of captured LNCaP cells with nuclei stained with DAPI, CEPX (green) and AR gene locus (red). (G) Micrograph of a fluorescently labeled PC3 cell captured on the HB-Chip (top) and subsequent micrograph taken of the same cell stained with H and E. (Scale bar: 10  $\mu\text{m}$ ). (Reproduced from Stott *et al.* [32] with permission from the Proceedings of the National Academy of Sciences of the United States of America (*PNAS*)).....32

Figure 1.8 (A) GEDI microfluidic device design and (B) Image of silicon device with silicon gasket. (C) Top view of microfluidic obstacle array with array geometric parameters.  $\Delta$  = obstacle offset.  $\Lambda$  = obstacle spacing in the direction of bulk flow.  $\Gamma$  = obstacle spacing in the direction orthogonal to bulk flow.  $2r$  = obstacle diameter. Streamlines (gray) denote fluid flow. Path lines (various colors) denote trajectories of cells of different diameters. Obstacle array spacing and orientation parameters are also defined. (D) The rate of cell-wall collisions for cells traveling through the array is a strong function of the offset parameter of the array; the GEDI design methodology implies use of an offset parameter that leads to size-dependent collision rates. The

results predicted for the flow through the geometry at left are shown at right by the solid line; the four specific cell sizes lead to results denoted by the four colored dots on this graph. Other geometric arrangements lead to different results, shown at right in the dotted and dashed lines. (E) Devices with the same surface area to volume ratio give vastly different results: straight arrays lead to collisions that decrease as the blood travels through the device; GEDI arrays lead to collisions that increase with travel through the device. (Reproduced from Kirby *et al.* [29] with permission from the author) .....34

Figure 1.9 (A) Schematic operation of the HT-CTC module with 50 parallel, sinusoidal microchannels and inlet/outlet channels arranged in the z-configuration. The large arrow indicates sample flow direction through the selection channels. (B) SEM of the selection bed showing high aspect ratio sinusoidal microchannels and the output channel (top). (C) SEM of one of the high aspect ratio sinusoidal channels. (D) Fluid dynamics simulation results showing the distribution of flow velocities and shear stress in microfluidic selection channels. (E) Box plot from CTCs isolated from 7 metastatic PDAC patients, 5 healthy donors, and 5 local resectable PDAC patients. Reproduced from Kamande *et al.* [34] with permission .....35

Figure 1.10 Schematic of the horizontally packed TiNFs for improved CTC capture through combining cell-capture-agent (i.e., Anti-EpCAM) and cancer cell-preferred nano-scale topography ( Reproduced from Zhang *et al.* [151] with permission) .....39

Figure 1.11 APO Cell device (A) Schematic of the top view of the flow chamber showing sample injection and sample collection port locations. (B) Still image from video demonstrating the flow and collection of fluorescently labeled SKOV3 cancer cells through the collection port in the ApoStream flow chamber. Cancer cells are collected into the collection port when the DEP field is activated. (C) Still image from video demonstrating the flow of fluorescently labeled PBMCs through ApoStream flow chamber. The first half of the video (10 s) demonstrates that most PBMCs fall into the collection port when the DEP field is not active. (Reproduced from Gupta *et al.* [191] with permission).....48

Figure 1.12 Outline of the Gilupi nanodetector (A) Section of the guidewire which remains inside the puncture cannula (B) 20 mm long gold coated tip of the stainless steel guidewire which is in direct contact with the blood circulation and biofunctionalized with EpCAM antibodies to target CTC. (Reproduced from Saucedo-Zeni *et al.* [193] with permission.).....50

Figure 1.13 Viability and proliferation of circulating cells isolated by CAM from blood of breast cancer patients. (A) A mixture of live green fluorescent cells and dead red fluorescent cells were seen in the cell fraction of pre-CAM enrichment. Bar = 40  $\mu$ m. (B) Viability of circulating cells prior to and post to CAM enrichment. Percentages of live cells in pre- and post-CAM fractions were measured as percentage of green cells in

both green and red cells. (c, d) CAM-enriched cells were cultured on the CAM scaffold for 1–33 days. Live cells were photographed under phase contrast microscopy (PCM) and fluorescence microscopy (CAM, to reveal CAM uptake/labeling of tumor cells). Tumor cells grew as time increased. On day 1 (C), tumor cells were seen to associate with CAM uptakes and as round cells (large white arrows) larger than hematologic cells (small yellow arrowheads). On day 10 (D), tumor cells were seen as round cells (white arrows) larger than hematologic cells (red arrows). By day 33 (E), tumor cells grew in clusters with large epithelioid cells (open arrows) but hematologic cells decreased their number and not seen in the field. Reproduced from Lu *et al.* [217] with permission .....58

Figure 2.1 Modular microfluidic system for CTC analysis. (A) Schematic representation of the operation of the system and the three modules comprising the system including the HT-CTC module, the impedance sensing module and the staining and imaging module. Arrows indicate flow of sample (1 and 1'), wash buffer (2 and 2'), CTC release buffer (3 and 3'), and fixation and staining reagents (4 and 4'). For detailed operational procedures please refer to the Experimental Section. (B) Picture of the assembled system. Roman numerals correspond to modules described in (A). (C) Micrographs and data plots showing the various outputs of the three different task-specific modules including: (I) HT-CTC selection module, which used anti-EpCAM-coated sinusoidal microchannels for the positive selection of CTCs; (II) electrical signatures of CTCs obtained using the impedance sensor module; and (III) images of CTCs stained with DAPI and collected at the staining and imaging module. ....89

Figure 2.2 (A) Schematic operation of the HT-CTC module with 50 parallel, sinusoidal microchannels and inlet/outlet channels arranged in the z-configuration. The large arrow indicates sample flow direction through the selection channels. (B) SEM of the selection bed showing high-aspect ratio sinusoidal microchannels and the output channel (top). (C) SEM of one of the high-aspect ratio sinusoidal channels. (D) SEM image of a portion of the high-precision micromilled brass molding tool showing the sample inlet port with continuously changing width and height for minimizing unswept volumes during sample (*i.e.*, blood) introduction. (E) Assembled HT-CTC modules with different numbers of microfluidic sinusoidal channels designed for efficient processing of various sample volumes.....90

Figure 2.3 Staining and imaging module. (A) Assembly process; (a) – cover plate with an array of  $8 \times 6 \mu\text{m}^2$  channels, which form pores for retaining cells between the interleaving inlet and outlet channels (b). (B) Schematic of an assembled module and its operation; Red – input channels; Blue – output channels; Yellow – interconnecting channels. (C) Image of the staining and imaging module filled with fluorescein. The lower fluorescence intensity in the interconnecting channels is due to the smaller cross-sectional area of these channels compared to the input/output channels. (D) Fluorescence image of CTCs retained by pores. The cells were stained with DAPI for visualization. (E) High magnification fluorescence image of Hs578T cells retained at the

pore structures of the staining and imaging module. These cells were stained with PKH67 lipid membrane green fluorescent dye for visualization. ....93

Figure 2.4 (A) Various stages of filling a 320-channel HT-CTC module (20 mm length) with a dye solution. (B) Numerical simulation results showing the distribution of flow velocities for different configurations of the CTC selection beds arranged in a z-configuration. (C) Average linear velocity of fluid in 16 groups of 20 adjacent sinusoidal high aspect ratio microchannels based on the results depicted in Figure 2.4A (filled bars) and theoretical values obtained via numerical simulation (empty bars). (D) Distribution of cells selected in 20 mm long microchannels .....101

Figure 2.5 Recoveries of MCF-7 cells using selection beds modified with EpCAM antibody at different antibody concentrations. Results were normalized to recovery obtained for antibody concentration of 1 mg/mL .....104

Figure 2.6 Capture efficiencies of MCF-7 cells using isolation beds with varying channel length. Zone 1 first 50% of channel length, zone 2 – 50-75% of channel length, zone – 75 – 100% of the channel length .....106

Figure 2.7 Single-cell electrical impedance sensing. (A) Histograms for impedance response for leukocytes (blue bars) and SW620 cancer cells (red bars). (B) SW620 (red bars) and leukocyte (blue bars) cell sizes measured optically.....108

Figure 2.8 Fluorescent images of CTCs collected in the staining and imaging module. (A-D) Images of a CTC from a PDAC patient after being released from the selection bed, impedance counted, and collected at a pore on the staining and imaging module followed by fixation and staining with DAPI, anti-cytokeratin antibodies (8/19) labeled with Texas Red, and FITC-labeled leukocyte antibody marker for CD45. (E) Fluorescent image of a CTC with the cytoplasm partially deformed and pulled into the pore and the interconnecting channel. Dashed lines indicate the edges of the input channel and the interconnecting channel. Scale bar is 10  $\mu\text{m}$  in all cases. ....110

Figure 2.9 (A) Impedance counts generated from CTCs selected from 2.0 mL of blood from a patient with metastatic PDAC. The sample was processed through the HT-CTC selection module at a linear flow velocity of 2.0 mm/s. CTCs were then released from the selection bed using a CTC release buffer at a volumetric flow rate of 10  $\mu\text{L}/\text{min}$ . A total of 14 CTCs were enumerated using impedance sensing based on a signal-to-noise threshold of 3 (dotted line). The red dotted line represents the threshold level, which was used to differentiate ‘true’ events from noise. Data presented here were smoothed using algorithms described in the Experimental Section. After impedance counting, the cells were directed to the staining and imaging module for phenotypic identification (DAPI, CD45 and cytokeratins). (B) Plot showing the correlation between the impedance counts versus CTCs enumerated via immuno-staining on the staining and

imaging module for 4 different metastatic PDAC patient samples. (●) Represents expected numbers of CTC events based on the impedance signatures and (□) shows the experimental enumeration data from the staining and imaging module ( $r = 0.93$ ). (C) Interface between a capillary and plastic module showing the capillary inserted into a guide channel to accommodate the 365  $\mu\text{m}$  od capillary and stepping to a channel size of 150  $\mu\text{m}$ , which matches the id of the interconnect capillary. ....112

Figure 2.10 Staining and enumeration of CTCs via immunophenotyping. (A) Box plot representing results from the phenotypic enumeration of CTCs isolated from 7 PDX and 3 healthy mice. (B) Box plot from CTCs isolated from 7 metastatic PDAC patients, 5 healthy controls and 5 local resectable PDAC patients. (C) Fluorescence images of various selected cells from a metastatic PDAC patient: (i) CTC; (ii) two white blood cells; and (iii) cluster of CTCs. (b, f, j) CTC marker for Cytokeratin 8/19 (red) with b, j positive for this marker and f negative for this marker; and (c, g, k) leukocyte antigen marker CD45 (green) with c, k negative for this marker and g positive for this marker. Micrographs (i-l) are of an aggregate of 6 CTCs captured in the HT-CTC module. This aggregate showed positive for cytokeratins 8/19 (j) and negative for leukocyte marker CD45 (k). In all of these panels the nuclei were stained with DAPI (blue). Bars are 10  $\mu\text{m}$ . ....116

Figure 3.1 Diagrams of the microfluidic system made *via* micro-replication into PMMA from a metal mold master. and agarose gel electrophoresis of the PCR products. (A) Cell selection HTMSU. The capture bed consisted of curvilinear channels that were 30 mm wide and 150 mm deep (51 channels). (B) Brightfield images represents time lapse micrographs of a captured SW620 cell(a) under 0.25%w/w trypsin processing which took 20 min for release(b). Flow rate for cell capture was 27 $\mu\text{l}/\text{min}$ . linear flow velocity of 2mm/s (C) Impedance readout of approximately 26 SW620 cells released from the capture bed at linear velocity of 2mm/s. PCR was set for 32 cycles. Each cycle: 94 °C (30 s), 60 °C (30 s),72 °C (40 s). Gel stained with EtBr products separated at 4.8 V/cm. (D) Gel Electropherogram for PCR performed on standard SW620 samples (a) no gDNA template, Negative control; (b) DNA from 10 SW620 cells; (c) DNA from 20 SW620 cells; (d) DNA from 50 SW620 cells; (e) DNA from 100 SW620 cells; (f) DNA from 500 SW620 cells; (g) DNA from 1,000 SW620 cells; (h) DNA from 5,000 SW620 cells; (i) gDNA template from SW620, Positive control; Lanes a-i contains 3  $\mu\text{L}$  of DNA amplicons. (E) Gel Electropherogram for PCR performed on SW620 cells obtained from HTMSU selection followed by electrokinetic enrichment a) gDNA template from SW620, Positive control; (b) PCR product from 10 SW620 cells selected from whole blood using HTMSU (c) PCR product from whole blood with no SW620 cells (d) no gDNA template, Negative control. Lanes a-d contains 3  $\mu\text{L}$  of DNA amplicons. ....141

Figure 3.2 The LDR mixtures contained a discriminating and common primers for *KRAS* c12.2V, could selectively detect mutations in G12V. Two  $\mu\text{L}$  of amplicons from PCR with SW620 (mutant) were used for analyzing point mutation in the *KRAS* gene. LDR was set for 20 cycles. Initial denaturation 95 °C for 2 min. Each cycle consisted of: 95 °C

(30s), 65 °C (2 min), and 4 °C as final hold. LDR was performed at capillary temperature of 60°C, denaturation temperature of 90 °C (3 min), Injection at 2.0 kV (30 s) and separation at 6.0 kV (20 min). Peak a represents the primer and peak b is the LDR product. CGE analysis was acquired for the following samples; A) 0 B) 10 C) 20 D) 50 E) 100 F) 500 and G) 5,000 SW620 CTCs. The insets shown in (A) and (B) represent a magnified view of the LDR product peaks. H) CGE trace for LDR analysis of 50 HT29 CTCs. DNA size markers of 20 and 80 nt were co-electrophoresed with the LDR products. ....143

Figure 3.3 Two µl of amplicons from PCR were used for analyzing point mutation in the *KRAS* gene for blood samples spiked with and without 10 SW620s. The LDR products were analyzed using capillary electrophoresis. The capillary electrophoresis responses for sample after processing blood with no SW620 are shown in A, and B shows the electropherogram for 10 spiked SW620s in blood. Peak ‘a’ represents the primer and peak ‘b’ is the LDR product for SW620. ....144

Figure 4.1 Fluorescence dot plots showing typical CD antigen expression on RPMI-8226 cells. All plots were gated on CD45<sup>-</sup>. The resulting dot plots indicate: (A) 74% of these cells express CD56<sup>+</sup>; (quadrant R6); (B) 90% of the cells express CD138<sup>+</sup> (quadrant R6); and (C) 98% of the cells express CD38<sup>+</sup> (quadrant R6). Fluorochromes used for each antibody was PE for CD56, APC for CD38, Pacific blue for CD138 and FITC for CD45.....166

Figure 4.2 (A) Schematic of the CMMC selection device with an array of 50 parallel sinusoidal microchannels and inlet/outlet channels arranged in a z-configuration. Flow of blood is indicated by the green arrow. (B) SEM of the selection bed depicting high-aspect ratio (30 x 150 µm, w x d) sinusoidal microchannels and the output channel. (C) Blood processing setup in a biological safety hood showing blood filled syringes set on a Harvard apparatus multi-syringe pump. The syringes are each connected to inlet capillaries interfaced to the CMMC selection devices. (D) DAPI fluorescent image of CMMCs captured on either side of a sinusoidal microchannel.....168

Figure 4.3 (A) Graph showing cell capture efficiency versus cell translational velocity. In these experiments an estimated 500 RPMI-8226 cells were seeded into RPMI-1640 total cell medium. The cells were prestained with a live nuclei cell dye and were introduced in the CMMC selection device at linear velocities ranging from 0.4-2 mm/s. Capture efficiency was determined by the ratio of RPMI-8226 cells captured on the CMMC selection device to the total number of RPMI-8226 cells selected on chip and collected in the effluent. Number of cells captured was determined by both brightfield and fluorescence microscopy. (B) Calibration plot of RPMI-8226 cells seeded (20-500 cells/0.5 mL) of healthy donor blood and processed through the device at the optimized linear velocity of 1.1 mm/s. Capture sensitivity for the CMMC selection assay was given by the slope ( $m = 0.6865$ ,  $r^2 = 0.9994$ ). ....171

Figure 4.4 In-situ immunophenotyping and cytoplasmic staining of CMMCs. Panels (A) and (B) represent RPMI-8226 cells and CMMCs selected in a polymer microchannel via anti-human CD138/CD138, respectively. Positive CMMC surface markers are presented by micrographs: (b,g) CD56-PE; (c,h) CD38-APC; while (d,i) are negative control marker CD45-FITC for leukocyte identification. DAPI was used for nuclei identification (a,f,l). Panel (C) represents cytoplasmic staining of RPMI-8226 cells, which are the  $\lambda$  light chain expressing cells, using anti human Ig $\kappa$ -PE (m) and anti-human Ig $\lambda$ -APC (n). (D) H&E image of a released plasma cell from the CMMC selection bed using enzymatic release via trypsin. All bars represent 10  $\mu$ m. ....173

Figure 4.5 Alternative confirmatory phenotypes for CMMCs isolated from a patient sample. Panel (A) represents 6 CD138 selected cells that were found to be CD56<sup>+</sup> (b) and CD38<sup>-</sup> (c). Panel (B) shows a mix of two phenotypes side-by-side, 3 CD38<sup>+</sup>/CD56<sup>+</sup> positive cells (g,h) next to 2 CD56<sup>+</sup>/CD38<sup>-</sup> cells (h). Both panels show dim to no expression of CD45 (c,i). Nuclei were stained with DAPI (a,f). Composite images are shown in e & j for both panels. ....175

Figure 4.6 Panels A and B represent cytoplasmic staining of a clinical sample with active MM (B) using anti-human Ig  $\kappa$ -PE (b,e) and anti-human Ig  $\lambda$ -APC (c,f) and (C) cytoplasmic staining of RPMI-8226 cells as a control. Results indicated strong Kappa expression for approximately 70% of the cells enumerated and weak expression of about 10% of the total cells captured on the device for the clinical sample. Imaging conditions: 5x objective, 1.2 s exposure time for PE (Kappa) and 9 s exposure time for APC (Lambda). Bars represent 150 $\mu$ m. ....176

Figure 4.7 Box plots presenting count of CMMCs selected in chip from MM patient blood samples. Data are normalized to 1 mL. Lower and upper edges of box show 25th and 75th percentiles, respectively. Solid line in box represents median, and solid diamond represents mean. Error bars show maximum and minimum values. ....177

Figure 4.8 Agarose gel electrophoresis of PCR products generated from (A) RPMI-8226 cells and (B) CMMCs from 4 patient samples. PCR was run with 35 cycles with an initial denaturation step of 2 min and final extension for 7 min. Each cycle consisted of: 94°C (30 s), 59°C (30 s), 72°C (40 s). The gel was stained with ethidium bromide and run at 4.8 Vcm<sup>-1</sup>. (A) Gel electropherogram for PCR performed on RPMI-8226 cells with; (a) no gDNA template; (b) gDNA template from HT-29 directly (positive control); (c) gDNA from 20 RPMI-8226 cells; (d) gDNA from 150 RPMI-8226 cells; (e) gDNA from 500 RPMI-8226 cells; and (f) gDNA from 750 RPMI-8226 cells. Lanes a-f contain 5  $\mu$ L of DNA amplicons. (B) Gel electropherogram for PCR performed on CMMCs obtained from 4 clinical samples analyzed using the CMMC selection device: (a) No gDNA and used as a negative control; (b) gDNA template from RPMI-8226 directly used as a positive control. (c) gDNA from patient 35; (d) gDNA from patient 36; (e) gDNA from patient 37; (f) gDNA from patient 38. Positive controls consisted of harvesting either HT-



29 or RPMI-8226 cells from the culturing dish (~1,000 cells), lysing them, performing a solid-phase extraction of the gDNA followed by PCR of the purified sample.....180

Figure 4.9 LDR and Sanger sequence analysis of sequence variations in the *KRAS* gene for codons 12 and 13 with the gDNA secured from RPMI-8226 cells, HT-29 cells, and CMMCs isolated from clinical samples. LDR consisted of 20 cycles. Initial denaturation was performed at 95°C for 2 min. Each cycle consisted of: 95°C (30 s); 60°C (2 min); and 4°C as a final hold. LDR products were analyzed using CGE performed at a capillary temperature of 60°C with an initial denaturation step prior to injection at 90°C for 3 min. CGE injection was performed at 2.0 kV for 30 s and separation was done at 6.0 kV. CGE electropherograms for various samples are shown in (A-F). LDR product peaks are represented with an asterisk \*. (A) shows the 49 nt LDR product denoting the G12A mutation found in RPMI-8226; (B) and (D) show no LDR products at the c12.2 C locus for HT-29 and patient 35, respectively; (C) shows a 54 nt LDR product denoting the G12S mutation for patient 35; and (E) shows a 42 nt product denoting the G13D mutation for patient 36. DNA size markers of 20 and 80 nt were co-electrophoresed with the LDR products. (F) Sanger sequencing trace for gDNA secured from patient 36 at codons 12 and 13 with an additional peak at c13.1A denoting the presence of mutant copies bearing the G13S mutation.....182

Figure 5.1 Schematic of the bio-processor, an integral component of the CTC workstation. The bio-processor is composed of modules for CTC affinity selection (Sepase and EpCAM), impedance sensor (CD), cell array with valving fluidic layer, SPE module, and imaging module for the real-time monitoring of molecular beacons via FRET produced as a result of a successful LDR. The fluidic motherboard also contains continuous flow thermal reactors for lysis, PCR and LDR. The PCR is multiplexed containing primers for the appropriate gene fragments to be interrogated. The LDRs are spatially multiplexed with each thermal reactor monitoring a specific locus. While the system shows a 6-plex LDR, this can be scaled for higher multiplexing as needed. The workstation also contains a scanning microscope for phenotyping cells in the 2D array, the imaging microscope for CCD-TDI readout, thermal control units, electronic control boards for data processing, and fluid handling hardware (syringe pumps), which are not shown.....194

Figure 5.2 Effect of thermal fusion bonding on the stability of oligonucleotide bifunctional linkers. After modified oligonucleotide linkers were covalently attached to UV-activated PMMA, the PMMA was (A) heated to 107°C for 20 min or (B) not heated. The fluorescence intensity profiles from a vertical section of two spots (see dotted yellow line) in (A) and (B) are shown in (C). To interrogate the stability of the attached oligonucleotide linkers, solution complements to the linkers bearing a fluorescent reporter were hybridized to the linkers. As can be seen in (C), no difference in the fluorescence intensity resulted. (D) UV-activated PMMA reacted with EDC/NHS coupling reagents and a single-stranded oligonucleotide linker containing a 5' amino group and Cy3 at its 3' end. A single dU residue was added internally to the linker. After

coupling, the linker was subjected to the USER system, which cleaves the linker at the dU residue. The loss of fluorescence is indicative of the cleavage. Spot (a) is a linker with no dU residue, while spot (b) contained the dU residue in the linker .....197

Figure 5.3 The top panel shows the process strategy for performing 3D molding using a PDMS intermediate molding tool containing nano-textures. The finished nano-textured chip is shown with ridges, but the nano-structure architecture can be altered through lithographic changes imposed on the PDMS intermediate molding tool. (A-C, E) SEM images of PMMA CTC selection channels containing nano-textures with bumps that range from 200 nm (A-D) to 5  $\mu\text{m}$  (E). (D, F) Fluorescence microscope images of nano-textured channels that were sealed with a cover plate using solvent-assisted bonding. Fluorescein was used as the dye seed in a 1X TBE buffer (pH = 8.5). These images demonstrate no leakage following cover plate bonding. For SEMs (A, E), the CTC device was sealed with a cover plate, dipped in liquid N<sub>2</sub> and fractured so as to produce a cross section of the nano-textured channel to show the integrity of the nano-features. In (A), the nano-texture structures are not visible at the magnification used but can be seen in (B), before cover plate bonding; (C), after cover plate bonding. In (E), the features are clearly visible. ....199

Figure 5.4 Expression differences of Sepsase and EpCAM for various cancer cell lines .....200

Figure 5.5 Single-cell electrical impedance detection. (A) Histograms for impedance response for leukocytes (blue bar) and SW620 cancer cells (red bar). (B) SW620 (red) and leukocyte (blue) cell size measured optically. (C) Plot of impedance response, phase and magnitude, as a function of the voltage frequency applied to the electrodes. Taken from ref.[42] with permission. (D) New electrode design in which thin films electrodes are deposited on both top and bottom plates. ....202

Figure 5.6 (A) Schematic of the 2D cell array. The array consists of microwells made from PMMA and a transparent FEP layer (3 layers) that serve as the fluidic, valving and through-hole units for this module. (B) Fabrication method for the polymer valves; this is accomplished using 2-sided embossing and laser drilling. The small arrows show the flow direction when the valve is open. To close the valve, a mechanical solenoid is used.[29] (C) Cross-sectional view of the microwell with the FEP layers serving as the well floor with access hole to the fluidic network. The total force ( $F_T$ ) acting on the cell to resist movement is gravity ( $F_G$ ), hydrodynamic (if applied,  $F_H$ ) and Stokes ( $F_S$ ). For a HeLa-type cell,  $F_T \approx F_G \approx 29.9$  pN. For a 1064-nm laser beam of modest intensity, a scattering force,  $F_S$ , will be able to eject the cell from this well.  $F_H$  is applied using either positive or negative operation of a syringe pump and valves, poised on the backside of this module (they are not visible in this schematic). ....205

Figure 5.7 (A) Schematic of the optical readout module that consists of input connects to accept the output of each LDR thermal reactor, which are poised on the motherboard.

This module consists of a cover plate with an embedded COC planar waveguide and readout channels that are approximately 2  $\mu\text{m}$  in width and 350-500 nm in depth at the detection zone (evanescent excitation of solution molecular beacons). (B) Molding tool is prepared via UV-LiGA. ....211

## LIST OF SCHEMES

Scheme 3.1 Overview of the molecular profiling strategy adopted for CTCs resident in peripheral blood .....130

Scheme 3.2 CTC selection assay on PMMA based HTMSU device. First panel illustrates the exposure of PMMA to UV radiation to generate a monolayer of carboxylic acid moieties that facilitate antibody attachment. The second panel shows the selection of CTCs from blood after covalent attachment of anti- EpCAM to the PMMA substrate. Third panel illustrates the elution of unbound cells (RBCs and WBCs) from the captured CTCs and the release of CTCs for downstream processing. ....137

Scheme 5.1 Single-stranded oligonucleotide bifunctional linkers used for covalently attaching mAbs to polymer surfaces bearing accessible carboxylic acids. The oligonucleotide linkers (see upper left) can contain any sequence, but is shown with a string of ~15 dT units that do not contain a primary amine so as not to be cross-linked to the surface. X1,2 can be a uracil or photocleavable residue as seen in the upper right. Following device incubation with target cells, they can be released from the selection surface. ....196

## ABBREVIATIONS

Ab	-	antibody
APC	-	allophycocyanin
AR	-	androgen receptor
A <sub>c</sub>	-	antigen density
BRAF	-	v-raf murine sarcoma viral oncogene homolog B1
BD	-	becton dickinson
CTC	-	circulating tumor cells
CTC-iChip	-	inertial focusing Chip
CMMC	-	circulating multiple myeloma cell
CMC	-	circulating melanoma cells
CTM	-	circulating tumor microemboli
COC	-	cyclic olefin copolymer
CRC	-	colorectal cancer
CE	-	capillary gel electrophoresis
CK	-	cytokeratin
CCC	-	cancer cell culture media
CCD	-	charged coupled device
CCD-TDI	-	charged coupled device-time delay and integration
CEC	-	circulating endothelial cells
CMP	-	chemical mechanical polishing
CPC	-	circulating progenitor cells
CAM	-	cell adhesion matrix
CNC	-	computer numerical control
CD 38	-	myeloid and lymphocyte surface receptor
CD 45	-	leukocyte-specific surface receptor
CD 138	-	plasma- specific surface receptor
CD 56	-	neural cell adhesion molecule
CD 146	-	melanoma cell adhesion molecule
CRAB	-	hypercalcemia, renal insufficiency, anemia, bone lesions
D	-	diluted
DAPI	-	4', 6-diamidino-2-phenylindole
DEP	-	dielectrophoresis
DEP-FFF	-	dielectrophoresis flow fraction
DRIE	-	deep reactive ion etching
D-PBS	-	dulbecco's phosphate buffer
DVD	-	digital video disc
ECM	-	extracellular matrix
Ep-CAM	-	epithelial cell adhesion molecule
EGFR	-	epidermal growth factor
EMT	-	epithelial to mesenchymal transition
ε <sub>M</sub>	-	permittivity of the suspending medium
ERMS	-	electric field strength
FDEP	-	dielectrophoresis force

FA	-	adhesion force
FS	-	shear force
fc	-	bond strength between a single antigen-antibody complex
F <sub>c</sub>	-	fragment crystallizable
F <sub>ab</sub>	-	fragment antigen binding
FRET	-	forster resonance energy transfer
FEP	-	fluorinated ethylene propylene
FSMW	-	biofunctionalized structured medical seldinger guidewire wire
FITC	-	fluorescein isothiocyanate
GMBS	-	N-(γ-maleimidobutyryloxy) succinimide ester
glyco A	-	glycophorin A
GED1	-	geometrically enhanced differential
hGBM	-	human glioblastoma
Her2	-	human epidermal growth factor receptor 2
Hb-Chip	-	herringbone chip
HTMSU	-	high throughput microsampling unit
ITO	-	indium titanium oxide
IMWG	-	international myeloma working group
IgG	-	immunoglobulin G
Igκ	-	immunoglobulin kappa
Igλ	-	immunoglobulin lambda
KRAS	-	kirsten RNA associated rat sarcoma 2 virus gene
LMD	-	laser microdissection
LiGA	-	lithography, electroplating, and molding
LnCAP	-	prostate cancer cell line
LDR	-	ligase detection reaction
MFC	-	multiparametric flow cytometry
mAb	-	monoclonal antibody
mCRC	-	metastatic colorectal cancer
mPDAC	-	metastatic pancreatic ductal adenocarcinoma
mRNA	-	messenger ribonucleic acid
MPTMS	-	3-mercaptopropyltrimethoxysilane
MMP	-	micromilling machine
MUC1	-	mucin 1
MM	-	multiple myeloma
MGUS	-	monoclonal gammopathy of undetermined significance
MDA MB231	-	breast cancer cell line
NHDF	-	normal human dermal fibroblasts
NR	-	not reported
N <sub>L</sub>	-	ligand density
pMOFF	-	parallel multiorifice flow fractionation device
PBS	-	phosphate buffer
PBMC	-	peripheral blood mononuclear cells
PEG	-	polyethylene glycol
Pt	-	platinum

PEEK	-	polyetheretherketone
PFA	-	paraformaldehyde
PFD	-	portable filter based microdevice
PIPAAM	-	poly (N-isopropyl acrylamide)
PMMA	-	poly(methylmethacrylate)
PDAC	-	pancreatic ductal adenocarcinoma
PDX	-	patient derived xenografts
PDMS	-	poly(dimethyl siloxane)
PLGA	-	poly(lactic-co-glycolic acid)
PC	-	poly(carbonate)
PC3	-	bone metastasis prostate cancer cells
RBC	-	red blood cells
RNA-ISH	-	rna in situ hybridization assay
RT-PCR	-	reverse transcriptase polymerase chain reaction
SMM	-	smoldering multiple myeloma
SHM	-	somatic hypermutations
SiNP	-	silicon nanopillar
SMCC	-	succinimidyl trans-4(maleimidymethyl) cyclohexane-1-carboxylate
SERPINE 1	-	serpin peptidase inhibitor
TGF $\beta$	-	transforming growth factor beta
TAK1	-	transforming growth factor-beta-activated kinase
U	-	undiluted
USER	-	uracil-specific excision reagent
UDG	-	uracil-DNA glycosylase
VLBD	-	versatile label free chip
VACNT	-	vertically aligned carbon nanotubes
WBC	-	white blood cells
WNT2	-	wingless-type MMTV integration site family member 2
$\mu$ -Hall	-	micro hall detector device
$\mu$ -Sieve	-	microsieve FISH device

## ABSTRACT

Cancer research is centered on the discovery of new biomarkers that could unlock the obscurities behind the mechanisms that cause cancer or those associated with its spread (*i.e.*, metastasis). Circulating tumor cells (CTCs) have emerged as attractive biomarkers for the management of many cancer-related diseases due primarily to the ease of securing them from a simple blood draw. However, their rarity (~1 CTC per mL of whole blood) makes enrichment analytically challenging. Microfluidic systems are viewed as exquisite platforms for the clinical analysis of CTCs due to their ability to be used in an automated fashion, minimizing sample loss and contamination. This has formed the basis of the reported research, which focused on the development of microfluidic systems for CTC analysis. The system reported herein consisted of a modular design and targeted the analysis of CTCs using pancreatic ductal adenocarcinoma (PDAC) as the model disease for determining the utility of the system. The system was composed of 3 functional modules; (i) a thermoplastic CTC selection module consisting of high aspect ratio (30  $\mu\text{m}$  x 150  $\mu\text{m}$ ) channels; (ii) an impedance sensor module for label-less CTC counting; and (iii) a staining and imaging module for phenotype identification of selected CTCs. The system could exhaustively process 7.5 mL of blood in <45 min with CTC recoveries >90% directly from whole blood. In addition, significantly reduced assay turnaround times (8 h to 1.5 h) was demonstrated. We also show the ability to detect *KRAS* gene mutations from CTCs enriched by the microfluidic system. As a proof-of-concept, the ability to identify *KRAS* point mutations using a PCR/LDR/CE assay from as low as 10 CTCs enriched by the integrated microfluidic system was demonstrated. The clinical utility of the polymer-based



microfluidic device for the analysis of circulating multiple myeloma cells (CMMCs) was demonstrated as well. Parameters such as translational velocity and recovery of CMMCs were optimized and found to be 1.1 mm/s and 71%, respectively. Also demonstrated was on-chip immunophenotyping and clonal testing of CMMCs, which has been reported to be prognostically significant. Further, a pilot study involving 26 patients was performed using the polymer microfluidic device with the aim of correlating the number of CMMCs with disease activity. An average of 347 CMMCs/mL of whole blood was recovered from blood volumes of approximately 0.5 mL.

# CHAPTER 1. MATERIALS AND MICROFLUIDICS: ENABLING THE CLINICAL UTILITY OF CIRCULATING TUMOR CELLS

## 1.1 Introduction

CTCs are exfoliated cells from primary or secondary neoplasms that have been implicated in metastasis. [1] Studies based on mouse models indicate that growing or regressing tumors shed  $\sim 3.2$  to  $4.1 \times 10^6$  cells per day per g of tissue. [2] [3] Although a great number of these cells turn out to be apoptotic, [4, 5] there exists a certain aggressive population that under particular micro-environmental conditions, may acquire mesenchymal characteristics, evade the body's immune surveillance system and infiltrate distant organs giving rise to metastasis. [6, 7] Recent findings have suggested CTCs exist in circulation as single cells or aggregates (CTM-circulating tumor microemboli) of which the latter have been found to be associated with increased metastatic potential (see Figure 1.1). [8, 9] Clinical studies based on CTCs have associated the frequency of occurrence of these cells with poor progression free and overall survival for metastatic breast, colorectal and prostate cancer. [10-12] Consequently, they have been viewed as attractive new cancer biomarkers for managing many cancer diseases. CTCs have been suggested to serve as surrogates for tumor biopsy tissue allowing for less invasive sampling, which is especially beneficial for cancers that are anatomically inaccessible, such as pancreatic tumors. They can also be a source of material for understanding basic tumor biology, such as genotype or protein profile investigational studies or for drug targeting/discovery applications. [13-15]

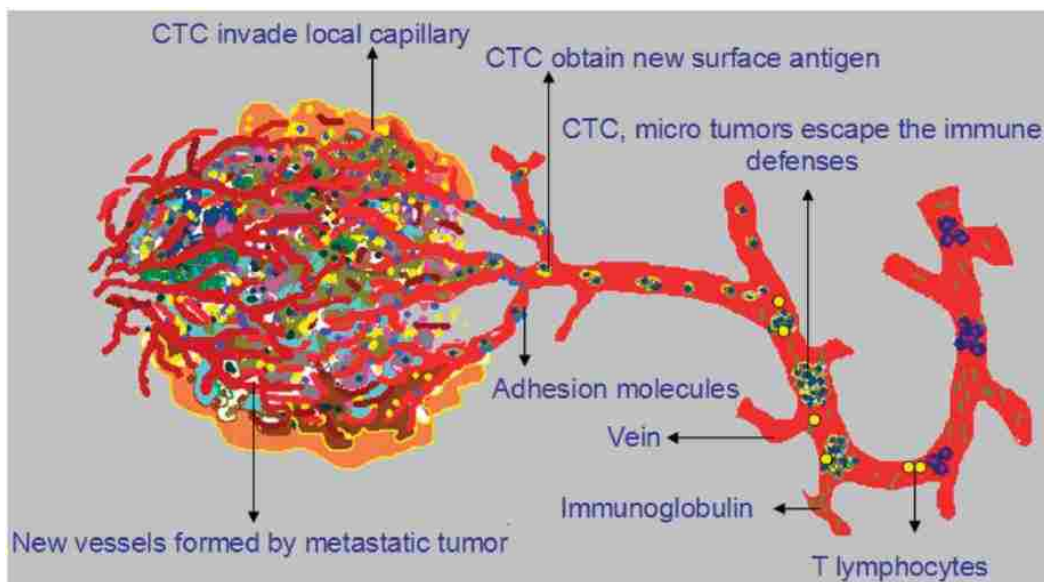


Figure 1.1 CTCs escape immune surveillance and result in metastatic malignancy. (Reproduced from Elshimali *et al.* [16] with permission)

Ninety percent of all cancer-related deaths are due to metastatic disease. Unfortunately, many conventional methods for cancer diagnosis, such as imaging with the appropriate contrast agents, are not sensitive enough to detect micro-metastatic or pre-metastatic conditions, where treatment interventions can result in improved overall survival compared to therapies administered after the onset of metastatic disease. A number of studies have indicated that CTCs can be used for detection of pre-metastatic conditions besides being restricted to managing metastatic disease only. [17-19]

Various technologies have been used to isolate and enumerate CTCs from blood, however, in spite of the rapidly evolving technology there are still challenges. CTCs are a very rare population in blood, which is populated with a variety of cell types in much higher abundance than CTCs. Further, CTCs are phenotypically heterogeneous with a short half-life; 1 – 2.4 h in circulation. [20, 21] In addition, CTC enrichment can be complicated by the fact that their genotype and phenotype profiles

are likely to be modified dynamically once exfoliated due to EMT-like (Epithelial-Mesenchymal Transition) processes. [21-23] There is currently no single antigenic marker that is uniformly expressed on all CTCs that can effectively be used to identify the various sub-populations of CTCs that may be present in circulation and be key effectors in the metastatic cascade. [24] Enrichment strategies ( $>10^9$ ) are therefore necessary to obtain various CTC sub-populations possibly found in circulation and also, secure pure populations of these CTCs so as to enable downstream characterization of such sub-populations via genotyping or the propagation of these cells for biological studies.

CellSearch™ (Veridex LLC) is the only system cleared by the FDA as a diagnostic tool for the enrichment and enumeration of CTCs, but only for metastatic breast, colon and prostate cancers. This system is based on antibody functionalized magnetic particles that specifically bind to CTCs expressing unique antigen(s), such as the epithelial cell adhesion molecule, EpCAM. Upon application of a magnetic field, CTCs bound to the magnetic particles are extracted and further identified with tumor specific phenotypic markers. The technology has been clinically validated by several studies. [11, 25] Advantages of CellSearch include; its ability to predict progression free and overall survival of breast cancer patients; and it is a semi-automated process that has facilitated use in several centers where clinical trials are currently being carried out. [26] However, it suffers from low purity (0.01-0.1%) and low clinical sensitivity with recent reports indicating very low CTC median yields (1 CTC/7.5 ml) in some cancers. [27, 28]

Newer platforms, such as microfluidics, have demonstrated higher purities and clinical yields. [29-34] Microfluidic devices are attractive platforms for the analysis of CTCs for several reasons: (i) They can be configured to select CTCs based on several different modalities including biological cell properties, such as expression of antigens specific to the CTC type or physical cell properties, such as cell size or deformability; (ii) microfluidic devices operate in a closed architecture minimizing the potential of sample contamination artifacts that may provide false positive results, especially in clinical laboratory settings; (iii) microfluidics can be produced in a high production mode and at low-cost. For example, devices can be produced in thermoplastics using micro-replication, the same technology used to produce CDs and DVDs; (iv) CTC selection devices can be integrated to other steps to fully automate sample processing negating the need for operator intervention and thus, minimizing false negative or false positive results. [35, 36] [34]

Challenges with microfluidics include the high surface-to-volume ratio associated with these devices requiring special attention to engineer surfaces that reduce non-specific adsorption artifacts, especially when dealing with clinical samples such as whole blood. Also, microfluidics are many times incompatible with high throughput processing; for typical volume flow rates of 300 nL/min ( $50 \times 50 \mu\text{m}^2$  microchannel cross-section,  $0.2 \text{ cm s}^{-1}$  linear velocity), 3,333 min (55.5 h) would be required to exhaustively process 1 mL of sample.

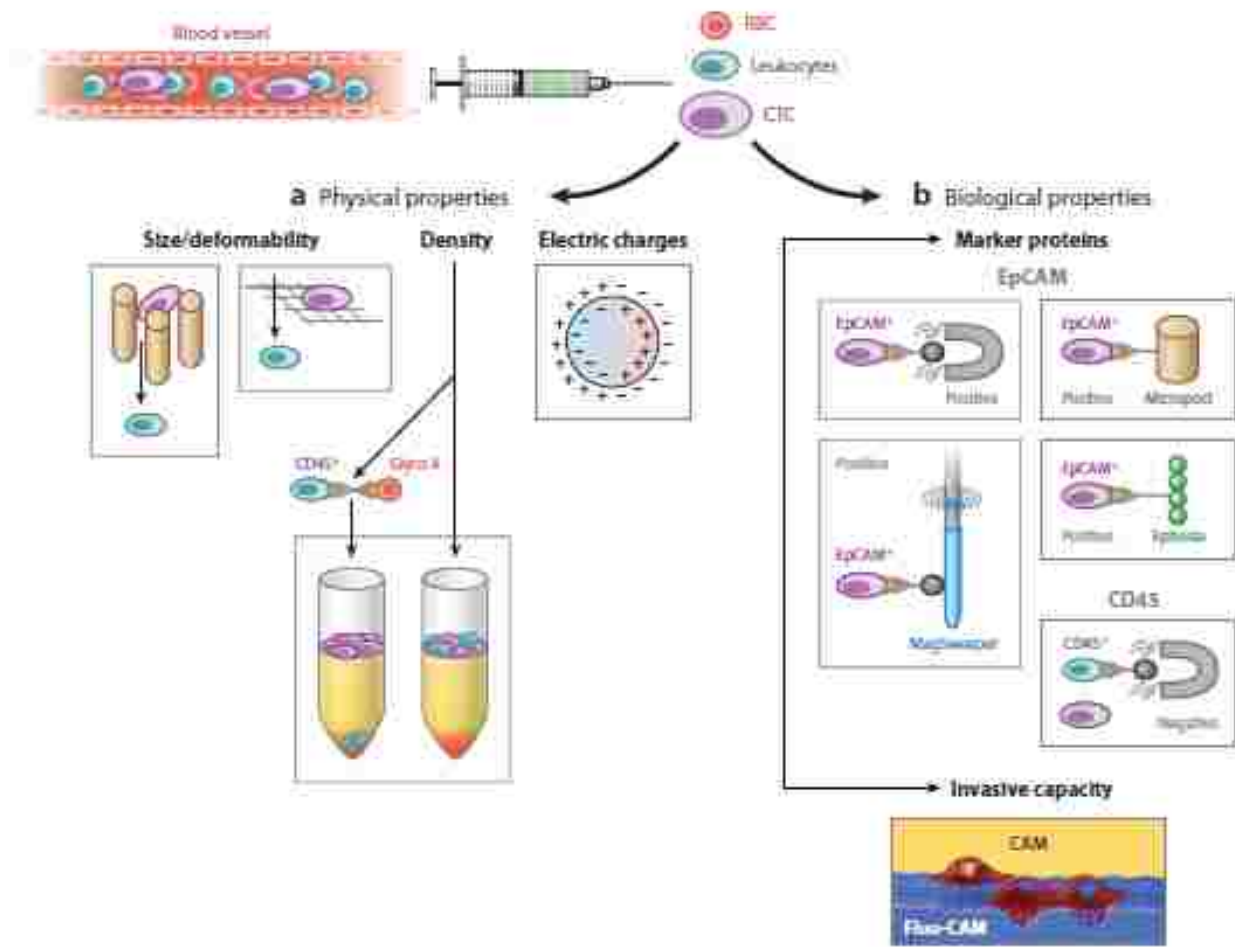


Figure 1.2 Enrichment of circulating tumor cells (CTCs) from the peripheral blood of cancer patients is based on physical or biological properties of CTCs. (A) Physical properties include size (membrane filter devices), deformability (microfluidic system in a chip), density (Ficoll centrifugation), and electric charge (dielectrophoresis). (B) Biological properties include expression of cell surface markers and invasive capacity. Cell surface markers include an epithelial cell adhesion molecule (EpCAM) for positive selection and CD45 for negative selection; anti-EpCAM or anti-CD45 antibodies conjugated with magnetic beads, used to enrich CTCs in a magnetic field; and anti-EpCAM antibodies on microposts or columns of nanobeads. Invasive capacity refers to adherence and invasion of fluorescent matrix. Abbreviations: glyco A, glycophorin A (a 131-amino-acid protein present at the extracellular surface of the human red blood cell); CAM, cell adhesion matrix; fluo-CAM, fluorescent cell adhesion matrix; RBC, red blood cells. (Reproduced from Alix-Panabières *et al.* [38] with permission)

CTC enrichment from blood is based on two criteria that differentiate CTCs from normal hematopoietic cells: (i) Biological properties, such as surface and cytoplasmic protein expression, viability, and invasion capacity. CTCs can be directly targeted, in which case, this is referred to as positive selection while the converse, negative selection clears hematopoietic cells to obtain CTC fractions indirectly; (ii) physical properties such as size, density, cell membrane electric potential, and deformability (see Figure 1.2). [37, 38]

Assessment of CTC enrichment technologies is based on 5 important figures-of-merit: (i) Throughput, defined as the maximum volume processing rate; (ii) recovery, an indicator of the number of target cells selected from the input sample with respect to the seed level of the target in that same sample; (iii) purity, which is defined as the ratio of CTCs selected to the total number of cells enriched; (iv) clinical sensitivity, which refers to the ability of the assay to correctly identify those patients with the disease; and (v) clinical specificity, which refers to the ability of the assay to correctly identify those patients without the disease. [39, 40] While throughput is primarily a function of the mechanical properties of the device, purity is in most cases material dependent whether the selection modality is based on biological or physical properties of the CTC. Clinical sensitivity and specificity are a complex function of the biological and physical properties of the CTC, but also on the topographical features of the device.

Material considerations play an important role in the development of devices targeted for CTC enrichment, especially for microfluidic-based devices. For example, many CTC selection platforms utilize immunomagnetic selection that employ magnetic

beads decorated with antibodies directed against antigens unique to the CTC. The magnetic susceptibility of these particles must be sufficient to collect with high efficiency all CTCs, even those with low expression levels of the target antigen. In addition, devices with biocompatible surfaces are required so as to maintain CTC integrity and viability as well as minimize non-specific adsorption of hematopoietic cells to their surfaces. From a commercial perspective, material selection can determine the cost and manufacturability of the CTC device. The manufacturing modality is highly dictated by the type of material used; for example thermoplastics can be produced in high production modes and at low cost using micro-replication. These considerations are important in order to facilitate the use of devices in clinical-based settings, where a high turnover is expected for cancer screening and diagnosis and the fact that devices are used for only one assay and then, discarded to minimize false positive results. [41, 42]

As noted, material properties play an integral role in determining the performance characteristics of a device irrespective of the selection modality employed (*i.e.*, biological or physical). For selection based on the CTC's biological properties, device surface properties are dictated by the pendant functional groups found on the substrate material both in terms of number density and type. These functional groups and their surface density determine the surface load of affinity agents, such as antibodies used for CTC enrichment. Typically, high loads of antibodies are required to select with high efficiency CTCs, especially those with low antigen expression. The topography of the surface is critical as well, because it can increase the contact area between the CTC and selection surface for devices using affinity selection; large contact areas enhance



recovery of CTCs even with low antigen expression levels. Optical transparency of the substrate is an important consideration as well because efficient enumeration of the CTCs utilizes immunofluorescence, where low-levels of fluorescence must be detected. In addition, the substrate material must accommodate the fluorescence microscope used to image the CTCs, such as the refractive index and cover slip thickness to provide high image quality of the CTCs. For devices and assays based on IMAC (immunomagnetic assisted cell sorting), the magnetic susceptibility of the beads is critical for effective enrichment of CTCs from complex sample matrices. For CTC microfluidic devices based on physical selection, such as micro-filters, the material selection is based upon the ability to generate reproducible and accurate pore or filter structure dimensions optimized for CTC selection while at the same time minimizing non-specific adsorption of hematopoietic cells.

While many CTC reviews have appeared in the literature, the primary goal of these reviews have been to focus on the enrichment protocols employed to select CTCs and/or clinical studies. [38, 43-46] This review is unique in that it will provide an overview on the interplay of materials and microfluidics for CTC enrichment. Specifically, we will discuss the role of material considerations on the performance metric(s) of the microfluidic selection mechanism for CTC analysis including, recovery, throughput, purity and clinical sensitivity/specificity.

## **1.2 Substrates Commonly Used by Microfluidics for CTC Enrichment**

Material options for any microfluidic device depend on several factors such as machinability, optical transparency, inertness to the assay conditions, thermal tolerances and a surface conducive to modification. [42, 43, 47, 48] Silicon, glass, polymers and magnetic beads are commonly employed in CTC enrichment microfluidic devices. Here we will look at how these materials have been selected for the fabrication of various CTC enrichment devices and the material property effects on CTC enrichment.

### **1.2.1 Silicon and Glass Materials for CTC Enrichment Microfluidic Devices**

Silicon and glass and their hybrids are the most commonly used materials for CTC enrichment microfluidic devices primarily because of their well-established surface-modification chemistries. Silicon is a semiconductor material that has been well characterized in terms of its physical and chemical properties as well as micromachining techniques used to form structures relevant for the device's operation. Silicon has been used in both for the affinity and size selection of CTC using microfluidic devices. [31, 49-51] Characteristics that make silicon an attractive material for CTC enrichment are its solvent compatibility and well established surface chemistries for ligand attachment. In the case of size selection, silicon offers good mechanical stability, especially in the construction of different filter structures such as pores, slots and traps for high throughput blood processing. [49, 50]

Silicon can also be used as a master in soft lithography for the fabrication of PDMS microfluidic devices for CTC enrichment. [52-54] Microfabrication of silicon can be carried out using photolithography followed by wet etching, plasma etching or reactive ion etching. [55] More specifically, deep reactive ion etching (DRIE) has been utilized to create micropost structures as deep as 50 to 100  $\mu\text{m}$  for CTC selection devices based on affinity capture, [31] and the GEDI (geometrically enhanced differential) devices, [29] both of which utilize affinity capture of CTCs. Nanostructured silicon nanopillar (SiNP) devices for CTC capture were fabricated using a wet etching method implementing a micro-electrochemical redox reaction involving HF and silver nitrate. [56]

Filter-based microfluidic devices for CTC enrichment have also used silicon as the substrate material for the generation of pore or filtering structures. One such example was the multi-obstacle architecture device that utilized silicon-on-glass (SOG) to create high-aspect ratio microfilter structures for CTC isolation. Basically, lapping and chemical/mechanical polishing (CMP) were performed on the silicon layer, which determined the optimal height of the structures (50  $\mu\text{m}$ ). Glass was bonded onto the silicon using anodic methods. As a consequence, CTC visualization was enabled through the use of optical microscopy with high aspect ratio structures generated for CTC isolation. [50] In another report, the authors produced uniform depth honeycomb structures on a silicon micro-sieve (see Figure 1.3) to generate a CTC enrichment device. The fabrication strategy employed a SOI (silicon-on-insulator) wafer instead of silicon to prevent DRIE over-etching due to the embedded silicon dioxide layer. After the

structures were formed, the embedded SiO<sub>2</sub> layer was then removed by dielectric reactive ion etching. [49]

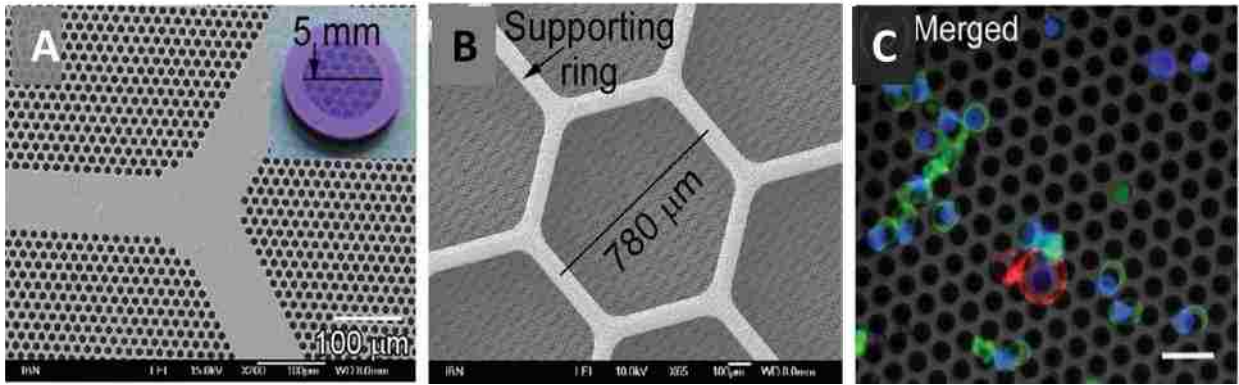


Figure 1.3 (A) SEM image of a silicon microsieve filter with uniform honeycomb pore structures fabricated using silicon on insulator technology (SOI), (B) SEM image of the backside of the microsieve membrane showing the supporting rings. The dimension of the silicon microsieve and membrane area is 7.5 mm and 5 mm in diameter, respectively. (C) Composite fluorescent images of enriched MCF-7 cells (red and blue) and leukocytes (green and blue) stained with fluorescent labeled antibodies against membrane antigens EpCAM (red) and leukocyte marker CD45 (green). All nuclei were stained with DAPI. Scale bar: 30  $\mu\text{m}$  (20 $\times$ ). (Reproduced from Lim *et al.* [49]with permission).

Glass microfluidic devices are particularly favored due to their well-defined surface chemistry and outstanding optical properties. These properties are highly desired for maximizing signal output during the fluorescence imaging phases of the assay to allow for immunophenotyping of the cells. In fact, a number of CTC microfluidic devices consist of hybrid forms of two materials, such as glass and silicon or glass and PDMS where glass is primarily used as a cover plate for high resolution imaging purposes. For example, a herringbone device, which consisted of a PDMS substrate

bonded to a glass cover plate, enabled high-resolution imaging for in situ FISH assays and RNA ISH analysis of WNT2 gene expression of CTCs enriched by the device from both human and patient-derived xenograft models. [57] [32]

There are some challenges involved with the fabrication of both glass and silicon-based microfluidic devices. First, glass is limited to the production of low aspect ratio structures due to the isotropic nature of wet etching producing shallow structures. [47, 58] While this can be alleviated using DRIE dry etching techniques, it makes the fabrication protocol more costly compared to wet-etching microstructures. Also, both materials involve at least 5 fabrication steps with some requiring harmful and toxic agents, such as acids for wet etching. This necessitates the need to use clean room facilities, which also adds to the cost of producing devices, which can be problematic for scenarios where *in vitro* diagnostics are required such as CTC assays, which require one-time use operation. Device cost is compounded by low manufacturing yields when using DRIE as well. [59, 60]

### **1.2.2 Polymer Substrates for Microfluidic Devices used for CTC Enrichment**

To ensure clinical accessibility of microfluidic devices for CTC diagnostics, low-cost and high fidelity large-scale production of single-use devices is critical. [61, 62] For this, polymers, such as poly (methylmethacrylate), PMMA, cyclic olefin copolymer, COC, poly(carbonate), PC, or poly(dimethyl siloxane), PDMS, are well suited. Microfluidic devices fabricated in silicon [62-66] require time-consuming photolithography and etching (wet or dry) to microstructure components required for each device adding to device cost and reduced production rates. Alternatively, reverse polarities of the desired

microstructures can be patterned into silicon substrates [62, 67-69] or spin-coated photoresist layers [70-78] that can be used as molding masters. PDMS can be cast against a mold master and cured to form the desired microstructures; this curing process requires from 45 min to 24 h. [62, 67-79] The elastomeric PDMS is then peeled from the master and the microstructured PDMS sealed against a glass cover plate; both are treated with oxygen plasma and irreversibly bonded to yield the sealed device. After removing the PDMS, the molding master is free for repetitive uses and the time and expense of lithography for producing each device eliminated. [62, 67-79] However, this process requires several hours of curing time and thus, is difficult to effectively compete with the throughput capabilities offered by hot embossing or injection molding, where thermoplastic replicas can be produced within a few seconds with high fidelity. [34, 61, 70, 80, 81]

Thermoplastics, such as PMMA and COC for selection of CTCs and PC have been hot embossed from a metal molding master. In many cases, the master can be mechanically machined into brass using micrometer-sized milling bits and thus, no clean room is required. [61, 80] Alternative strategies, such as UV or X-ray LiGA (lithography, electroplating, and molding) offer the ability to fabricate sub-micrometer structures with high fidelity. [79, 82] Hot embossing consists of heating a thermoplastic substrate to above its glass transition temperature ( $T_g$ ) and under controlled pressure, transferring the master's microstructures into the heated substrate, then cooling and releasing the patterned substrate. [61, 79, 80] Figure 1.4 shows pictures of a micromilling machine used to produce mold masters and a hot embossing machine

used to micro-mold devices from the metal masters generated via micromilling. Similarly, injection molding can be used to create devices via micro-replication and requires pellets of the thermoplastic to be passed through a heated barrel with the molten thermoplastic forced through a nozzle and into a cavity produced by the molding master. The thermoplastic then solidifies following cooling transferring the master mold's structures into the polymer. [79] While set up costs for injection molding are higher than that associated with hot embossing, production rates for injection molding are typically much higher than that associated with hot embossing.



Figure 1.4 (A) Kern micromilling machine (MMP) is a computer numerically controlled (CNC) milling machine that is used to pattern microstructures on metal mold inserts using very small milling bits (down to 25  $\mu\text{m}$  diameter) rotated at very high speeds in the range of 40,000 – 200,000 rpm. Mold inserts can then be used as masters for the production of microstructures on polymer substrates (B) Hex03 hot embossing equipment capable of molding polymer parts containing features with micro- and nano-dimensions including high aspect ratios (>10 : 1) through a combination of heat and pressure. It is commonly used to produce polymer microfluidic chips for biomedical applications.

Because both hot embossing and injection molding use a top-down fabrication approach leaving open-faced microstructures, sealing the patterned thermoplastic must be undertaken to form the final device. Sealing strategies can employ simple approaches such as the use of commercially available adhesive coverslips.[83] However, the fluidic pressure of processing whole blood within micrometer-sized channels necessitates strong sealing of the coverslip to the substrate to prevent device failure. Thus, thermal fusion bonding has been employed due to the high tensile strength bonding between the substrate and coverslip it generates. Here, a thin (125 – 500  $\mu\text{m}$ ) coverslip composed of the same thermoplastic as that used for the substrate is pressed against the patterned substrate and the pair is heated to near their glass transition temperature, which allows the polymer chains to rearrange, bond, and seal the microfluidic device with similar tensile strengths as PDMS-to-glass bonding. [34, 61, 80, 81]

Whichever fabrication modality is used, the polymer substrate must possess the following characteristics to serve as a viable substrate for fluidic devices targeted for the selection of CTCs: (i) Functional scaffold for the surface attachment of the affinity agent (antibody, peptide, aptamer); (ii) optically transparent and void of autofluorescence; and (iii) surfaces that show minimal amounts of non-specific adsorption of blood cells to their surfaces to provide high purity of the enriched CTC fractions; and (iv) biocompatible surfaces so as not to compromise the viability of isolated CTCs for on-chip culturing or drug delivery studies. Point (i) is particularly important for CTC selection modality using biological CTC selection because of the need for covalently attaching is high.



Strategies for immobilizing affinity agents to polymers are diverse amongst current CTC technologies but for either PDMS or thermoplastics, successful immobilization of the affinity agents has been demonstrated by introducing reactive functional groups onto the substrate. For example, PDMS surfaces use alkoxy silane molecules,[63, 67, 84] while thermoplastics depend on generating carboxylic acid moieties for amide coupling of affinity agents; the activating source for generating these functional scaffolds typically use UV or ozone. [61, 80, 81] [34] Furthermore, thermoplastic UV/ozone modifications require the thermoplastic to be sufficiently transparent to provide uniform modification throughout the CTC selection conduit. [81]

A polymer's optical qualities also impacts the identification or enumeration process of the isolated CTCs via immunofluorescence.[62] PDMS's optical transparency is nearly glass-like making it ideal for fluorescence visualization.[85] Both unmodified or UV/ozone modified PMMA and COC thermoplastics have comparable fluorescence backgrounds to glass, [85, 86] and thus, they are certainly compatible with immunofluorescence identification of CTCs. [61, 80, 81] [34] PC, however, has a much higher fluorescence background,[86] and following UV/ozone modification for the attachment of affinity agents, the polymer's autofluorescence overwhelms CTC fluorescence, disqualifying it in many cases for CTC isolation and immunofluorescence analysis. [81]

Lastly, the hydrophobicity of native PMMA, [87] COC, [88] and PDMS [89] lends to issues related to biocompatibility. But, modifications of the polymer using, for example, oxygen plasma treatment of PDMS or UV/ozone treatment of thermoplastics,

[81] is necessary to improve the material's biocompatibility. In the case of PDMS, hydrophobic recovery can affect the surface's biocompatibility (adherent cells were ~98% viable after 24 h [90]), while for thermoplastics, hydrophobic recovery is not as pervasive, but thermal processing above the  $T_g$  of the material can enhance this process.[81] UV/ozone treated COC exhibited the same biocompatibility as PDMS, [90] but the UV/ozone treated PMMA exhibited elevated cytotoxicity (~89% viability after 24 h [90]) due to the leaching of peroxide and oligomeric and monomeric methyl methacrylate by-products following the UV/ozone activation process. [81, 90]

Further aspects of thermoplastic biocompatibility are more subtle. Firstly, if CTC culturing is attempted on-chip, the CTCs must be provided with an adequate supply of carbon dioxide and oxygen to maintain pH; [90] the gas permeability (permeability constants given in Table 1.1) of elastomeric PDMS is far greater than most thermoplastics, [91-96] thereby requiring continuous flow of fresh media to cells cultured within thermoplastic devices. [90] Secondly, on-chip monitoring of cellular response to drugs can be biased by adsorption of small, hydrophobic molecules to the polymeric substrate; this effect has been shown to occur in PDMS [90, 97, 98] and PMMA [90] (detailed values are shown in Table 1.1).

As a final note, thermoplastics can be used for the fabrication of filters for size-based selection of CTCs from other mononucleated blood cells. [99, 100] Commercially-available PC filters are track-etched; [101] this process produces pores randomly distributed across the filter and larger, fused pores through which rare CTCs may pass. Consequently, clogging is common and recoveries are poor (50-60%). [102, 103]

Table 1.1 Various polymer materials used in CTC enrichment devices

Quality	Specific Criteria (ref)	PDMS	COC	PMMA	PC
Manufacturability	Master Mold Fabrication [79]	Lithographic	Micromilling or LIGA		
	(Material) [79]	(Si or photoresist)	(Brass or Nickel)		
	Time for Replication [79]	Mediocre (hours)	Mass-Production (seconds)		
Immobilization of Affinity Agents	Functionalization [84]	Excellent	Excellent	Moderate	Poor/Moderate
	(Method) [84]	(alkoxysilane)	(UV/ozone)	(UV/ozone)	(UV/ozone)
Immunofluorescence Visualization	Autofluorescence [85, 86]	Very Low	Low	Low	Very High
Biocompatibility	Cytotoxicity [90]	Excellent	Excellent	Moderate	Excellent
	(Viability after 24 h)	(98%)	98%	89%	98%
	Adsorption of Hydrophobic Molecules (7-EC <sup>†</sup> ) [90]	20%	0%	20%	0%
	CO <sub>2</sub> Permeability <sup>‡</sup> (P × 10 <sup>13</sup> )	3489	1.77	2.33	22.23
	O <sub>2</sub> Permeability <sup>‡</sup> (P × 10 <sup>13</sup> )	695	0.765	0.0653	2.96

<sup>†</sup> 7-EC ≡ 7 ethoxycoumarin. Similar results were found for testosterone.

<sup>‡</sup> Permeability constant (P) units:  $\left(\frac{cm^3 \cdot cm}{cm^2 \cdot s \cdot Pa}\right)$ .

\* References [93-96].

Measurements were done at standard pressure and the temperatures were 25 °C for COC and PC and 35 °C for PDMS and PMMA.

To this end, microfabrication techniques utilizing photoresists and reactive ion etching have been used to construct 2-D and 3-D filters with controlled pore sizes and spacing. Three-D filters offer lower fluidic stress on filtered CTCs for the isolation of live rather than fixed cells. [99, 100, 104] Parylene C has also been used as a polymeric substrate for these filters due to its mechanical flexibility, biocompatibility, and optical transparency for immunofluorescence CTC enumeration. [99]

### **1.2.3 Magnetic Materials for CTC Enrichment using Microfluidic Devices**

The use of magnetic particles for CTC isolation is ubiquitous largely because the CellSearch technology remains the only FDA approved assay for CTC enrichment and analysis. In this section, we will focus on several technologies that utilize magnetic particles and discuss how the nature of the particles affects the CTC enrichment process.

Magnetic particles have been researched for over two decades, resulting in the commercialization of an array of products, including those catered specifically for the isolation of CTCs. Many other commercially available products or slight modifications thereof are used for CTC isolation. [105] The choice of magnetic particles for CTC enrichment is predicated on the requirement of only low strength magnets (such as inexpensive neodymium magnets generating on the order of a T) necessary to remove these magnetic particles and their payload from solution (achieving saturation magnetization in fields on the order of tens to hundreds of mT). [105-108] There are material properties that should be assessed when considering magnetic particles for the isolation of CTCs, especially when utilized in conjunction with a microfluidic device. [68]

To process a blood sample using CellSearch, a pre-processed blood sample is dosed with a ferrofluid consisting of ~100 nm iron oxide nanoparticles [108] coated with a polymer to improve solubility [109] with the particles functionalized with anti-EpCAM antibodies. [110] After incubation, cells bound to these magnetic nanoparticles are isolated by applying an external magnetic field. [105, 106, 110] Rigorous evaluations of the CellSearch technology have shown a recovery of ~85%; [110, 111] however, the purity is poor (<0.01-0.1%) complicating further characterizations of the isolated CTCs. [112-115] Because the interaction of the nanoparticles with cells occurs by diffusion, shear forces are not induced that could disrupt weak, nonspecific interactions of contaminant cells; the use of shear forces to improve purity is a fundamental construct of the MagSweeper. [115, 116]

The MagSweeper utilizes a magnetic stirring rod with a non-adherent, 25  $\mu\text{m}$  thick plastic sheath to isolate cells that have been labeled with 4.5  $\mu\text{m}$  magnetic beads in a similar fashion as that of CellSearch. By sweeping through a diluted blood sample contained in a well, the MagSweeper captures labeled cells under shear stress, thereby detaching nonspecifically and weakly adhering cells to achieve higher purities compared to CellSearch. Of 50 MCF-7 cells, a metastatic breast cancer cell line, spiked into a diluted blood sample, 62  $\pm$ 7% were isolated with a purity of 51  $\pm$ 18%. [115] A second generation MagSweeper device was compared directly with CellSearch for patients with metastatic prostate cancer. The MagSweeper exhibited similar recoveries to that of CellSearch, but with lower purity. [116] The lower purity may have been attributed to either different blood preparation steps or the use of custom-labeled 1.5  $\mu\text{m}$  magnetic

beads; [116] the authors previously iterated that antibody specificity and micro-bead quality was critical for assay purity because contaminating cells are generally attached to the magnetic beads rather than to the sheathed magnetic rod itself. [115]

A challenge in terms of clinical utility of the MagSweeper is its incompatibility with whole blood. The high viscosity, cell density, and protein content of whole blood caused magnetic micro-beads to aggregate, precipitate, and/or prevent antibody-antigen complexation. [117] Thus, additional workflow was necessary to process blood samples, for example removal of RBCs or dilution. [68, 111, 115-117]

For nanoparticle-based technologies, CTC isolation from whole blood has been demonstrated using 30 nm, iron oxide nanoparticles functionalized with amphiphilic polymers (providing stability in whole blood matrices) and capture antibodies. From unprocessed, unfractionated whole blood, cultured SK-BR3 cells were isolated with a 73.6% recovery and 33.2% purity. [117] However, to our knowledge, clinical demonstrations of using magnetic nanoparticles in unprocessed whole blood have not been demonstrated.

Compared to magnetic micro-beads, iron oxide nanoparticles offer several advantages: (i) The nanoparticle solution is quasi-homogenous, improving the kinetics of cell-particle interactions; and (ii) more of the cell's surface is reactive (by approximately two to three orders of magnitude) due to the nanoparticle's enhanced surface area to volume ratio. [117] However, there are limitations as to the use of nanoparticles, many of which arise from cellular uptake of the nanoparticles Xu, Aguilar [117] This imparts unavoidable cell contamination due to cellular uptake, reduction in

CTC viability, and alteration of the CTC's molecular profile. [109, 118] Even with CellSearch, it has been shown that many CTCs isolated are apoptotic. [119, 120] In comparison, great care was taken to ensure that the MagSweeper did not induce any statistically significant change in the viability of the selected CTCs and had minimal effects on single cell transcriptomes. [116] In contrast to the free solution mixing of functionalized magnetic particles with their target cells, the Ephesia microchip utilizes magnetic micro-beads in a unique format (see Figure 1.5). A PDMS casted microchannel was sealed over a glass coverslip previously patterned with magnetic ink by micro-printing. Upon the application of a magnetic field, the magnetic inks concentrated the magnetic field lines vertically and 4.5  $\mu\text{m}$  antibody-coated magnetic micro-beads self-assembled into high aspect ratio pillars that were used for CTC isolation. [105, 121] The Ephesia chip achieved >94% recovery with 78 – 97% purity for the isolation of cultured Raji (B-lymphocyte) cells mixed with different numbers of Jurkat (T-lymphocyte) cells (minimum ratio of 1 Raji cell to 100 Jurkat cells). Furthermore, B-lymphocytes were isolated from blood and fine needle aspirate patient samples; good correlation with flow cytometry was observed for cell morphology and antigen expression. [105] The Ephesia chip is compatible with mass-production modalities such as those used for the production of thermoplastic devices and the batch functionalization of micro-beads simplifies the practical aspects of functionalizing individual devices. [105] A concern with the Ephesia chip was that it was designed for processing very low sample volumes (10  $\mu\text{L}$ ). The stability of the micro-bead pillars limited linear velocities of up to 0.1 mm/s, corresponding to a volumetric throughput of

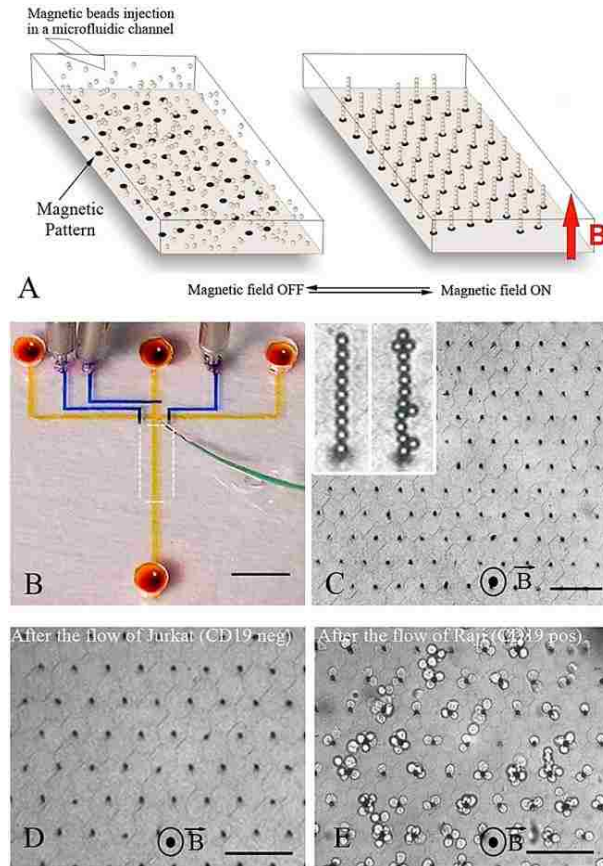


Figure 1.5 (A) Principle of magnetic self-assembly. A hexagonal array of magnetic ink is patterned at the bottom of a microfluidic channel. Beads coated with an antibody are injected in the channel. Beads are submitted to Brownian motion. The application of an external vertical magnetic field induces the formation of a regular array of bead columns localized on top of the ink dots. (B) Two levels PDMS integrated microchip. Channels were filled with colored water. Delivery and separation channels for the cells appear in yellow. Inlets ports appear in orange. The separation channel is the longer vertical branch. The area bearing magnetic posts is marked by the dotted white box. Channels in the upper PDMS layer, controlling the opening and closing of the inlet channels, appear in blue. The green wire is a thermocouple for in situ control of the temperature in the system. (Scale bar: 0.5 cm.) (C) Magnetically assembled array of columns of 4.5  $\mu\text{m}$  beads coated with anti-CD19 mAb (specifically retaining Raji B-Lymphocytes). Typical column shapes are shown in the insets. (Scale bar: 80  $\mu\text{m}$ .) (D) Optical micrograph of the columns after the passage of 1,000 Jurkat cells. No cell can be seen. (Scale bar: 80  $\mu\text{m}$ .) (E) After the passage of 400 Raji cells, numerous ones are captured and rosetted on the columns. (Scale bar: 80  $\mu\text{m}$ .) (Reproduced from Saliba *et.al* [122] with permission from the Proceedings of the National Academy of Sciences of the United States of America (*PNAS*))



3.6  $\mu\text{L}/\text{h}$ . The low throughput was also partly due to the constrained size of the microfluidic channel (40 x 250  $\mu\text{m}$ , W x D). [105]

### **1.3 Biological and Physical Properties for CTC Enrichment**

CTCs possess intrinsic properties that differentiate them from hematopoietic cells, the major component of peripheral blood. These properties can be placed into two broad categories. Biological properties, which are primarily focused on tumor associated surface antigen expression, viability and invasion capacity while physical properties take into account cell size, density, electrical charges and deformability. A plethora of microfluidic technologies have adopted different formats that target either biological or physical or both properties for CTC enrichment. In the following sections, we will discuss microfluidic devices based on biological or physical selection and how material properties affect the performance of these devices.

#### **1.3.1 Microfluidics for CTC Enrichment Based on Biological Properties**

These mainly employ affinity-based assays for CTC enrichment. These assays use specific but non-covalent interactions between a ligand (antibody, aptamers, and peptide) to a tumor specific membrane protein. CTC selection involves a solid phase (glass, silicon, polymers) in which the recognition element is covalently tethered to the surface of a fluidic conduit. [39] The correct choice of a solid surface and the application of suitable surface chemistry that is compatible with a diverse set of proteins and at the same time maintaining their native conformation and biological function are necessary.

Blood samples are passed through the appropriately prepared conduit to invoke the CTC selection process. The following strategies are considered in order to maximize interactions of the blood-borne CTCs and the surface immobilized ligands: (i) geometrical configurations of the fluidic conduit that affect the fluid dynamics; (ii) the nature of the surface chemistry of the solid phase; and (iii) attachment chemistry of the bound ligand.

### 1.3.1.1 Immobilization Strategies

Critical to a positive or negative CTC selection assay is the immobilization of a biologic capture element, be it a protein (antibody, Ab), aptamer, or peptide, to the surface of a microfluidic channel. For the enrichment of CTCs from a clinical sample, which have varying levels of antigenic expression, [123] it is critical that a maximum number of *active* capture elements be immobilized onto a surface. As the surface density of these active elements increases, so does the adhesion force ( $F_A$ ) of an isolated CTC to the capture surface as noted by equation (1):

$$F_A = \left( \frac{2A_c k_B \theta N_R}{l_b} \right) \ln \left( 1 + \frac{N_L}{\eta K_D} \right), \quad (1)$$

where  $A_c$  is the cell's contact area to the surface,  $k_B$  is Boltzmann's constant,  $\theta$  is the absolute temperature,  $N_R$  is the receptor density (the CTC's antigen expression level),  $l_b$  is the extent of stretch to reach before breaking the antigen/Ab association,  $N_L$  is the surface density of active mAbs,  $K_D$  is the antigen/Ab dissociation constant, and  $\eta$  is an

adjustable fitting parameter. Increasing  $F_A$  by ensuring a large  $N_R$  (active capture element surface density) prevents a captured CTC from being removed from the surface by hydrodynamic shear force, especially when antigen expression of the CTC ( $N_L$ ) is low. [61, 63, 81, 124] Critical to efficient CTC capture, then, is a strategy by which selection elements are immobilized in high densities. Attachment of the selection element can use either passive adsorption or covalent attachment techniques.

For passive adsorption, reduction of Ab activity by physisorption is well known; it has been shown that 90% of Abs lose their activity through this process.[125] For this reason, few researchers directly adsorb CTC capture elements to their surfaces. However, an example has been documented; adsorption of epithelial antibodies and selection proteins onto halloysite coated microtubes to induce CTC capture along the microtube surface. [126, 127] In the majority of other cases where passive adsorption has been employed, a scaffolding protein such as an avidin protein, [116, 128] biotinylated BSA (subsequently following by an avidin protein), [71] or protein G [127] have been passively adsorbed first. Then, either biotinylated Abs are bound to the avidin decorated surface via strong avidin-biotin linkages or unmodified Abs are bound to the surface using protein G. In the latter case, protein G binds Abs specifically to the Ab's Fc region, thereby ensuring the Ab is optimally oriented with its Fab regions (antigen binding regions) exposed to solution for binding CTCs. This is not true for avidin linkages, because biotinylation may occur with any reactive residue present in the Ab (*i.e.*, on the Fc or Fab regions); [129] this results in a surface of Abs with non-uniform orientation where only those with Fab regions exposed to solution are capable

of CTC capture (effective reduction of  $N_R$  in Eq. (1)). [130] Considering the costs of avidin proteins and protein G (as well as the analogous protein A) are comparable and the benefits of controlled Ab orientation are well established for bioassays in general, [131] the use of protein G in place of an avidin moiety is wise due to a higher percentage of effectively active Abs. In either case, the passive adsorption of biologic CTC recognition elements is attractive due to simplicity (no additional linkers or coupling agents are required).

For the covalent attachment of Ab to selection surfaces, functional scaffolds must first be generated to which the Abs may be coupled via covalent bonds, typically involving primary amine groups present within the Fc or Fab regions of the Abs. For glass/PDMS substrates, the use of 3-mercaptopropyltrimethoxysilane (MPTMS) is commonly used to generate sulfhydryl surface groups after which a sulfhydryl-amine crosslinker, (N-( $\gamma$ -maleimidobutyryloxy) succinimide ester, GMBS), is employed. [63, 67, 73, 132] The succinimide ester of GMBS permits covalent amide linkages to lysine and/or arginine (primary amine) residues on the Abs. [84] The use of MPTMS and GMBS on glass/PDMS substrates has exclusively been used to immobilize neutravidin for subsequent introduction of biotinylated Abs. [63, 67, 73, 132] Alternatively, researchers utilizing magnetic nanoparticles coated with a polymer containing carboxylic acid moieties have directly immobilized peptides and Abs via the succinimide ester (generated via the ubiquitous 1-ethyl-3-(3-dimethylaminopropyl)carbodiimide (EDC) and N-hydroxysuccinimide (NHS) crosslinking reagents) rather than proceed through the neutravidin intermediate. [117, 133] As the neutravidin bridging strategy

does not guarantee Ab orientation and adds several steps to the workflow and cost by the use of additional reagents, direct tethering between surface-confined carboxylic acid groups and Abs is an attractive approach.

Myung, *et al.* used EDC and NHS crosslinking to activate carboxylated PAMAM dendrimers (7<sup>th</sup> generation), which were immobilized on a PEGylated surface and immediately reacted them with epithelial antibodies. These dendrimers served two purposes: (i) To increase the surface's antibody load by multivalency per unit surface area; and (ii) to decrease the antibody/antigen dissociation constant (by six orders of magnitude), again by multivalent cell adhesion. However, the capture efficiency enhancements observed under flow were modest, 1.5 to 2.2 fold improvements compared to a PEGylated surface only. [134] However, a 1.1 to 1.7 fold improvement for the PEGylated surface relative to a bare surface, where the antibodies were covalently attached to an epoxy modified surface, was observed. [134]

The use of PEG monolayers is well known in bioassays as they reduce nonspecific adsorption artifacts (enhancing the purity of isolated CTCs) and protein denaturation (retaining capture antibody activity) by entropic resistance to PEG-protein interactions. [104, 131] But, PEG coatings [133, 135] as well as polymeric linkers [136] or amphiphilic triblock polymers, [117] can improve solubility of inorganic nanoparticles permitting functionalization of the nanoparticles for targeting CTCs and increasing *in vivo* circulation time. [104, 137-139]

It is also possible to directly and covalently tether CTC selection Abs (or recognition element in general) via an amide linkage to microchannel surfaces molded

into thermoplastics. Here, thermoplastic-based microfluidic devices for the analysis of CTCs must contain surface-confined carboxylic acids for EDC/NHS coupling of the selection Ab to the microchannel wall. The generation of carboxylic acids by UV/ozone treatment in three different thermoplastics has been reported (PMMA, PC and COC). [140] For this process, the polymer's optical transparency to the 254 nm activating light was critical for high density carboxylic acid generation throughout the microchannel's depth; PMMA's absorption of the modifying radiation decreased carboxylic acid generation, especially in microchannels possessing high aspect ratios. COC's superior optical transmissivity permitted higher carboxylic acid surface yields, and this was shown to directly impact CTC selection from whole blood in terms of both efficiency and purity (see Figure 1.6). [81]

Lastly, we address the use of aptamers for CTC selection and their attachment to microfluidic device channels. In one case, an RNA aptamer with a pendant amino group on its 5' end was immobilized to a PMMA surface in the same manner as an antibody, utilizing EDC and NHS coupling agents for covalent attachment. In another aptamer immobilization strategy, the researchers employed a biotinylated primer sequence bound to the surface via passively adsorbed avidin that annealed a circular DNA template containing an aptamer sequence.

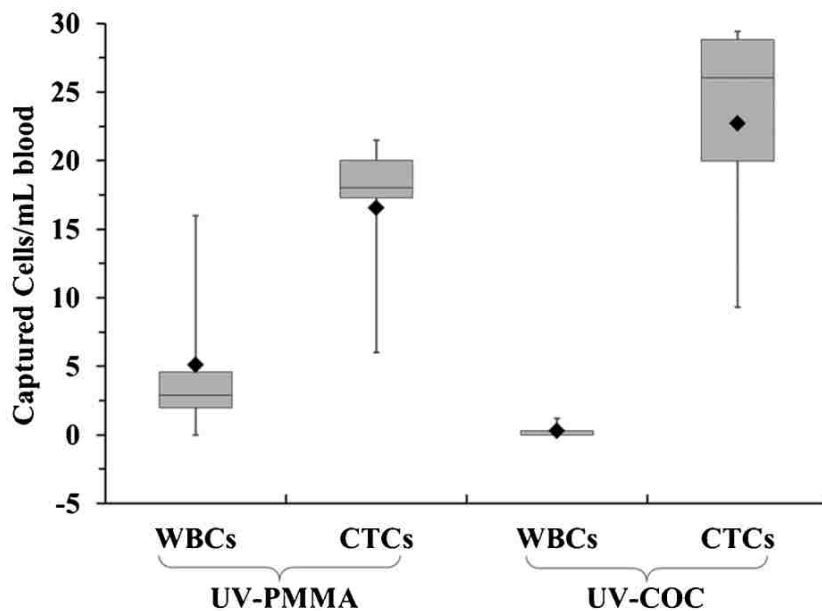


Figure 1.6 Box plots presenting count of CTCs and WBCs selected in UV-PMMA (5 PDX (Patient Derived Xenograft models)) and UV-COC (4 PDX) chip from mice blood samples. Data are normalized to 1 mL. Lower and upper edges of box show 25th and 75th percentiles, respectively. Solid line in box represents median, and solid diamond represents mean. Error bars show maximum and minimum values. (Reproduced from Jackson *et al.* [30] with permission from the Royal Society of Chemistry)

Then, they enzymatically polymerized the DNA template by rolling circle amplification creating long (on the order of 0.1 to 100  $\mu\text{m}$  in length), repetitive patterns of CTC-binding aptamers extending into solution. [74] While the avidin layer is arguably unnecessary in this design, the utilization of rolling circle amplification to construct or rather extend, a pre-immobilized aptamer was a unique strategy that can be applied to essentially any microfluidic geometry.

### 1.3.1.2 Geometrical Configurations for Biological Property CTC Selection

Various geometrical configurations have been adapted using microfluidics with positive selection of CTCs to induce particle displacement in laminar flow, which is characteristic in micro-dimensions due to low Reynolds numbers. [141] The main objective is to increase the encounter rates between CTCs and the solid phase onto which the target ligands are attached. In one microfluidic rendition, 78,000 functionalized microposts covering an area of 970 mm<sup>2</sup> whose size, spacing and arrangement were optimized to yield non-linear flow streams and low shear forces. A 50 µm vertical periodic shift was applied every 3<sup>rd</sup> micropost row to change the trajectory of the CTC to enhance the collision probability between CTCs and the posts. An equilateral micropost array arrangement was the best configuration that resulted in the highest hydrodynamic recovery (65%) for CTCs irrespective of their EpCAM expression level. This device was used in clinical studies for lung, breast, prostate, pancreatic and colon cancer. [31]

This CTC chip later adopted a staggered herringbone (Hb) mixer format (see Figure 1.7).[72] The Hb CTC chip consisted of 8 herringbone channels with a channel height of 50 µm and groove height of 45 µm. Chaotic flow was induced by the variation of the shape of the grooves as a function of the axial position of the channels. The Hb chip was found to be more efficient than its predecessor (CTC chip) in terms of throughput (from 1 mL/h to 4.8 mL/h), which resulted in a decreased processing time. Recovery also improved by 26.3% and an increase in purity levels from 9 ±0.1% to 14 ±0.1% was



also observed. [32] The Hb CTC chip has since then been used for various clinical studies. [32]

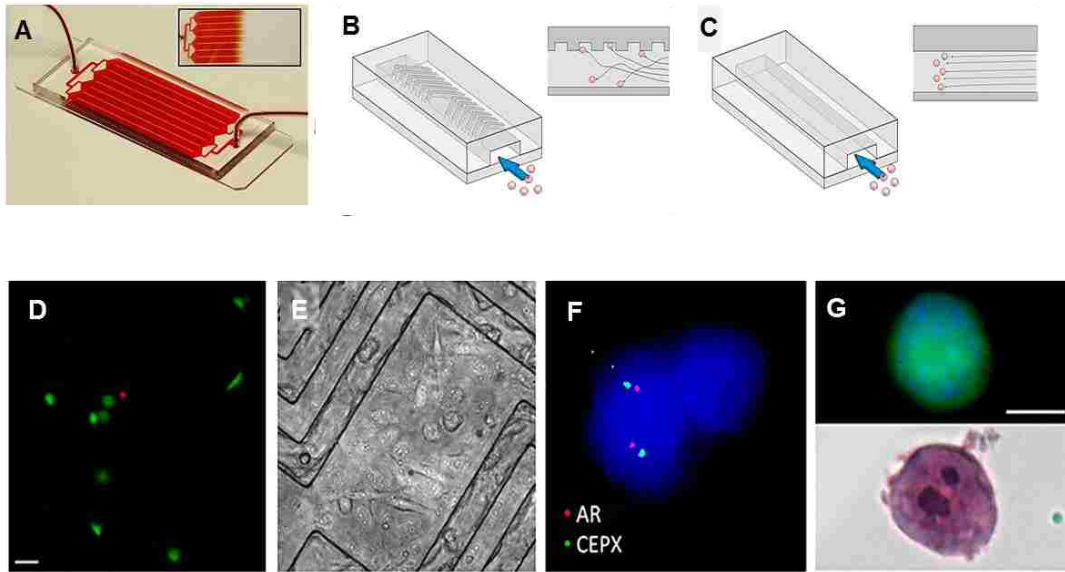


Figure 1.7 (A) The HB-Chip consists of a microfluidic array of channels with a single inlet and exit. Inset illustrates the uniform blood flow through the device. (B) Cartoon illustrating the cell-surface interactions in the HB-Chip, and (C) a traditional flat-walled microfluidic device. (D) Micrograph of spiked cancer cells captured on the HB-Chip, representative of capture cell viability (LIVE/DEAD). (Scale bar: 40  $\mu\text{m}$ ). (E) Micrograph of spiked cells captured on the herringbone chip and subsequently cultured on the device for 21 d. (F) On-chip FISH of captured LNCaP cells with nuclei stained with DAPI, CEPX (green) and AR gene locus (red). (G) Micrograph of a fluorescently labeled PC3 cell captured on the HB-Chip (top) and subsequent micrograph taken of the same cell stained with H and E. (Scale bar: 10  $\mu\text{m}$ ). (Reproduced from Stott *et al.* [32] with permission from the Proceedings of the National Academy of Sciences of the United States of America (PNAS))

Kirby and coworkers adopted a similar approach to Toner groups first CTC chip where they developed a micropost array in a device consisting of 5000 circular of hexagonal or circular posts (100 $\mu\text{m}$  tall and 80 $\mu\text{m}$  in diameter) centered in an 8 mm by 25 mm channel (see Figure 1.8). In the geometrical enhanced immunocapture device

(GEDI) the posts were arranged in way to create size dependent trajectories while creating maximum streamline distortions. The arrangement ensured the reduced capture of contaminating leukocytes by achieving a purity of 68% for LNCaP prostate cells spiked in blood and 62% for PCTCs from patient samples.

The High Throughput Microsampling Unit (HTMSU) developed by Adams and coworkers adopted sinusoidal parallel channels. In this format travelling CTCs were propelled to the outer edges of the selection channel walls using curved channels due to cross stream velocities and centrifugal forces acting on the wall. A total of 51 channels were deployed to increase the throughput and using a 2 mm/s volumetric linear velocity, selected to optimize CTC recovery, ~37 min was required to process 1 mL of whole blood. Recoveries of 97% were reported for MCF7 cells spiked into rabbit blood.

The same group modified the HTMSU to adopt a z-configuration of sinusoidal microchannels to provide a higher number of channels (320) for higher throughput processing (7.5 mL of whole blood processed in <20 min).[34] Using this design (see Figure 1.9), the group demonstrated that high purity CTC fractions was achievable for devices made from COC (98%) with recoveries >90% for MCF-7 CTC surrogates was shown. In addition, findings based on computational simulations on the fluid dynamics revealed that higher shear forces  $13.3 \text{ dyn/cm}^2$  were obtainable for blood in the sinusoidal channels than posts ( $0.4 \text{ dyn/cm}^2$ ) or herringbone structured channels, which was adequate to release loosely bound leukocytes.[30] The CTC selection device could be coupled with an impedance sensor for the label-less counting of single CTCs

following release from the capture surface and finally, the released CTCs shuttled to a staining and imaging device where the CTCs could be enumerated and phenotyped. (see Figure 1.9).

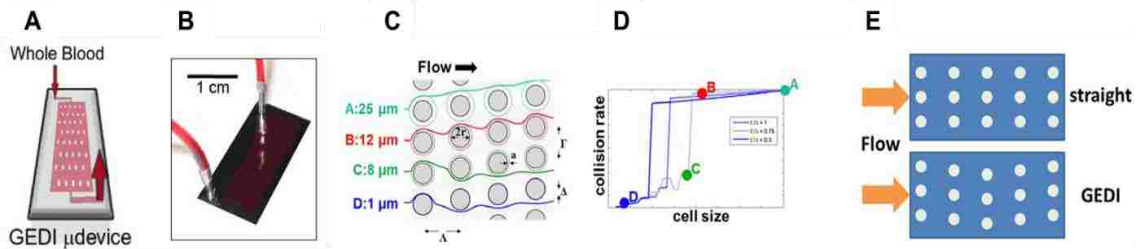


Figure 1.8 (A) GEDI microfluidic device design and (B) Image of silicon device with silicon gasket. (C) Top view of microfluidic obstacle array with array geometric parameters.  $\Delta$  = obstacle offset.  $\Lambda$  = obstacle spacing in the direction of bulk flow.  $\Gamma$  = obstacle spacing in the direction orthogonal to bulk flow.  $2r$  = obstacle diameter. Streamlines (gray) denote fluid flow. Path lines (various colors) denote trajectories of cells of different diameters. Obstacle array spacing and orientation parameters are also defined. (D) The rate of cell-wall collisions for cells traveling through the array is a strong function of the offset parameter of the array; the GEDI design methodology implies use of an offset parameter that leads to size-dependent collision rates. The results predicted for the flow through the geometry at left are shown at right by the solid line; the four specific cell sizes lead to results denoted by the four colored dots on this graph. Other geometric arrangements lead to different results, shown at right in the dotted and dashed lines. (E) Devices with the same surface area to volume ratio give vastly different results: straight arrays lead to collisions that decrease as the blood travels through the device; GEDI arrays lead to collisions that increase with travel through the device. (Reproduced from Kirby *et al.* [29] with permission from the author)

Using this system, whole blood from locally resectable and metastatic pancreatic ductal adenoma carcinoma (PDAC) patients were analyzed. Using the CellSearch technology, metastatic PDAC patients typically yield 0-1 CTC per 7.5 mL of whole blood.[11, 142] Using this device and system, the authors demonstrated selection of EpCAM positive CTCs from PDAC patients in high purity (>86%) and with excellent yields (mean = 53 CTCs per mL for metastatic PDAC patients). In addition, they

demonstrated the ability to detect CTCs in PDAC patients with locally resectable disease (mean = 11 CTCs per mL). [34]

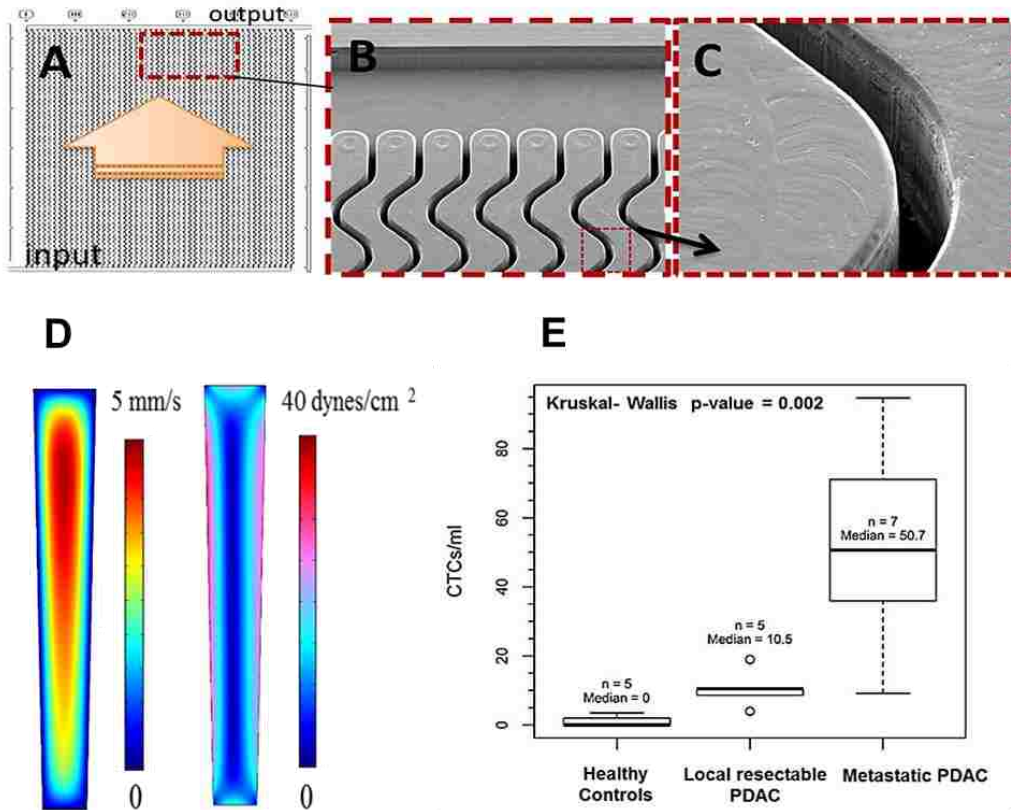


Figure 1.9 (A) Schematic operation of the HT-CTC module with 50 parallel, sinusoidal microchannels and inlet/outlet channels arranged in the z-configuration. The large arrow indicates sample flow direction through the selection channels. (B) SEM of the selection bed showing high aspect ratio sinusoidal microchannels and the output channel (top). (C) SEM of one of the high aspect ratio sinusoidal channels. (D) Fluid dynamics simulation results showing the distribution of flow velocities and shear stress in microfluidic selection channels. (E) Box plot from CTCs isolated from 7 metastatic PDAC patients, 5 healthy donors, and 5 local resectable PDAC patients. Reproduced from Kamande *et al.* [34] with permission

In all these cases, the geometry adapted for the CTC enrichment device plays a critical role in shaping the fluid dynamics within the device. The linear velocity and the shear forces experienced by the target cells of interest affect the recovery as well as the

purity. Recovery is maximized when shear rate is low in order to reduce the shear forces acting on the captured cells thus maintaining their viability as demonstrated by Nagrath and coworkers. [31] However this is at the expense of purity because low shear forces may not remove nonspecifically bound contaminating cells. A summary of the clinical performance metrics and comparisons to CellSearch™ technology, of the above mentioned devices in this section has been listed in Table 1.2.

### **1.3.1.3 Nature of the Solid Phase Surface**

Various materials and surface textures have been applied by groups to enhance recovery of CTCs based on their external morphological characteristics. One approach is to mimic the nano-scale topography of the extra-cellular matrix (ECM) onto which epithelial tumor cells are firmly held. [143, 144] The ECM proteins located on the surface of the basement membrane contribute to the nanotextured surface which aid in cell anchorage and proliferation. [145-147] Results indicate significantly improved CTC recoveries from nanotextured surfaces in comparison to smooth surfaces. This occurs through the morphological differences seen on tumor cells, which possess filopodia and microvilli containing selection antigens.

A nanotextured surface with silicon nanopillars (SiNP) coated with antibodies targeting EpCAM on CTCs has been reported. [69, 132, 148-151] The goal was to enhance local topographical interactions along with specific bioaffinity targets to increase the recovery for CTCs with filopodia and microvilli extensions. In an example using Si nanopillars, [69] the dimensions of the nanopillars were 100-200 nm in diameter and 25  $\mu\text{m}$  in height enclosed in a serpentine microchannel with dimensions of

800 mm in length by 1 mm width. Fishbone structures were later incorporated into the serpentine channel in order to induce chaotic mixing to enhance recovery. [132] Results indicated a recovery of 4-14% on a flat Si substrate and 45-65% recovery for MCF-7 cells using the nanostructured Si substrate. [69] Although an increased recovery was demonstrated by the incorporation of nanostructures, the ability to release the captured CTCs was only about 10% with a poor viability using the nanopillars format. Later, the authors utilized a thermoresponsive polymer, (poly (N-isopropyl acrylamide), PIPAAM, covalently grafted onto the SiNW substrate (P-SiNW). The P-SiNW was functionalized with anti-EpCAM for CTC capture. At 37°C, the biotinylated anti-EpCAM Abs on the P-SiNW were exposed on the nano-substrate surface for CTC contact. However, when the temperatures was reduced to 4°C, conformational changes on the polymer backbone led to the internalization of anti-EpCAM Abs within the polymer backbone resulting in release of the CTCs. Results indicated recoveries of ~70% and a release efficiency of 90% with a viability of 90%. [148]

As an alternative to vertically aligned silicon nanopillars, horizontally oriented inorganic TiO<sub>2</sub> nanofibers were demonstrated for CTC selection, which also consisted of anti-EpCAM antibodies grafted onto the nanofibers. [151] Several advantages of using this material were noted: i) The horizontal orientation was more representative of the nanostructures embedded in the ECM matrix leading to improved cell-to-substrate affinity; ii) more precise control over the packing density of the TiO<sub>2</sub> nanofibers (TiNF) using electrospinning (see Figure 1.10); and iii) flexibility in the choice of material that could be electrospun onto any given substrate, such as glass or silicon (not only limited

to TiO<sub>2</sub>). The authors demonstrated that the horizontal fibers were more sensitive and specific to EpCAM expressing cells. The CTC recovery was also found to be highly dependent on electrospinning time; greater than 60 min electrospinning time resulted in maximum recoveries. [151]

A second generation device was designed to facilitate single CTC molecular analysis by the incorporation laser microdissection (LMD) to the platform, thus eliminating the concern of contaminating leukocytes affecting the analysis. The substrate consisted of a transparent LMD slide onto which poly(lactic-co-glycolic acid), PLGA, nanofibers were electrospun. These fibers were functionalized with a melanoma-specific antibody (CD146) for the isolation of circulating melanoma cells (CMCs). The LMD microscope was used to cut out and harvest a positively identified CMC for further molecular analyses. Results indicated 87% recovery for the M229 cell line seeded into a cell culture medium at a flow rate of 0.5 ml hr<sup>-1</sup>. Molecular analysis from single CMCs isolated using the device from 2 patient samples successfully found BRAF<sup>V600E</sup> mutations using Sanger sequencing with results consistent with the patient's tumor biopsy. [149]

Nano-textured PDMS substrates for CTC isolation was also demonstrated to yield higher recoveries in comparison to glass and smooth PDMS substrates. [152] In this study, a 3D nanotextured PDMS substrate was prepared by casting PDMS over a nano-textured surface, such as NaOH-treated poly (D, L-lactide-co-glycolide), PLGA polymer. Aptamers against EGFR were immobilized onto the nano-textured PDMS substrate and human glioblastoma (hGBM) cells were used as a model for CTC

isolation. Findings from this study found an increase in probe density on the nano-textured PDMS surface compared to a planar glass or PDMS substrates without the nano-texturing. However a decrease in specificity was observed when a mixture of fibroblasts and hGBM cells were sampled. [152]

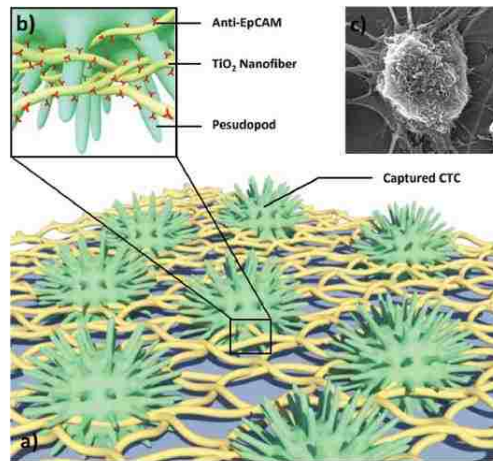


Figure 1.10 Schematic of the horizontally packed TiNFs for improved CTC capture through combining cell-capture-agent (i.e., Anti-EpCAM) and cancer cell-preferred nano-scale topography ( Reproduced from Zhang *et al.* [151] with permission)

Recently, nanoporous posts instead of solid posts were found to increase the recovery of CTCs by increasing the interception efficiency (the fraction of particles in flow intercepted by a collector) and the association strength between the particles and affinity-agent decorated surface. The use of highly porous vertically aligned carbon nanotubes (VACNT) allowed fluid streamlines to pass through the posts bringing cells into direct contact with the posts, thus resolving the no-slip boundary condition observed at the liquid-to-solid post interphase. Secondly, the highly porous surface reduced



hydrodynamic resistance observed for solid posts. As a result, higher recoveries for PC3 cells (0.8%) within the first row of nanoporous posts was observed compared to solid posts (0.2%). [153]

In a similar manner, Hughes and coworkers used halloysite nanotubes (300 nm diameter) along with a bimolecular surface of E-selectin to promote CTC rolling for EpCAM specific CTC capture in a microfluidic device. [127] The halloysite tube led to increased roughness that extended into the flow channel thereby increasing contact with CTCs. Increased purity of CTC fractions were observed due to less leukocyte spreading on the nanotube-coated surface compared to a smooth surface. Consequently, a recovery of 50% was obtained with purities of 18-80% for clinical samples of breast, prostate, lung and ovarian cancers.

#### **1.3.1.4 Negative Enrichment**

Negative enrichment of CTCs utilizes leukocyte-specific markers, such as CD45, for the depletion of these cell types from whole blood leaving an unbiased population of CTCs following erythrocyte removal. Further, the EMT hypothesis suggests that down-regulation of epithelial markers, such as EpCAM, is more apparent in circulation where CTCs take on mesenchymal characteristics; as such, not all CTCs express EpCAM. [24] Therefore, the reliance on EpCAM solely for the capture of CTCs in most technologies may exclude sub-populations of CTCs with different phenotypes lacking epithelial markers. [154-156] A common strategy used by various reports incorporates RBC lysis or density gradient centrifugation[157] followed by CD45 leukocyte depletion via magnetic separation, which is accomplished by introducing functionalized magnetic

particles into the sample. [158] [159] The enriched sample is subsequently analyzed using confocal imaging, [160] flow cytometry [51] or molecular analyses, such as the use of RT-PCR for EGFR expression. [156, 160, 161]

Few reports on microdevices have documented the use of CTC negative enrichment. Hyun and coworkers reported on a herringbone device termed the geometrically activated surface interaction device (GASI). [162] This device consisted of a PDMS-glass hybrid substrate with channels coated with CD45 antibodies for leukocyte capture with the CTCs collected in the effluent. The device was found to generate a capture efficiency <88% for leukocytes at a cell population of  $10^6$ - $10^7$  cells/ml. GASI is an enhanced version of the original device with altered channel dimensions such as increased apex dimensions, which resulted in 98.94% leukocyte capture efficiency. Demonstrations on using GASI for CTC isolation from clinical samples was reported for breast, lung and gastric cancers.

Chen *et al.* reported a disk-based microfluidic platform capable of isolating CTCs via negative immunomagnetic separation. [163] Here, non-magnetically labeled MCF7 cells were used as model CTCs while magnetically labeled Jurkat cells or MNCs (mononucleated cells) from blood were used as non-target cells. The device included a multistage magnet configuration and double trapping region to enhance depletion efficiency of non-target cells (~99%) while enhancing the collection of MCF7s (recovery ~60%).

One of the drawbacks to negative selection is the comparatively low purity of isolated CTCs (0.94%-3.64%). [162] Huang *et al.* recently reported a study that

improved the purity of CTCs by integrating optical-induced dielectrophoretic (ODEP) force, which is based on cell manipulation for a laminar flow microfluidic system. CTCs were further separated from leukocytes into two flow streams based on cell size and electrical properties after conventional negative enrichment. The device consisted of a multilayer layered structure consisting of PDMS, indium tin oxide coated glass, adhesive tape with microfabricated channels and a lower ITO glass substrate coated with photoconductive material for ODEP manipulations. Purities of 74-82% and 64-66% were obtained for PC3 and OECM-1 cells, respectively. [150]

Advantages of negative enrichment are that they do not rely on the specific phenotype of tumor cells for CTC enrichment. Thus, other rare cells can be enriched as well such as, circulating endothelial cells (CECs), cancer stem cells (CSCs), circulating progenitor cells (CPCs), and nucleated red blood cells (nRBC). Moreover, CTCs remain intact without any alteration and are available for downstream processing. However, the challenges are the relatively poor purities attained as well as the low CTC yields. Pre-processing steps such as erythrocyte lysis and centrifugation may also contribute to low CTC yields.

Materials that have been utilized in the above mentioned devices are similar to devices used for positive enrichment, such as PDMS, whose material properties are well suited for bio-affinity selection of CD45 expressing cells. A magnetic disk was utilized for the separation of magnetically-labeled leukocytes from unlabeled CTCs and finally, the ODEP integrated to a PDMS microfluidic platform consisted of ITO glass with photoconductive material selected to facilitate ODEP cell manipulations.

### 1.3.1.5 Miscellaneous Microfluidic Devices for Positive or Negative Selection of CTCs

Issadore and coworkers developed a  $\mu$ Hall (micro-Hall) device for the detection of immunomagnetically functionalized CTCs from ovarian cancer patients. The  $\mu$ Hall detector consisted of an array of 8 micro hall sensors that were able to sense the characteristic magnetic moments of cells in flow that had been immunolabeled with magnetic nanoparticles (MNPs). The signals generated depended upon the quantity of MNPs bound to the cells, which in turn were directly proportional to their targeted tumor marker expression level such as EpCAM, Her2/Neu, EGFR and Mucin1 (MUC1). Thus, CTCs with a high expression of these markers could be distinguished from leukocytes with low expressing tumor markers. The array was enclosed in PDMS with a chevron structured channel to facilitate hydrodynamic focusing of the cells over the hall sensors. A comparative study of 20 ovarian patient samples between the  $\mu$ Hall detector and CellSearch<sup>TM</sup> indicated a high diagnostic accuracy rate of 96% for the  $\mu$ Hall detector compared to 15% for CellSearch. The  $\mu$ Hall device was fabricated from relatively low cost hall sensors adapted from the semiconductor industry and herringbone channels on the PDMS material. [164]

CTC-iChip (inertial focusing Chip) is an integrated microfluidic platform that was recently developed by Ozkumur and coworkers that could be configured for either positive (<sup>pos</sup>CTC-iChip) or negative enrichment (<sup>neg</sup>CTC-iChip). [165] It was designed to integrate 3 sorting techniques in a single device. Briefly, the first section was the deterministic lateral displacement of nucleated cells from red blood cells (RBCs). The

second section consisted of the alignment of nucleated cells within a single microfluidic channel using inertial focusing and finally, the third section was based on the displacement of magnetically labeled cells in a collection channel. The device could process large volumes of blood at a reasonable rate (8 mL/h). <sup>pos</sup>CTC-iChip recovery rates for high EpCAM expressing SKBR3 cells was 98% while low EpCAM expressing MDA-MB231 was 78% with a sample purity of 0.2 to 43%. For <sup>neg</sup>CTC-iChip, the average depletion rate of white blood cells (WBCs) was 32,000 WBCs/mL with a recovery of 97% for mesenchymal expressing MCF10A-LBX1 cells. Also the <sup>pos</sup>CTC-iChip was found to be more sensitive for CTC capture than CellSearch™ for patients that had low disease burden.

### **1.3.2 Microfluidics for CTC Enrichment Based on Physical Properties**

Physical-based assays are able to discriminate CTCs from hematopoietic cells on the basis of size, density, electric charges, or deformability. CTC diameters range from 10 µm to 30 µm while hematopoietic cells are typically below 8 µm in diameter. Reports on size-based separation devices have employed a number of strategies, such as microfabricated filter pores, traps and slots for the entrapment of CTCs from whole blood. [49, 50, 52, 68, 100, 166-168] A number of reviews have adequately discussed physical CTC enrichment devices. [38, 43, 169, 170] Table 1.2 lists some of these devices and shows their performance metrics for sample processing as well as compares their clinical metrics with the current FDA approve CellSearch™ technology.

These devices achieve higher throughputs than biological enrichment microdevices and as a result can process large volumes of blood at shorter times. However, this is at

the expense of purity values which are considerably much lower than biological enrichment microdevices (see Table 1.2).

### **2.1.3.1 Dielectrophoretic Microdevices for CTC Enrichment**

There have been a number of reports on the enrichment of CTCs using dielectrophoretic separation. Dielectrophoresis is based on the inherent differences in the dielectric properties of CTCs from normal hematopoietic cells, which is dictated by their physical and electrical properties such as morphology, bilipid membrane characteristics, internal structure, cytosolic constitution, and nucleus size. [171, 172] Dielectrophoretic separations is based upon two dissimilar neutral particle populations subjected to non-uniform electric fields, which induce differences in translational motion and/or reorientation of the particles due to their dielectric properties. [173, 174]

Within certain frequency ranges, cells tend to move in the direction of increasing electric field (towards the electrode); this is termed positive DEP while the converse is negative DEP. The DEP crossover frequency is the frequency at which the DEP force makes the transition from negative to a positive force and is dependent of the cell and medium conductivity and permittivity. [175][176][172] CTCs are attracted by positive DEP forces while blood cells remain levitated by negative DEP forces resulting in the separation of these two cell populations in a hydrodynamic flow. It has been documented that the mean crossover frequencies for breast, lung and ovarian cancer cells are low, 30-40 kHz compared to 90-140 kHz for the majority of peripheral blood cells. This difference forms the basis of CTC separation from the bulk of the blood cell components when a frequency range of 45-84 kHz is applied where CTC experience

positive DEP force while peripheral blood cells remain in the bulk fluid resulting in separation. The DEP force is given by;

$$F = 2\pi r^3 \varepsilon_m R_e[K] \nabla E^2 \quad (2)$$

where  $\varepsilon_m$  is the absolute permittivity of the suspending medium,  $\nabla E$  is the local electric field (rms) intensity,  $R_e [K]$  is the real part of the dipolar Clausius-Mossotti factor and determines the sign of the force (positive or negative) being defined as:

$$K = \frac{\varepsilon_p^* - \varepsilon_m^*}{\varepsilon_p^* + 2\varepsilon_m^*}, \varepsilon^* = \varepsilon - j \frac{\sigma}{\omega} \quad (3)$$

where  $\varepsilon_p^*$  and  $\varepsilon_m^*$  are the complex permittivity of the particle and medium, respectively.

The complex permittivity for a dielectric material can be described by its permittivity  $\varepsilon$  and conductivity  $\sigma$  where  $\omega$  is the angular frequency of the applied electric field  $E$ . [177]

DEP force is strongly dependent on the volume of the particle and the gradient of the electric field. [178] Devices for CTC separation have been documented using different formats, such as electrode affinity columns, [172, 179-182] DEP-field flow fractionation devices, [176, 183-185] 3D asymmetric devices with continuous variation in electric responses [186, 187] and DEP devices with planar electrode configurations. [188, 189]

We shall briefly highlight a few examples. Gupta and coworkers recently reported a device that is now commercially available, called the ApoStream™ device, which is based on DEP-FFF (field flow fractionation). DEP-FFF uses the effect of viscous flow of liquid near a surface and the application of a force field that will place different particles at different heights from the surface. Particles will travel at different speeds according to their distance above the surface and thus, when they are introduced to the force field at

the same time and point, they will exit the device at different times according to their heights above the surface and their reaction to the imposed field. [190] DEP-FFF uses a continuous flow mode rather than a batch processing configuration resulting in high throughput processing. The device consisted of a flow chamber with the floor containing a polyimide film sheet with electroplated copper and gold electrodes while acrylic sheets formed the ceiling of the chamber and a gasket formed the side walls. Here, high EpCAM expressing ovarian cancer model cells SKOV3 as well as low EpCAM expressing model breast cancer cells, MDAMB-231 spiked into PBMCs were continuously introduced at a low flow rate. Upon application of an AC electric field to the flow chamber, the CTCs were separated from the PBMC fraction. CTC recoveries as high as 75% and reduction efficiencies of the PBMCs of ~99% were obtained. Viability of CTCs obtained was as high as 98%. [191]

DEP devices have been used in combination with other techniques in order to attain higher purities of CTC fractions. Moon and coworkers combined multi-orifice flow fractionation along with DEP for the isolation of MCF7 model breast cancer cells from RBCs and WBCs. MOFF involves microparticles that are moved laterally by hydrodynamic inertial forces driven by a multiorifice structure.



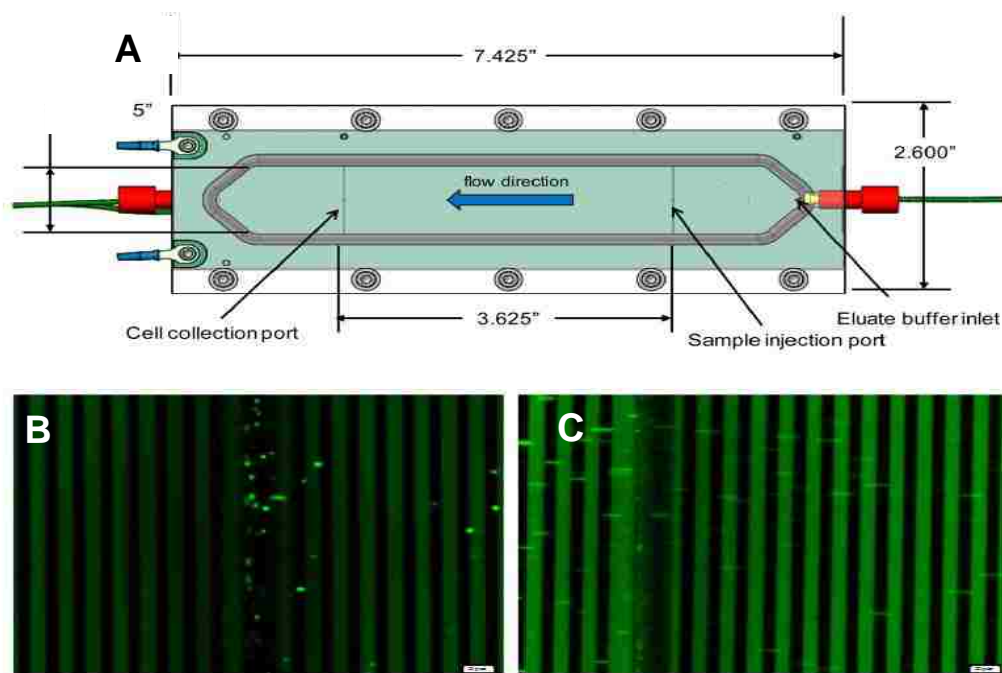


Figure 1.11 APO Cell device (A) Schematic of the top view of the flow chamber showing sample injection and sample collection port locations. (B) Still image from video demonstrating the flow and collection of fluorescently labeled SKOV3 cancer cells through the collection port in the ApoStream flow chamber. Cancer cells are collected into the collection port when the DEP field is activated. (C) Still image from video demonstrating the flow of fluorescently labeled PBMCs through ApoStream flow chamber. The first half of the video (10 s) demonstrates that most PBMCs fall into the collection port when the DEP field is not active. (Reproduced from Gupta *et al.* [191] with permission)

Extent of lateral movement varies according to particle size. Although this method has a throughput of 300  $\mu\text{L}/\text{min}$ , the reduction efficiencies of both RBCs and WBCs were 88% and 61%, respectively. Addition of a DEP module with electrodes consisting of gold and chromium sputtered onto glass and sealed with PDMS resulted in a 162-fold increase in the separation efficiency of MCF7 as well as 99% and 92% reduction in

RBC and WBCs fractions, respectively. In this report both high processing speeds and high purities were attained through the integration of these two techniques. [53]

Materials used for DEP CTC enrichment devices are mainly selected to be compatible with biological-based separations. Joule heating is one of the major factors affecting DEP separations. In order to lower thermal heating in DEP devices, the application of 3D silicon electrodes instead of planar electrodes has been shown to maintain suitable temperatures for cell manipulations even as the voltage increases. [192] For optical DEP cell manipulations, Indium Titanium Oxide (ITO) over glass has been used as an alternative to gold or platinum electrodes due its transparency. [150]

Recently a nanodetector referred to as the Gilupi device was designed for the *in vivo* detection and collection of CTCs. It has been made commercially available by GILUPI GmbH medical technology company. The device consists of an anti-EpCAM biofunctionalized structured medical seldinger guidewire wire (FSMW) that can be inserted into the vein of a patient's arm by the use of a 20 gauge needle (see Figure 1.12). The needle is a stainless steel wire coated with a gold layer and an anti-EpCAM functionalized hydrogel. It is inserted into the arm for a total of 30 min and over that time period, 1500 mL of blood is sampled allowing the potential for the capture of large numbers of CTCs. This device has been used in patients with breast, lung and prostate cancer and has successfully identified CTCs in 80% of these patients. Material considerations were mainly devoted to minimizing *in vivo* cytotoxicity. FSMW was compared to copper wire and Teflon as alternatives by looking at the viability of normal

human dermal fibroblasts (NHDF) after contact. It was found that FSMW gave the highest cell viability while copper wire gave the lowest. [193]

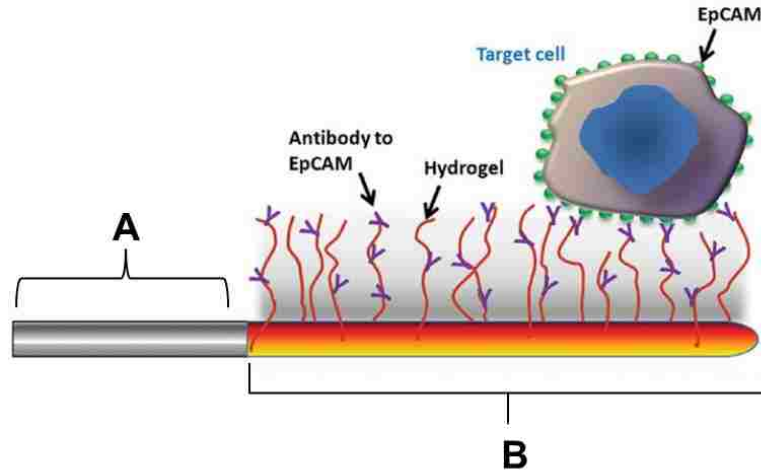


Figure 1.12 Outline of the Gilupi nanodetector (A) Section of the guidewire which remains inside the puncture cannula (B) 20 mm long gold coated tip of the stainless steel guidewire which is in direct contact with the blood circulation and biofunctionalized with EpCAM antibodies to target CTC. (Reproduced from Saucedo-Zeni *et al.* [193] with permission.)

The application of functional assays can be used as a means for the detection of viable CTCs. Epispot (epithelial immunospot) assay is based on the secretion of specific marker proteins. Nitrocellulose membranes are coated with an antibody against a specific protein marker. Cells are seeded and cultured for 48 h during which time secretion of proteins are directly captured on the plate. Cells are then washed off and fluorescently labeled secondary antibodies are then added. Immunospots are then detected via video camera imaging, which signifies the presence of viable cells. CK19 and MUC1 have been used for breast cancer CTC detection while prostate specific antigen (PSA) was used for prostatic CTC detection for clinical trials. Findings indicated

90% of breast cancer patients secreted MUC1 marker, 54% secreted CK19 while 83.3% of prostate cancer patients secreted PSA.[45]

Similarly, the collagen adhesion matrix (CAM) technology has the ability to enrich CTCs based on their avidity to invade the CAM. [196] This assay targets more aggressive and invasive phenotypes of CTCs, which are capable of ingesting CAM. Mononucleated cell fractions from patient blood were placed in fluorescently labeled CAM coated 16-well chamber slides distributed by Vitatex Inc. and cultured with cancer cell culture (CCC) media. Studies on breast cancer patients revealed that enriched CTCs using this assay had distinct populations and were capable of propagation. Results indicated a CTC recovery rate of 54%, assay purity range of 0.5 - 35% and a 100 assay positivity rate. [197]

AdnaTest is a molecular-based assay that selects CTCs via immunomagnetic enrichment after which gene expression profiling is performed using a multiplex RT-PCR to evaluate tumor associated transcripts such as HER2, MUC-1n and GA773-2 for breast cancer specifically. This method boasts higher sensitivity compared to CellSearch™ with about 2 CTCs per 1 ml of blood.<sup>[26]</sup> CTCs were detected in 69% of breast cancer patients and their expression profiles shown to be heterogeneous. [198]

## **1.4 Beyond Enumeration of CTCs**

### **1.4.1 Phenotypic Characterization of CTCs**

CellSearch™, which is the only FDA approved technology for the isolation of CTCs from epithelial cancers such as breast, colorectal and prostate uses 4 markers to

phenotype CTCs: 1) EpCAM, which is usually used as the selection target; 2) cytoplasmic cytokeratins (8, 18, 19); 3) nuclear component confirmed by DAPI or Hoechst staining; and 4) CD45 as a negative indicator (indicative of leukocyte). Events are scored as CTCs if they stain positive with DAPI and cytokeratins, but negative for CD45. In addition, CTCs tend to have a larger nucleus to cytoplasmic ratio than leukocytes. Optical and fluorescence imaging is usually used to identify the phenotype of CTCs. [199] As a result CTCs enriched from blood using microfluidic devices typically follow the same labeling protocol for establishing CTC phenotypes. [30-32, 34, 57]

However, studies on the EMT hypothesis suggests that CTCs are heterogeneous with mesenchymal as well as epithelial characteristics. [200] [201] Moreover, recent reports on CTC enrichment using the Herringbone device among others, identified cells that stained positive for both epithelial (CK 8, 18, 19) and CD45 markers. [32] [34] These cells could also be considered as artifacts in the device or nonviable cells that may nonspecifically absorb the staining markers.

Studies also indicate a down regulation of EpCAM expression for metastatic cases thus technologies that use EpCAM as a selection target may miss CTCs with absent or low expressing epithelial antigens. Recent CTC enrichment devices are using different strategies such as negative enrichment [71, 163, 202] or the use of both epithelial and mesenchymal antibodies to select both CTC types. [33] As a result, increased CTC recoveries have been observed.[33] However, the use of multiple selection markers decreases the specificity of cells captured and thus the sample purity is in turn adversely affected.

The process of CTC phenotype identification also requires the use of fixatives and permeabilization agents that can render the cells unusable for downstream analysis, such as propagation or genomic profiling. Due to the lack of consensus in CTC phenotyping, additional identification criteria such as CTC molecular analysis for gene expression or mutation analysis should be used as well.

#### **1.4.2 Genotype Characterization of CTCs selected by Microfluidics**

Cancers typically result from the disruption of cell signaling pathways that lead to the alteration of genes. This in turn leads to the formation of cells with uncontrolled growth patterns compared to normal cells. [41, 203, 204] Gene expression profiling is a genomic technique used to investigate genes encoded in the genome of cells. These genes are transcribed into mRNA, which dictates protein synthesis in a cell. Gene expression is a major determinant of the behavior of both normal and malignant cells. Studies have shown that gene expression profiling can be used to predict clinical outcomes of breast, prostate and colorectal cancer patients. [205-210] It has also been used to predict the therapeutic response for drugs against cancer, such as docetaxel in breast cancer. [211] CTCs are also good candidates for tumor biology studies. Their molecular characterization may give insight to aberrant pathways, such as TGF- $\beta$  signaling, Wnt signaling, and EMT markers associated with tumor development and progression. In addition they may be used to investigate drug targeting markers and cancer stem cell markers. Various techniques can be used for gene expression profiling such as reverse transcriptase polymerase chain reaction (RT-PCR), cDNA microarrays and in-situ hybridization.

Due to the higher purity many times obtained through the use CTC microfluidic devices compared to CellSearch™, molecular characterization studies are feasible. The capacity to isolate concentrated, viable CTCs makes the microfluidic devices for CTC enrichment ideal tools for molecular access to rare CTC subpopulations such as metastatic precursor cells or cancer stem cells. To highlight a few examples, the PSA gene marker KLK3 was found expressed in CTCs isolated from metastatic prostate cancer patients as well as the TTF-1 (thyroid transcription factor-1) from pulmonary adenocarcinoma patients using a posted CTC microfluidic chip. [31] Protein expression was first determined by immunostaining and then cells were lysed on chip to extract genomic material. RT-PCR was used to interrogate the KLK3 and the PCR product was detected using slab gel electrophoresis. This was achievable due to the purity level of ~ 50% obtained from the CTC microchip assay. [31]

Using a Herringbone microfluidic chip, various molecular tests on CTCs have been carried. For example, FISH analysis on spiked cells for prostate cancer as well as CTCs isolated from prostate patient samples were analyzed; the androgen receptor gene (AR) as well as TMPRSSR-Exon1 and –ERG in Exon 5 fusion transcripts were evaluated. [32]

More recently, Min and coworkers developed a quantifiable dual colorimetric RNA-in situ hybridization assay to analyze epithelial transcripts Keratins (KRT 5, 7, 8, 18 and 19) and EpCAM, and mesenchymal transcripts, FNI fibronectin, CDH2 (cadherin 2) and SERPINE1 (Serpin peptidase inhibitor) in CTCs isolated from metastatic breast cancer patients. Important findings based on the EMT hypothesis were found using

RNA-ISH on CTCs; i) CTCs expressed more EMT markers than tumor cells within the tissue of the primary tumor; and ii) a prominent association of the presence of mesenchymal markers were found in CTC clusters rather than in single migratory cells suggesting mesenchymal transformation of epithelial cells mediated by TGF- $\beta$  release from platelets. [33]

In another study, isolated CTCs from genetically modified mouse models as well as pancreatic cancer patient samples were analyzed for the WNT gene. [57] This gene is associated with an increased metastatic propensity *in vivo* through the suppression of anoikis and also enhances anchorage independent sphere formation in tumor cells. The Wnt gene is also a potential drug target for metastasis, because the suppression of TAK1 kinase suppresses the WNT effect. A RNA single-molecule sequence analysis assay was developed for digitized gene expression profiling (DGE) as a result of the minute amount of CTCs captured and low purity levels (0.1-6%) generated by the selection device.

#### **1.4.3 Drug Targeting and Response Monitoring from Microfluidically Selected CTCs**

In many cases, obtaining tumor tissue may involve invasive surgery and/or fine needle aspirations to secure material for various drug targeted studies. This has further led to the significance of CTCs as an important biomarker due to the ease of accessibility. [44, 46] [37, 38] Patient treatment response monitoring could be simplified if CTC changes were used as a response marker during the course of therapy. Specific genotypes expressed in tumor tissues are associated with more aggressive forms of



disease and worse prognosis, such as HER2 gene expression in breast cancer patients. [212-214] Drug targeting studies as well as response to treatment have been employed in clinical studies involving CTC enrichment microfluidics.

The posted CTC chips were the first microfluidic devices used for monitoring drug efficacy for patients by observing changes in CTC numbers and correlating them to clinical and radiographical changes. Gefitinib, an EGFR inhibitor was administered to 9 patients with non-small cell lung cancer were serially monitored over the course of their therapy. A significant correlation (Pearson's correlation = 0.68) was observed between the change in quantity of CTCs captured and the response to treatment measured by CT scans. [215]

The GEDI device was also used to monitor CTC numbers during drug studies specifically for the assessment of microtubulin bundling upon application of Paclitaxel.[216] The GEDI devices with CTCs captured from prostate patient samples were placed in culture dishes and treated with Paclitaxel for 24 h. In all samples, microtubule bundling was clearly evident by the distorted shape orientation of microtubules as observed with increased fluorescence intensity indicating the effectiveness of the drug. [29]

In another the report, a lectin aided filter-based CTC microfluidic device facilitated *in vitro* studies of Cytarabine, a leukemia drug that inhibits DNA and RNA polymerases on a K562 model leukemia cell line. Viability of filtered K562 cells greatly decreased with increase concentration of Cytarabine. [52]

#### 1.4.4 Culture of Viable CTCs Isolated from CTC Enrichment Microdevices

CTCs carry pertinent oncogenic information because they are shed from primary and metastatic tumors. It therefore follows that they could be used as surrogates for tumor tissue for tumor biology studies. Propagation of CTCs is one of the main interests for tumor biologists and a number of studies have demonstrated the ability to culture CTCs directly from patient blood. One such study utilized the CAM assay, which separates invasive CTC sub-populations by their ability to ingest collagenous matrices. CTCs enriched are cultured with cancer cell culture (CCC) media consisting of 1:1 mixture of Dulbecco's modified Eagles medium and RPMI 1640 medium supplemented with serum and glutamine and streptomycin for 12 h (see Figure 1.13). CTCs cultured using this method have been subjected to both cellular and molecular analysis such as gene expression profiling which revealed that subpopulations retained both epithelial and EMT stem cell ( CD44 and TWIST1) genes. [218, 219]

Bo and coworkers used biocompatible parylene slot filter device to capture PC3 cells spiked into whole blood. Selected PC3 cells were cultured on or off the device. For off device culture, the PC3 cells were selectively removed from the slot filter device using a glass micropipette with a tip diameter of 20  $\mu\text{m}$  suctioned by a P-87 micropipette and placed into culture media for 3 to 6 d. In both cases more than 90% of the PC3 cells were found to be viable.[166] For liquid-based non-adherent CTCs, Raji cells, which are immortalized B chronic lymphocytes, were captured on magnetic bead columns (Ephesia device). The cells were cultured *in vitro* with CO<sub>2</sub> independent growth media

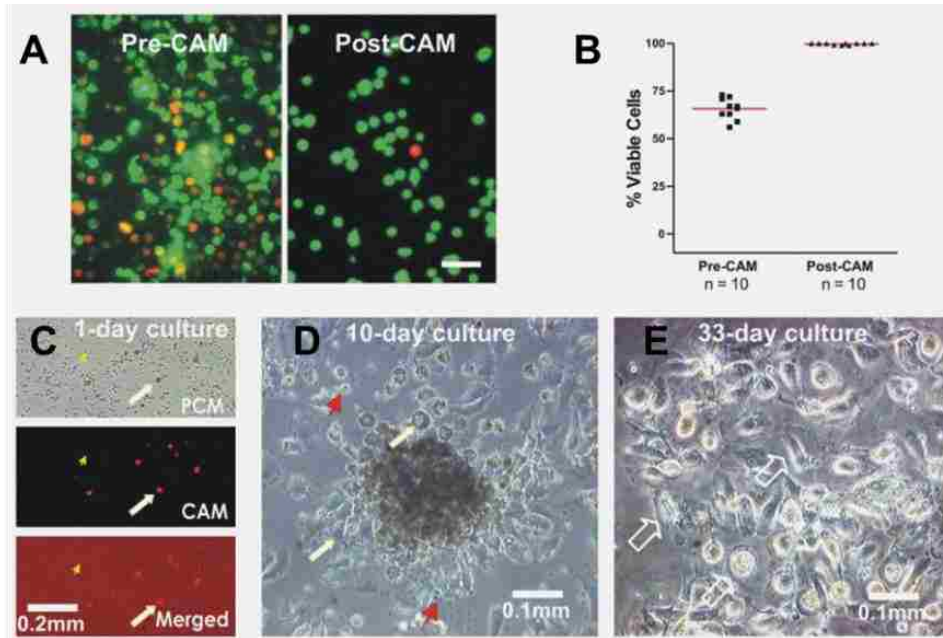


Figure 1.13 Viability and proliferation of circulating cells isolated by CAM from blood of breast cancer patients. (A) A mixture of live green fluorescent cells and dead red fluorescent cells were seen in the cell fraction of pre-CAM enrichment. Bar = 40  $\mu$ m. (B) Viability of circulating cells prior to and post to CAM enrichment. Percentages of live cells in pre- and post-CAM fractions were measured as percentage of green cells in both green and red cells. (c, d) CAM-enriched cells were cultured on the CAM scaffold for 1–33 days. Live cells were photographed under phase contrast microscopy (PCM) and fluorescence microscopy (CAM, to reveal CAM uptake/labeling of tumor cells). Tumor cells grew as time increased. On day 1 (C), tumor cells were seen to associate with CAM uptakes and as round cells (large white arrows) larger than hematologic cells (small yellow arrowheads). On day 10 (D), tumor cells were seen as round cells (white arrows) larger than hematologic cells (red arrows). By day 33 (E), tumor cells grew in clusters with large epithelioid cells (open arrows) but hematologic cells decreased their number and not seen in the field. Reproduced from Lu *et al.* [217] with permission

infused through the device while maintaining temperature between 36°C and 37°C via a microthermocouple embedded into the device with mitosis observed after 12 h of culture. [122]

Unfortunately, very few reports involving microfluidic devices have shown the ability to culture actual CTCs isolated from clinical samples. There are controversies

with regards to the use of cell lines as representative of tumor cells because they are already immortalized and adapted to growth in culture and as a result, are expandable without limitation. Some of the challenges involved with the culture of primary cells compared to established cell lines are: 1) Primary cells have a limited life span in culture and are not accustomed to culture media created for established cell lines; 2) primary cells are slow in proliferation; and 3) CTCs isolated from patient blood samples constitute heterogeneous populations and may contain contaminating cells that may not adapt well in existing growth media used for cell lines.

Kirby and coworkers were able to demonstrate the culture of CTCs isolated from patient blood samples using the GEDI device for the purposes of drug target engagement. This was achievable due to their reported purity of 68% and high viability of the CTCs captured. Briefly, the GEDI microfluidic device containing CTCs enriched from prostate cancer clinical samples was placed in a culture dish with RPMI-1640 media containing 2% serum and supplemented with either 0.1% DMSO control or paclitaxel at concentrations of 100 nM or 1 mM and incubated at 37°C for 24 h. Although the authors were able to demonstrate culture of CTCs from clinical samples for purposes of drug target engagement, CTCs grown in culture were fixed after a short time frame of 24 h; these conditions may not be a suitable for continuous long term propagation of CTCs derived from patient samples. [29]

Table 1.2 Clinical performance metrics of CTC enrichment devices for various cancers

Cancer Type	Device	Sample pre-processing required	Volumetric velocity (mL/h)	Processing Time for 7.5ml (h)	No. of CTCs/7.5 ml CTCs /7.5 ml by Veridex	Assay Positivity (%)	Purity (%)	Refs
Localized Prostrate	CTC Chip	no	1-2	3.8-7.5	705 (n = 7)	NR	53	[31]
	SiNP	yes <sup>†</sup>	1	10.6	12 (n = 2)	NR	NR	[51]
Advanced Prostrate	CTC Chip	no	1-2	3.8-7.5	645 (n=19)	100	49	[31]
	HB Chip	no	4.8	1.6	2895 (n=15)	93	14	[220]
	SiNP	yes <sup>†</sup>	1	10.6	51 (n=24), <b>5</b>	81	NR	[51]
	GEDI	no	1	7.5	405( n=30), <b>2</b>	100	68	[29]
	PFD	no	108	0.07	96( n=28), <b>18</b>	100	NR	[221]
	μSieve	yes <sup>‡</sup>	<120	0.06-0.13	37.5 (U),22.5 (D) ( n=1)	100	<0.01	[49]
Breast	CTC Chip	no	1-2	3.8-7.5	593 (n=10)	100	60	[31]
	PFD	no	108	0.07	25 (n=11), <b>12</b>	100	NR	[221]
	p-MOFF	yes <sup>†</sup>	36	0.2	1 - 21 (n=24)	79	NR	[53]
	μSieve	yes <sup>‡</sup>	<120	0.06-0.13	218 (U),60 (D) (n=3)	100	<0.01	[49]
Pancreatic	CTC Chip	no	1-2	3.8-7.5	1470 (n=15)	100	53	[31]
	HB Chip	no	4.8	1.6	135 (n= 15)	73	0.1-6	[220]
	HT-CTC	no	1.65	4.5	390 (n=7)	100	86	[34]
Colorectal	CTC Chip	no	1-2	3.8-7.5	908 (n=10)	100	67	[31]
	PFD	no	108	0.07	10 (n=12), <b>0.3</b>	81	NR	[221]
	μSieve	yes <sup>‡</sup>	<120	0.06-0.13	60 (U),128 (D) (n=3)	100	<0.01	[49]
Lung	CTC Chip	no	1-2	3.8-7.5	1163 (n=55)	100	52	[31]
	VLBD	no	2	3.8	187 (n=5)	100	83	[168]
Bladder	PFD	no	108	0.07	10 (n=6), <b>0.3±0.5</b>	50	NR	[221]
Ovarian	μ-Hall	no	0.1-1	7.5-75	57 (n=20), <b>1</b>	100	100	[64]
Cervical	μSieve	yes <sup>‡</sup>	<120	0.06-0.13	22.5 (U), 45(D) (n=1)	100	<0.01	[49]

NR (Not Reported)

† Blood sample was subjected to RBC lysis and centrifugation

‡ Blood sample diluted with PBS, U (Undiluted blood sample) and D (Diluted blood sample)

## 1.5 References

1. Steeg, P.S., *Tumor metastasis: mechanistic insights and clinical challenges*. Nature Medicine, 2006. **12**(8): p. 895-904.
2. Butler, T.P. and P.M. Gullino, *Quantitation of Cell Shedding into Efferent Blood of Mammary Adenocarcinoma*. Cancer Research, 1975. **35**(3): p. 512-516.
3. Liotta, L.A., Kleiner, J., and G.M. Saidel, *QUANTITATIVE RELATIONSHIPS OF INTRAVASCULAR TUMOR-CELLS, TUMOR VESSELS, AND PULMONARY METASTASES FOLLOWING TUMOR IMPLANTATION*. Cancer Research, 1974. **34**(5): p. 997-1004.
4. Glinsky, G.V., *Apoptosis in metastatic cancer cells*. Critical Reviews in Oncology/Hematology, 1997. **25**(3): p. 175-186.
5. Larson, C.J., et al., *Apoptosis of circulating tumor cells in prostate cancer patients*. Cytometry Part A, 2004. **62A**(1): p. 46-53.
6. Christiansen, J.J. and A.K. Rajasekaran, *Reassessing Epithelial to Mesenchymal Transition as a Prerequisite for Carcinoma Invasion and Metastasis*. Cancer Research, 2006. **66**(17): p. 8319-8326.
7. Tsuji, T., et al., *Epithelial-Mesenchymal Transition Induced by Growth Suppressor p12(CDK2-AP1) Promotes Tumor Cell Local Invasion but Suppresses Distant Colony Growth*. Cancer Research, 2008. **68**(24): p. 10377-10386.
8. Al-Mehdi, A.B., et al., *Intravascular origin of metastasis from the proliferation of endothelium-attached tumor cells: a new model for metastasis*. Nature Medicine, 2000. **6**(1): p. 100-102.
9. Läubli, H., et al., *L-Selectin Facilitation of Metastasis Involves Temporal Induction of Fut7-Dependent Ligands at Sites of Tumor Cell Arrest*. Cancer Research, 2006. **66**(3): p. 1536-1542.
10. Cristofanilli, M. and S. Braun, *Circulating Tumor Cells Revisited*. Jama-Journal of the American Medical Association, 2010. **303**(11): p. 1092-1093.

11. Cristofanilli, M., G.T. Budd, and M.J. Ellis, *Circulating tumor cells, disease progression, and survival in metastatic breast cancer*. New England Journal of Medicine, 2004. **351**: p. 781-791.
12. Cristofanilli, M., J. Reuben, and J. Uhr, *Circulating tumor cells in breast cancer: Fiction or reality?* Journal of Clinical Oncology, 2008. **26**(21): p. 3656-3657.
13. Gradilone, A., et al., *Circulating tumor cells (CTCs) in metastatic breast cancer (MBC): prognosis, drug resistance and phenotypic characterization*. Annals of Oncology, 2011. **22**(1): p. 86-92.
14. Ma, P.C., et al., *Circulating tumor cells and serum tumor biomarkers in small cell lung cancer*. Anticancer Res., 2003. **23**(Copyright (C) 2010 American Chemical Society (ACS). All Rights Reserved.): p. 49-62.
15. Punnoose, E.A., et al., *Molecular Biomarker Analyses Using Circulating Tumor Cells*. Plos One, 2010. **5**(9).
16. Elshimali, Y.I. and W.W. Grody, *The clinical significance of circulating tumor cells in the peripheral blood*. Diagnostic Molecular Pathology, 2006. **15**(4): p. 187-194.
17. Nakagawa, T., et al., *Detection of Circulating Tumor Cells in Early-Stage Breast Cancer Metastasis to Axillary Lymph Nodes*. Clinical Cancer Research, 2007. **13**(14): p. 4105-4110.
18. Stathopoulou, A., et al., *Molecular Detection of Cytokeratin-19–Positive Cells in the Peripheral Blood of Patients With Operable Breast Cancer: Evaluation of Their Prognostic Significance*. Journal of Clinical Oncology, 2002. **20**(16): p. 3404-3412.
19. Xenidis, N., et al., *Predictive and Prognostic Value of Peripheral Blood Cytokeratin-19 mRNA-Positive Cells Detected by Real-Time Polymerase Chain Reaction in Node-Negative Breast Cancer Patients*. Journal of Clinical Oncology, 2006. **24**(23): p. 3756-3762.
20. Meng, S., et al., *Circulating Tumor Cells in Patients with Breast Cancer Dormancy*. Clinical Cancer Research, 2004. **10**(24): p. 8152-8162.
21. Deng, G., et al., *Enrichment with anti-cytokeratin alone or combined with anti-EpCAM antibodies significantly increases the sensitivity for circulating tumor cell detection in metastatic breast cancer patients*. Breast Cancer Research, 2008. **10**(4).

22. Thurm, H., et al., *Rare Expression of Epithelial Cell Adhesion Molecule on Residual Micrometastatic Breast Cancer Cells after Adjuvant Chemotherapy*. *Clinical Cancer Research*, 2003. **9**(7): p. 2598-2604.
23. Rao, C.G., et al., *Expression of epithelial cell adhesion molecule in carcinoma cells present in blood and primary and metastatic tumors*. *International Journal of Oncology*, 2005. **27**(1): p. 49-57.
24. Went, P.T.H., et al., *Frequent EpCam protein expression in human carcinomas*. *Human Pathology*, 2004. **35**(1): p. 122-128.
25. Riethdorf, S., et al., *Detection of circulating tumor cells in peripheral blood of patients with metastatic breast cancer: A validation study of the CellSearch system*. *Clinical Cancer Research*, 2007. **13**(3): p. 920-928.
26. Van der Auwera, I., et al., *Circulating tumour cell detection: a direct comparison between the CellSearch System, the AdnaTest and CK-19/mammaglobin RT-PCR in patients with metastatic breast cancer*. *British Journal of Cancer*, 2010. **102**(2): p. 276-284.
27. Allard, W.J., et al., *Tumor Cells Circulate in the Peripheral Blood of All Major Carcinomas but not in Healthy Subjects or Patients With Nonmalignant Diseases*. *Clinical Cancer Research*, 2004. **10**(20): p. 6897-6904.
28. Attard, G., et al., *Characterization of ERG, AR and PTEN Gene Status in Circulating Tumor Cells from Patients with Castration-Resistant Prostate Cancer*. *Cancer Research*, 2009. **69**(7): p. 2912-2918.
29. Kirby, B.J., et al., *Functional Characterization of Circulating Tumor Cells with a Prostate-Cancer-Specific Microfluidic Device*. *Plos One*, 2012. **7**(4): p. 1-10.
30. Jackson, J.M., et al., *UV activation of polymeric high aspect ratio microstructures: ramifications in antibody surface loading for circulating tumor cell selection*. *Lab on a Chip*, 2014.
31. Nagrath, S., et al., *Isolation of rare circulating tumour cells in cancer patients by microchip technology*. *Nature (London, U. K.)*, 2007. **450**(Copyright (C) 2010 American Chemical Society (ACS). All Rights Reserved.): p. 1235-1239.
32. Stott, S.L., et al., *Isolation of circulating tumor cells using a microvortex-generating herringbone-chip*. *Proceedings of the National Academy of Sciences*, 2010. **107**(43): p. 18392-18397.
33. Yu, M., et al., *Circulating Breast Tumor Cells Exhibit Dynamic Changes in Epithelial and Mesenchymal Composition*. *Science*, 2013. **339**(6119): p. 580-584.



34. Kamande, J.W., *et al.*, *Modular Microsystem for the Isolation, Enumeration, and Phenotyping of Circulating Tumor Cells in Patients with Pancreatic Cancer*. *Analytical Chemistry*, 2013. **85**(19): p. 9092-9100.
35. Dharmasiri, U., *et al.*, *High-Throughput Selection, Enumeration, Electrokinetic Manipulation, and Molecular Profiling of Low-Abundance Circulating Tumor Cells Using a Microfluidic System*. *Anal. Chem.* (Washington, DC, U. S.), 2011. **83**(Copyright (C) 2011 American Chemical Society (ACS). All Rights Reserved.): p. 2301-2309.
36. Adams, A.A., *et al.*, *Highly Efficient Circulating Tumor Cell Isolation from Whole Blood and Label-Free Enumeration Using Polymer-Based Microfluidics with an Integrated Conductivity Sensor*. *J. Am. Chem. Soc.*, 2008. **130**(Copyright (C) 2010 American Chemical Society (ACS). All Rights Reserved.): p. 8633-8641.
37. Bednarz-Knoll, N., C. Alix-Panabieres, and K. Pantel, *Clinical relevance and biology of circulating tumor cells*. *Breast Cancer Research*, 2011. **13**(6).
38. Alix-Panabières, C., H. Schwarzenbach, and K. Pantel, *Circulating tumor cells and circulating tumor DNA*. *Annual review of medicine*, 2012. **63**: p. 199-215.
39. Dharmasiri, U., *et al.*, *Microsystems for the Capture of Low-Abundance Cells*, in *Annual Review of Analytical Chemistry, Vol 3*, E.S.Z.R.N. Yeung, Editor 2010. p. 409-431.
40. Lalkhen, A.G. and A. McCluskey, *Clinical tests: sensitivity and specificity*. *Continuing Education in Anaesthesia, Critical Care & Pain*, 2008. **8**(6): p. 221-223.
41. Soper, S.A., *et al.*, *Point-of-care biosensor systems for cancer diagnostics/prognostics*. *Biosens. Bioelectron.*, 2006. **21**(Copyright (C) 2013 American Chemical Society (ACS). All Rights Reserved.): p. 1932-1942.
42. Henares, T.G., F. Mizutani, and H. Hisamoto, *Current development in microfluidic immunosensing chip*. *Analytica Chimica Acta*, 2008. **611**(1): p. 17-30.
43. Kovarik, M.L., *et al.*, *Micro Total Analysis Systems for Cell Biology and Biochemical Assays*. *Analytical Chemistry*, 2011. **84**(2): p. 516-540.
44. Alix-Panabières, C. and K. Pantel, *Circulating Tumor Cells: Liquid Biopsy of Cancer*. *Clinical Chemistry*, 2013. **59**(1): p. 110-118.
45. Alix-Panabières, C., *et al.*, *Detection and Characterization of Putative Metastatic Precursor Cells in Cancer Patients*. *Clinical Chemistry*, 2007. **53**(3): p. 537-539.

46. Pantel, K., R.H. Brakenhoff, and B. Brandt, *Detection, clinical relevance and specific biological properties of disseminating tumour cells*. Nature Reviews Cancer, 2008. **8**(5): p. 329-340.
47. Becker, H. and L.E. Locascio, *Polymer microfluidic devices*. Talanta, 2002. **56**(2): p. 267-287.
48. Soper, S.A., *et al.*, *Peer Reviewed: Polymeric Microelectromechanical Systems*. Analytical Chemistry, 2000. **72**(19): p. 642 A-651 A.
49. Lim, L.S., *et al.*, *Microsieve lab-chip device for rapid enumeration and fluorescence in situ hybridization of circulating tumor cells*. Lab on a Chip, 2012. **12**(21): p. 4388-4396.
50. Kim, M.S., *et al.*, *SSA-MOA: a novel CTC isolation platform using selective size amplification (SSA) and a multi-obstacle architecture (MOA) filter*. Lab on a Chip, 2012. **12**(16): p. 2874-2880.
51. Wang, S., *et al.*, *Highly Efficient Capture of Circulating Tumor Cells by Using Nanostructured Silicon Substrates with Integrated Chaotic Micromixers*. Angewandte Chemie-International Edition, 2011. **50**(13): p. 3084-3088.
52. Li, L., *et al.*, *Lectin-aided separation of circulating tumor cells and assay of their response to an anticancer drug in an integrated microfluidic device*. Electrophoresis, 2010. **31**(18): p. 3159-3166.
53. Moon, H.-S., *et al.*, *Continuous separation of breast cancer cells from blood samples using multi-orifice flow fractionation (MOFF) and dielectrophoresis (DEP)*. Lab on a Chip, 2011. **11**(6): p. 1118-1125.
54. Angell, J.B., S.C. Terry, and P.W. Barth, *Silicon Micromechanical Devices*. Scientific American, 1983. **248**(4): p. 44-55.
55. Börner, M.W., *et al.*, *Sub-micron LIGA process for movable microstructures*. Microelectronic Engineering, 1996. **30**(1-4): p. 505-508.
56. Peng, K.Q., *et al.*, *Synthesis of Large-Area Silicon Nanowire Arrays via Self-Assembling Nanoelectrochemistry*. Advanced Materials, 2002. **14**(16): p. 1164-1167.
57. Yu, M., *et al.*, *RNA sequencing of pancreatic circulating tumour cells implicates WNT signalling in metastasis*. Nature, 2012. **advance online publication**.

58. Soper, S., *et al.*, *Point-of-care biosensor systems for cancer diagnostics/prognostics*. *Biosensors and Bioelectronics*, 2006. **21**(10): p. 1932-1942.
59. Hupert, M.L., *et al.*, *High-precision micromilling for low-cost fabrication of metal mold masters*. *Proc. SPIE-Int. Soc. Opt. Eng.*, 2006. **6112**(Copyright (C) 2010 American Chemical Society (ACS). All Rights Reserved.): p. 61120B/1-61120B/12.
60. Hupert, M., *et al.*, *Evaluation of micromilled metal mold masters for the replication of microchip electrophoresis devices*. *Microfluidics and Nanofluidics*, 2007. **3**(1): p. 1-11.
61. Adams, A.A., *et al.*, *Highly Efficient Circulating Tumor Cell Isolation from Whole Blood and Label-Free Enumeration Using Polymer-Based Microfluidics with an Integrated Conductivity Sensor*. *J. Am. Chem. Soc.*, 2008. **130**(27): p. 8633-8641.
62. Ozkumur, E., *et al.*, *Inertial Focusing for Tumor Antigen-Dependent and –Independent Sorting of Rare Circulating Tumor Cells*. *Sci Transl Med*, 2013. **5**(179): p. 179ra47-179ra47.
63. Nagrath, S., *et al.*, *Isolation of rare circulating tumour cells in cancer patients by microchip technology*. *Nature*, 2007. **450**(7173): p. 1235-1239.
64. Issadore, D., *et al.*, *Ultrasensitive Clinical Enumeration of Rare Cells ex Vivo Using a Micro-Hall Detector*. *Sci Transl Med*, 2012. **4**(141): p. 141ra92-141ra92.
65. Asghar, W., *et al.*, *Electrical fingerprinting, 3D profiling and detection of tumor cells with solid-state micropores*. *Lab Chip*, 2012. **12**(13): p. 2345-2352.
66. Chung, Y.-K., *et al.*, *An electrical biosensor for the detection of circulating tumor cells*. *Biosensors and Bioelectronics*, 2011. **26**(5): p. 2520-2526.
67. Gleghorn, J.P., *et al.*, *Capture of circulating tumor cells from whole blood of prostate cancer patients using geometrically enhanced differential immunocapture (GEDI) and a prostate-specific antibody*. *Lab Chip*, 2010. **10**(1): p. 27-29.
68. Kang, J.H., *et al.*, *A combined micromagnetic-microfluidic device for rapid capture and culture of rare circulating tumor cells*. *Lab Chip*, 2012. **12**(12): p. 2175-2181.

69. Wang, S., et al., *Highly Efficient Capture of Circulating Tumor Cells by Using Nanostructured Silicon Substrates with Integrated Chaotic Micromixers*. *Angewandte Chemie, International Edition*, 2010. **50**: p. 3084-3088.
70. Saliba, A.E., et al., *Microfluidic sorting and multimodal typing of cancer cells in self-assembled magnetic arrays*. *PNAS*, 2010. **107**: p. 14524-14529.
71. Hyun, K.-A., T.Y. Lee, and H.-I. Jung, *Negative enrichment of circulating tumor cells using a geometrically activated surface interaction (GASI) chip*. *Anal Chem*, 2013.
72. Stott, S.L., et al., *Isolation of circulating tumor cells using a microvortex-generating herringbone-chip*. *Proc Natl Acad Sci U S A*, 2010. **107**(43): p. 18392-18397.
73. Yu, M., et al., *RNA sequencing of pancreatic circulating tumour cells implicates WNT signalling in metastasis*. *Nature*, 2012. **487**(7408): p. 510-513.
74. Zhao, W., et al., *Bioinspired multivalent DNA network for capture and release of cells*. *Proceedings of the National Academy of Sciences*, 2012.
75. Shim, S., et al., *Dielectrophoresis has broad applicability to marker-free isolation of tumor cells from blood by microfluidic systems*. *Biomicrofluidics*, 2013. **7**(1): p. 011808-12.
76. Doh, I. and Y.-H. Cho, *A continuous cell separation chip using hydrodynamic dielectrophoresis (DEP) process*. *Sensors and Actuators A: Physical*, 2005. **121**(1): p. 59-65.
77. Moon, H.-S., et al., *Continuous separation of breast cancer cells from blood samples using multi-orifice flow fractionation (MOFF) and dielectrophoresis (DEP)*. *Lab Chip*, 2011. **11**(6): p. 1118-1125.
78. Bhagat, A., S. Kuntaegowdanahalli, and I. Papautsky, *Inertial microfluidics for continuous particle filtration and extraction*. *Microfluidics and Nanofluidics*, 2009. **7**(2): p. 217-226.
79. Madou, M.J., *Fundamentals of microfabrication and nanotechnology*. 3rd ed2012, Boca Raton, FL: CRC Press.
80. Dharmasiri, U., et al., *Highly efficient capture and enumeration of low abundance prostate cancer cells using prostate-specific membrane antigen aptamers immobilized to a polymeric microfluidic device*. *Electrophoresis*, 2009. **30**(18): p. 3289-300.

81. Jackson, J.M., et al., *UV Activation of Polymeric High Aspect Ratio Microstructures: Ramifications in Antibody Surface Loading For Circulating Tumor Cell Selection*. Lab Chip, 2013: p. Submitted for publication.
82. Galloway, M., et al., *Contact conductivity detection in poly(methyl methacrylate)-based microfluidic devices for analysis of mono- and polyanionic molecules*. Anal Chem, 2002. **74**(10): p. 2407-15.
83. Chen, C.-L., et al., *Separation and detection of rare cells in a microfluidic disk via negative selection*. Lab Chip, 2011. **11**(3): p. 474-483.
84. Hermanson, G.T., *Bioconjugate techniques* 1996, San Diego: Academic Press. xxv, 785 p.
85. Piruska, A., et al., *The autofluorescence of plastic materials and chips measured under laser irradiation*. Lab Chip, 2005. **5**(12): p. 1348-1354.
86. Shadpour, H., et al., *Physiochemical properties of various polymer substrates and their effects on microchip electrophoresis performance*. Journal of Chromatography A, 2006. **1111**(2): p. 238-251.
87. Sakai, Y. and K. Nakazawa, *Technique for the control of spheroid diameter using microfabricated chips*. Acta Biomater, 2007. **3**(6): p. 1033-40.
88. Mehta, G., et al., *Hard top soft bottom microfluidic devices for cell culture and chemical analysis*. Anal Chem, 2009. **81**(10): p. 3714-22.
89. Leclerc, E., Y. Sakai, and T. Fujii, *Cell culture in 3-dimensional microfluidic structure of PDMS (polydimethylsiloxane)*. Biomedical Microdevices, 2003. **5**(2): p. 109-114.
90. van Midwoud, P.M., et al., *Comparison of Biocompatibility and Adsorption Properties of Different Plastics for Advanced Microfluidic Cell and Tissue Culture Models*. Anal Chem, 2012. **84**(9): p. 3938-3944.
91. Stern, S.A. and B.D. Bhide, *Permeability of silicone polymers to ammonia and hydrogen sulfide*. Journal of Applied Polymer Science, 1989. **38**(11): p. 2131-2147.
92. Stern, S.A., V.M. Shah, and B.J. Hardy, *Structure-Permeability Relationships in Silicone Polymers*. Journal of Polymer Science Part B-Polymer Physics, 1987. **25**(6): p. 1263-1298.
93. Brandrup, J., E.H. Immergut, and E.A. Grulke, *Polymer handbook, 4th edition*. 4th ed 2004, New York ; Chichester: Wiley.

94. Hu, C.-C., *et al.*, *Gas separation properties in cyclic olefin copolymer membrane studied by positron annihilation, sorption, and gas permeation*. Journal of Membrane Science, 2006. **274**(1–2): p. 192-199.
95. Chiou, J.S. and D.R. Paul, *Gas Permeation in Miscible Homopolymer Copolymer Blends .1. Poly(Methyl Methacrylate) and Styrene Acrylonitrile Copolymers*. Journal of Applied Polymer Science, 1987. **34**(3): p. 1037-1056.
96. Massey, L.K., *Permeability properties of plastics and elastomers : a guide to packaging and barrier materials*. 2nd ed2003, Norwich, NY, USA: Plastics Design Library/William Andrew Pub. xiv, 601 p.
97. Duffy, D.C., *et al.*, *Rapid prototyping of microfluidic systems in poly(dimethylsiloxane)*. Anal Chem, 1998. **70**(23): p. 4974-4984.
98. Toepke, M.W. and D.J. Beebe, *PDMS absorption of small molecules and consequences in microfluidic applications*. Lab Chip, 2006. **6**(12): p. 1484-1486.
99. Zheng, S., *et al.*, *Membrane microfilter device for selective capture, electrolysis and genomic analysis of human circulating tumor cells*. Journal of Chromatography A, 2007. **1162**(2): p. 154-161.
100. Zheng, S., *et al.*, *3D microfilter device for viable circulating tumor cell (CTC) enrichment from blood*. Biomedical Microdevices, 2011. **13**(1): p. 203-213.
101. Fleischer, R.L., *et al.*, *Particle Track Etching*. Science, 1972. **178**(4058): p. 255-263.
102. Rostagno, P., *et al.*, *Detection of rare circulating breast cancer cells by filtration cytometry and identification by DNA content: sensitivity in an experimental model*. Anticancer Res, 1997. **17**(4A): p. 2481-5.
103. Lara, O., *et al.*, *Enrichment of rare cancer cells through depletion of normal cells using density and flow-through, immunomagnetic cell separation*. Experimental Hematology, 2004. **32**: p. 891-904.
104. Myung, J.H., *et al.*, *The role of polymers in detection and isolation of circulating tumor cells*. Polymer Chemistry, 2012. **3**(9): p. 2336-2341.
105. Saliba, A.E., *et al.*, *Microfluidic sorting and multimodal typing of cancer cells in self-assembled magnetic arrays*. Proc Natl Acad Sci U S A, 2010. **107**(33): p. 14524-14529.
106. Yavuz, C.T., *et al.*, *Low-Field Magnetic Separation of Monodisperse Fe<sub>3</sub>O<sub>4</sub> Nanocrystals*. Science, 2006. **314**(5801): p. 964-967.

107. Wang, A.Y., *et al.*, *Study of magnetic ferrite nanoparticles labeled with Tc-99m-pertechnetate*. Journal of Radioanalytical and Nuclear Chemistry, 2010. **284**(2): p. 405-413.
108. Hoshino, K., *et al.*, *Microchip-based immunomagnetic detection of circulating tumor cells*. Lab Chip, 2011. **11**(20): p. 3449-3457.
109. Santhosh, P.B. and N.P. Ulrih, *Multifunctional superparamagnetic iron oxide nanoparticles: Promising tools in cancer theranostics*. Cancer Letters, 2013. **336**(1): p. 8-17.
110. Allard, W.J., *et al.*, *Tumor cells circulate in the peripheral blood of all major carcinomas but not in healthy subjects or patients with nonmalignant diseases*. Clin Cancer Res, 2004. **10**: p. 6897-904.
111. Dharmasiri, U., *et al.*, *Microsystems for the Capture of Low-Abundance Cells*. Annual Review of Analytical Chemistry, Vol 3, 2010. **3**: p. 409-431.
112. Zieglschmid, V., C. Hollmann, and O. Bocher, *Detection of disseminated tumor cells in peripheral blood*. Critical Reviews in Clinical Laboratory Sciences, 2005. **42**(2): p. 155-196.
113. Martin, V.M., *et al.*, *Immunomagnetic enrichment of disseminated epithelial tumor cells from peripheral blood by MACS*. Experimental Hematology, 1998. **26**(3): p. 252-264.
114. Racila, E., *et al.*, *Detection and characterization of carcinoma cells in the blood*. Proc Natl Acad Sci U S A, 1998. **95**(8): p. 4589-4594.
115. Talasz, A.H., *et al.*, *Isolating highly enriched populations of circulating epithelial cells and other rare cells from blood using a magnetic sweeper device*. Proceedings of the National Academy of Sciences, 2009. **106**(10): p. 3970-3975.
116. Cann, G.M., *et al.*, *mRNA-Seq of Single Prostate Cancer Circulating Tumor Cells Reveals Recapitulation of Gene Expression and Pathways Found in Prostate Cancer*. Plos One, 2012. **7**(11): p. e49144.
117. Xu, H., *et al.*, *Antibody conjugated magnetic iron oxide nanoparticles for cancer cell separation in fresh whole blood*. Biomaterials, 2011. **32**(36): p. 9758-9765.
118. Mi, Y., *et al.*, *Herceptin functionalized polyhedral oligomeric silsesquioxane - conjugated oligomers - silica/iron oxide nanoparticles for tumor cell sorting and detection*. Biomaterials, 2011. **32**(32): p. 8226-8233.

119. Rossi, E., et al., *M30 neoepitope expression in epithelial cancer: quantification of apoptosis in circulating tumor cells by CellSearch analysis*. Clin Cancer Res, 2010. **16**(21): p. 5233-43.
120. Deneve, E., et al., *Capture of Viable Circulating Tumor Cells in the Liver of Colorectal Cancer Patients*. Clin Chem, 2013.
121. Nagrath, S., et al., *Isolation of rare circulating tumour cells in cancer patients by microchip technology*. Nature, 2007. **450**: p. 1235-9.
122. Saliba, A.-E., et al., *Microfluidic sorting and multimodal typing of cancer cells in self-assembled magnetic arrays*. Proceedings of the National Academy of Sciences of the United States of America, 2010. **107**(33): p. 14524-14529.
123. Rao, C.G., et al., *Expression of epithelial cell adhesion molecule in carcinoma cells present in blood and primary and metastatic tumors*. Int J Oncol, 2005. **27**: p. 49-57.
124. Dharmasiri, U., et al., *Microsystems for the Capture of Low Abundant Cells*. Annual Review of Analytical Chemistry, 2010. **3**: p. 409-431.
125. Butler, J.E., et al., *The immunochemistry of sandwich elisas—VI. Greater than 90% of monoclonal and 75% of polyclonal anti-fluorescyl capture antibodies (CABs) are denatured by passive adsorption*. Molecular Immunology, 1993. **30**(13): p. 1165-1175.
126. Hughes, A.D. and M.R. King, *Use of Naturally Occurring Halloysite Nanotubes for Enhanced Capture of Flowing Cells*. Langmuir, 2010. **26**(14): p. 12155-12164.
127. Hughes, A.D., et al., *Microtube Device for Selectin-Mediated Capture of Viable Circulating Tumor Cells from Blood*. Clin Chem, 2012. **58**(5): p. 846-853.
128. Shah, A.M., et al., *Biopolymer System for Cell Recovery from Microfluidic Cell Capture Devices*. Anal Chem, 2012. **84**(8): p. 3682-3688.
129. Adamczyk, M., et al., *Region-Selective Labeling of Antibodies as Determined by Electrospray Ionization-Mass Spectrometry (ESI-MS)*. Bioconjugate Chemistry, 2000. **11**(4): p. 557-563.
130. Dugas, V., A. Elaissari, and Y. Chevalier, *Surface Sensitization Techniques and Recognition Receptors Immobilization on Biosensors and Microarrays*, in *Recognition Receptors in Biosensors*, M. Zourob, Editor 2010, Springer New York. p. 47-134.



131. Peluso, P., *et al.*, *Optimizing antibody immobilization strategies for the construction of protein microarrays*. Analytical Biochemistry, 2003. **312**(2): p. 113-124.
132. Wang, S.T., *et al.*, *Capture of circulating tumor cells with a highly efficient nanostructured silicon substrates with integrated chaotic micromixers*. European Biophysics Journal with Biophysics Letters, 2011. **40**: p. 235-235.
133. Galanzha, E.I., J.W. Kim, and V.P. Zharov, *Nanotechnology-based molecular photoacoustic and photothermal flow cytometry platform for in-vivo detection and killing of circulating cancer stem cells*. J Biophotonics, 2009. **2**(12): p. 725-35.
134. Myung, J.H., *et al.*, *Dendrimer-Mediated Multivalent Binding for the Enhanced Capture of Tumor Cells*. Angewandte Chemie International Edition, 2011. **50**(49): p. 11769-11772.
135. Galanzha, E.I., *et al.*, *In vivo magnetic enrichment and multiplex photoacoustic detection of circulating tumour cells*. Nat Nano, 2009. **4**(12): p. 855-860.
136. He, W., *et al.*, *In vivo quantitation of rare circulating tumor cells by multiphoton intravital flow cytometry*. Proc Natl Acad Sci U S A, 2007. **104**(28): p. 11760-5.
137. Owens, D.E., 3rd and N.A. Peppas, *Oponization, biodistribution, and pharmacokinetics of polymeric nanoparticles*. Int J Pharm, 2006. **307**(1): p. 93-102.
138. Zhang, Y., N. Kohler, and M. Zhang, *Surface modification of superparamagnetic magnetite nanoparticles and their intracellular uptake*. Biomaterials, 2002. **23**(7): p. 1553-61.
139. Sun, C., R. Sze, and M. Zhang, *Folic acid-PEG conjugated superparamagnetic nanoparticles for targeted cellular uptake and detection by MRI*. J Biomed Mater Res A, 2006. **78**(3): p. 550-7.
140. Jackson, J.M., *et al.*, *UV activation of polymeric high aspect ratio microstructures: Ramifications in antibody surface loading for circulating tumor cell selection*. Lab on a Chip, 2013. **13**.
141. Park, J.-S. and H.-I. Jung, *Multiorifice Flow Fractionation: Continuous Size-Based Separation of Microspheres Using a Series of Contraction/Expansion Microchannels*. Analytical Chemistry, 2009. **81**(20): p. 8280-8288.
142. Hayes, D.F. and J. Smerage, *Is there a role for circulating tumor cells in the management of breast cancer?* Clinical Cancer Research, 2008. **14**: p. 3646-3650.

143. Thapa, A., *et al.*, *Nano-structured polymers enhance bladder smooth muscle cell function*. *Biomaterials*, 2003. **24**(17): p. 2915-2926.
144. Miller, D.C., *et al.*, *Endothelial and vascular smooth muscle cell function on poly(lactic-co-glycolic acid) with nano-structured surface features*. *Biomaterials*, 2004. **25**(1): p. 53-61.
145. Liotta, L., *et al.*, *Metastatic potential correlates with enzymatic degradation of basement membrane collagen*. *Nature*, 1980. **284**(5751): p. 67-68.
146. Ruoslahti, E., *How cancer spreads*. *Scientific American*, 1996. **275**(3): p. 72-77.
147. Boot-Handford, R., *The extracellular matrix factsbook*, 1998.
148. Hou, S., *et al.*, *Capture and Stimulated Release of Circulating Tumor Cells on Polymer-Grafted Silicon Nanostructures*. *Advanced Materials*, 2013. **25**(11): p. 1547-1551.
149. Hou, S., *et al.*, *Polymer Nanofiber-Embedded Microchips for Detection, Isolation, and Molecular Analysis of Single Circulating Melanoma Cells*. *Angewandte Chemie International Edition*, 2013. **52**(12): p. 3379-3383.
150. Huang, S.-B., *et al.*, *High-purity and label-free isolation of circulating tumor cells (CTCs) in a microfluidic platform by using optically-induced-dielectrophoretic (ODEP) force*. *Lab on a Chip*, 2013. **13**(7): p. 1371-1383.
151. Zhang, N., *et al.*, *Electrospun TiO<sub>2</sub> Nanofiber-Based Cell Capture Assay for Detecting Circulating Tumor Cells from Colorectal and Gastric Cancer Patients*. *Advanced Materials*, 2012. **24**(20): p. 2756-2760.
152. Wan, Y., *et al.*, *Nanotextured substrates with immobilized aptamers for cancer cell isolation and cytology*. *Cancer*, 2012. **118**(4): p. 1145-1154.
153. Chen, G.D., *et al.*, *Nanoporous micro-element arrays for particle interception in microfluidic cell separation*. *Lab on a Chip*, 2012. **12**(17): p. 3159-3167.
154. Pecot, C.V., *et al.*, *A novel platform for detection of CK+ and CK- CTCs*. *Cancer Discovery*, 2011: p. 580-586.
155. Lustberg, M., *et al.*, *Emerging technologies for CTC detection based on depletion of normal cells*, in *Minimal Residual Disease and Circulating Tumor Cells in Breast Cancer 2012*, Springer. p. 97-110.

156. Yang, L., et al., *Optimization of an enrichment process for circulating tumor cells from the blood of head and neck cancer patients through depletion of normal cells*. Biotechnology and Bioengineering, 2009. **102**(2): p. 521-534.
157. Hayes, G.M., et al., *Isolation of malignant B cells from patients with chronic lymphocytic leukemia (CLL) for analysis of cell proliferation: Validation of a simplified method suitable for multi-center clinical studies*. Leukemia Research, 2010. **34**(6): p. 809-815.
158. Zigeuner, R.E., et al., *Isolation of Circulating Cancer Cells From Whole Blood By Immunomagnetic Cell Enrichment and Unenriched Immunocytochemistry In Vitro*. The Journal of Urology, 2003. **169**(2): p. 701-705.
159. Naume, B., et al., *Immunomagnetic techniques for the enrichment and detection of isolated breast carcinoma cells in bone marrow and peripheral blood*. Journal of Hematotherapy, 1997. **6**(2): p. 103-114.
160. Balasubramanian, P., et al., *Confocal Images of Circulating Tumor Cells Obtained Using a Methodology and Technology That Removes Normal Cells*. Molecular Pharmaceutics, 2009. **6**(5): p. 1402-1408.
161. Tong, X., et al., *Application of immunomagnetic cell enrichment in combination with RT-PCR for the detection of rare circulating head and neck tumor cells in human peripheral blood*. Cytometry Part B: Clinical Cytometry, 2007. **72B**(5): p. 310-323.
162. Hyun, K.-A., T.Y. Lee, and H.-I. Jung, *Negative Enrichment of Circulating Tumor Cells Using a Geometrically Activated Surface Interaction Chip*. Analytical Chemistry, 2013. **85**(9): p. 4439-4445.
163. Chen, C.-L., et al., *Separation and detection of rare cells in a microfluidic disk via negative selection*. Lab on a Chip, 2011. **11**(3): p. 474-483.
164. Issadore, D., et al., *Ultrasensitive Clinical Enumeration of Rare Cells ex Vivo Using a Micro-Hall Detector*. Science Translational Medicine, 2012. **4**(141): p. 141ra92.
165. Ozkumur, E., et al., *Inertial Focusing for Tumor Antigen–Dependent and –Independent Sorting of Rare Circulating Tumor Cells*. Science Translational Medicine, 2013. **5**(179): p. 179ra47.
166. Bo, L., et al. *Parylene membrane slot filter for the capture, analysis and culture of viable circulating tumor cells*. in *Micro Electro Mechanical Systems (MEMS), 2010 IEEE 23rd International Conference on*. 2010.

167. Hyun, K.-A., *et al.*, *Microfluidic flow fractionation device for label-free isolation of circulating tumor cells (CTCs) from breast cancer patients*. *Biosensors and Bioelectronics*, 2013. **40**(1): p. 206-212.
168. Tan, S.J., *et al.*, *Versatile label free biochip for the detection of circulating tumor cells from peripheral blood in cancer patients*. *Biosensors & Bioelectronics*, 2010. **26**(4): p. 1701-1705.
169. Williams, A., *et al.*, *Size-based enrichment technologies for CTC detection and characterization*, in *Minimal Residual Disease and Circulating Tumor Cells in Breast Cancer 2012*, Springer. p. 87-95.
170. Lianidou, E.S. and A. Markou, *Circulating tumor cells in breast cancer: detection systems, molecular characterization, and future challenges*. *Clinical Chemistry*, 2011. **57**(9): p. 1242-1255.
171. Fiedler, S., *et al.*, *Dielectrophoretic Sorting of Particles and Cells in a Microsystem*. *Analytical Chemistry*, 1998. **70**(9): p. 1909-1915.
172. Gascoyne, P.R.C., *et al.*, *Dielectrophoretic separation of cancer cells from blood*. *IEEE Transactions on Industry Applications*, 1997. **33**(3): p. 670-678.
173. Jones, T.B., *Electromechanics of particles* 2005: Cambridge University Press.
174. Iliescu, C., G. Tresset, and G. Xu, *Dielectrophoretic field-flow method for separating particle populations in a chip with asymmetric electrodes*. *Biomicrofluidics*, 2009. **3**(4): p. 044104-10.
175. Shim, S., *et al.*, *Dynamic physical properties of dissociated tumor cells revealed by dielectrophoretic field-flow fractionation*. *Integrative Biology*, 2011. **3**(8): p. 850-862.
176. Gascoyne, P.R.C., *et al.*, *Isolation of rare cells from cell mixtures by dielectrophoresis*. *Electrophoresis*, 2009. **30**(8): p. 1388-1398.
177. Gascoyne, P.R.C. and J. Vykoukal, *Particle separation by dielectrophoresis*. *Electrophoresis*, 2002. **23**(13): p. 1973-1983.
178. Çetin, B., *et al.*, *Continuous particle separation by size via AC-dielectrophoresis using a lab-on-a-chip device with 3-D electrodes*. *Electrophoresis*, 2009. **30**(5): p. 766-772.
179. Becker, F.F., *et al.*, *THE REMOVAL OF HUMAN LEUKEMIA-CELLS FROM BLOOD USING INTERDIGITATED MICROELECTRODES*. *Journal of Physics D- Applied Physics*, 1994. **27**(12): p. 2659-2662.

180. Becker, F.F., *et al.*, *SEPARATION OF HUMAN BREAST-CANCER CELLS FROM BLOOD BY DIFFERENTIAL DIELECTRIC AFFINITY*. Proceedings of the National Academy of Sciences of the United States of America, 1995. **92**(3): p. 860-864.
181. Cheng, J., *et al.*, *Isolation of cultured cervical carcinoma cells mixed with peripheral blood cells on a bioelectronic chip*. Analytical Chemistry, 1998. **70**(11): p. 2321-2326.
182. Huang, Y., *et al.*, *Dielectrophoretic cell separation and gene expression profiling on microelectronic chip arrays*. Analytical Chemistry, 2002. **74**(14): p. 3362-3371.
183. Huang, Y., *et al.*, *Introducing dielectrophoresis as a new force field for field-flow fractionation*. Biophysical Journal, 1997. **73**(2): p. 1118-1129.
184. Huang, Y., *et al.*, *The removal of human breast cancer cells from hematopoietic CD34(+) stem cells by dielectrophoretic field-flow-fractionation*. Journal of Hematotherapy & Stem Cell Research, 1999. **8**(5): p. 481-490.
185. Yang, J., *et al.*, *Cell separation on microfabricated electrodes using dielectrophoretic/gravitational field flow fractionation*. Analytical Chemistry, 1999. **71**(5): p. 911-918.
186. Park, J., *et al.*, *An efficient cell separation system using 3D-asymmetric microelectrodes*. Lab on a Chip, 2005. **5**(11): p. 1264-1270.
187. An, J., *et al.*, *Separation of malignant human breast cancer epithelial cells from healthy epithelial cells using an advanced dielectrophoresis-activated cell sorter (DACS)*. Analytical and Bioanalytical Chemistry, 2009. **394**(3): p. 801-809.
188. Sabuncu, A.C., *et al.*, *Dielectrophoretic separation of mouse melanoma clones*. Biomicrofluidics, 2010. **4**(2).
189. Yang, F., *et al.*, *Dielectrophoretic separation of colorectal cancer cells*. Biomicrofluidics, 2010. **4**(1).
190. Wang, X.B., *et al.*, *Cell separation by dielectrophoretic field-flow-fractionation*. Analytical Chemistry, 2000. **72**(4): p. 832-839.
191. Gupta, V., *et al.*, *ApoStream<sup>[sup [trademark sign]]</sup>, a new dielectrophoretic device for antibody independent isolation and recovery of viable cancer cells from blood*. Biomicrofluidics, 2012. **6**(2): p. 024133-14.
192. Iliescu, C., *et al.* *Manipulation of Biological Samples using Electric Field*. in *Semiconductor Conference, 2007. CAS 2007. International*. 2007.

193. Saucedo-Zeni, N., et al., *A novel method for the in vivo isolation of circulating tumor cells from peripheral blood of cancer patients using a functionalized and structured medical wire*. International Journal of Oncology, 2012. **41**(4): p. 1241.
194. Eifler, R.L., et al., *Enrichment of circulating tumor cells from a large blood volume using leukapheresis and elutriation: Proof of concept*. Cytometry Part B: Clinical Cytometry, 2011. **80B**(2): p. 100-111.
195. Schwella, N., et al., *Leukapheresis after high-dose chemotherapy and autologous peripheral blood progenitor cell transplantation: a novel approach to harvest a second autograft*. Transfusion, 2003. **43**(2): p. 259-264.
196. Ghersi, G., et al., *The Protease Complex Consisting of Dipeptidyl Peptidase IV and Seprase Plays a Role in the Migration and Invasion of Human Endothelial Cells in Collagenous Matrices*. Cancer Research, 2006. **66**(9): p. 4652-4661.
197. Paris, P.L., et al., *Functional phenotyping and genotyping of circulating tumor cells from patients with castration resistant prostate cancer*. Cancer Letters, 2009. **277**(2): p. 164-173.
198. ZIEGLSCHMID, V., et al., *Heterogeneous Expression of Tumor-associated Genes in Disseminated Breast Cancer Cells*. Anticancer Res, 2007. **27**(4A): p. 1769-1776.
199. Fehm, T., et al., *Methods for isolating circulating epithelial cells and criteria for their classification as carcinoma cells*. Cytotherapy, 2005. **7**(2): p. 171-185.
200. Yu, M., et al., *Circulating tumor cells: approaches to isolation and characterization*. The Journal of Cell Biology, 2011. **192**(3): p. 373-382.
201. Coumans, F.A.W., et al., *Challenges in the Enumeration and Phenotyping of CTC*. Clinical Cancer Research, 2012. **18**(20): p. 5711-5718.
202. Talasz, A.H., et al., *Isolating highly enriched populations of circulating epithelial cells and other rare cells from blood using a magnetic sweeper device*. Proceedings of the National Academy of Sciences of the United States of America, 2009. **106**(10): p. 3970-3975.
203. Zenonos, K. and K. Kyprianou, *RAS signaling pathways, mutations and their role in colorectal cancer*. World journal of gastrointestinal oncology, 2013. **5**(5): p. 97-101.
204. Dreesen, O. and A. Brivanlou, *Signaling Pathways in Cancer and Embryonic Stem Cells*. Stem Cell Reviews, 2007. **3**(1): p. 7-17.

205. Wang, Y., *et al.*, *Gene-expression profiles to predict distant metastasis of lymph-node-negative primary breast cancer*. *The Lancet*, 2005. **365**(9460): p. 671-679.
206. Chang, J.C., *et al.*, *Patterns of resistance and incomplete response to docetaxel by gene expression profiling in breast cancer patients*. *Journal of Clinical Oncology*, 2005. **23**(6): p. 1169-1177.
207. Glinsky, G.V., *et al.*, *Gene expression profiling predicts clinical outcome of prostate cancer*. *Journal of Clinical Investigation*, 2004. **113**(6): p. 913-923.
208. Khambata-Ford, S., *et al.*, *Expression of epiregulin and amphiregulin and K-ras mutation status predict disease control in metastatic colorectal cancer patients treated with cetuximab*. *Journal of Clinical Oncology*, 2007. **25**(22): p. 3230-3237.
209. Ghadimi, B.M., *et al.*, *Effectiveness of gene expression profiling for response prediction of rectal adenocarcinomas to preoperative chemoradiotherapy*. *Journal of Clinical Oncology*, 2005. **23**(9): p. 1826-1838.
210. Smirnov, D.A., *et al.*, *Global Gene Expression Profiling of Circulating Tumor Cells*. *Cancer Research*, 2005. **65**(12): p. 4993-4997.
211. Chang, J.C., *et al.*, *Gene expression profiling for the prediction of therapeutic response to docetaxel in patients with breast cancer*. *The Lancet*, 2003. **362**(9381): p. 362-369.
212. Khoury, T., *et al.*, *Breast carcinoma with amplified HER2: a gene expression signature specific for trastuzumab resistance and poor prognosis*. *Modern Pathology*, 2010. **23**(10): p. 1364-1378.
213. Hurvitz, S.A., *et al.*, *Current approaches and future directions in the treatment of HER2-positive breast cancer*. *Cancer Treatment Reviews*, 2013. **39**(3): p. 219-229.
214. Nadal, R., *et al.*, *Relevance of molecular characterization of circulating tumor cells in breast cancer in the era of targeted therapies*. *Expert Review of Molecular Diagnostics*, 2013. **13**(3): p. 295-307.
215. Maheswaran, S., *et al.*, *Detection of Mutations in EGFR in Circulating Lung-Cancer Cells*. *New England Journal of Medicine*, 2008. **359**: p. 366-377.
216. Checchi, P.M., *et al.*, *Microtubule-interacting drugs for cancer treatment*. *Trends in Pharmacological Sciences*, 2003. **24**(7): p. 361-365.

217. Lu, J., *et al.*, *Isolation of circulating epithelial and tumor progenitor cells with an invasive phenotype from breast cancer patients*. International Journal of Cancer, 2010. **126**(3): p. 669-683.
218. Kennedy, A., *et al.*, *Elevation of seprase expression and promotion of an invasive phenotype by collagenous matrices in ovarian tumor cells*. International Journal of Cancer, 2009. **124**(1): p. 27-35.
219. Fan, T., *et al.*, *Clinical significance of circulating tumor cells detected by an invasion assay in peripheral blood of patients with ovarian cancer*. Gynecologic Oncology, 2009. **112**(1): p. 185-191.
220. Stott, S.L., *et al.*, *Isolation and characterization of circulating tumor cells from patients with localized and metastatic prostate cancer*. Sci. Transl. Med., 2010. **2**(Copyright (C) 2010 American Chemical Society (ACS). All Rights Reserved.): p. No pp. given.
221. Lin, H.K., *et al.*, *Portable filter-based microdevice for detection and characterization of circulating tumor cells*. Clinical Cancer Research, 2010. **16**(20): p. 5011-5018.



## CHAPTER 2. MODULAR MICROSYSTEM FOR THE ISOLATION, ENUMERATION AND PHENOTYPING OF CIRCULATING TUMOR CELLS: MANAGING PATIENTS WITH PANCREATIC CANCER

### 2.1 Introduction

The presence of circulating tumor cells (CTCs) in cancer patients was documented as early as 1869. [1] They are shed from many solid tumors and have been implicated as key participants in the metastatic process. As such, CTCs have attracted considerable attention as an exciting new class of biomarkers that can provide valuable clinical information for staging of patients, early diagnosis of relapse, guiding therapy, monitoring response to particular therapies and detection of disease recurrence. [2-21] Another exciting attribute of CTCs is that they can easily be obtained through a simple blood draw (~7.5 mL), potentially obviating the need for securing biopsies, which can be anatomically difficult to obtain or problematic if monitoring response to therapy as this would require many biopsy samples taken over an extended period of time.

The main challenge associated with the analysis of CTCs is their low frequency; 1-100 CTCs per  $10^9$  erythrocytes. Thus, highly sensitive enrichment techniques are required to enable effective CTC clinical analysis. Three important metrics are considered when evaluating CTC enrichment techniques; (i) throughput, defined as the maximum volume processing rate; (ii) recovery, an indicator of the number of target cells selected from the input sample with respect to the seed level of the target in that same sample; and (iii) purity defined as the ratio of CTCs selected to the total number of cells enriched.

\* Reproduced with permission from the *Analytical Chemistry*.

CellSearch™ (Veridex) is the only FDA approved technology for CTC enrichment and has been approved for breast, prostate and colorectal cancers. It utilizes functionalized immunomagnetic beads that target tumor specific antigens associated with CTCs, which in most cases is the epithelial cell adhesion molecule, EpCAM. This system has been validated through many clinical reports, however, it suffers from low purity (0.01–0.1%) and poor clinical sensitivity; recent data has shown that 7/9 normal-type breast cancer cell lines could not be recovered using the CellSearch system. [22, 23] In addition significant sample preprocessing is required and the assay cost is prohibitively high. Thus, new technologies that can provide higher CTC sensitivity and specificity as well as automate the entire processing pipeline from CTC selection to enumeration are needed.

CellSearch typically recovers fewer CTCs from clinical samples than newer platforms, such as those based on microfluidics, [24] which can directly process whole blood and search for CTCs with high recovery. [25-31] Microfluidic devices are attractive platforms for the analysis of CTCs for several reasons: (i) they can be configured to select CTCs based on several different modalities including biological cell properties, such as expression of antigens specific to the CTC type or physical cell properties, such as size. [32] (ii) Microfluidic chips operate in a closed architecture, minimizing the potential of sample contamination artifacts that may provide false positive results, especially in clinical laboratory settings. (iii) Microfluidic devices can be produced in a high production mode and at low-cost. For example, devices can be produced in thermoplastics using micro-replication, the same technology used to produce

consumables such as CD and DVDs. [29, 33, 34] (iv) CTC selection devices can be integrated to other processing steps to fully automate sample processing negating the need for operator intervention and thus, minimizing false negative results.

Challenges with microfluidics include the high surface-to-volume ratio associated with these devices requiring special attention to engineer surfaces that reduce non-specific adsorption artifacts, especially when dealing with clinical samples such as whole blood. Also, microfluidics are many times incompatible with high throughput processing; for typical volume flow rates of 300 nL/min (50 x 50  $\mu\text{m}^2$  microchannel cross-section, 0.2  $\text{cm s}^{-1}$  linear velocity), 3,333 min (55.5 h) would be required to exhaustively process 1 mL of sample.

A common physical cell property used to enrich CTCs is based on differences in the size of a CTC compared to that of erythrocytes and leukocytes. Generally, these devices demonstrate very high throughputs (1 mL/min) but low purity. [35-40] For example, Hosokawa *et al.* reported a microcavity array device with circular pores possessing dimensions of 8.4  $\mu\text{m}$  – 9.1  $\mu\text{m}$  that could use flow rates of 0.2 – 1 mL/min with recoveries of 85%. [41] The device also demonstrated substantial amounts of leukocyte infiltration within the enriched samples; 1,000 – 3,000 per mL of processed blood. In addition, to secure high recoveries using size selection, the cells must be fixed prior to filtration, negating the ability to culture selected cells.

Microfluidic devices using affinity-based assays (*i.e.*, positive selection or biological cell property enrichment) typically demonstrate higher purities compared to their size-based counterparts, but at the expense of throughput. [29, 30, 33, 34, 42] CTC

affinity beds configured in microfluidic platforms have employed a variety of geometrical configurations (arrays of microposts, high aspect ratio microchannels) and fluid dynamics to optimize recoveries. [29, 30, 33, 34] Low throughputs result from the necessity of using low linear velocities imposed by the limitation set by the maximum shear forces that selected cells can withstand without being stripped from the selection surface. In addition, certain flow velocities must be employed to promote highly efficient antigen/antibody interactions. [29, 30] For example, a CTC chip utilizing a staggered arrangement of microposts produced a recovery of 65% at low shear ( $0.4 \text{ dynes/cm}^2$ ) with a throughput of 1 mL/h. [30] Other geometries have employed herringbone channels to induce chaotic mixing leading to recoveries on the order of 91% and purities from 9% to 14%. [43] Recently, a nanotextured herringbone device consisting of silicon nanopillars poised on a fluidic channel was reported. [44] A flow rate of 1 mL/h was used for CTC selection from clinical samples. Adams and coworkers utilized sinusoidal high aspect ratio microchannels to reduce pressure drops and increased throughput to 1.6 mL/h. A recovery of MCF 7 cells spiked into blood was reported to be 97%.

Irrespective of the CTC selection modality employed, the enumeration process, which consists of staining the selected cells with DAPI, anti-CD45 antibodies and a cytokeratin cocktail, has been difficult and tedious to undertake requiring imaging of large areas and, in some cases, several imaging planes. For example, using a positive selection CTC microfluidic device developed by our group, [29] 6 h of imaging time was required using a confocal microscope to enumerate the cells based on staining results, cell morphology and the nuclear-cytoplasmic ratio. As another example, Stott *et al.*

reported a total scan time of 8 h for a CTC microfluidic chip utilizing positive selection. [43] Another challenge that has been observed for CTC assays is that some epithelial cancers do not show high sensitivity to the CTC assay, for example pancreatic cancer. Pancreatic ductal adenocarcinoma, or PDAC, is one of the deadliest forms of pancreatic cancer and the fourth-leading cause of cancer-related deaths worldwide. According to the National Cancer Institute, it is one of the most prognostically unfavorable human cancers with the rate of incidence nearly equal to the rate of mortality. [45-48] Newly diagnosed patients have a median survival of 6 months and a 5-year survival rate of only 3 – 5%. Unfortunately, minimal advances have been made to improve patient outcome in PDAC over the past 20 years primarily because of failures at the diagnostic level. CTCs for this disease could be attractive biomarkers to manage this type of cancer. Unfortunately, several CTC technologies provide low clinical yields for this disease. For example, the CellSearch system demonstrated clinical CTC yields for metastatic PDAC patients in the range of 0-1 per 7.5 mL of blood using EpCAM-positive selection. [49, 50] With sized-based selection, the median yields are slightly higher (~9 CTCs per 7.5 mL) but at the expense of purity. [51, 52] Recently, a micro-pillar-based CTC fluidic device has generated fairly high yields of CTCs for PDAC patients when using anti-EpCAM antibodies as the selection marker. [30]

Herein we present a novel platform for the selection and subsequent analysis of CTCs directly from blood samples using a modular microfluidic system to achieve high throughput required for clinical sample processing, high recovery, high purity and full process automation with a short assay turnaround time. The three main components of

the modular system included: (i) A high throughput (HT) CTC selection module used for the affinity enrichment of CTCs with high recoveries and purities; (ii) an impedance sensor module for label-free enumeration; and (iii) a staining and imaging module for placing the CTCs in a small viewing area to reduce imaging time. The HT-CTC selection module consisted of a parallel network of high aspect ratio curvilinear channels (30  $\mu\text{m}$  wide and 150  $\mu\text{m}$  deep) arranged in a z-configuration. The z-configuration occupied a smaller footprint compared to our previously reported CTC selection device and allowed for uniform addressing of a large number of parallel microchannels. This module could be scaled from 50 to 320 microchannels depending on the blood volume processing needs while keeping the processing time below 45 min irrespective of the input volume. As a prescreening tool, we included an impedance sensor module that utilized two orthogonally placed Pt electrodes to enumerate CTCs released from the selection module. The third module, referred to as the staining and imaging module, was used for collection, staining, and visualization of the selected cells for phenotype identification. It consisted of a 2D array of 800 triangular-shaped microfabricated pores with dimensions of 8  $\mu\text{m}$  by 6  $\mu\text{m}$ . This module eliminated the arduous task of scanning large area selection beds by indexing CTCs within a small area and a single imaging plane. The clinical utility of this modular microsystem was tested using blood samples from PDX (patient derived xenograft) mouse models and from patients with local resectable and metastatic PDAC.

## 2.2 Experimental

### 2.2.1 Materials

Pt wires (75  $\mu\text{m}$  diameter) were purchased from Sigma-Aldrich (St. Louis, MO). COC (Topas 6013S-04) plates (1/8" thick) and films (250  $\mu\text{m}$  thick) were acquired from Topas Advanced Polymers, Florence KY. 1/8" thick PMMA hot embossing stock was acquired from SABIC Polymershapes (Raleigh, NC). 250  $\mu\text{m}$  thick PMMA films used as the imaging module cover plates were purchased from Goodfellow Corporation (Oakdale, PA). PEEK tubing and connectors were purchased from IDEX Health & Science (Oak Harbor, WA). Chemicals used for PMMA and COC surface cleaning and modification included reagent grade isopropyl alcohol, 1-ethyl-3-[3-dimethylaminopropyl] carbodiimide hydrochloride (EDC), N-hydroxysuccinimide (NHS), fetal bovine serum, and 2-(4-morpholino)-ethane sulfonic acid (MES) all of which were acquired from Sigma-Aldrich. Monoclonal anti-EpCAM antibody was obtained from R&D Systems (Minneapolis, MN). Tris-glycine buffer was obtained from Bio-Rad Laboratories (Hercules, CA). PBS buffer and trypsin from porcine were purchased from Sigma-Aldrich. For CTC immunostaining, the nuclear stain DAPI was obtained from Thermo Pierce Technologies (Rockford, IL). Anti-CD45-FITC antibody (HI30 clone) and anti-cytokeratin antibodies (8/19 conjugated to Texas Red) were purchased from eBiosciences (San Diego, CA). Bovine serum albumin (BSA) in PBS buffer (pH 7.4) was secured from Sigma-Aldrich. MEM-non essential amino acids were obtained from GIBCO (Grand Island, NY GEAA).

## **2.2.2 Fabrication of Microfluidic Modules**

The CTC processing system (see Figure 2.1) consisted of three separate, task-specific polymer modules: (1) HT-CTC selection module; (2) impedance sensing module; and (3) the staining and imaging module. Hot embossing and laser ablation were used as the primary tools for fabrication of the polymer fluidic modules as described previously.<sup>53</sup> Hot embossing mold masters were prepared in brass using high precision-micromilling (KERN 44, KERN Micro- und Feinwerktechnik GmbH & Co.KG; Murnau, Germany) and standard carbide bits (Performance Micro Tool, Janesville, WI).<sup>53</sup> Hot embossing of polymer modules was performed using a HEX03 embossing machine (Jenoptik Optical Systems GmbH, Jena, Germany). The embossing conditions consisted of a temperature of 155°C and 30 kN force for 120 s for cyclic olefin copolymer, COC, substrates and 160°C and 20 kN force for 240 s for poly(methylmethacrylate), PMMA, substrates. Laser milling was done using an ArF excimer laser (Rapid X 250, Resonetics Inc., Nashua, NH) with a laser fluence at the workpiece of ~15 J/cm<sup>2</sup> and a repetition rate of 50 Hz.

## **2.2.3 HT-CTC Selection Module**

The HT-CTC module (see Figure 2.2) was made from the thermoplastic, cyclic olefin copolymer, COC, due to its ability to be embossed with high aspect ratio microstructures, its optical clarity, its propensity to be UV functionalized with high efficiency irrespective of channel aspect ratio, and the minimal amounts of non-specific



adsorption of leukocytes it demonstrated providing high purity levels of enriched CTCs from whole blood. 54

The HT-CTC module consisted of an array of high-aspect ratio sinusoidal microchannels with a nominal width of 30  $\mu\text{m}$  and depth of 150  $\mu\text{m}$  serving as the CTC selection bed. Selection beds were addressed using a single inlet and outlet microchannel arranged in a unique z-configuration. The selection bed employed 50 to 320 sinusoidal microchannels with the maximum number of channels set by the maximum length of the chip, which was chosen to be 75 mm to match the length of a standard microscope slide, and the smallest channel-to-channel spacing that was machineable.

After hot embossing, the HT-CTC module and cover plate were flood exposed to broad band UV light at  $\sim 22 \text{ mW/cm}^2$  (measured at 254 nm) for 15 min using a home-built system employing a low pressure Hg grid lamp (GLF-42, Jelight Company Inc., Irvine, CA). UV exposure produced carboxylic acid surface scaffolds that were used for the covalent attachment of monoclonal antibodies for CTC selection (anti-EpCAM antibodies).<sup>55, 56</sup> After UV exposure, the substrate was enclosed with a cover plate by Thermal fusion bonding at a temperature of 132°C and a bonding pressure of  $\sim 1 \text{ N/cm}^2$ . Bonding conditions were carefully selected to achieve high bond strength, but preserve structural integrity of the high-aspect ratio microchannels.

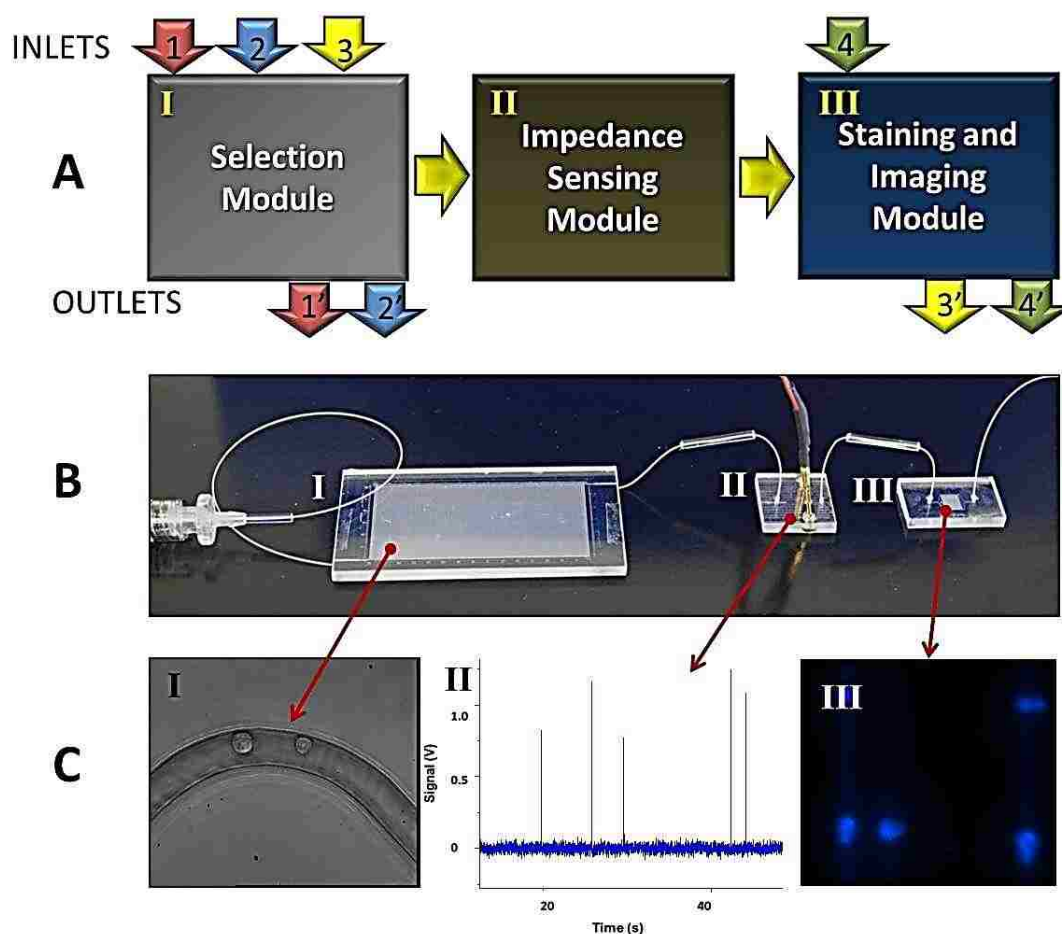


Figure 2.1 Modular microfluidic system for CTC analysis. (A) Schematic representation of the operation of the system and the three modules comprising the system including the HT-CTC module, the impedance sensing module and the staining and imaging module. Arrows indicate flow of sample (1 and 1'), wash buffer (2 and 2'), CTC release buffer (3 and 3'), and fixation and staining reagents (4 and 4'). For detailed operational procedures please refer to the Experimental Section. (B) Picture of the assembled system. Roman numerals correspond to modules described in (A). (C) Micrographs and data plots showing the various outputs of the three different task-specific modules including: (I) HT-CTC selection module, which used anti-EpCAM-coated sinusoidal microchannels for the positive selection of CTCs; (II) electrical signatures of CTCs obtained using the impedance sensor module; and (III) images of CTCs stained with DAPI and collected at the staining and imaging module.

After assembly, the surface of the microfluidic channels was modified using EDC-NHS chemistry. This consisted of 50 mg/mL EDC (1-Ethyl-3-[3-dimethylaminopropyl]carbodiimide hydrochloride), 5 mg/mL NHS (N-hydroxysuccinimide) in 100 mM MES (pH 6), followed by incubation with a solution of anti-EpCAM monoclonal antibodies (0.5 mg/mL; 150 mM PBS buffer, pH 7.4) overnight at 4°C. The optimum concentration of the antibody was chosen based on studies to optimize CTC recovery (see Figure 2.5).

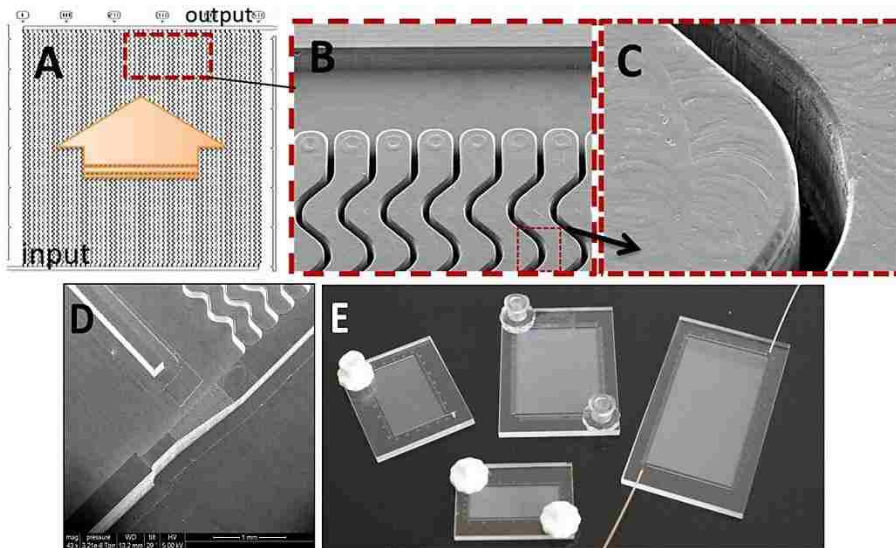


Figure 2.2 (A) Schematic operation of the HT-CTC module with 50 parallel, sinusoidal microchannels and inlet/outlet channels arranged in the z-configuration. The large arrow indicates sample flow direction through the selection channels. (B) SEM of the selection bed showing high-aspect ratio sinusoidal microchannels and the output channel (top). (C) SEM of one of the high-aspect ratio sinusoidal channels. (D) SEM image of a portion of the high-precision micromilled brass molding tool showing the sample inlet port with continuously changing width and height for minimizing unswept volumes during sample (*i.e.*, blood) introduction. (E) Assembled HT-CTC modules with different numbers of microfluidic sinusoidal channels designed for efficient processing of various sample volumes

#### **2.2.4 Evaluation of Flow Uniformity in HT-CTC Selection Bed**

Video microscopy was used to study the uniformity of the linear flow velocities through the HT-CTC selection bed with inlet and outlet all arranged in z-configuration. The HT-CTC chip with 320, 20 mm long sinusoidal microchannels was used for these experiments. The experimental setup for these measurements consisted of a syringe pump connected to the HT-CTC chip through a manual HPLC sample injector equipped with a 20  $\mu\text{L}$  volume sample loop. During measurements, buffer solution was continuously pumped through the HT-CTC chip at volumetric a flow rate of 176  $\mu\text{L}/\text{min}$ , which produced an average linear flow velocity in the sinusoidal microchannels of 2 mm/s. Aliquots of 20  $\mu\text{L}$  of red food dye were injected into the clear buffer solution and the time required for the dye plug to travel from the inlet channel to the outlet channel was then recorded. Because monitoring of the filling time for individual channels was not feasible due to the overall size of the chip and the limited optical resolution of our video recording system, the chip was divided into 16 observation windows with roughly 20 selection microchannels per window and an average filling time was recorded for each window. The recorded times were divided by the channel length (20 mm) to obtain the average linear velocity as presented in Figure 2.4C.

#### **2.2.5 Impedance Module**

The impedance sensing module, which was made in poly(methylmethacrylate), PMMA, and consisted of two perpendicular microchannels. A microchannel with dimensions of 50  $\mu\text{m}$  width x 75  $\mu\text{m}$  depth served as a conduit for cells flowing through

this module. The second microchannel ( $75 \times 75 \mu\text{m}^2$ ) was used as guides to place two Pt wires, which were used as electrodes for making the single-cell impedance measurements. Impedance measurements were conducted using previously described circuitry. [29] Data were collected and analyzed using a NI-USB-6009 (National Instruments) data acquisition board and software written in LabView (National Instruments). Data were collected at 2 kHz, which allowed for sample processing through the sensor at a maximum flow rate of  $20 \mu\text{L}/\text{min}$  ( $80 \text{ mm}/\text{s}$ ) without generating signal aliasing. The raw output data was subjected to a 1,000 point adjacent averaging algorithm to establish the baseline for the measurement without generating signal bias. Baseline was then subtracted from the data in order to correct for signal drift.

### **2.2.6 Staining and Imaging Module**

The design of the staining and imaging module is presented in Figure 2.3. It consisted of two independent microchannel networks, one consisting of an array of smaller microchannels laser machined into the module cover plate and a second set of fluidic channels embossed into the substrate, which consisted of interleaving input/output channels of larger cross section. The smaller channels on the cover plate were positioned perpendicular to the interleaved input/output channels contained within the substrate. The input/output channels ( $50 \mu\text{m}$  depth; varying width) were hot embossed into PMMA using a high precision micromilled mold master. Laser ablation was used to fabricate the array of smaller microchannels into a thin PMMA film serving as the module cover plate. Both parts were thermal fusion bonded at  $106^\circ\text{C}$  and a

pressure of  $\sim 3 \text{ N/cm}^2$  with the patterned surfaces facing each other. The staining and imaging module possessed 800 pores arranged in a 2D matrix and spaced by  $100 \mu\text{m}$

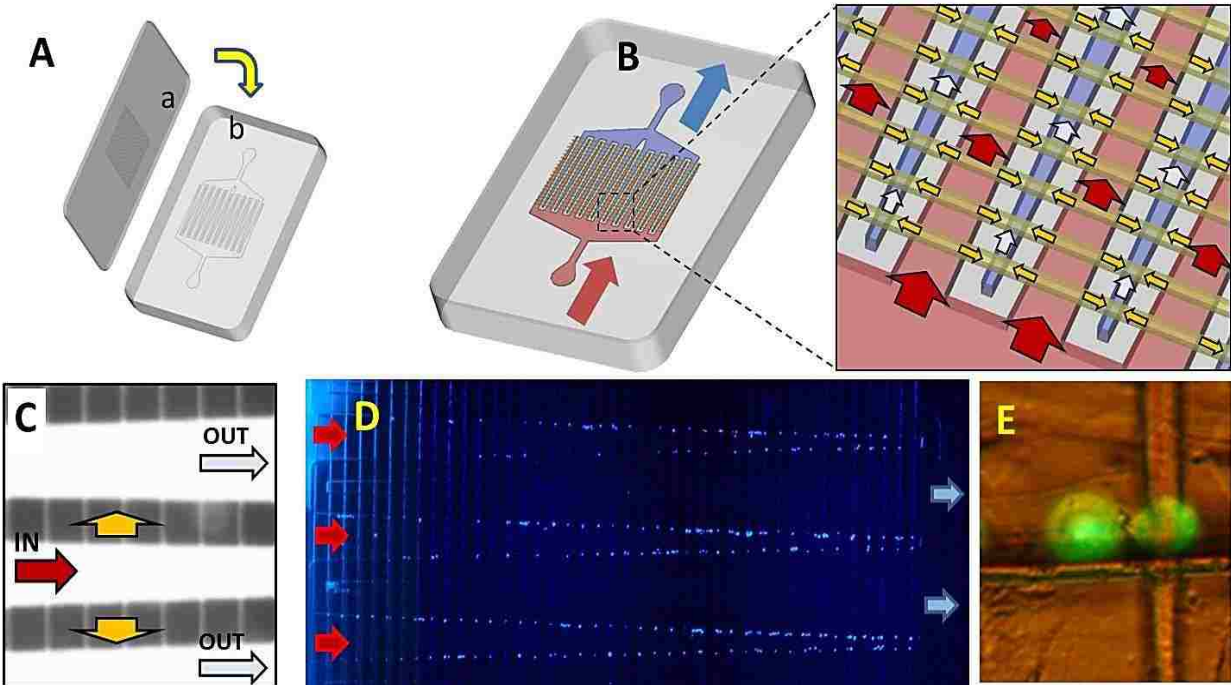


Figure 2.3 Staining and imaging module. (A) Assembly process; (a) – cover plate with an array of  $8 \times 6 \mu\text{m}^2$  channels, which form pores for retaining cells between the interleaving inlet and outlet channels (b). (B) Schematic of an assembled module and its operation; Red – input channels; Blue – output channels; Yellow – interconnecting channels. (C) Image of the staining and imaging module filled with fluorescein. The lower fluorescence intensity in the interconnecting channels is due to the smaller cross-sectional area of these channels compared to the input/output channels. (D) Fluorescence image of CTCs retained by pores. The cells were stained with DAPI for visualization. (E) High magnification fluorescence image of Hs578T cells retained at the pore structures of the staining and imaging module. These cells were stained with PKH67 lipid membrane green fluorescent dye for visualization.

Addressing of the microfluidic networks and connection between modules was accomplished using glass capillaries (Polymicro Technologies, Phoenix, AZ) affixed to inlet and outlet ports of each module via epoxy (Permapoxy, Permatex, Hartford, CT).

Capillaries were connected to each other using low dead volume interconnects secured from Polymicro.

### **2.2.7 Cell Culture**

MCF-7 (breast), Hs578T (breast) and SW620 (colorectal) cancer cell lines were purchased from American Type Culture Collection (ATCC, Manassas, VA) and cultured according to recommended conditions. Briefly, all cell lines were incubated at 37°C under a 5% CO<sub>2</sub> atmosphere. Eagles minimum essential medium (MCF-7 and Hs578T) and Dulbecco's minimum essential medium (SW620s) containing 1.5 mM L-glutamine supplemented with 10% FBS (GIBCO, Grand Island, NY) was used. A 0.01mg/mL solution of bovine insulin (GIBCO, Grand Island, NY) was added to the complete growth media for the MCF-7 cells. The Hs578T cell line required 1X non-essential amino acids to complete the final growth medium. The cell lines were grown as adherent monolayers in T75 culture flasks (Corning) to 80-95% confluence with media changes every 2-3d. Cells were washed in a flask with Dulbecco's phosphate buffered saline, DPBS (GIBCO, Grand Island, NY), dissociated by using TrypLE™ Express (1X) (GIBCO, Grand Island, NY) at 37°C for 5-7 min and subsequently seeded into culture flasks at a low concentration.

### **2.2.8 Patient Samples**

Patients with pancreatic cancer were recruited according to a protocol approved by the University of North Carolina's IRB. Blood specimens from healthy volunteers were collected under a separate IRB-approved protocol. A total of 8 patients with known

metastatic PDAC and 6 patients with non-metastatic PDAC were used as positive controls. Five non-cancer patients also served as negative controls. All specimens were collected into BD Vacutainer® (Becton-Dickinson, Franklin Lakes, NJ) tubes containing the anticoagulant EDTA and were processed within 5 h of the blood draw.

### **2.2.9 Patient-derived Xenograft (PDX) Models**

Tumors from de-identified PDAC patients were grafted onto the flanks of immunocompromised mice under approval by the Institutional Animal Care and Use Committee. Terminal bleeds were obtained via cardiac puncture. Blood samples from the PDX models were then analyzed using the microfluidic system.

#### **2.2.10 Staining Procedure**

The staining protocol was as follows: 0.25% BSA in PBS buffer (pH 7.4) was infused through the staining and imaging module at a flow rate of 20  $\mu\text{L}/\text{min}$ . Next, 100 $\mu\text{L}$  of 0.0025mg/mL anti-human CD45-FITC was infused at a flow rate 10  $\mu\text{L}/\text{min}$  and allowed to incubate at 4°C followed by a 5 min wash with 0.02%TX-100/PBS at 20  $\mu\text{L}/\text{min}$ . For fixation and permeabilization, 2-4% paraformaldehyde in PBS buffer was infused at a flow rate of 15  $\mu\text{L}/\text{min}$  followed by 0.1%TX-100 in PBS buffer at the same flow rate. Next, 100  $\mu\text{L}$  of 0.01mg/mL anti-cytokeratins 8/19 labeled with Texas Red was infused at 10  $\mu\text{L}/\text{min}$  and incubated at 4°C followed by a 10 min wash consisting of 0.25%BSA in PBS at 20  $\mu\text{L}/\text{min}$ . For nuclear staining, 0.001mg/mL DAPI in PBS was infused at a flow rate of 15  $\mu\text{L}/\text{min}$  followed by a wash with 0.25% BSA in PBS.



### 2.2.11 HT-CTC Module Operation

Prior to analysis of all samples, the HT-CTC selection module was thoroughly washed with PBS buffer at a flow rate of 40  $\mu\text{L}/\text{min}$  for at least 5 min in order to remove unbound antibody from the microchannel walls. Blood specimens collected into BD Vacutainer® tubes were placed on a nutator for at least 10 min to allow for homogenous distribution of blood components. Following homogenization, 3 mL of patient blood or approximately 1 mL of PDX blood was transferred into a disposable Luer Lok™ syringe (BD Biosciences, Franklin Lakes, NJ) using a BD vacutainer female luer transfer adapter. Immediately after transfer, blood samples were processed through the HT-CTC selection module. A PHD2000 syringe pump (Harvard Apparatus, Holliston, MA) was used to hydrodynamically drive the blood through the HT-CTC selection module at the appropriate volume flow rate to attain an optimal average linear velocity of sample through the sinusoidal microchannels (2 mm/s) to maximize recovery.[29] During the course of blood sample introduction, the syringe was rotated by 180° along its longitudinal axis and lightly tapped in order to prevent sedimentation of the blood components inside the syringe to assure exhaustive and representative sample introduction. Finally, the HT-CTC selection bed was flushed with 2.5 mL of PBS at a linear velocity of 4 mm/s to remove any nonspecifically bound cells.

During blood infusion into the HT-CTC module and the subsequent washing step, the output capillary to this module was disconnected from the impedance sensing module and inserted into a microfuge tube for waste collection. When the release buffer, which contained trypsin, was introduced into the HT-CTC module, the output capillary

was reconnected to the impedance sensing module. The output port of the impedance sensing module was connected to the input port of the imaging and staining module (see Figure 2.1).

### **2.2.12 Operation of the Integrated System and Data Collection and Analysis**

All three modules were connected in series using glass capillaries (see Figure 2.1). Following HT-CTC module washing, 200  $\mu\text{L}$  of the CTC release buffer consisting of 0.25% w/v trypsin in 25 mM TRIS/192 mM glycine buffer (pH 7.4) was infused through the HT-CTC selection module to allow for the release of CTCs from the antibody-containing selection channels and into the downstream processing modules. As the CTCs traversed through the impedance sensor, an electrical signal was recorded using in-house designed and built electronics as described previously. [29] The raw output data was subjected to a 1,000 point adjacent averaging algorithm to establish the baseline for the measurement without generating signal bias. Baseline was then subtracted from the data in order to correct for signal drift. Impedance responses generated from CTCs were counted when the signal-to-noise ratio exceeded 3:1. Cells counted were directed into the staining and imaging module for staining with fluorescently labeled markers including cytokeratins 8/19, the nuclear stain (DAPI), and a negative control consisting of FITC labeled anti-CD45 antibodies.

The staining protocol was as follows: 0.25% BSA in PBS buffer (pH 7.4) was infused through the staining and imaging module at a flow rate of 20  $\mu\text{L}/\text{min}$ . Next, 100  $\mu\text{L}$  of 0.0025 mg/ml anti-human CD45-FITC was infused at a flow rate 10  $\mu\text{L}/\text{min}$  and allowed to incubate at 4°C followed by a 5 min wash with 0.25% BSA/PBS at 20  $\mu\text{L}/\text{min}$ . For

fixation and permeabilization, 2-4% paraformaldehyde in PBS buffer was infused at a flow rate of 15  $\mu\text{L}/\text{min}$  followed by 0.1%TX-100 in PBS buffer at the same flow rate. Next, 100  $\mu\text{L}$  of 0.01 mg/ml anti-cytokeratins 8/19 labeled with Texas Red was infused at 10  $\mu\text{L}/\text{min}$  and incubated at 4°C followed by a 10 min wash consisting of 0.25% BSA in PBS at 20  $\mu\text{L}/\text{min}$ . For nuclear staining, 0.001 mg/ml DAPI in PBS was infused at a flow rate of 15  $\mu\text{L}/\text{min}$  followed by a wash with 0.25% BSA in PBS.

The stained cells were imaged using an inverted Olympus 1X71 microscope (Center Valley, PA) using 10x, 20x, 40x, and 60x dry objectives equipped with a high resolution (1344 x 1024) CCD camera (Hamamatsu ORCA-03G) and a mercury arc lamp as an illumination source. Images were collected using 40 $\times$  (0.6 NA) and 60 $\times$  (0.7 NA) dry lens objectives and analyzed using Metamorph software (Olympus). Exposure times for the DAPI, FITC/CD45, and Texas Red/CK channels were 50, 600, and 600 ms, respectively.

Statistical analysis was performed using the Kruskal-Wallis Test ( $p = 0.05$ ) for three sample groups of healthy, non-metastatic and metastatic PDAC patients. For pairwise test analysis, Wilcoxon Rank-Sum ( $p = 0.05$ ) was applied..

## **2.3 Results and Discussion**

### **2.3.1 HT-CTC Module**

The HT-CTC module utilized COC as the substrate material. COC demonstrates higher UV transmissivity compared to PMMA, therefore generating a higher surface density of carboxylic acid groups on channel walls. These surface-confined carboxyl

groups serve as functional scaffolds for the attachment of CTC recognition elements. [53, 54] Higher UV transmission also resulted in a more uniform modification of the high-aspect ratio microchannel walls when made from COC. COC also demonstrated higher CTC purities due to lower non-specific adsorption of hematopoietic cells to its surface compared to PMMA. [54]

Considering the requirements for the microfluidic channel geometry and linear velocity of the sample through the selection channels to maximize recovery, [29] it was clear that higher throughput could be achieved by either increasing the number of parallel microchannels or increasing the depth of the microchannels without changing the width. For results reported herein, we used larger number of parallel channels as a method for increasing throughput. For example, the previously reported device used 51 parallel channels (cross-section  $30\ \mu\text{m} \times 150\ \mu\text{m}$ ) and could process 1 mL of whole blood in 37 min. Thus, it would take nearly 4.7 h for this device to process 7.5 mL. By increasing the number of channels to 320, 7.5 mL input volumes could be processed in <45 min using an average linear velocity of 2 mm/s.

To uniformly address all parallel channels within the selection bed employing large numbers of parallel sinusoidal channels, we adopted a unique z-configuration (Figure 2.2). In this configuration, fluid enters the selection bed through a single inlet channel with a larger cross-sectional area and exits through a single outlet channel also possessing a larger cross-section compared to the sinusoidally-shaped selection channels (see Supporting Information). Both inlet and outlet channels were perpendicular to an array of high aspect ratio channels comprising the selection bed

(Figure 2.2A). The z-configuration provides the smallest possible footprint for addressing the isolation bed and allows for easy scaling of the CTC isolation bed size. For example, in a recently proposed fluidic design for neutrophil isolation [55], bifurcation was used for addressing parallel channels of the isolation bed, which nearly doubled the footprint of the proposed device in order to allocate space for the fluid distribution network. Furthermore, compared to previously reported design, [29] the high linear fluid velocities in the inlet and outlet channels of z-configuration allow for more efficient removal of persistent air bubbles that are inevitably introduced into device architectures during operation and may interfere with the fluid flow.

Uniformity of the fluid flow in z-configuration is highly dependent on the flow resistance ratio between the inlet/outlet channels and the flow resistance in the parallel channels. In general, wider (lower fluidic resistance) inlet channels and longer and/or narrower (higher fluidic resistance) parallel channels show higher flow uniformity throughout the array. Inhomogeneity of the flow rate is exacerbated by the number of parallel channels in the array. As seen in Figure 2.4A, a parabolic fill profile was observed over the entire selection bed during filling. Qualitatively, if each channel of the array was filling under a constant linear velocity, the filling profile of the array should show a linear gradient.

To evaluate flow uniformity in the CTC selection beds with various numbers of sinusoidal channels and for various lengths of the selection bed, we performed numerical simulations to establish average linear velocities of fluid in individual

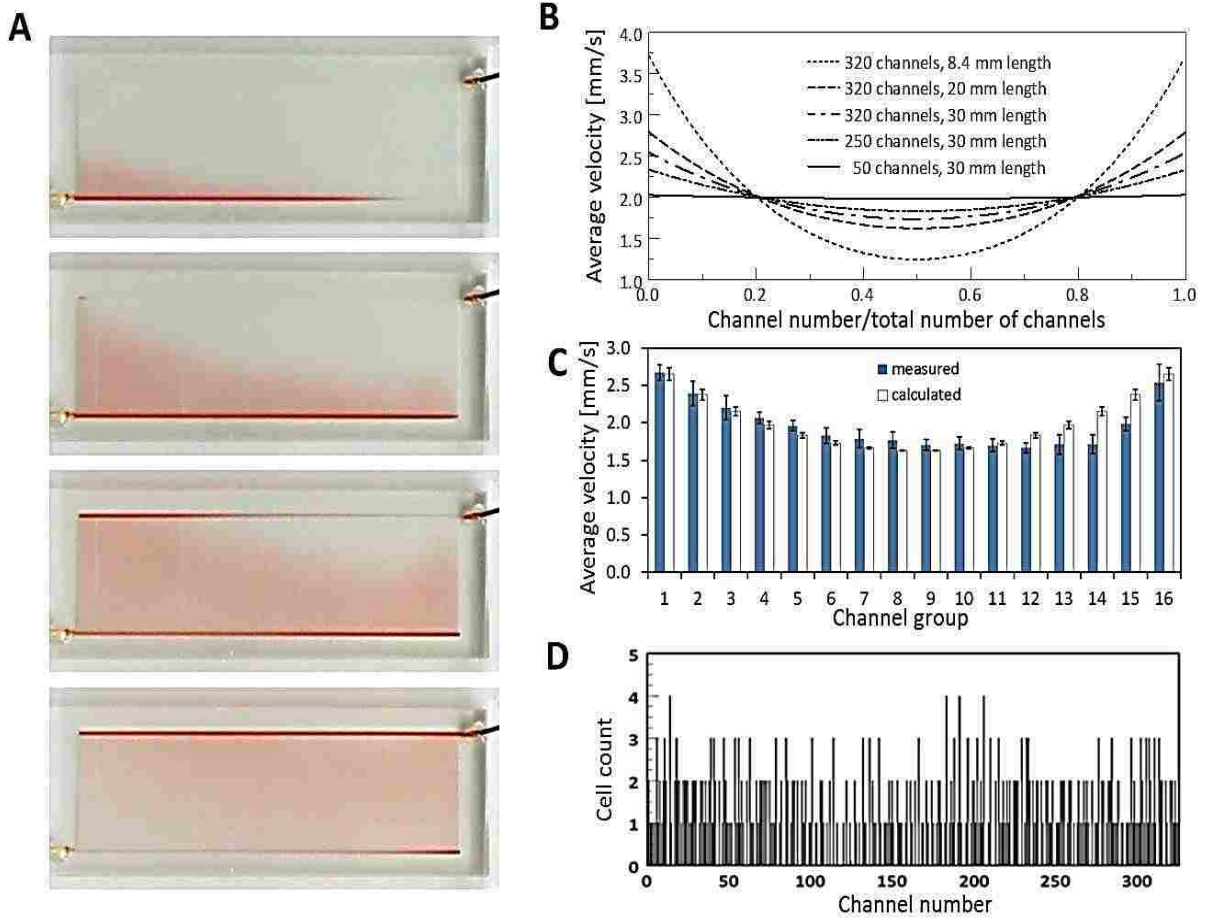


Figure 2.4 (A) Various stages of filling a 320-channel HT-CTC module (20 mm length) with a dye solution. (B) Numerical simulation results showing the distribution of flow velocities for different configurations of the CTC selection beds arranged in a z-configuration. (C) Average linear velocity of fluid in 16 groups of 20 adjacent sinusoidal high aspect ratio microchannels based on the results depicted in Figure 2.4A (filled bars) and theoretical values obtained via numerical simulation (empty bars). (D) Distribution of cells selected in 20 mm long microchannels

sinusoidal microchannels. Due to the numerical limits of simulating large geometries using computational fluid dynamics (CFD), we employed a method described by Zhang and coworkers. [56] This method splits the selection bed into an interconnected system

of individually defined parallel channels and the addressing inlet/outlet channels. Each channel segment was treated as a fluidic resistor, and the flow dynamics through the entire system was described by pressure and mass balance equations. [56]

Figure 2.4B presents solutions for microfluidic selection beds with 50, 250 and 320 channels possessing dimensions of  $0.03 \times 0.15 \times 30 \text{ mm}^3$  along with the results for 320 channels with varying lengths of 30, 20 and 8.4 mm. As can be seen from this data, for the 320 channel device with 8.4 mm selection channel lengths, the maximum and minimum flow velocities fall outside the range of 1 mm/s – 4 mm/s, a range that was determined to provide CTC recoveries >80%. [29] However, when using 320 channels and incorporating a length of 30 mm, the average flow velocity remains within an acceptable range for maximum CTC recovery. The simulated results were also confirmed experimentally (Figure 2.4C). The results indicated good agreement with the simulation results; the slowest flow rates were observed in the middle and fastest at the outer channels with an RSD of 16%. We also evaluated the distribution of selected MCF-7 cells inside a HT-CTC bed modified with anti-EpCAM antibodies. MCF-7 cells (~500) labeled with a PKH 67 fluorescent membrane dye were spiked into normal blood and processed using the selection bed comprised of 320 channels and the numbers of MCF-7 cells per channel were counted using a fluorescence microscope. Figure 2.4D shows the selected cell distribution within individual channels. A uniform distribution of cells across the entire series of microchannels occurred with most of the channels capturing 1 or 2 cells and only a few capturing 3 - 4 cells or no cells at all. The overall average CTC recovery for these experiments was  $83.1\% \pm 5.2\%$  ( $n = 4$ ). Selection beds

with at least 30 mm channel lengths were necessary to achieve recoveries >90% (see section on the effect of bed length on recovery).

### **2.3.2 Optimization of anti-EpCAM Antibody Concentration**

In order to increase the probability of interaction between antigens on the CTC surface and selection channel wall bound antibodies, it is critical that there be a maximum coverage of the antibody on the channel walls. On the other hand, the amount of antibody used for the reaction should be kept to a minimum in order to keep the cost of the assay low. The amount of antibody required to produce a monolayer coverage of the walls within the selection bed can be estimated using the following assumptions. Theoretically, a monolayer of an IgG-type antibody has been reported to be on the order of  $1.1 \text{ pmol}\cdot\text{cm}^{-2}$ . [57] For comparison, the surface density of carboxylic acid moieties produced on a polymer surface using UV activation has been reported to be on the order of  $1 \text{ nmol}\cdot\text{cm}^{-2}$ , indicating significant excess of carboxylic acid moieties compared to the surface density of antibodies for a monolayer coverage. [58] In studies previously published by our group describing CTC isolation using polymer microfluidic devices, a relatively high concentration of anti-EpCAM antibody was used (1 mg/mL). [29, 33] For microchannels with cross-sectional dimensions of  $30 \text{ }\mu\text{m}$  wide x  $150 \text{ }\mu\text{m}$  deep, a solution of antibody at 1mg/mL concentration injected into the microchannels provides an amount of antibody corresponding to nearly 10x excess to the theoretical amount required to achieve complete monolayer coverage. One has to also note that the maximum surface coverage is not a single parameter for determining optimal



performance of the CTC recovery process as the activity of surface bound antibodies is important as well. The activity of the antibody is dependent on its conformation on the surface and possible steric effects caused by crowding.

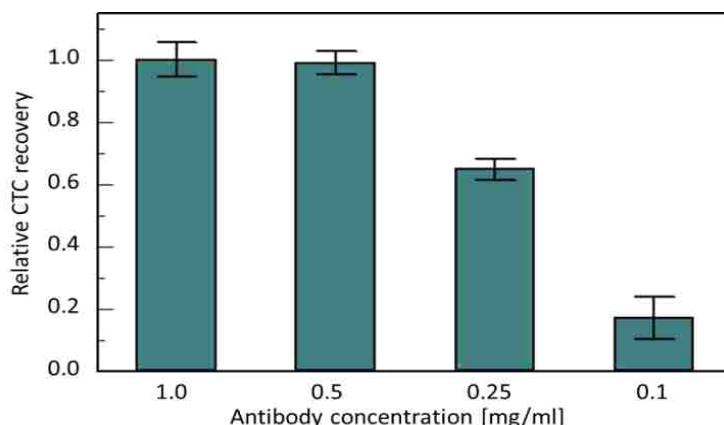


Figure 2.5 Recoveries of MCF-7 cells using selection beds modified with EpCAM antibody at different antibody concentrations. Results were normalized to recovery obtained for antibody concentration of 1 mg/mL.

In order to establish the optimum concentration of anti-EpCAM antibody required during the covalent attachment process to optimize recovery, we evaluated the recoveries of MCF-7 cells obtained using selection beds prepared with different concentrations of antibodies. Figure 2.5 presents a summary of these experiments using beds modified with 1 mg/mL, 0.5 mg/mL, 0.25 mg/mL, and 0.1 mg/mL of anti-EpCAM antibody. As can be seen from this data, there seems to be no difference in recovery when the antibody concentration is reduced 2-fold to 0.5 mg/mL. However, further reductions in the amount of antibody leads to significant drop in the recovery of

the MCF-7 cells. Therefore, the concentration of 0.5 mg/mL was used throughout this work.

### **2.3.3 Effect of CTC Selection Bed Length on Recovery**

We were also interested in evaluating whether the length of the selection channels was critical in regards to CTC recovery. The use of shorter selection channels can reduce pressure drops within the selection channels and require less use of antibody. To evaluate selection bed length on recovery, the location of MCF-7 cells recovered using 8, 20, and 26 mm long beds (320 channels) were recorded and assigned to one of three equidistant zones along the microchannel length (see Figure 2.6). The overall average recovery for beds with 8 mm long channels was 67%, the 20 mm long channels was 83% and the 26 mm length channels was 93%. Inspection of the location of the selected CTCs along the 20 mm length channel bed indicated that 69% of the cells captured were found in a 0-10 mm region of the channel (the 0 coordinate is the input end of the channel), 23% were 10-15 mm region from the inlet and 8% were within the 15-20 mm zone with comparable numbers seen for the other two channel lengths. It is important to note that although the majority of the selected cells were captured within the first half-length of the selection channels, there was still a relatively large number of cells captured in the second half of the channels indicating that shorter selection beds do not provide optimal CTC recoveries. Indeed, evaluation of 8 mm long channels comprising the selection bed produced an overall recovery of 67%. For comparison, the original CTC selection beds employed by Adams, *et al.* [29] used 26 mm long sinusoidal

microchannels and demonstrated recoveries >90% (see Figure 2.6). Therefore, all of the results reported herein used selection beds with channels ~30 mm in length.

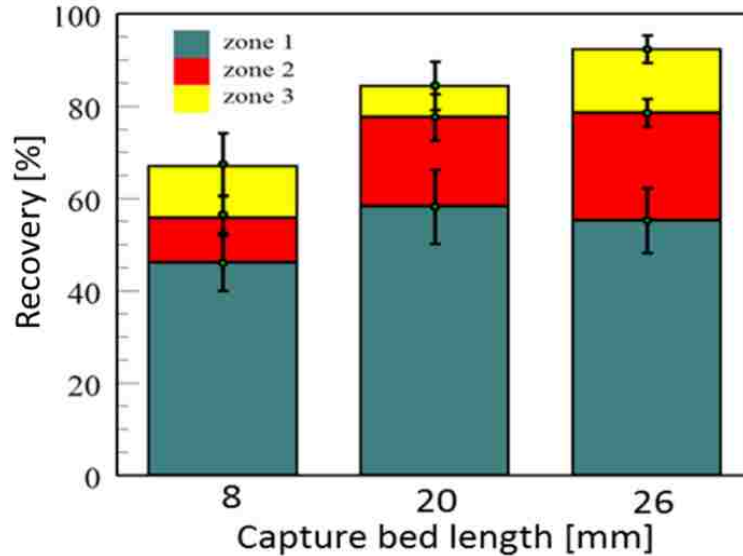


Figure 2.6 Capture efficiencies of MCF-7 cells using isolation beds with varying channel length. Zone 1 first 50% of channel length, zone 2 – 50-75% of channel length, zone – 75 – 100% of the channel length

### 2.3.4 Impedance Sensor Module

The impedance sensor adopted a geometry similar to that reported previously by our group. [29, 33, 59][29] Using this sensor, we were interested in determining the ability to discriminate between leukocytes and CTCs based on size differences, which is the cell characteristic measured at the operating frequency (40 kHz). At this frequency, the amplitudes of signals produced by single cells are dominated by cell size. [59] This module was fabricated in PMMA and consisted of a pair of Pt electrodes placed orthogonally to a 50  $\mu\text{m}$  channel through which released CTCs traversed. Figure 2.7A

provides results for SW620 cells spiked into buffer and traversing through the pair of Pt wires. Also shown are leukocytes that were isolated from a buffy coat of blood secured from a healthy donor and measured using the impedance sensor. There was only a slight overlap in the signal amplitudes between the two cell types with a misclassification frequency of ~15%. Similar results were observed when the cell sizes for the same populations were measured using an optical imaging technique (Figure 2.7B). A 100% concurrence between the impedance sensor response and passing cells were observed when using a microscope to watch the passage of single cells through the pair of electrodes (data not shown). However, because there was some size overlap between CTCs and leukocytes, we could not clearly distinguish between these two cell types based solely on the magnitude of the impedance response. In spite of this limitation, the high purity of our selected CTC fractions from whole blood (>80%, see below) indicates that the leukocyte infiltration is low anyway. Nevertheless, the impedance sensor in its current format can measure signatures from single cells that are unlabeled and thus, can serve as a prescreening tool for assessing the need to immunocytochemically stain for CTCs. If no impedance signals are generated, the sample can be considered negative for CTCs and thus, forgo the need for staining reducing assay cost and operator time.

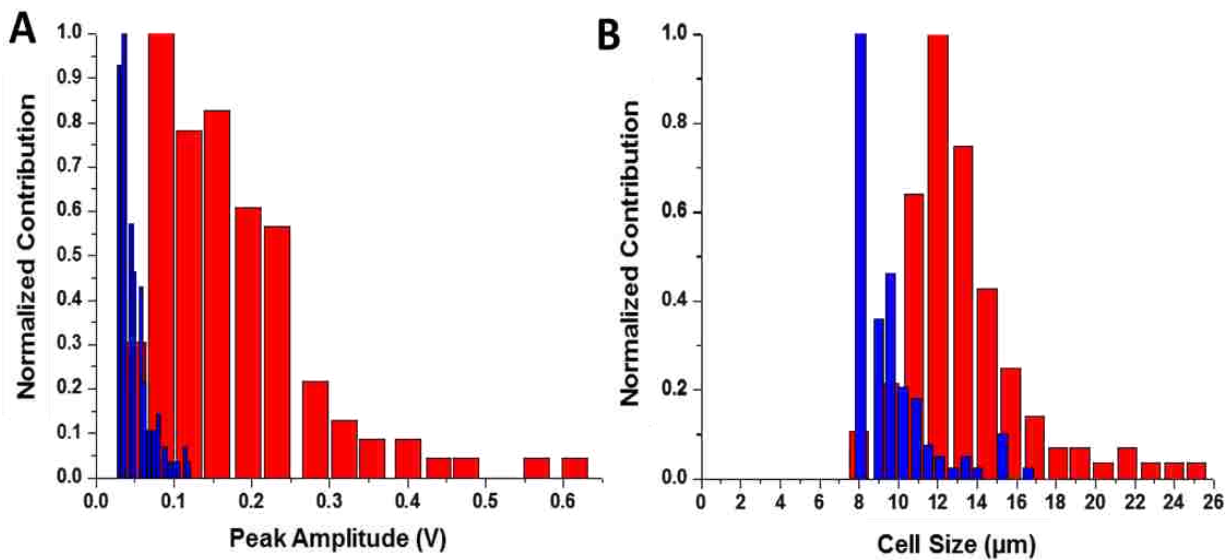


Figure 2.7 Single-cell electrical impedance sensing. (A) Histograms for impedance response for leukocytes (blue bars) and SW620 cancer cells (red bars). (B) SW620 (red bars) and leukocyte (blue bars) cell sizes measured optically

### 2.3.5 Staining and Imaging Module

PMMA was selected as the substrate of choice for the staining and imaging module due to the high quality machining it generated using laser ablation as well as its favorable optical properties. [60] The design and operation of the novel 2D imaging module are shown in Figure 2.3. It consisted of two independent networks of channels; an interleaving input/output channel network interconnected using an array of smaller channels positioned orthogonally to the input/output channels. The interconnecting/feed channel interface generated a pore structure, whose dimensions were determined by the size of the interconnecting channel (8  $\mu\text{m}$  base and 6  $\mu\text{m}$  height). During operation, CTCs released from the primary selection bed were transported through the impedance sensor to the staining and imaging module where they were retained due to their larger

size as compared to the size of the pore. After collection at each pore, CTCs could be fixed, permeabilized, and immunostained directly within the staining and imaging module followed by fluorescence imaging.

The unique geometry of the staining and imaging module offered important benefits: (i) A small footprint ( $0.16 \text{ cm}^2$ ) as compared to the primary selection bed ( $4 \text{ cm}^2$  for the 50-channel z-configuration selection module), which significantly reduced the time required for imaging; (ii) cells are brought to a single focal plane further reducing imaging time; and (iii) the highly ordered configuration of the pores allowed for indexing cell position, which also reduced imaging time.

To validate the performance of the staining and imaging module, we determined the collection efficiency of fixed and unfixed cells at a flow rate that was used to move the released CTCs from the selection channels to the staining and imaging module. We used Hs578ST cells seeded into PBS as a model for these studies. The collection efficiency was defined as the ratio of cells collected at the pores to the number of cells enumerated by the impedance sensor (see Figure 2.9). We determined that for fixed cells, the collection efficiency of the staining and imaging module was  $96 \pm 6\%$  ( $n=5$ ) while for unfixed cells, the collection efficiency was  $85 \pm 11\%$  ( $n=5$ ). The difference in the collection efficiency is indicative of the higher deformability of unfixed cells compared to those that are fixed (see Figure 2.8). [61]

We also found that the cells resident within a pore adhered to the pore structure even when the solution flow was terminated. Therefore, the cells could be trapped at the pore without requiring boundary conditions to contain the cells. Because of this adhesion, we could remove the staining and imaging module from the system and place it on a conventional microscope stage without losing cells from their respective pore location.

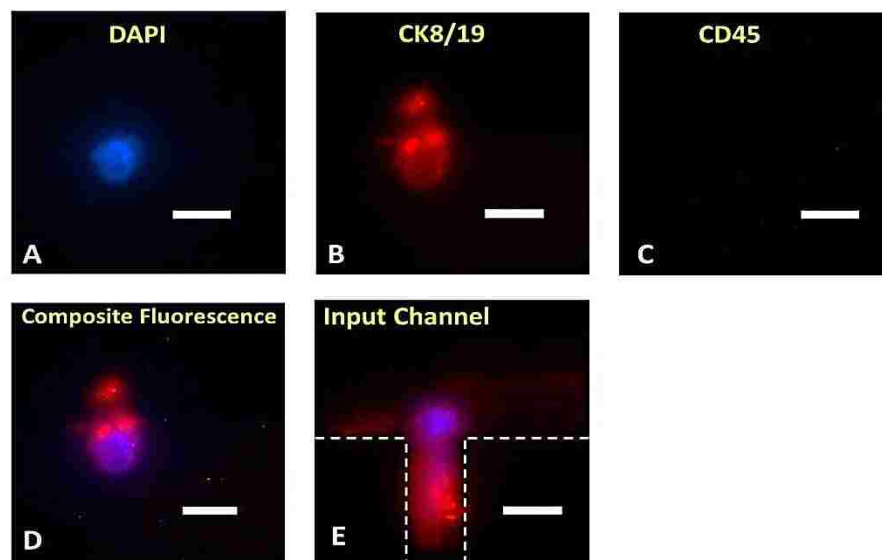


Figure 2.8 Fluorescent images of CTCs collected in the staining and imaging module. (A-D) Images of a CTC from a PDAC patient after being released from the selection bed, impedance counted, and collected at a pore on the staining and imaging module followed by fixation and staining with DAPI, anti-cytokeratin antibodies (8/19) labeled with Texas Red, and FITC-labeled leukocyte antibody marker for CD45. (E) Fluorescent image of a CTC with the cytoplasm partially deformed and pulled into the pore and the interconnecting channel. Dashed lines indicate the edges of the input channel and the interconnecting channel. Scale bar is 10  $\mu\text{m}$  in all cases.

### 2.3.6 Correlation of Impedance Responses with Imaging Data

We next evaluated the collection efficiency of the staining and imaging module for patient samples (n = 4, PDAC). Impedance responses from each sample were analyzed and correlated to the number of CTCs collected using the staining and imaging module that were scored as CTCs (DAPI(+), CD45(-) and CK(+)). A Pearson correlation of 0.93 (n=4) was obtained between the impedance responses and the CTCs collected at the staining and imaging module. As seen from the impedance trace for one patient (Figure 2.9A), 14 peaks were assigned as cell events. Variations of the peak amplitude responses for the impedance trace were most likely due to differences in CTC size and/or transduction of leukocytes (see Figure 2.7). The CTCs collected on the staining and imaging module were found to be 8 for this same sample and were definitively identified as CTCs by their staining pattern. For all PDAC samples analyzed, the collection efficiency of CTCs by the staining and imaging module was  $72 \pm 13\%$  (see Figure 2.9). While the staining and imaging module demonstrated higher collection efficiencies for the Hs578T cell line compared to the clinical samples, this difference could have arisen from impedance signals recorded for leukocytes as well as the CTCs, which were not present in the cell line studies. Also, most of the CTCs are in an apoptotic state and therefore, their cell membrane may not be rigid enough to withstand the pressure exerted on the cell by the pore structure (see Figure 2.8). [62-64]



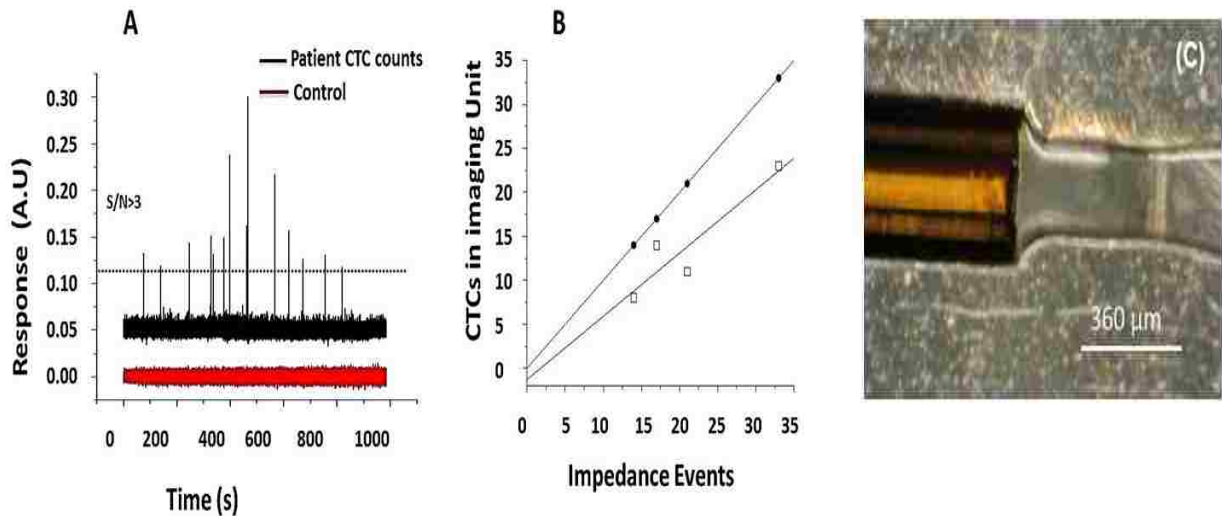


Figure 2.9 (A) Impedance counts generated from CTCs selected from 2.0 mL of blood from a patient with metastatic PDAC. The sample was processed through the HT-CTC selection module at a linear flow velocity of 2.0 mm/s. CTCs were then released from the selection bed using a CTC release buffer at a volumetric flow rate of 10  $\mu\text{L}/\text{min}$ . A total of 14 CTCs were enumerated using impedance sensing based on a signal-to-noise threshold of 3 (dotted line). The red dotted line represents the threshold level, which was used to differentiate ‘true’ events from noise. Data presented here were smoothed using algorithms described in the Experimental Section. After impedance counting, the cells were directed to the staining and imaging module for phenotypic identification (DAPI, CD45 and cytokeratins). (B) Plot showing the correlation between the impedance counts versus CTCs enumerated via immunostaining on the staining and imaging module for 4 different metastatic PDAC patient samples. (●) Represents expected numbers of CTC events based on the impedance signatures and (□) shows the experimental enumeration data from the staining and imaging module ( $r = 0.93$ ). (C) Interface between a capillary and plastic module showing the capillary inserted into a guide channel to accommodate the 365  $\mu\text{m}$  od capillary and stepping to a channel size of 150  $\mu\text{m}$ , which matches the id of the interconnect capillary.

The high correlation between the impedance responses and those ascertained through immunostaining using the staining and imaging module also indicated that

minimal cell loss was induced by the capillary interconnections between modules. Any potential loss of cells by these interconnects could be induced by shearing effects at module/capillary junctions or the unswept volumes created by these same junctions. However, the relatively large size of the CTCs and the small capillary diameters used as the interconnects (id = 150  $\mu\text{m}$ ) as well as the carefully designed capillary-to-module interface minimized unswept volumes. The interface between the capillary and module was accomplished by using multiple levels of microstructures. A guide channel for the capillary matching the capillary od (365  $\mu\text{m}$ ) was used as the capillary holder and the fluidic channel dimensions matched that of the capillary id (150  $\mu\text{m}$ ). Figure 2.9C shows this interface.

### **2.3.7 Preclinical Studies Using PDX Models**

We processed blood samples from PDX models (n = 7) that were engrafted with biopsy tissue from metastatic PDAC patients. In addition, we analyzed blood from healthy mice (n = 3) to serve as negative controls. Cells were classified as CTCs only if they met the following criteria; (i) intact cells with nuclei; (ii) immunocytochemically positive for cytokeratins 8/19 and negative for leukocyte marker CD45; and (ii) morphological characteristics such as having a nucleus to cytoplasm ratio of 2:1 with a large visible nucleus (Figure 2.10C i. a-d). CTCs generated from PDX models were isolated within a range of 13 to 112 CTCs/mL (median = 24/mL, mean = 44  $\pm$ 36/mL), while healthy mice (n = 3) generated a mean of 0.83 /mL (p = 0.022). A summary of this data can be seen in the box plot shown in Figure 2.10A.

### 2.3.8 Clinical Studies in Metastatic and Local Resectable PDAC Patients

For metastatic PDAC patient blood samples, we isolated an average of  $53 \pm 29$  CTCs/mL, median = 51/mL with a range of 9 to 95 CTCs/mL. To establish assay reproducibility, we also processed three aliquots from the same patient sample through three different HT-CTC modules. An RSD value of 14% ( $n = 3$ ) was obtained. CTCs were selected in all patients with metastatic PDAC. For the healthy blood donors, in most cases no CTCs were observed ( $p = 0.004$ ). Metastatic patients had a statistically significant higher CTC count compared to healthy patients ( $p = 0.008$ ).

We also analyzed blood from 5 patients who had been determined to have local resectable PDAC by CT scans. We found an average of 12 CTCs/mL for this group of patients. Based on the Kruskal-Wallis test ( $p = 0.002$ ), there was a significant difference in the CTCs/mL between metastatic, local resectable, and healthy patients. Pairwise Wilcoxon Rank-Sum tests suggested that there was a significant difference between metastatic and healthy patients ( $p = 0.005$ ). Between local resectable PDAC and healthy patients there was also a statistically significant difference in terms of CTC numbers ( $p = 0.011$ ). Comparison between metastatic and local resectable patients also indicated a significant CTC number difference ( $p = 0.023$ ). These results remained significant when accounting for multiple testing using the Hochberg method ( $p$ -values of 0.016, 0.022, and 0.023). This data is summarized in the box plot shown in Figure 2.10B. The presence of CTCs from locally resectable patients may be indicative of micrometastasis, which is undetectable by conventional diagnostic methods. CT scans, which are commonly used for tumor imaging, are less informative with regard to the

micrometastatic nature of the tumor because they cannot detect tumors smaller than 1 cm and thus, may not be effective for assessing the micrometastatic nature of PDAC as our assay has demonstrated. [45] Continuous monitoring of CTC counts from this group of patients may be important in predicting the reoccurrence of the disease after surgical resection.

The purity of the assay when processing clinical blood samples was determined as well. The purity was calculated using the ratio of the number of CTCs selected to the total number of cells selected and was found to be  $86 \pm 12\%$  for all samples analyzed. For many CTC selection platforms, purity is calculated as the ratio of CTCs (DAPI(+), CK(+) and CD45(-)) divided by the total number of selected DAPI(+) cells. Unfortunately, the purity number when calculated in this fashion can be biased if the leukocyte numbers are relatively constant, but the CTC number per patient varies (can vary over 3-orders of magnitude). We show in Table 2.1 the numbers of those cells selected and classified as CTCs and cells classified as leukocytes or double stained cells (CK(+) and CD45(+)) for several patients (n=4) with different states of disease as well as healthy donors.

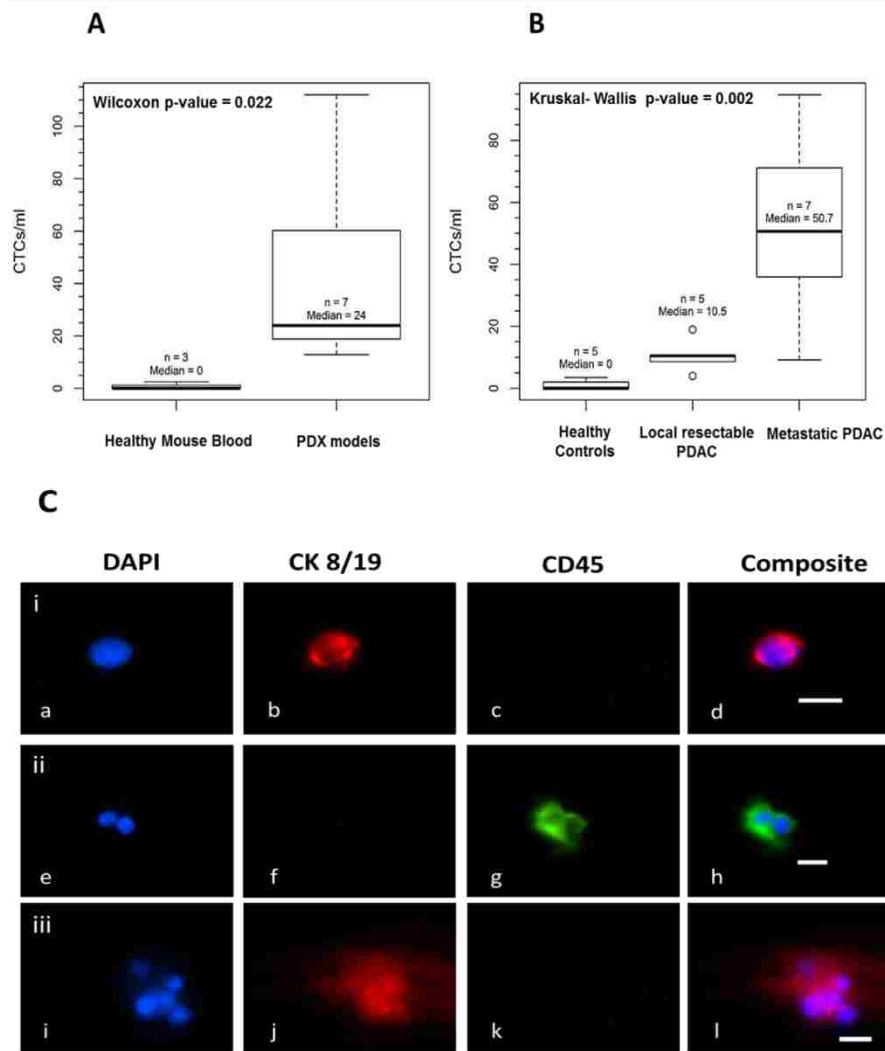


Figure 2.10 Staining and enumeration of CTCs via immunophenotyping. (A) Box plot representing results from the phenotypic enumeration of CTCs isolated from 7 PDX and 3 healthy mice. (B) Box plot from CTCs isolated from 7 metastatic PDAC patients, 5 healthy controls and 5 local resectable PDAC patients. (C) Fluorescence images of various selected cells from a metastatic PDAC patient: (i) CTC; (ii) two white blood cells; and (iii) cluster of CTCs. (b, f, j) CTC marker for Cytokeratin 8/19 (red) with b, j positive for this marker and f negative for this marker; and (c, g, k) leukocyte antigen marker CD45 (green) with c, k negative for this marker and g positive for this marker. Micrographs (i-l) are of an aggregate of 6 CTCs captured in the HT-CTC module. This aggregate showed positive for cytokeratins 8/19 (j) and negative for leukocyte marker CD45 (k). In all of these panels the nuclei were stained with DAPI (blue). Bars are 10  $\mu$ m.

For these studies, the cells were not released from the selection module using trypsin, but were enumerated directly within the selection module following staining within the same module. Without release using trypsin, potential damage to antigenic membrane targets could be avoided, which could misrepresent specific cell population numbers, including the leukocyte population. The purity for the PDX models was found to be  $89 \pm 16\%$ . The high purity levels observed in our studies compared to others were mainly due to the relatively high shear forces applied to the selected cells during the post selection wash, which used a linear velocity of  $4 \text{ mms}^{-1}$ . While the CTCs selected on the channel walls remained unaffected by the high shear forces due to the high  $K_d$  value ( $3.3 \times 10^8 \text{ M}^{-1}$ ) between the EpCAM antigen and EpCAM antibody and the multi-point contact, [29] the non-specifically adsorbed leukocytes are more easily removed from the surface due to their apparent lower adhesion force to the surface.

As can be seen from this data, the number of leukocytes selected ranged from approximately 1 – 9 per mL of blood processed with the lowest infiltration rate of leukocytes found for the local resectable PDAC patients and highest numbers associated with the metastatic PDAC patients. Also, the CTC number varied tremendously as would be expected and as shown in Figure 2.10 of the main text for these three cases. From this data, the purity level as calculated using the method described previously was 86% for the metastatic PDAC patients

Table 2.1 Average number of CTCs, leukocytes and double-stained cells selected using the HT CTC selection module depicted in Figure 2.2 for two different PDAC pathologies and healthy donors. For this data, the selected cells were stained within the selection module and not released from the surface using trypsin. The cells were stained with DAPI (nucleus), cytokeratins and CD45. Each row of the data set corresponds to a different patient analyzed, which was performed in triplicate (blood sample, split into three equal volumes and run on three different HT-CTC modules). The number shown represents the mean for each patient.

Pathology		CTCs/mL	Leukocytes/mL	Double Stained Cells/mL
Healthy Donors		0	7	0
		2	2	2
		0	2	0
		0	2	0
Means		0.5 ( $\pm 1$ )	3 ( $\pm 2$ )	0.5 ( $\pm 1$ )
Local	Resectable	10.5	1	1
		8	0	0
		19.0	2	0
		10.5	0	0
Means		12 ( $\pm 4$ )	0.8 ( $\pm 0.9$ )	0.3 ( $\pm 0.5$ )
Metastatic PDAC		34.0	12.0	3
		68.3	9	2
		94.7	10.7	1
		73.8	2	1
Means		68 ( $\pm 25$ )	9 ( $\pm 4$ )	2

Also seen in this data for the healthy donors, one case we detected CTCs, which could be classified as a false positive result. However, follow up on this individual may be warranted because the CTC number may be indicative of a non-diagnosed micrometastatic or metastatic condition for not just PDAC, but any solid tumor that can produce CTCs. In addition, our data clearly shows that all cases that were diagnosed as metastatic or micrometastatic (local resectable), CTCs were found indicating that the

false negative rate is 0 in this limited data set. However, a larger cohort of samples still needs to be analyzed to reach a concise clinical decision as to the false positive and false negative rate of CTC detection using our assay. This is currently ongoing in our laboratory. In addition, a rigorous comparison to the standard CTC analysis platform, CellSearch, must be undertaken and this work is also currently being undertaken in our laboratory and will be reported in subsequent manuscripts.

We also noticed microclusters of CTCs in some of the PDAC blood samples (71%) that were processed (Figure. 7C i-l). These clusters were predominantly found near the entrance to the sinusoidal microchannels of the HT-CTC selection module. Recent reports on CTC isolation have cited the presence of similar clusters or microemboli. [43] It is speculated that these clusters form in circulation or break off from the primary tumor as a cohort of cells. As a cluster, CTCs can escape the immune surveillance system more readily than individual CTCs and can be indicative of an increased metastatic potential of the cancer. [6, 65]

We also noted the presence of cells that stained positive for all three markers (DAPI, cytokeratins, and CD45). The frequency of the "triple positive" cells was on the order of  $1.6 \pm 2.0$  cells/mL, which was lower than the CTC and/or leukocyte occurrence. This is contrary to other reports, which indicated a much higher frequency of such cells. [43] Although at this point we do not understand the origin of these cells, they could be a sub-population of CTCs acquiring mesenchymal markers or leukocytes with an abnormally increased cytokeratin expression. In current studies these cells were not



classified as CTCs, however, they were included in purity calculations as contaminating cells

## **2.4 Conclusion**

In this study we adopted a modular approach with 3 task-specific modules for processing CTCs in an automated fashion. The first module consisted of a HT-CTC selection module designed with a z-configuration to obtain uniform flow properties throughout an array of microchannels and was scalable to process volumes of 7.5 mL in less than 45 min. The selected cells could be released from the antibody-decorated selection surface and shuttled through an impedance sensor module. The inclusion of the impedance sensor module was useful as a prescreening tool to allow the user to make decisions based on the impedance response as to whether staining and imaging of selected CTC fractions was necessary, which can result in a significant reduction in assay cost and time.

We also described a unique staining and imaging module consisting of a high density array of pore structures made at the intersection of large input channels and smaller interconnecting channels. This module demonstrated a significant reduction in the analysis time for CTC imaging; 6 h processing time for analyzing cells in the selection module to 10 min when using the staining and imaging module. Although the collection efficiencies were slightly lower for CTCs generated from clinical samples compared to cell lines, this can be rectified by re-engineering the pore structures comprising this device to possess smaller dimensions and at the same time increasing the number of pores.

Using this system, we have achieved some interesting clinical data for PDAC as well, both local resectable and metastatic PDAC. We have detected CTCs in all patients diagnosed with PDAC (see SI Table 2.1) and with high purity resulting from the high shear forces exerted on the cells following selection in the HT-CTC module. This high purity level should provide the ability to secure high quality molecular profiles of the CTCs that can be used to guide therapy by stratifying patients with PDAC and other solid tumors.

Using our integrated and modular system, CTC assay time was significantly reduced compared to the approach requiring manual processing. For the manual case, the assay time was found to be ~8 h (CTC selection, staining and imaging) with the majority of time relegated to imaging the relatively large selection bed. For the microsystem presented in this manuscript, the assay time was reduced to 1.5 h (45 min CTC selection time even for 7.5 mL of blood, 15 min release time, 20 min fixation, permeabilization and staining time and 10 min imaging time).

The modular approach presented herein provides multiple advantages toward constructing integrated, sample-to-answer systems. These include: (i) flexibility in the selection of materials used for construction of task-specific modules to optimize performance for each processing step; (ii) ease of reconfiguration of fluidic cartridges without re-engineering the entire system in order to accommodate alternative and/or improved processing steps; (iii) ability to use separate production schemes optimized for each module in order to reduce the overall assay cost; and (iv) high production yields of integrated systems. The main challenge when using modular approach lies

with the proper interconnection technologies which will minimize the potential CTC loss during processing due to existence of unswept volumes that may trap the CTCs. Our current efforts are directed toward integrating the modular assay using interconnects recently described by our group which will provide zero-dead volume fluidic path. [66]

\* All technical and clinical data were mainly contributed by authors J.Kamande and M. Hupert. Collaborator and author J.J Yeh mainly obtained the blood samples under an approved IRB #11-1924 (see appendix and permissions sections).

## 2.5 References

1. Paget, S., *THE DISTRIBUTION OF SECONDARY GROWTHS IN CANCER OF THE BREAST*. The Lancet, 1889. **133**(3421): p. 571-573.
2. Elshimali, Y.I. and W.W. Grody, *The clinical significance of circulating tumor cells in the peripheral blood*. Diagnostic Molecular Pathology, 2006. **15**(4): p. 187-194.
3. Jacob, K., C. Sollier, and N. Jobodo, *Circulating tumor cells: detection, molecular profiling and future prospects*. Expert Review of Proteomics, 2007. **4**(6): p. 741-756.
4. Loberg, R.D., *et al.*, *Detection and isolation of circulating tumor cells in urologic cancers: A review*. Neoplasia, 2004. **6**(4): p. 302-309.
5. Mocellin, S., *et al.*, *The prognostic value of circulating tumor cells in patients with melanoma: A systematic review and meta-analysis*. Clinical Cancer Research, 2006. **12**(15): p. 4605-4613.
6. Paterlini-Brechot, P. and N.L. Benali, *Circulating tumor cells (CTC) detection: Clinical impact and future directions*. Cancer Letters, 2007. **253**(2): p. 180-204.
7. Pelkey, T.J., H.F. Frierson, and D.E. Bruns, *Molecular and immunological detection of circulating tumor cells and micrometastases from solid tumors*. Clinical Chemistry, 1996. **42**(9): p. 1369-1381.
8. Tsouma, A., *et al.*, *Circulating Tumor Cells in Colorectal Cancer: Detection Methods and Clinical Significance*. Anticancer Research, 2008. **28**(6B): p. 3945-3960.
9. Wong, I.H.N., *Transcriptional profiling of circulating tumor cells: Quantification and cancer progression (Review)*. Oncology Reports, 2003. **10**(1): p. 229-235.

10. Arrazubi, V., *et al.*, *Circulating tumor cells: Prognostic factor for metastatic colorectal cancer*. *Annals of Oncology*, 2010. **21**: p. 80-80.
11. Cristofanilli, M. and S. Braun, *Circulating Tumor Cells Revisited*. *Jama-Journal of the American Medical Association*, 2010. **303**(11): p. 1092-1093.
12. Jiao, L.R., *et al.*, *Circulating Tumor Cells and Sample Size: The More, the Better Reply*. *Journal of Clinical Oncology*, 2010. **28**(17): p. E290-E290.
13. Konigsberg, R., *et al.*, *Circulating tumor cells in metastatic colorectal cancer: Efficacy and feasibility of different enrichment methods*. *Cancer Letters*, 2010. **293**(1): p. 117-123.
14. Lalmahomed, Z.S., *et al.*, *Circulating Tumor Cells and Sample Size: The More, the Better*. *Journal of Clinical Oncology*, 2010. **28**(17): p. E288-E289.
15. Li, Q., *Circulating Tumor Cells: Determining Its Number and What It Means*. *Cytometry Part A*, 2010. **77A**(3): p. 211-212.
16. Maheswaran, S. and D.A. Haber, *Circulating tumor cells: a window into cancer biology and metastasis*. *Current Opinion in Genetics & Development*, 2010. **20**(1): p. 96-99.
17. Negin, B.P. and S.J. Cohen, *Circulating Tumor Cells in Colorectal Cancer: Past, Present, and Future Challenges*. *Current Treatment Options in Oncology*, 2010. **11**(1-2): p. 1-13.
18. Nelson, N.J., *Circulating Tumor Cells: Will They Be Clinically Useful?* *Journal of the National Cancer Institute*, 2010. **102**(3): p. 146-U11.
19. Punnoose, E.A., *et al.*, *Molecular Biomarker Analyses Using Circulating Tumor Cells*. *Plos One*, 2010. **5**(9).
20. Rahbari, N.N., *et al.*, *Meta-analysis Shows That Detection of Circulating Tumor Cells Indicates Poor Prognosis in Patients With Colorectal Cancer*. *Gastroenterology*, 2010. **138**(5): p. 1714-U20.
21. Raimondi, C., *et al.*, *Circulating Tumor Cells in Cancer Therapy: Are we off Target?* *Current Cancer Drug Targets*, 2010. **10**(5): p. 509-518.
22. Sieuwerts, A.M., *et al.*, *Anti-epithelial cell adhesion molecule antibodies and the detection of circulating normal-like breast tumor cells*. *Journal of the National Cancer Institute*, 2009. **101**: p. 61-66.

23. Mostert, B., *et al.*, *Detection of circulating tumor cells in breast cancer may improve through enrichment with CD-146*. *Breast Cancer Research and Treatment*, 2011. **127**: p. 33-41.
24. Dharmasiri, U., *et al.*, *Microsystems for the Capture of Low-Abundance Cells*, in *Annual Review of Analytical Chemistry, Vol 3*, E.S. Yeung and R.N. Zare, Editors. 2010. p. 409-431.
25. Kuo, J.S., *et al.*, *Deformability considerations in filtration of biological cells*. *Lab Chip*, 2010. **10**: p. 837-842.
26. Lin, Y.G., *et al.*, *Rare circulating tumor cells can be reliably and efficiently detected using a novel microfluidics and micro-electromechanical systems (MEMS)-based rare cell recovery platform: Preclinical and clinical data*. *Gynecologic Oncology*, 2009. **112**(2): p. 230.
27. Maheswaran, S., *et al.*, *Detection of Mutations in EGFR in Circulating Lung-Cancer Cells*. *New England Journal of Medicine*, 2008. **359**: p. 366-377.
28. Xu, Y., *et al.*, *Aptamer-Based Microfluidic Device for Enrichment, Sorting, and Detection of Multiple Cancer Cells*. *Analytical Chemistry*, 2009. **81**(17): p. 7436-7442.
29. Adams, A.A., *et al.*, *Highly efficient circulating tumor cell isolation from whole blood and label-free enumeration using polymer-based microfluidics with an integrated conductivity sensor*. *Journal of the American Chemical Society*, 2008. **130**(27): p. 8633-8641.
30. Nagrath, S., *et al.*, *Isolation of rare circulating tumour cells in cancer patients by microchip technology*. *Nature (London, U. K.)*, 2007. **450**(Copyright (C) 2010 American Chemical Society (ACS). All Rights Reserved.): p. 1235-1239.
31. Tan, S.J., *et al.*, *Microdevice for the isolation and enumeration of cancer cells from blood*. *Biomedical Microdevices*, 2009. **11**(4): p. 883-892.
32. Williams, A., *et al.*, *Size-Based Enrichment Technologies for CTC Detection and Characterization*, in *Minimal Residual Disease and Circulating Tumor Cells in Breast Cancer*, M. Ignatiadis, C. Sotiriou, and K. Pantel, Editors. 2012, Springer Berlin Heidelberg. p. 87-95.
33. Dharmasiri, U., *et al.*, *Highly efficient capture and enumeration of low abundance prostate cancer cells using prostate-specific membrane antigen aptamers immobilized to a polymeric microfluidic device*. *Electrophoresis*, 2009. **30**(Copyright (C) 2010 American Chemical Society (ACS). All Rights Reserved.): p. 3289-3300.

34. Dharmasiri, U., et al., *High-Throughput Selection, Enumeration, Electrokinetic Manipulation, and Molecular Profiling of Low-Abundance Circulating Tumor Cells Using a Microfluidic System*. *Analytical Chemistry*, 2011. **83**(6): p. 2301-2309.
35. Chen, Z.Z., et al., *Pool-dam structure based microfluidic devices for filtering tumor cells from blood mixtures*. *Surface and Interface Analysis*, 2006. **38**(6): p. 996-1003.
36. Lim, L.S., et al., *Microsieve lab-chip device for rapid enumeration and fluorescence in situ hybridization of circulating tumor cells*. *Lab on a Chip*, 2012. **12**(21): p. 4388-4396.
37. Zheng, S., et al., *Membrane microfilter device for selective capture, electrolysis and genomic analysis of human circulating tumor cells*. *Journal of Chromatography A*, 2007. **1162**(2): p. 154-161.
38. Lin, H.K., et al., *Portable Filter-Based Microdevice for Detection and Characterization of Circulating Tumor Cells*. *Clinical Cancer Research*, 2010. **16**(20): p. 5011-5018.
39. Bo, L., et al. *Parylene membrane slot filter for the capture, analysis and culture of viable circulating tumor cells*. in *Micro Electro Mechanical Systems (MEMS), 2010 IEEE 23rd International Conference on*. 2010.
40. Xu, T., et al., *A Cancer Detection Platform Which Measures Telomerase Activity from Live Circulating Tumor Cells Captured on a Microfilter*. *Cancer Research*, 2010. **70**(16): p. 6420-6426.
41. Hosokawa, M., et al., *Size-Selective Microcavity Array for Rapid and Efficient Detection of Circulating Tumor Cells*. *Analytical Chemistry*, 2010. **82**(15): p. 6629-6635.
42. Saliba, A.-E., et al., *Microfluidic sorting and multimodal typing of cancer cells in self-assembled magnetic arrays*. *Proceedings of the National Academy of Sciences*, 2010. **107**(33): p. 14524-14529.
43. Stott, S.L., et al., *Isolation and characterization of circulating tumor cells from patients with localized and metastatic prostate cancer*. *Science Translational Medicine*, 2010. **2**(Copyright (C) 2010 American Chemical Society (ACS). All Rights Reserved.): p. No pp. given.
44. Wang, S., et al., *Highly Efficient Capture of Circulating Tumor Cells by Using Nanostructured Silicon Substrates with Integrated Chaotic Micromixers*. *Angewandte Chemie-International Edition*, 2011. **50**(13): p. 3084-3088.

45. Riker, A., S.K. Libutti, and D.L. Bartlett, *Advances in the early detection, diagnosis, and staging of pancreatic cancer*. Surgical Oncology, 1997. **6**(3): p. 157-169.
46. Hariharan, D., A. Saied, and H.M. Kocher, *Analysis of mortality rates for pancreatic cancer across the world*. HPB, 2008. **10**(1): p. 58-62.
47. Hezel, A.F., *et al.*, *Genetics and biology of pancreatic ductal adenocarcinoma*. Genes & Development, 2006. **20**(10): p. 1218-1249.
48. Grasso, D., M.N. Garcia, and J.L. Iovanna, *Autophagy in pancreatic cancer*. Int J Cell Biol, 2012. **2012**: p. 760498.
49. Cristofanilli, M., G.T. Budd, and M.J. Ellis, *Circulating tumor cells, disease progression, and survival in metastatic breast cancer*. New England Journal of Medicine, 2004. **351**: p. 781-791.
50. Hayes, D.F. and J. Smerage, *Is there a role for circulating tumor cells in the management of breast cancer?* Clinical Cancer Research, 2008. **14**: p. 3646-3650.
51. Khoja, L., *et al.*, *A pilot study to explore circulating tumour cells in pancreatic cancer as a novel biomarker*. British Journal of Cancer, 2012. **106**: p. 508-516.
52. Kurihara, T., *et al.*, *Detection of circulating tumor cells in patients with pancreatic cancer: A preliminary result*. Journal Hepatobiliary Pancreatic Surgery, 2008. **15**: p. 189-195.
53. McCarley, R.L., *et al.*, *Resist-Free Patterning of Surface Architectures in Polymer-Based Microanalytical Devices*. Journal of the American Chemical Society, 2004. **127**(3): p. 842-843.
54. Jackson, J.M., *et al.*, *UV Modification of Polymeric High Aspect Ratio Microstructures: Ramifications in Antibody Surface Loading For Circulating Tumor Cell Selection*. Lab Chip, 2013, submitted for publication.
55. Kotz, K.T., *et al.*, *Clinical microfluidics for neutrophil genomics and proteomics*. Nature Medicine, 2010. **16**(9): p. 1042-1047.
56. Zhang, W., *et al.*, *Analysis and optimization of flow distribution in parallel-channel configurations for proton exchange membrane fuel cells*. Journal of Power Sources, 2009. **194**(2): p. 931-940.
57. Herron, J.N., *et al.*, *Surfactant Science Series*, 2003. **110**: p. 155-163.

58. Wei, S.Y., *et al.*, *Photochemically patterned poly(methyl methacrylate) surfaces used in the fabrication of microanalytical devices*. Journal Of Physical Chemistry B, 2005. **109**(35): p. 16988-16996.
59. Sun, T. and H. Morgan, *Single-cell microfluidic impedance cytometry: a review*. Microfluidics and Nanofluidics, 2010. **8**: p. 423-443.
60. Shadpour, H., *et al.*, *Physiochemical properties of various polymer substrates and their effects on microchip electrophoresis performance*. Journal of Chromatography A, 2006. **1111**(2): p. 238-251.
61. Kuo, J.S., *et al.*, *Deformability considerations in filtration of biological cells*. Lab on a Chip, 2010. **10**(7): p. 837-842.
62. Méhes, G., *et al.*, *Circulating Breast Cancer Cells Are Frequently Apoptotic*. The American Journal of Pathology, 2001. **159**(1): p. 17-20.
63. Glinsky, G.V., *Apoptosis in metastatic cancer cells*. Critical Reviews in Oncology/Hematology, 1997. **25**(3): p. 175-186.
64. Larson, C.J., *et al.*, *Apoptosis of circulating tumor cells in prostate cancer patients*. Cytometry Part A, 2004. **62A**(1): p. 46-53.
65. Christiansen, J.J. and A.K. Rajasekaran, *Reassessing Epithelial to Mesenchymal Transition as a Prerequisite for Carcinoma Invasion and Metastasis*. Cancer Research, 2006. **66**(17): p. 8319-8326.
66. Wang, H., *et al.*, *Fully Integrated Thermoplastic Genosensor for the Highly Sensitive Detection and Identification of Multi-Drug-Resistant Tuberculosis*. Angewandte Chemie International Edition, 2012. **51**(18): p. 4349-4353.



## CHAPTER 3. MOLECULAR PROFILING OF ENRICHED LOW-ABUNDANCE CIRCULATING TUMOR CELLS (CTCS) USING A HIGH-THROUGHPUT MICROFLUIDIC SYSTEM.

### 3.1 Introduction

Propagated malignancy is the main cause of cancer-related deaths. Despite the harmful and destructive growth at the site of origin, primary tumors are only responsible for only 10% of cancer-related deaths while 90% are due to metastases occurring at the time of diagnosis or as a recurrence of a previously diagnosed cancer [1-3]. It has been speculated that cancerous tissues shed cells into the bloodstream, which are responsible for the metastasis of cancer. This process is not well understood however, mouse models of tumor spread have implicated the process of an epithelial to mesenchymal transition (EMT) by which adherent epithelial cells acquire migratory cell fates. These models, however, differ significantly from human cancer metastases and therefore the study of this process in mouse models is limited [4]. A better understanding of human metastases can be obtained only from the study of Circulating Tumor Cells (CTCs). In carcinomas, CTCs are epithelial in origin; they overexpress EpCAM surface antigens, which is only expressed on malignant tumors derived from epithelia and is usually targeted in peripheral blood using monoclonal antibodies specific for EpCAM. CTCs appear at very low frequencies of about 1 CTC in  $1 \times 10^9$  hematological cells.

-----

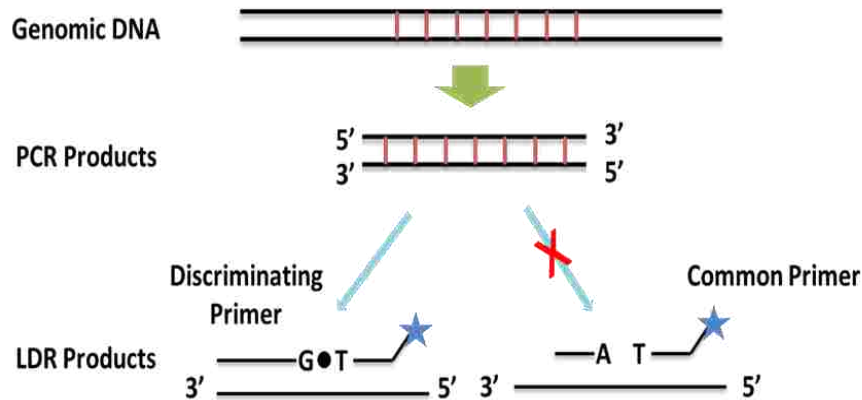
\* Reproduced with permission from the *Analytical Chemistry*. Work presented in this chapter is centered on the molecular profiling of colorectal CTCs and authors JK, UD, and NK were the major contributors to this section.

Elucidating the quantity of CTCs in peripheral blood can serve as an indicator for the clinical management of several cancer-related diseases by providing information on the success/failure of therapeutic intervention and disease stage forecasting. Isolation and enumeration of exfoliated CTCs in peripheral blood or bone marrow for a variety of cancer-related diseases has already been reported such as breast, colorectal, prostate, renal, bladder and non-small cancers. [5-9] Studies have shown that the presence of >5 CTCs in 7.5 mL of blood from metastatic breast cancer patients has been associated with poor prognosis and overall survival. [3, 9, 10]

Multiple approaches have been used to detect CTCs, ranging from size-based separations to the use of immunomagnetic beads containing antibodies directed against EpCAM [11, 12]. Although the establishment of CTC levels in peripheral blood has been associated with poor prognosis, there are reports suggesting that this information may not correlate with the degree of metastases, but their molecular profiles should be more informative [13-16]. Tumors contain genetically heterogeneous cell subpopulations with different propensities to spawn metastatic disease and therefore, if the CTC population responsible for metastasis could be identified through unique genetic profiles, oncologists could match proper therapy to the individual patient. Molecular profiling of CTCs can provide additional clinical information that cannot be garnered simply by enumerating the selected cells. For example, mutations in certain gene fragments that are associated with metastasis, such as the *KRAS* mutations in colorectal cancer, can provide opportunities for personalized treatment of a patient. It has already been shown that metastatic CRC patients with mutated *KRAS* do not benefit from anti-EGFR mAb

therapy, whereas patients with wild-type *KRAS* genotypes do benefit from ceturimab and panitumumab-based treatments. [17-19] In addition, it has been noted that non-tumor epithelial cells can also be present in the blood and express antigens that would select these cells as well.

Human colorectal carcinomas harbor 19 different *KRAS* mutations the majority of which are clustered in two codons. Approximately 90% of the activating mutations in the *KRAS* gene are scored in codon 12 (wild type: GGT) and 13 (wild type: GGC) in exon 1 while only 5% are located in codon 61 (wild type: CAA) in exon 2. PCR/LDR assay is a sensitive and specific method to identify and score the presence of *KRAS* mutations. This assay was developed by Barany *et al.* and is presented schematically in Scheme 3.1 [28-31].



Scheme 3.1 Overview of the molecular profiling strategy adopted for CTCs resident in peripheral blood

The attractive nature of this assay strategy for the mass-limited samples anticipated for CTC analyses is that two stages of amplification are used; exponential amplification associated with the polymerase chain reaction, PCR, and also a linear amplification using the ligase detection reaction LDR. In addition the assay can be configured in a highly multiplexed fashion to search for many mutations in a single processing step.

In this Chapter, we will primarily focus on *KRAS* mutational analysis of CRC CTCs that were enriched via a previously reported microfluidic system. [20] The system included; (i) Selection, release and subsequent enumeration of CTCs via a previously reported high-throughput microsampling unit (HTMSU) (see Figure 3.1); and (ii) an electrokinetic micromanipulation unit for enrichment of low-abundant CTCs for subsequent molecular profiling of rare point mutations in gDNA of the CTCs. CTCs were enriched into a reservoir (2  $\mu$ L) for subsequent molecular interrogation for detection of point mutations in gDNA. SW620 cells from colorectal circulating cancer cell line were used as a model. The selected cells were enumerated using on-chip conductivity transducer, thereby, the enumerated cells were directed to a manipulation section for pre-enrichment into a cell collection cassette. The enriched CTCs were collected and gDNA was extracted for genotyping. Because most *KRAS* mutations are localized to codon 12 and to a lesser extent codons 13 and 61, the PCR/LDR/CE assay was performed on *KRAS* oncogenes (codons 12) to detect the presence/absence of point mutations possessing clinical relevance for the diagnosis/prognosis of colorectal cancers.

## 3.2 Experimental

### 3.2.1 Materials and Reagents

PMMA substrates and cover plates (0.5 mm thickness) were purchased from Good Fellow (Berwyn, PA). Platinum wires were purchased from Alfa Aesar (Boston, MA). Polyimidecoated fused silica capillaries were purchased from Polymicro Technologies (Phoenix, AZ). Chemicals used for the PMMA surface cleaning and modification included reagent grade isopropyl alcohol, 1-ethyl-3-[3-dimethylaminopropyl] carbodimide hydrochloride (EDC), N-hydroxysuccinimide (NHS), fetal bovine serum and 2-(4-morpholino)-ethane sulfonic acid (MES) and these were purchased from Sigma-Aldrich (St. Louis, MO). Monoclonal anti-EpCAM antibody was obtained from R&D Systems (Minneapolis, MN). The SW620 (colorectal cancer cell line), growth media, HEPES buffer, Phosphate Buffered Saline (PBS) and trypsin were purchased from American Type Culture Collection (Manassas, VA). Citrated rabbit blood was purchased from Colorado Serum Company (Denver, CO). TRIS-glycine buffer was obtained from Bio-Rad Laboratories (Hercules, CA). All solutions were prepared in nuclease-free water, Invitrogen (Carlsbad, CA). Nuclease-free microfuge tubes were purchased from Ambion (Foster City, CA) and were used for preparation and storage of all samples and reagents. A fluorescein derivative, PKH67, was purchased from Sigma-Aldrich. Oligonucleotide probes and primers were obtained from two different sources, Integrated DNA technologies (Coralville, IA).

### **3.2.2 Cell Culture and Imaging**

SW620 cells were cultured to 80% confluence in Dulbecco's Modified Eagle's Medium supplemented with high glucose containing 1.5 g/L sodium bicarbonate ( $\text{NaHCO}_3$ ), 15 mM HEPES buffer, and 10% fetal bovine serum. A cell stripper solution was prepared in 150 mM PBS and used to harvest the SW620 cells from the culturing plate. SW620 cells were stained with PKH67 for microscopic visualization experiments using fluorescence. A modified protocol for cell staining was implemented whereby the dye concentration was increased twofold resulting in more evenly distributed fluorescent labels over the cell's periphery. Cell counts were determined by counting three aliquots of cells in succession using a hemacytometer. The cell count accuracy was within 10%.

In cases where the cells required optical visualization to assist in the operational optimization of the HTMSU or the electro-manipulation unit, the PMMA devices were fixed onto a programmable motorized stage of an Axiovert 200M (Carl Zeiss, Thornwood, NY) microscope and video images were collected during each experiment at 30 frames/s using a monochrome CCD (JAI CV252, San Jose, CA). A Xe arc lamp was used to excite the fluorescent dyes incorporated into the cells' membrane.

### **3.2.3 Fabrication of Microsampling Unit**

The microfluidic chips were hot embossed into PMMA substrates via micro-replication from a metal mold master. A detailed description of the HTMSU fabrication protocol was given in Adams *et al.* [21] The HTMSU consisted of a series of 51 high-aspect ratio curvilinear channels that in concert formed the cell capture bed. Each

channel was 150  $\mu\text{m}$  (depth)  $\times$  30  $\mu\text{m}$  (width) and shared common inlet/outlet ports (Figure 3.1A). Curvilinear shaped capture channels were used to improve the cell capture efficiency as described previously. [21] The cell-free marginal zone apparent in straight channels was not observed in curvilinear channels and the cell radial distribution was unaffected by changes in cell translational velocity. Cells migrate to the outside of the curved channels due to centrifugal forces acting on the cells and the cross-stream velocity component due to the reversal of the direction of curvature. The result is an increase in the antibody/antigen encounter rate as the cells moved through the capture beds at the relatively high-linear velocities used here. The channel width of the cell capture bed (30  $\mu\text{m}$ ) was comparable with the average target cell diameter, which was used to increase the probability of cell–antigen interactions with the solution-borne target cells. The large channel depth (150  $\mu\text{m}$ ) was selected to reduce the pressure drop in high-volume flow rates and also, to increase sample processing throughput.

Before final assembly, 1 mm holes were drilled into the electro-manipulation unit reservoirs, input port and electrodes. Then, the chips were washed with ~0.5% Alconox solution, rinsed and ultrasonicated with DI water followed by rinsing with 2-propanol, and again ultrasonication for 15 min in DI water. The channels were examined under a microscope to ensure they were not filled with debris. The embossed devices were assembled by heat annealing a coverplate made from the same material to the substrate. The coverplate and substrate were clamped together and placed in a convection oven for ~20 min at 101 °C for UV-modified HTMSU and 105 °C for UV-

unmodified HTMSU. After successful heat annealing, the 125  $\mu\text{m}$  diameter Pt wire wrapped Cu electrodes were placed into the drilled holes in electro-manipulation unit. The other end of the Pt wire was inserted into the holes drilled in opposite ends of the microchannel.

Appropriately cleaned PMMA HTMSUs devices and cover plates were exposed through a mask to UV radiation resulting in the formation of carboxylate moieties only in the exposed areas of the PMMA. The exposed areas were restricted to only the cell capture bed region of the device. UV irradiation was performed through an aluminum mask for 10 min at  $15 \text{ mWcm}^{-2}$  to facilitate the formation of the carboxylated scaffold.

Pt electrodes ( $d = 76 \mu\text{m}$ ) served as the contact conductivity sensor in the detection zone of the HTMSU and were placed into guide channels that were positioned orthogonal to the fluidic output channel following thermal assembly. Then, Pt wires positioned in HTMSU and the cover plate were aligned and clamped together between two borosilicate plates. Insertion of the electrodes was monitored using a microscope to carefully control the inter-electrode gap ( $\sim 50 \mu\text{m}$ ). The cell constant of the Pt conductivity sensor,  $K$ , was  $\sim 0.01 \mu\text{m}^{-1}$ , which allowed for the specific detection of SW620 cells based on their average size (diameter= $25 \mu\text{m}$ ).

### **3.2.4 Antibody Immobilization**

Antibody immobilization was carried out in a two-step process. The UV-modified thermally assembled HTMSU device was loaded with a solution containing 4mg/mL EDC, 6 mg/mL NHS in 150 mM MES (pH $\sim$ 6) for 1h at room temperature to obtain the succinimidyl ester intermediate. After this incubation, the EDC/NHS solution was



removed by flushing nuclease-free water through the device. Then, an aliquot of 1.0 mg/mL of the monoclonal anti-EpCAM antibody solution contained in 50 mM PBS (pH~7.4) was introduced into the HTMSU and allowed to react for 4 h. The device was then rinsed with a solution of PBS (pH~7.4) to remove any non-specifically bound anti-EpCAM antibodies.

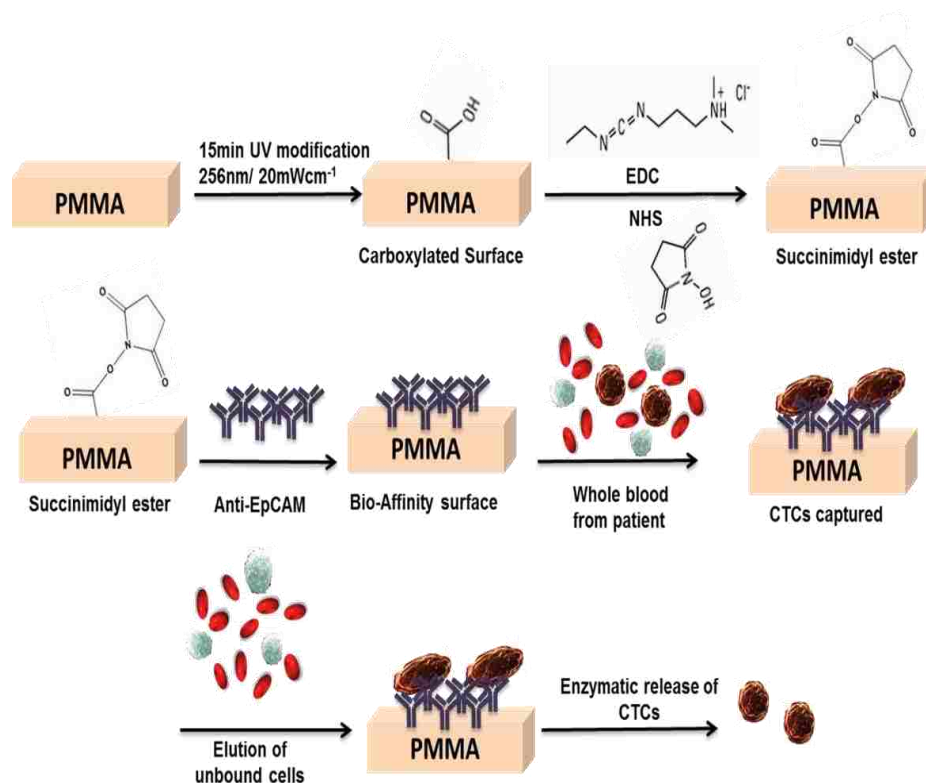
### **3.2.5 SW620 Cell Capture, Release and Enumeration Using the HTMSU**

To connect the HTMSU to the pump, a luer lock syringe (Hamilton, Reno, NV) was placed on the pump equipped with a luer-to-capillary adapter (Inovaquartz, Phoenix, AZ). This was then attached to the capillary that was sealed to the input port of the HTMSU. A pre-capture rinse was performed with 0.2 mL of 150 mM PBS at 50 mm/s linear velocity to maintain isotonic conditions. Then, the appropriate volume of a cell suspension was introduced at the 27.5  $\mu$ L/min volumetric flow rate, which is optimized by Adams *et al.* to produce the desired linear velocity of 2 mm/s in each microchannel comprising the capture bed. Next, a post-capture rinse was performed with 0.2 mL of 150 mM PBS at 50 mm/s to remove any non-specifically adsorbed cells.

Following a post cell capture rinse, a 0.25% trypsin solution in 0.2 mM TRIS/ 19.2 mM glycine buffer (pH ~8.3) was infused into the HTMSU. The captured cells could be observed under a microscope until they were enzymatically removed with Stoke's forces acting on the wall.

The released cells from the capture surface were traversed at 1  $\mu$ L/min (mm/s) linear flow rate through a set of Pt electrodes. We used a specially designed circuit as described earlier to measure the changes in solution conductivity due to single cell

passing the detector as a function of time to create the desired conductivity trace from which cell numbers were determined. (see scheme 3.2 summary of the CTC selection assay).



Scheme 3.2 CTC selection assay on PMMA based HTMSU device. First panel illustrates the exposure of PMMA to UV radiation to generate a monolayer of carboxylic acid moieties that facilitate antibody attachment. The second panel shows the selection of CTCs from blood after covalent attachment of anti- EpCAM to the PMMA substrate. Third panel illustrates the elution of unbound cells (RBCs and WBCs) from the captured CTCs and the release of CTCs for downstream processing.

### **3.2.6 DNA Extraction**

Genomic DNA (gDNA) was extracted from captured cells using Lyse-and-Go PCR reagent (Pierce Biotechnology, IL, USA). Following the manufacturer's recommendations, 5  $\mu$ L of Lyse-and-Go PCR reagent was added to a known number of cells and thermocycled using the following temperatures: 65 °C for 30 s; 8 °C for 30 s; 65 °C for 90 s; 97 °C for 180 s; 8 °C for 60 s; 65 °C for 180 s; 97 °C for 60s; 65 °C for 60 s. Prior to the addition of the PCR cocktail, the samples were put to hold at 80 °C

### **3.2.7 PCRs, LDRs and CE**

PCR amplifications were carried out to generate 290 bp amplicons of SW620 using the gene-specific primer sequences: exon 1 forward –5' TTA AAA GGT ACT GGT GGA GTA TTT GAT A 3', ( $T_m = 55.4$  °C) and exon 1 reverse – 5' AAA ATG GTC AGA GAA ACC TTT ATC TGT 3'( $T_m = 56.3$  °C). In here, 45  $\mu$ L of a PCR cocktail containing 10 mM TRIS–HCl buffer (pH~8.3), 50 mM KCl, 1.5 mM MgCl<sub>2</sub>, 200  $\mu$ M dNTPs, and 0.4  $\mu$ M of each forward and reverse primers (sequences shown above) was added to the cell lysate previously held at 80 °C in the thermo cycler. After a 2-min initial denaturation, 1.5 U of AmpliTaq DNA polymerase (Applied Biosystems, Foster City, CA, USA) was added under hot-start conditions and amplification was achieved by thermally cycling for 30 cycles at 95 °C for 30 s, 60 °C for 2 min, and a final extension at 72 °C for 3 min.

To test the fidelity and yield of the PCR, slab gel electrophoresis was run on an aliquot of each reaction. From each aliquot either 2  $\mu$ L PCR product for standard cell solutions or 3  $\mu$ L PCR product for microchip processed solutions was mixed with 1  $\mu$ L

loading dye and 3  $\mu$ L of 1X TBE buffer for standard cell solution or 2  $\mu$ L of 1X TBE buffer for microchip processed solution, then the mixture was loaded into an individual well of a Ethidium bromide prestained 3% agarose gel (Bio-Rad Laboratories, Hercules, CA). The slab gel electrophoresis was typically run at 5 V/cm for 30 min. The developed slab gel images were captured using Gel Logic 200 Visualizer (Carestream Molecular imaging, New Haven, CT)

Bench-top LDRs were executed in a total volume of 20  $\mu$ L in 0.2 mL polypropylene microtubes using a commercial thermal cycling machine (Eppendorf Thermal Cycler (Brinkmann Instrument, Westbury, NY, USA). The reaction cocktail typically employed in this work consisted of 10 mM TRIS-HCl (pH~8.3), 25 mM KCl, 10 mM MgCl<sub>2</sub>, 0.5 mM NAD<sup>+</sup> (nicotinic adenine dinucleotide, a cofactor for ligase enzyme), and 0.01% Triton X-100, 2  $\mu$ L of 100 nM of the discriminating primer: 5' AAAGTTGTGGTAGTTGGAGCTGT 3' ( $T_m$ =71.3 °C) and fluorescently labeled freshly phosphorylated common primer: 5' Phos/TGGCGTAGGCAAGAGTGCCT/Cy5.5Sp 3' ( $T_m$  = 63.5 °C) and 2  $\mu$ L of the PCR product as template. 40 U of Taq DNA ligase (New England Biolabs) was added to the cocktail under hotstart conditions and the reactions were thermally cycled 20 times for 30 s at 94 °C and 2 min at 65 °C. The LDR products were stored at 4 °C until needed for capillary gel electrophoresis (CGE).

The LDR products were separated using a CEQ 8000 Genetic Analysis System (Beckman Coulter, Fullerton, CA, USA). Data acquisition was performed using the Beckman P/ACE software.

### 3.3 Results and Discussion

#### 3.3.1 PCRs/LDRs/CE

A method that can detect single point mutations in DNA is the ligase detection reaction (LDR) coupled to a PCR.[22-30] A schematic of the PCR/LDR is depicted in Scheme 3.1. Following PCR amplification of the appropriate gene fragments, which contain sections of the gene with point mutation(s), the amplicon is mixed with two LDR primers: common and discriminating that flank the point mutation of interest. The discriminating primer contains a base at its 3'-end that coincides with the single base mutation site. If bases are mismatched, ligation of the two primers does not occur. A perfect match, however, results in a ligation of the two primers and product length that is the sum of nucleotides from two primers.

In our experiment, captured and enumerated cells (see Figure 3.1) were lysed and PCR/LDR assay has been performed using their purified genetic material. Specifically, point mutations in codon 12 in the *KRAS* gene (12.2V) have been targeted that occurs in cell line SW620. Most of *KRAS* mutations are localized in codon 12, but they are also present in 13 and 61 [31-38] and they are found in nearly 35–50% of all patients with colorectal cancer. [39-41] Once acquired, *KRAS* mutations are conserved throughout the course of disease progression.

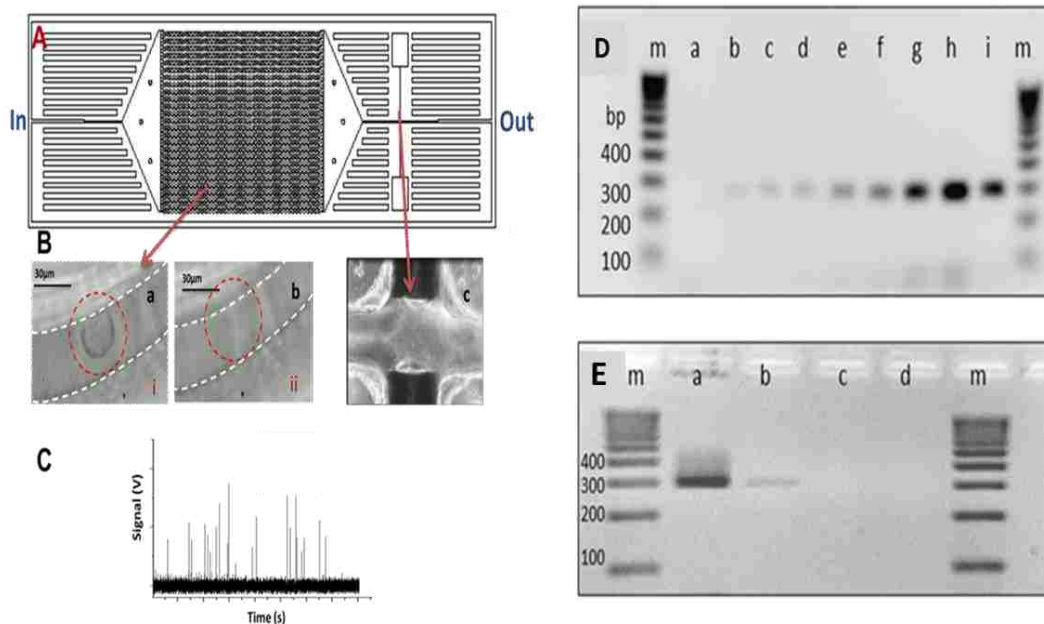


Figure 3.1 Diagrams of the microfluidic system made *via* micro-replication into PMMA from a metal mold master. and agarose gel electrophoresis of the PCR products. (A) Cell selection HTMSU. The capture bed consisted of curvilinear channels that were 30 mm wide and 150 mm deep (51 channels). (B) Brightfield images represents time lapse micrographs of a captured SW620 cell(a) under 0.25%w/w trypsin processing which took 20 min for release(b). Flow rate for cell capture was 27 $\mu$ L/min. linear flow velocity of 2mm/s (C) Impedance readout of approximately 26 SW620 cells released from the capture bed at linear velocity of 2mm/s. PCR was set for 32 cycles. Each cycle: 94 °C (30 s), 60 °C (30 s),72 °C (40 s). Gel stained with EtBr products separated at 4.8 V/cm. (D) Gel Electropherogram for PCR performed on standard SW620 samples (a) no gDNA template, Negative control; (b) DNA from 10 SW620 cells; (c) DNA from 20 SW620 cells; (d) DNA from 50 SW620 cells; (e) DNA from 100 SW620 cells; (f) DNA from 500 SW620 cells; (g) DNA from 1,000 SW620 cells; (h) DNA from 5,000 SW620 cells; (i) gDNA template from SW620, Positive control; Lanes a-i contains 3  $\mu$ L of DNA amplicons. (E) Gel Electropherogram for PCR performed on SW620 cells obtained from HTMSU selection followed by electrokinetic enrichment a) gDNA template from SW620, Positive control; (b) PCR product from 10 SW620 cells selected from whole blood using HTMSU (c) PCR product from whole blood with no SW620 cells (d) no gDNA template, Negative control. Lanes a-d contains 3  $\mu$ L of DNA amplicons.

Before cells from the chip were tested using PCR/LDR, an assay was tested on varying number of SW620 cells; 10, 20, 50, 100, 500, 1,000, and 5,000 cells to acquire information on limit of detection of the assay. As shown in the gel image in Figure 3.1D, cells ranging from 5,000 to as low as 10 were successfully amplified to yield 300 bp PCR product. To demonstrate the capability of the integrated microenrichment system in the pre-concentration of the selected CTCs for subsequent molecular profiling, an average volume (~1 mL) of whole blood containing low abundant CTCs was processed. As a result, 10 SW620 cells were selected and enriched from 1 mL of whole blood and subjected to PCR yielding the results shown in the Figure 3.1E lane b. The presence of mutations within the amplified DNA sequence (~ 300 bp) was discerned by a follow-up allele-specific ligation. The LDR common primer possessed a Cy5.5 fluorescent label and a 5' phosphorylation modification to facilitate covalent coupling with the unmodified discriminating primer in the event of successful ligation. Point mutations were confirmed by the formation of a 43 nt LDR product, which indicated that the ligation event had occurred between a 23 nt and 20 nt long discriminating and common primers. The capillary gel electrophoresis results of LDR product separation generated from PCR products of different number of cells are shown in Figures 3.2A-H. Clearly, LDR results showed a detectable signal generated from CTCs samples (43 nt peak labeled (b)) in Figure 3.2A -H from as low as 10 CTCs

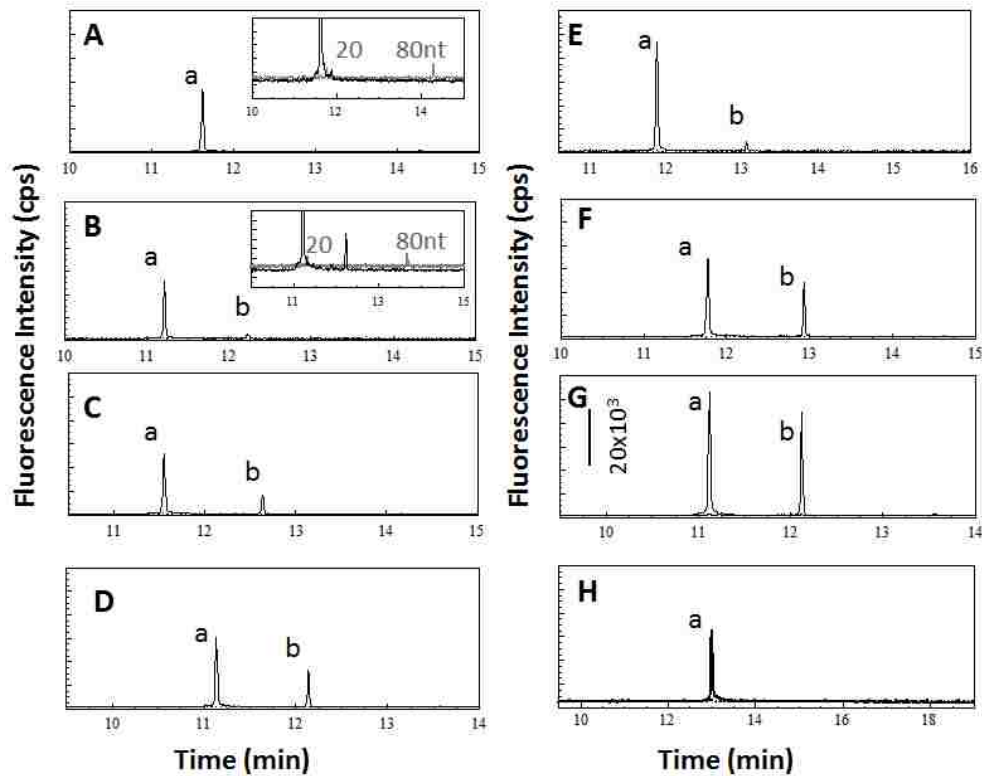


Figure 3.2 The LDR mixtures contained a discriminating and common primers for *KRAS* c12.2V, could selectively detect mutations in G12V. Two  $\mu\text{L}$  of amplicons from PCR with SW620 (mutant) were used for analyzing point mutation in the *KRAS* gene. LDR was set for 20 cycles. Initial denaturation 95 °C for 2 min. Each cycle consisted of: 95 °C (30s), 65 °C (2 min), and 4 °C as final hold. LDR was performed at capillary temperature of 60°C, denaturation temperature of 90 °C (3 min), Injection at 2.0 kV (30 s) and separation at 6.0 kV (20 min). Peak a represents the primer and peak b is the LDR product. CGE analysis was acquired for the following samples; A) 0 B) 10 C) 20 D) 50 E) 100 F) 500 and G) 5,000 SW620 CTCs. The insets shown in (A) and (B) represent a magnified view of the LDR product peaks. H) CGE trace for LDR analysis of 50 HT29 CTCs. DNA size markers of 20 and 80 nt were co-electrophoresed with the LDR products.



Whole blood without CTCs and whole blood containing 10 CTCs was processed via HTMSU and electro-manipulation system, the results of which are shown in Figure 3.3A and 3.3B respectively. As expected, our results showed no mutation in the whole blood that contained no CTCs (Figure 3.3A) while the results of whole blood containing 10 SW620 cells were positive (Figure 3.3B). These results indicated that the HTMSU and electro-manipulation system were very efficient platforms, which can be adopted for cell capture, release and enumeration for subsequent highly specific mutation profiling of low abundant CTCs.

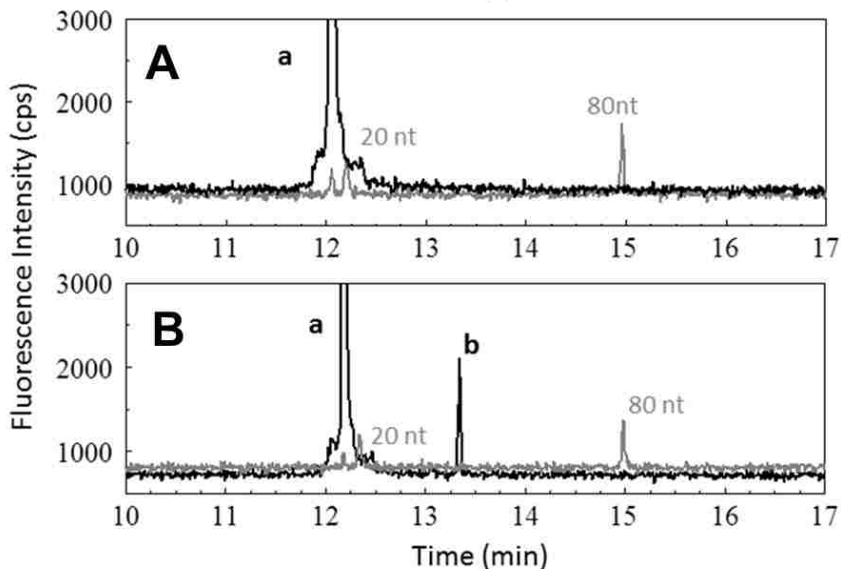


Figure 3.3 Two  $\mu$ l of amplicons from PCR were used for analyzing point mutation in the *KRAS* gene for blood samples spiked with and without 10 SW620s. The LDR products were analyzed using capillary electrophoresis. The capillary electrophoresis responses for sample after processing blood with no SW620 are shown in A, and B shows the electropherogram for 10 spiked SW620s in blood. Peak 'a' represents the primer and peak 'b' is the LDR product for SW620.

### 3.4 Conclusion

We have successfully demonstrated the ability to carry out *KRAS* mutational analysis from as low as 10 CTCs in blood using an integrated system via a high throughput microsampling unit (HTMSU) for selection and enumeration followed by the electrokinetic manipulation unit for pre-concentrating the cells into as low volumes of 2  $\mu$ L. Though only a single point mutation was analyzed as a proof of concept for CTC genotyping using the microfluidic system, we envision our technique being multiplexed through the use of a primary PCR of the gene of interest. This could be followed by multiplex LDR with different primer pairs that flank multiple mutation sites being interrogated. Finally, moving the PCR/LDR step to a microfluidic chip could reduce processing time, eliminate the potential of contamination when implemented in a centralized laboratory, and provide full process automation. Work is currently underway in our laboratory to realize such a system. Ultimately, evaluation of this assay for uncovering the presence/absence of prognostic mutations in the genome of CTCs isolated from blood samples secured from patients with metastatic CRC is the next step in evaluating the utility of our assay for assisting in the management of CRC-related diseases.

### 3.5 References

1. Bell, G.I., *Models for the specific adhesion of cells to cells*. Science, 1978. **200**(Copyright (C) 2010 U.S. National Library of Medicine.): p. 618-27.
2. Maheswaran, S. and D.A. Haber, *Circulating tumor cells: a window into cancer biology and metastasis*. Curr Opin Genet Dev, 2010. **20**(Copyright (C) 2010 U.S. National Library of Medicine.): p. 96-9.

3. Gerges, N., J. Rak, and N. Jabado, *New technologies for the detection of circulating tumour cells*. Br Med Bull, 2010. **94**(Copyright (C) 2010 U.S. National Library of Medicine.): p. 49-64.
4. Kalluri, R. and R.A. Weinberg, *The basics of epithelial-mesenchymal transition*. J. Clin. Invest., 2009. **119**(Copyright (C) 2010 American Chemical Society (ACS). All Rights Reserved.): p. 1420-1428.
5. Kurusu, Y., J. Yamashita, and M. Ogawa, *Detection of circulating tumor cells by reverse transcriptase-polymerase chain reaction in patients with resectable non-small-cell lung cancer*. Surgery, 1999. **126**(Copyright (C) 2010 U.S. National Library of Medicine.): p. 820-6.
6. Wood, D.P., Jr. and M. Banerjee, *Presence of circulating prostate cells in the bone marrow of patients undergoing radical prostatectomy is predictive of disease-free survival*. J Clin Oncol, 1997. **15**(Copyright (C) 2010 U.S. National Library of Medicine.): p. 3451-7.
7. Uemura, H., *Molecular detection of circulating cancer cells in patients with renal cell carcinoma*. Hinyokika Kyo, 1999. **45**(Copyright (C) 2010 U.S. National Library of Medicine.): p. 571-5.
8. Molnar, B., et al., *Circulating tumor cell clusters in the peripheral blood of colorectal cancer patients*. Clin Cancer Res, 2001. **7**(Copyright (C) 2010 U.S. National Library of Medicine.): p. 4080-5.
9. Cristofanilli, M., et al., *Circulating tumor cells, disease progression, and survival in metastatic breast cancer*. N. Engl. J. Med., 2004. **351**(Copyright (C) 2010 American Chemical Society (ACS). All Rights Reserved.): p. 781-791.
10. Stott, S.L., et al., *Isolation and characterization of circulating tumor cells from patients with localized and metastatic prostate cancer*. Sci. Transl. Med., 2010. **2**(Copyright (C) 2010 American Chemical Society (ACS). All Rights Reserved.): p. No pp. given.
11. Moreno, J.G., et al., *Changes in circulating carcinoma cells in patients with metastatic prostate cancer correlate with disease status*. Urology, 2001. **58**(Copyright (C) 2010 U.S. National Library of Medicine.): p. 386-92.
12. Wang, Z.P., et al., *Identification and characterization of circulating prostate carcinoma cells*. Cancer, 2000. **88**(Copyright (C) 2010 U.S. National Library of Medicine.): p. 2787-95.
13. Sotiriou, C. and M.J. Piccart, *Taking gene-expression profiling to the clinic: when will molecular signatures become relevant to patient care?* Nat. Rev. Cancer,

2007. **7**(Copyright (C) 2010 American Chemical Society (ACS). All Rights Reserved.): p. 545-553.
14. Klein, C.A., *The direct molecular analysis of metastatic precursor cells in breast cancer: A chance for a better understanding of metastasis and for personalized medicine*. Eur. J. Cancer, 2008. **44**(Copyright (C) 2010 American Chemical Society (ACS). All Rights Reserved.): p. 2721-2725.
  15. Shaffer, D.R., et al., *Circulating Tumor Cell Analysis in Patients with Progressive Castration-Resistant Prostate Cancer*. Clin. Cancer Res., 2007. **13**(Copyright (C) 2010 American Chemical Society (ACS). All Rights Reserved.): p. 2023-2029.
  16. Ma, P.C., et al., *Circulating tumor cells and serum tumor biomarkers in small cell lung cancer*. Anticancer Res., 2003. **23**(Copyright (C) 2010 American Chemical Society (ACS). All Rights Reserved.): p. 49-62.
  17. Lievre, A., et al., *KRAS mutations as an independent prognostic factor in patients with advanced colorectal cancer treated with cetuximab*. J. Clin. Oncol., 2008. **26**(Copyright (C) 2010 American Chemical Society (ACS). All Rights Reserved.): p. 374-379.
  18. Lievre, A., et al., *KRAS Mutation Status Is Predictive of Response to Cetuximab Therapy in Colorectal Cancer*. Cancer Res., 2006. **66**(Copyright (C) 2010 American Chemical Society (ACS). All Rights Reserved.): p. 3992-3995.
  19. Di, F.F., et al., *Clinical relevance of KRAS mutation detection in metastatic colorectal cancer treated by Cetuximab plus chemotherapy*. Br. J. Cancer, 2007. **96**(Copyright (C) 2010 American Chemical Society (ACS). All Rights Reserved.): p. 1166-1169.
  20. Dharmasiri, U., et al., *High-Throughput Selection, Enumeration, Electrokinetic Manipulation, and Molecular Profiling of Low-Abundance Circulating Tumor Cells Using a Microfluidic System*. Analytical Chemistry, 2011. **83**(6): p. 2301-2309.
  21. Adams, A.A., et al., *Highly Efficient Circulating Tumor Cell Isolation from Whole Blood and Label-Free Enumeration Using Polymer-Based Microfluidics with an Integrated Conductivity Sensor*. Journal of the American Chemical Society, 2008. **130**(27): p. 8633-8641.
  22. Hashimoto, M., et al., *Ligase detection reaction/hybridization assays using three-dimensional microfluidic networks for the detection of low-abundant DNA point mutations*. Analytical Chemistry, 2005. **77**(10): p. 3243-3255.
  23. Barany, F., *Genetic disease detection and DNA amplification using cloned thermostable ligase*. Proc Natl Acad Sci U S A, 1991. **88**(1): p. 189-93.

24. Favis, R., et al., *Universal DNA array detection of small insertions and deletions in BRCA1 and BRCA2*. Nature Biotechnology, 2000. **18**(5): p. 561-564.
25. Khanna, M., et al., *Multiplex PCR/LDR for detection of K-ras mutations in primary colon tumors*. Oncogene, 1999. **18**(1): p. 27-38.
26. Wang, Y., et al., *Microarrays assembled in microfluidic chips fabricated from poly(methyl methacrylate) for the detection of low-abundant DNA mutations*. Analytical Chemistry, 2003. **75**(5): p. 1130-1140.
27. Situma, C., et al., *Fabrication of DNA microarrays onto poly(methyl methacrylate) with ultraviolet patterning and microfluidics for the detection of low-abundant point mutations*. Anal Biochem, 2005. **340**(1): p. 123-35.
28. Khanna, M., et al., *Ligase detection reaction for identification of low abundance mutations*. Clin Biochem, 1999. **32**(4): p. 287-90.
29. Gerry, N.P., et al., *Universal DNA microarray method for multiplex detection of low abundance point mutations*. Journal of Molecular Biology, 1999. **292**(2): p. 251-262.
30. Cheng, Y.W., et al., *Multiplexed profiling of candidate genes for CpG island methylation status using a flexible PCR/LDR/Universal Array assay*. Genome Res, 2006. **16**(2): p. 282-9.
31. Bos, J.L., *The ras gene family and human carcinogenesis*. Mutat Res, 1988. **195**(3): p. 255-71.
32. Breivik, J., et al., *K-ras mutation in colorectal cancer: relations to patient age, sex and tumour location*. Br J Cancer, 1994. **69**(2): p. 367-71.
33. Capella, G., et al., *Frequency and spectrum of mutations at codons 12 and 13 of the c-K-ras gene in human tumors*. Environ Health Perspect, 1991. **93**: p. 125-31.
34. Finkelstein, S.D., et al., *Determination of tumor aggressiveness in colorectal cancer by K-ras-2 analysis*. Arch Surg, 1993. **128**(5): p. 526-31; discussion 531-2.
35. Forrester, K., et al., *Detection of high incidence of K-ras oncogenes during human colon tumorigenesis*. Nature, 1987. **327**(6120): p. 298-303.
36. Losi, L., J. Benhattar, and J. Costa, *Stability of K-ras mutations throughout the natural history of human colorectal cancer*. Eur J Cancer, 1992. **28A**(6-7): p. 1115-20.

37. Smith, A.J., *et al.*, *Somatic APC and K-ras codon 12 mutations in aberrant crypt foci from human colons*. *Cancer Res*, 1994. **54**(21): p. 5527-30.
38. Vogelstein, B., *et al.*, *Genetic alterations during colorectal-tumor development*. *N Engl J Med*, 1988. **319**(9): p. 525-32.
39. Andersen, S.N., *et al.*, *K-ras mutations and prognosis in large-bowel carcinomas*. *Scand J Gastroenterol*, 1997. **32**(1): p. 62-9.
40. Chiang, J.M., *Role of K-ras mutations in colorectal carcinoma*. *Cancer Lett*, 1998. **126**(2): p. 179-85.
41. Rothschild, C.B., *et al.*, *Detection of colorectal cancer K-ras mutations using a simplified oligonucleotide ligation assay*. *J Immunol Methods*, 1997. **206**(1-2): p. 11-9.

## **CHAPTER 4.ISOLATION AND CHARACTERIZATION OF CIRCULATING MULTIPLE MYELOMA CELLS (CMMCS) USING A POLYMER MICROFLUIDIC DEVICE**

### **4.1 Introduction**

Multiple myeloma (MM) is an incurable hematological neoplasm, which constitutes 1% of all cancers diagnosed. [1, 2] This condition is associated with the abnormal expansion of terminally differentiated B clonal plasma cells in the bone marrow. DNA breaks as a result of additional variable diversity joining (VDJ) gene rearrangements, hypersomatic genetic changes and isotype class switching that occur in the Ig heavy chain variable region in post germinal centers give rise to malignant clonal plasma cells. [3, 4] These pathological cells produce a toxic monoclonal-paraprotein in the serum, which in turn affects the kidneys leading to renal failure. Anemia is also associated with MM as a result of suppression of other vital blood-forming cells in the bone marrow by the plasma cells.[5]

The prognosis for this condition is dim with a 5 year survival rate of 40%. High dose chemotherapy followed by autologous transplantation is the only current treatment option for this condition. The International myeloma working group (IMWG), has defined three stages of progression for MM: (i) MGUS (monoclonal gammopathy of undetermined significance), considered as the premalignant stage of MM. It is characterized by the presence of low monoclonal protein in the serum of less than 30g/L, less than 10% of clonal plasma cells in the bone marrow and no symptoms of end organ damage such as hypercalcemia, renal insufficiency and bone lesions (CRAB). (ii) SMM (smoldering multiple myeloma) is a more advanced stage of MGUS

with a higher risk progression to symptomatic myeloma (10% per year) than MGUS (1% per year). It is characterized by the presence of equal or more than 30g/L of monoclonal protein in the serum and/or a proportion of more than 10% of clonal plasma cells in the bone marrow but no symptoms of end organ stage damage (CRAB). (iii) Final advanced stage is the symptomatic myeloma stage referred to as active MM and is characterized by greater than 10% of clonal plasma cells in the bone marrow, presence of monoclonal protein in the serum ( $\geq 30\text{g/L}$ ) and urine and evidence of end organ stage damage (CRAB). [2, 6]

The presence of circulating multiple myeloma cells (CMMCs) in peripheral blood have been considered clinically significant because: (i) Studies have shown that the frequency of occurrence of CMMCs can be used as a measure of disease activity; [7] (ii) CMMCs can serve as an independent prognostic factor for survival in MGUS, SMM and active MM; [8] and (iii) CMMC presence in blood may hinder autologous transplantation protocols that rely on circulating stem cells in the peripheral blood. [1, 7, 9] It therefore follows that CMMCs have the potential to be viewed as critical biomarkers for MM disease staging, designing therapy, and monitoring patients with minimal residual disease. Furthermore, CMMCs could be used as surrogates for tissue biology studies.

However, CMMCs are rarely found in the peripheral blood and when present, constitute approximately 0.1% of the total blood composition. [1] Conventional techniques for CMMC detection have been primarily based on slide-based immunofluorescence, [10-12] multiparametric flow cytometry (MFC), [9, 13, 14] and/or



molecular methods for Ig gene rearrangements. [15] Slide-based immunofluorescence techniques are routinely used for the clinical assessment of blood smears, however they suffer from poor sensitivity and thus, unsuitable for very low level of CMMC detection, especially in the asymptomatic MGUS stage. Though flow cytometry has been shown to be more sensitive (1 CMMC per 10,000 peripheral blood cells, PBCs) than morphological based methods, flow cytometry requires a large sample volume and many complex sample processing steps such as red blood cell lysis and cell staining procedures that may lead to CMMC loss. Molecular methods, on the other hand, have been documented to be more sensitive (1 CMMC : 100,000 PBCs). [15]

Microfluidic devices have been shown to provide better sensitivity for the detection and enumeration of low abundant samples, such as circulating tumor cells (CTCs) in blood whose frequency of occurrence are on the order of  $1:10^9$  PBCs. [16-24] Advantages of using microfluidics for the enrichment of rare cells are;(i) they have the ability to select CTCs with low expression of the target antigen; (ii) there is less damage to fragile cells due to low shear stress; and (iii) minimal sample preparation is required prior to analysis. The detection of CMMCs in peripheral blood can be paralleled to the detection of epithelial CTCs in peripheral blood when considering the analysis modality based upon a positive selection process in which antibodies are used to capture cells expressing unique antigens targeted by the selection antibody. CTCs and CMMCs are both low abundant and have prognostic significance; the only difference is that CTCs are epithelial-based cells while CMMCs are from a hematopoietic origin.

A number of studies for the microfluidic enrichment of CTCs have been documented and have demonstrated superior performance criteria in terms of throughput, purity, and recovery compared to slide-based immunofluorescence, flow cytometry, and molecular techniques for the detection of these rare cells. [18, 22, 25] Microfluidics could offer several advantages for CMMC analysis such as: (i) Requiring smaller input volumes than flow cytometry as well as minimal reagents for staining producing a reduced assay cost; (ii) selected cells may be made available for post analysis, such as gene profiling and propagation; and (iii) in-situ immunofluorescence as well as in-situ FISH assays are feasible, which is significant for prognostic studies involving MM.

In a pilot study involving 20 MM patients with different disease classifications of SMM and active MM, we demonstrate the diagnostic utility of a polymer-based microfluidic device (coined here as a CMMC selection device) for the high sensitivity analysis of CMMCs directly from peripheral blood. We have previously demonstrated the isolation and enumeration of pancreatic CTCs using a similar device, which provided high purity (~86%) of the selected cell fraction and high sensitivity (51 CTCs/mL) for clinical samples and utilized anti-EpCAM antibodies for the selection of the CTCs bearing EpCAM antigens. [24] In this work, we demonstrate the ability to select CMMCs via affinity selection using anti-human CD138 as the selection antibody. In addition, we perform in-situ immunophenotyping by using fluorescently-labeled CD56<sup>+</sup>/CD38<sup>+</sup>/CD45<sup>-</sup> markers for the positive identification of CMMCs with respect to other infiltrating leukocytes. For selected samples, we also demonstrate the

identification of monoclonal CMMCs by cytoplasmic immunoglobulin (cIg) light-chain staining for the  $\kappa$  and  $\lambda$  light chains. The data presented in this work also describes the ability to correlate the number of CMMCs selected with disease classification (SMM and MM). Finally, we assess the ability to determine the *KRAS* mutational status of gDNA isolated from CMMCs selected from patient samples using a highly sensitive PCR/LDR/CE assay. To the best of our knowledge, this is the first report on the use of a microfluidic device for the analysis of CMMCs directly from clinical patient samples.

## **4.2 Experimental**

### **4.2.1 Fabrication of the CMMC Selection Device**

Hot embossing and laser ablation were used as the primary tools for fabrication of the CMMC selection device as described previously.[26] Mold masters used for hot embossing were prepared in brass using high precision-micromilling (KERN 44, KERN Micro- und Feinwerktechnik GmbH & Co.KG; Murnau, Germany) and standard carbide bits (Performance Micro Tool, Janesville, WI).[26] Hot embossing of polymer microfluidic devices was performed using a HEX03 hot embossing machine (Jenoptik Optical Systems GmbH, Jena, Germany). The embossing conditions consisted of a temperature of 155°C and 30 kN force for 120 s for the cyclic olefin copolymer, COC, substrates and 160°C and 20 kN force for 240 s for poly(methylmethacrylate), PMMA, substrates. Laser milling was accomplished using an ArF excimer laser (Rapid X 250, Resonetics Inc., Nashua, NH) with a laser fluence at the workpiece of  $\sim 15 \text{ J/cm}^2$  and a repetition rate of 50 Hz.

The CMMC selection device (see Figure 4.2) was made from the thermoplastic, cyclic olefin copolymer, COC, due to its ability to be embossed with high aspect ratio microstructures, its optical clarity, its propensity to be UV functionalized with high efficiency irrespective of channel aspect ratio, and the minimal amounts of non-specific adsorption of contaminating cells as reported elsewhere. [27] The CMMC selection device consisted of an array of high-aspect ratio sinusoidal microchannels with a nominal width of 30  $\mu\text{m}$  and depth of 150  $\mu\text{m}$  serving as the selection bed. Selection beds consisted of 50 sinusoidal microchannels, which were addressed using a single inlet and outlet microchannel arranged in a unique z-configuration.

After hot embossing, the CMMC selection device and cover plate, both of which were made from the same material, were flood exposed to broad band UV light at  $\sim 22$   $\text{mW}/\text{cm}^2$  (measured at 254 nm) for 15 min using a home-built system employing a low pressure Hg grid lamp (GLF-42, Jelight Company Inc., Irvine, CA). UV exposure produced carboxylic acid surface scaffolds that were used for the covalent attachment of monoclonal antibodies for CMMC selection (anti-CD138 antibodies).[28, 29] After UV exposure, the substrate was enclosed with the cover plate by thermal fusion bonding at a temperature of 132°C and a bonding pressure of  $\sim 1$   $\text{N}/\text{cm}^2$ . Bonding conditions were carefully selected to achieve high bond strength to accommodate the high pressures generated from pumping high viscosity fluids (*i.e.*, whole blood) at relatively high volume flow rates ( $\sim 27$   $\mu\text{L}/\text{min}$ ), but preserve structural integrity of the high-aspect ratio microchannels (aspect ratio = 5:1).

After assembly, the surface of the microfluidic channels was modified using EDC-NHS chemistry. This consisted of 50 mg/mL EDC (1-Ethyl-3-[3-dimethylaminopropyl]carbodiimide hydrochloride), 5 mg/mL NHS (N-hydroxysuccinimide) in 100 mM MES (pH 6) followed by incubation with a solution of anti-CD138 monoclonal antibodies (0.5 mg/mL; 150 mM PBS buffer, pH 7.4) overnight at 4°C. The optimum concentration of the antibody was chosen based on studies to optimize CTC recovery as reported elsewhere. [24]

In the case of impedance sensing of single cells, a separate device, which was made in PMMA, consisting of two perpendicular microchannels was fabricated via hot embossing from a mold master. A microchannel with dimensions of 50  $\mu\text{m}$  width x 75  $\mu\text{m}$  depth served as a conduit for cells flowing through this module. The second microchannel (75 x 75  $\mu\text{m}^2$ ) was used as guides to place two Pt wires, which were used as electrodes for making the single-cell impedance measurements. Impedance measurements were conducted using previously described circuitry.[30] Data were collected and analyzed using a NI-USB-6009 (National Instruments) data acquisition board and software written in LabView (National Instruments). Data were collected at 2 kHz, which allowed for sample processing through the sensor at a maximum flow rate of 20  $\mu\text{L}/\text{min}$  (80 mm/s) without generating signal aliasing.

Addressing the microfluidic network and connection between the CMMC selection device and the impedance sensor device was accomplished using glass capillaries (Polymicro Technologies, Phoenix, AZ) affixed to inlet and outlet ports configured on each module; the capillaries were sealed to the devices using epoxy

(Permapoxy, Permatex, Hartford, CT). Capillaries were connected to each other using low dead volume interconnects secured from Polymicro.

#### **4.2.2 Materials**

Pt wires (75  $\mu\text{m}$  diameter) were purchased from Sigma-Aldrich (St. Louis, MO). COC (Topas 6013S-04) plates (1/8" thick) and films (250  $\mu\text{m}$  thick) were acquired from Topas Advanced Polymers, Florence KY. 1/8" thick PMMA hot embossing stock was acquired from SABIC Polymersshapes (Raleigh, NC). 250  $\mu\text{m}$  thick PMMA films were used as cover plates for the impedance devices and were purchased from Goodfellow Corporation (Oakdale, PA). PEEK tubing and connectors were purchased from IDEX Health & Science (Oak Harbor, WA). Chemicals used for PMMA and COC surface cleaning and modification included reagent grade isopropyl alcohol, 1-ethyl-3-[3-dimethylaminopropyl] carbodiimide hydrochloride (EDC), N-hydroxysuccinimide (NHS), fetal bovine serum, and 2-(4-morpholino)-ethane sulfonic acid (MES) all of which were acquired from Sigma-Aldrich. Monoclonal anti-CD138 antibody was obtained from R&D Systems (Minneapolis, MN). Tris-glycine buffer was obtained from Bio-Rad Laboratories (Hercules, CA). PBS buffer and trypsin from porcine were purchased from Sigma-Aldrich. For CMMC immunostaining, the nuclear stain DAPI was obtained from Thermo Pierce Technologies (Rockford, IL). For immunofluorescence analysis, antibodies, such as anti-CD138 pacific blue, anti-CD45-FITC (HI30 clone), anti-CD56-PE, anti-CD38-APC, anti-Ig kappa light chain-FITC, and anti-Ig lambda light chain-APC, were purchased from eBiosciences (San Diego, CA). Propidium Iodide for viability analysis in flow cytometry studies was obtained from Thermo Pierce Technologies (Rockford, IL).

Bovine serum albumin (BSA) in PBS buffer (pH 7.4) was secured from Sigma-Aldrich. MEM-non essential amino acids were obtained from GIBCO (Grand Island, NY GEAA). QIAamp DNA Mini Kit (Valencia, CA) for genomic DNA isolation and purification, custom made oligonucleotide probes and primers for both PCR and LDR reactions were obtained from Integrated DNA Technologies (IDT, Coralville, IA). Taq 2X master mix and Taq DNA ligase were purchased from New England Biolabs (NEB; Ipswich, MA).

### **4.2.3 Cell Culture**

The RPMI-8226 (multiple myeloma) cancer cell line was purchased from American Type Culture Collection (ATCC, Manassas, VA) and cultured according to recommended conditions. Briefly, the cell line was incubated at 37°C under a 5% CO<sub>2</sub> atmosphere. RPMI 1640 with 2.5 mM L-glutamine supplemented with 10% FBS (GIBCO, Grand Island, NY) was used. For subculturing conditions, RPMI-8226 cells were grown as non-adherent cell suspensions in T25 culture flasks (Corning) by maintaining a cell density between 5 x 10<sup>5</sup> and 2 x 10<sup>6</sup> viable cells/mL with fresh media changes every 2-3 d either via dilution or replacement of new medium.

### **4.2.4 Flow Cytometry: RPMI-8226 Surface Antigen Characterization**

All flow studies were performed at the UNC Flow Cytometry Core Center. A Beckman Coulter (Dako) Cyan ADP instrument equipped with 11 parameter analysis capability – forward and side scatter and 9 colors of fluorescence using 405 nm, 488 nm and 635 nm excitations – was used. The software, which provided instrument control and data acquisition for the Cyan, was Summit. For sample preparation, approximately

$10^6$  RPMI-8226 cells obtained from total culture media were centrifuged and resuspended in cold 0.5% BSA/PBS buffer in a 1.5 mL microcentrifuge tube. One- $\mu$ g of Fc blocker (Human IgG) was added to the cell suspension and left to incubate on ice for 15 min. Ten- $\mu$ l of fluorescently-labeled antibody or Isotype control was added to the cell suspension and left to incubate for 45 min at 4°C under dark conditions. Upon completion of immobilization of the surface antibody, cells were washed 3 times by centrifuging and replacing the buffer with cold 0.5% BSA/PBS. Right before flow cytometry analysis, propidium iodide (PI) was added for viability testing.

#### **4.2.5 Clinical Samples**

Patients with different clinical stage classifications of multiple myeloma (MGUS, SMM or active MM) were recruited according to a protocol approved by the University of North Carolina's IRB. Blood specimens from healthy volunteers were collected under a separate IRB-approved protocol. A total of 20 patients with unknown disease classifications were analyzed for CMMCs while a total of 6 healthy donor blood samples served as negative controls. All specimens were collected into BD Vacutainer® (Becton-Dickinson, Franklin Lakes, NJ) tubes containing the anticoagulant EDTA and were processed within 5 h of the blood draw.

#### **4.2.6 CMMC Selection Device Operation**

Prior to blood sample infusion, the CMMCs selection module was thoroughly washed with 0.5%BSA/PBS buffer at a flow rate of 40  $\mu$ L/min for at least 5 min in order to remove unbound antibody from the microchannel walls. Blood specimens collected



into BD Vacutainer® tubes were placed on a nutator for at least 10 min to allow for homogenous distribution of blood components. Following homogenization, 0.5 mL to 2 mL of patient blood was transferred into a disposable Luer Lok™ syringe (BD Biosciences, Franklin Lakes, NJ) using a BD vacutainer female luer transfer adapter. Immediately after transfer, blood samples were processed through the CMMC selection device. A PHD2000 syringe pump (Harvard Apparatus, Holliston, MA) was used to hydrodynamically drive the blood through the CMMC selection device at the appropriate volume flow rate to attain an average linear velocity of sample through the sinusoidal microchannels (1.1 mm/s) that would maximize recovery of the CMMCs. During the course of blood sample introduction, the syringe was rotated by 180° along its longitudinal axis and lightly tapped in order to prevent sedimentation of the blood components inside the syringe to assure exhaustive and representative sample introduction. Finally, the CMMC selection device was flushed with 2.5 mL of 0.5% BSA/PBS at a linear velocity of 4 mm/s to remove any nonspecifically bound cells. At this point, the device was either submitted for on-chip immunofluorescence staining for phenotype identification or prepared for trypsin release of captured cells for impedance sensing of the selected CMMCs.

#### **4.2.7 On-chip Immunostaining of Phenotypic Cell Surface Antigens and Light Chain Cytoplasmic Immunoglobulins ( $\lambda$ light chains and $\kappa$ light chains)**

Selected cells were analyzed for surface antigens via immunostaining by; (i) Treating with Fc blocker (IgG); (ii) incubation with anti-human CD45-FITC Abs, anti-human CD38-APC, and anti-human CD56-PE for 30 min; (iii) cell fixation with 2% PFA;

(iv) permeabilization with 0.1% Triton-X100; and incubation with nuclear staining dye, DAPI. For clonal population staining, selected cells were; (i) Fixed with 2% PFA; (ii) permeabilized with 0.1% Triton-X-100; and (iii) incubated with anti-human-Ig kappa light chain-FITC, and anti-human Ig lambda light chain-APC. The stained cells were imaged using an inverted Olympus 1X71 microscope (Center Valley, PA) using 10x, 20x, 40x, and 60x dry objectives equipped with a high resolution (1344 x 1024) CCD camera (Hamamatsu ORCA-03G) and a mercury arc lamp as an illumination source. Images were collected and analyzed using Metamorph imaging software (Olympus).

#### **4.2.8 Impedance Sensing**

Following CMMC selection device rinsing, 200  $\mu$ L of the CMMC release buffer consisting of 0.25% w/v trypsin in 25 mM TRIS/192 mM glycine buffer (pH 7.4) was infused through the CMMC selection device to allow for the release of CMMCs from the antibody-containing selection channels and the subsequent collection of the released CMMCs into a microcentrifuge tube. As the CMMCs traversed through the impedance sensor, an electrical signal was recorded using in-house designed and built electronics as described previously. [30] The raw output data was subjected to a 1,000 point adjacent averaging algorithm to establish the baseline for the measurement without generating signal bias. Baseline was then subtracted from the data in order to correct for signal drift. Impedance responses generated from CTCs were counted when the signal-to-noise ratio exceeded 3:1. Note that during blood infusion into the CMMC selection bed and the subsequent washing step, the output capillary of the CMMC selection device was disconnected from the impedance sensing device with the output

going into a microfuge tube for waste collection. When the release buffer was introduced into the CMMC selection bed, the output capillary was then reconnected to the impedance sensing device. The output port of the impedance sensing device was also inserted into a 1.5 mL microcentrifuge tube where all released cells were collected for subsequent molecular analysis.

#### **4.2.9 *KRAS* Mutational Analysis of CMMCs**

Genomic DNA (gDNA) was extracted and purified from HT-29 and RPMI-8226 cell lines and released CMMCs using a QIAamp DNA Mini Kit (Valencia, CA). For on chip gDNA extraction, the lysing buffers provided in the kit were infused through the device and eluent was further processed and purified following the recommendations of the manufacturer.

PCR amplifications were carried out to generate 290 bp amplicons of gDNA from HT-29, RPMI-8226 and CMMCs from clinical samples using gene-specific primer sequences (see Table 4.1 for *KRAS* primer sequence). The PCR cocktail consisted of a 50  $\mu$ L reaction consisting of 10 mM Tris-HCl, 50 mM KCl, 1.5 mM MgCl<sub>2</sub>, 0.2 mM dNTPs, 5% Glycerol, 0.08% IGEPAL® CA-630, 0.05% Tween® 20, 25 units/mL Taq DNA Polymerase, (pH 8.6) and cellular gDNA. Amplification was achieved by thermally cycling for 35 cycles at 94°C for 30 s, 59°C for 2 min and a final extension at 72°C for 3 min. PCR was carried out using an Eppendorf Thermal Cycler (Brinkmann Instrument Inc., Westbury, NY).

Table 4.1 *KRAS* PCR primer sequences

<i>KRAS</i> PCR	Sequence	Bases	T <sub>m</sub> (°C)
<i>KRAS</i> - Forward	TTAAAAGGTACTGGTGGAGTATTTGATA	28	54.0
<i>KRAS</i> - Reverse	AAAATGGTCAGAGAAACCTTTATCTGT	27	54.8

Slab gel electrophoresis was performed on an aliquot of the PCR products using a 3% agarose gel (Bio-Rad Laboratories, Hercules, CA) prestained with ethidium bromide. Amplicons were indexed against a DNA sizing ladder (50 – 1,000 bp, Molecular Probes, Eugene, OR). Separation was performed at 4.8 V/cm in 164 1x TBE (Tris/Boric Acid/EDTA, Bio-Rad Laboratories). After separation, the gels were imaged using a Logic Gel imaging system (Eastman Kodak). For *KRAS* mutational analysis, the PCR amplicons were either submitted for Sanger sequencing by Genewiz Technologies (Research Triangle Park N.C) or used for subsequent LDR analysis. For Sanger sequencing, DNA analyzer ABI 3730xl was used for capillary electrophoresis and fluorescent dye termination detection

Bench-top LDRs were performed in a total volume of 20 µL in 0.2 mL polypropylene microtubes using a commercial thermal cycling machine (Eppendorf Thermal Cycler (Brinkmann Instrument, Westbury, NY, USA). The reaction cocktail typically employed in this work consisted of 10 mM TRIS–HCl (pH~8.3), 25 mM KCl, 10 mM MgCl<sub>2</sub>, 0.5 mM NAD<sup>+</sup> (nicotinic adenine dinucleotide, a cofactor for ligase enzyme), and 0.01% Triton X-100, 2 µL of 50 nM of the discriminating primers and fluorescently labeled freshly phosphorylated common primers (see Table 4.2 for the LDR common and discriminating primer sequences) and 2 µL of the PCR product as template. Forty

U of Taq DNA ligase (New England Biolabs) was added to the cocktail under hot-start conditions and the reactions were thermally cycled 20 times for 30 s at 94°C and 2 min at 60°C. The LDR products were stored at 4°C until needed for capillary gel electrophoresis (CGE). The LDR products were separated using a CEQ 8000 Genetic Analysis System (Beckman Coulter, Fullerton, CA, USA). Data acquisition was performed using the Beckman P/ACE software.

Table 4.2 *KRAS* LDR primer sequences

LDR primer	5'-Sequence-3'	Bases	T <sub>m</sub>
Common_12.1	GTGGCGTAGGCAAGAGTGCCAA-Cy5	22	62.2
Common_12.2	TGGCGTAGGCAAGAGTGCCCT-Cy5	20	61.5
Common_13.3	GCGTAGGCAAGAGTGCCCTTGA-Cy5	21	59.9
Common_13.4	CGTAGGCAAGAGTGCCCTTGAC-Cy5	21	58.1
<i>KRAS</i> 12.1 WT	TTTTTTTTTTTTTTTTTATATAAACTTGTGGTAGTTG	43	58.4
<i>KRAS</i> 12.1 A	TTTTATATAAACTTGTGGTAGTTGGAGCTA	30	54.5
<i>KRAS</i> 12.1 C	TTTTTATATAAACTTGTGGTAGTTGGAGCTC	32	55.8
<i>KRAS</i> 12.1 T	TTTTTTTTATATAAACTTGTGGTAGTTGGAGCTT	34	56.1
<i>KRAS</i> 12.2 WT	TTTTTTTTTTTTTTTTTTTAACTTGTGGTAGTTGG	43	60.0
<i>KRAS</i> 12.2 A	TTAACTTGTGGTAGTTGGAGCTGA	25	56.3
<i>KRAS</i> 12.2 C	TTTTAACTTGTGGTAGTTGGAGCTGC	27	57.8
<i>KRAS</i> 12.2 T	TTTTTAACTTGTGGTAGTTGGAGCTGT	29	57.3
<i>KRAS</i> 13.1 WT	TTTTTTTTTTTTTTTTTTTGTGGTAGTTGGAGCTGG	39	59.9
<i>KRAS</i> 13.1 A	CTTGTGGTAGTTGGAGCTGGTA	22	56.4
<i>KRAS</i> 13.2 WT	TTTTTTTTTTTTTTTTTTTGTGGTAGTTGGAGCTGG	40	61.0
<i>KRAS</i> 13.2 A	TGTGGTAGTTGGAGCTGGTGA	21	58.2

## 4.3 Results and Discussion

### 4.3.1 Flow Cytometry Phenotype Characterization of RPMI-8226 as a Model Cell Line for CMMC

Multiple myeloma cells have a characteristic antigen surface expression that distinguishes them from normal B-plasma cells. Normal B plasma cells go through somatic hypermutations (SHM) in the Ig gene that take place during the germinal center stage of differentiation while malignant clonal plasma cells are formed at the post germinal center stage of differentiation and do not go through SHM processes resulting in a different in surface antigen expression from normal B-plasma cells. The criteria for MM phenotype identification that has been well documented indicates that primary myeloma cells strongly express CD38 and CD138 and in some cases, the expression of CD56 is also observed. In addition, a weak to almost no expression of CD45 is observed in most stages of MM. [31] A number of studies have utilized cells lines as models for primary myeloma cells as they share some essential features, such as Ig gene re-arrangement, cytoplasmic idiotype expression and surface antigen expression. [31] In this study, we selected RPMI-8226 cells as a model for primary multiple myeloma cells.

We first performed phenotypic characterization of these cells using flow cytometry in order to evaluate the fraction of RPMI-8226 cells expressing key myeloma surface antigens. Results indicated that out of a defined population of approximately 60,000 RPMI-8226 cells, 98% expressed CD38, 90% expressed CD138, 74% expressed CD56 while <0.01% showed minimal expression of CD45 (see Figure 4.1). This agrees well with studies that utilized the same cell line.[31] Though a greater fraction of RPMI 8226

expressed CD38 than CD138, we chose to use anti-CD138 as the selection agent for CMMCs because CD138 is solely and strongly expressed on plasma cells as opposed to CD38, which is expressed in both lymphoid and myeloid cells and thus may not provide the necessary specificity. [31, 32]

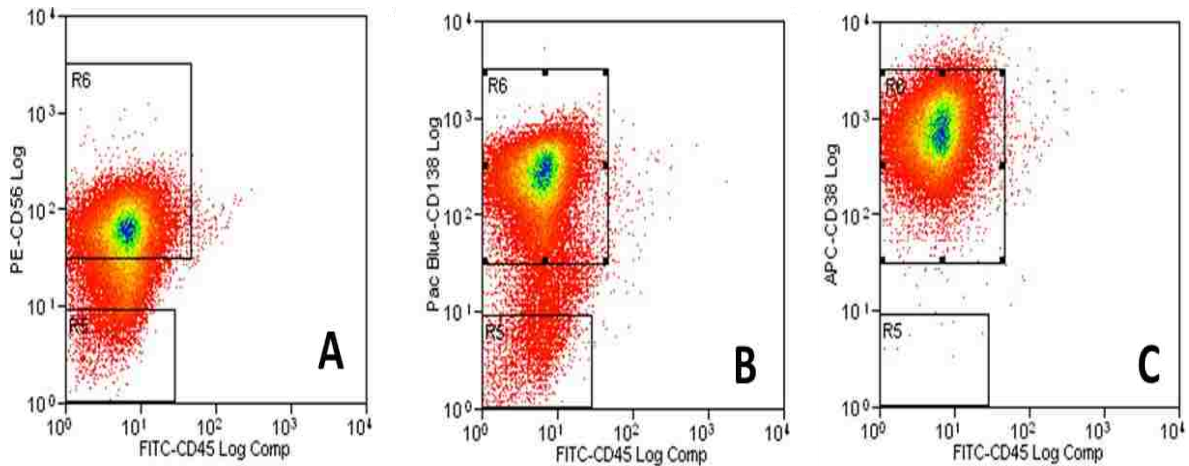


Figure 4.1 Fluorescence dot plots showing typical CD antigen expression on RPMI-8226 cells. All plots were gated on CD45<sup>-</sup>. The resulting dot plots indicate: (A) 74% of these cells express CD56<sup>+</sup>; (quadrant R6); (B) 90% of the cells express CD138<sup>+</sup> (quadrant R6); and (C) 98% of the cells express CD38<sup>+</sup> (quadrant R6). Fluorochromes used for each antibody was PE for CD56, APC for CD38, Pacific blue for CD138 and FITC for CD45

#### 4.3.2 RPMI-8226 Cell Translational Velocity Optimization for Capture on the CMMC Selection Device

The CMMC selection device has been utilized in previous studies in our research group for the specific selection of CTCs on the basis of antigen-antibody interactions (*i.e.*, positive selection). [23, 24, 30, 33] The selection bed consisted of 50 high aspect ratio curvilinear channels with dimensions of 30  $\mu\text{m}$  (width) and 150  $\mu\text{m}$  (depth) arranged in a z-configuration format (see figure 4.2 a & b). The channel

width dimension was designed to be as close as possible to the CTC diameters, which ranged from 10-25  $\mu\text{m}$ , while a depth of 150  $\mu\text{m}$  was selected to increase the throughput of the device. [30] Similarly, plasma cells have been found to be oval with diameters ranging from 9-20  $\mu\text{m}$ ; the average cell diameter for RPMI-8226 was measured to be  $13.7 \pm 2 \mu\text{m}$  via optical analysis. Based on the similar dimensions of CTC and CMMCs, we sought to use the same device for the selective capture of CMMCs.[34] Figure 4.2 d indicate DAPI stained CMMCs captured along the walls of a curvilinear channel in the CMMC selection device.

In previous studies, tumor specific antibodies such as anti-EpCAM were immobilized onto the walls of a selection bed via commonly used peptide chemistry following activation of the selection bed surfaces with UV light to generate carboxylic acid moieties. [18, 30, 35] Based on the same premise, CD138 was anchored onto the channels walls of the CMMC selection device and used as the selection antibody for CMMCs.

Optimal capture conditions for cells travelling through curvilinear channels were based on the Chang and Hammer model, which describes the dependence of the linear velocity of solution containing antigenic-bearing targets on the encounter rate and probability of reaction between solution-borne cells and surface tethered cell affinity agents. [36] We proceeded to investigate the optimal linear velocity in order to obtain the maximum recovery for CMMCs using RPMI-8226 as a model for this study.



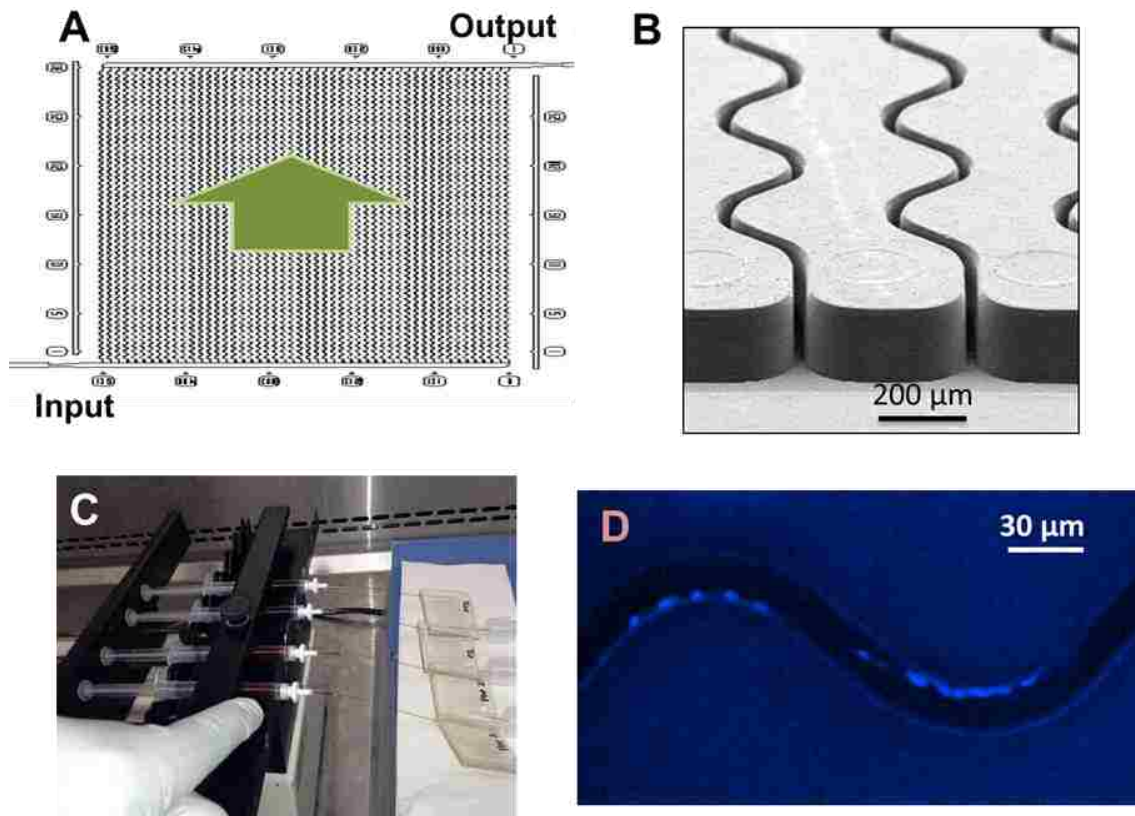


Figure 4.2 (A) Schematic of the CMMC selection device with an array of 50 parallel sinusoidal microchannels and inlet/outlet channels arranged in a z-configuration. Flow of blood is indicated by the green arrow. (B) SEM of the selection bed depicting high-aspect ratio ( $30 \times 150 \mu\text{m}$ ,  $w \times d$ ) sinusoidal microchannels and the output channel. (C) Blood processing setup in a biological safety hood showing blood filled syringes set on a Harvard apparatus multi-syringe pump. The syringes are each connected to inlet capillaries interfaced to the CMMC selection devices. (D) DAPI fluorescent image of CMMCs captured on either side of a sinusoidal microchannel.

Based on our findings as presented in Figure 4.3A, the maximum cell capture efficiency ( $71\% \pm 6\%$ ) was found to occur at a translational velocity of 1.1 mm/s under the conditions employed. These flow rate dependent capture studies followed the same trend as seen in previous studies for CTCs, which indicated that the cell

capture efficiency maximized by balancing conditions to optimize the encounter rate, which increases at higher flow rates, and the antigen/antibody reaction time, whose probability is reduced at higher flow rates. [37, 38] From previous studies, the optimal linear velocity for CTC recovery was found to be 2.0 mm/s. However, our findings indicated that the optimal translational velocity was less than that for CTCs (1.1 mm/s) indicating that the reaction rate is much slower for the anti-CD138/CD138 interaction compared to the anti-EpCAM/EpCAM association. A number of factors determine the rate dependent probability of association; (i) the expression level of the target molecule on the surface of the cell; (ii) adhesion strength between the antibody and antigen; and (iii) the accessibility of the antibody to its recognition element.[30, 38] CTCs are adherent cells and have a tendency to stick onto surfaces, which could increase reaction time lowering the strict dependency on flow rate. Also, the expression level of epithelial adhesion molecules in many cell types is very high; approximately 500,000 for breast cancer cell lines and 1,000,000 for colorectal cancer cell lines. [39, 40] However for CMMCs, which are primarily hematopoietic cells, they tend to be non-adherent and thus, have less of a tendency to stick onto surfaces. Though the exact expression level of CD138, which is the selection antigen we are using herein, has not been documented for CMMC model cells lines, we can assume that it is lower than CTC model cell lines as seen in tissue culture of both cells types. RPMI 8226 cells expand as suspended cells in growth media while MCF 7s (epithelial based CTCs) tend to attach and flatten onto the surface of tissue culture plate with the growth media covering the cells.

Lower reaction rates of the anti-CD138/CD138 pair in the case of CMMCs compared to the anti-EpCAM/EpCAM pair can be attributed to the expression of the antigen molecule CD138 also referred to as Syndecan-1 molecule. In MM, the systems of adhesion are regulated by cytoplasmic and extracellular mechanisms. Syndecan-1 molecules are the principal MM receptor systems of the extracellular matrix. Major roles of these molecules are to control tumor cell survival, growth, adhesion and bone cell differentiation in MM. Reports have indicated that the expression of CD138 is significantly decreased in MM cells and this has been associated with poor clinical outcomes. [41-45] Also the loss of Syndecan-1 is associated with the loss of anchorage dependent growth. Therefore, MM cells adapt a mesenchymal morphology and behavior. [43, 45] This low expression may result in a lower reaction rate requiring lower linear velocities to maximize the recovery as observed in the CMMC translational studies

In order to evaluate the capture sensitivity of the CMMC selection assay, we seeded 20, 150, 250 and 500 RPMI-8226 cells per 500  $\mu$ l of blood. The best-fit linear function to the data plotted in Figure 4.3B had a slope of 0.6865 ( $r^2 = 0.9994$ ). This demonstrated the ability of the assay to maintain capture recovery at different seed levels within the tested range. In addition the ability to detect varying numbers of cells makes this assay suitable for the detection of varying numbers of CMMCs from patient with different disease classification from MGUS to SMM to fully active MM. [1, 7]

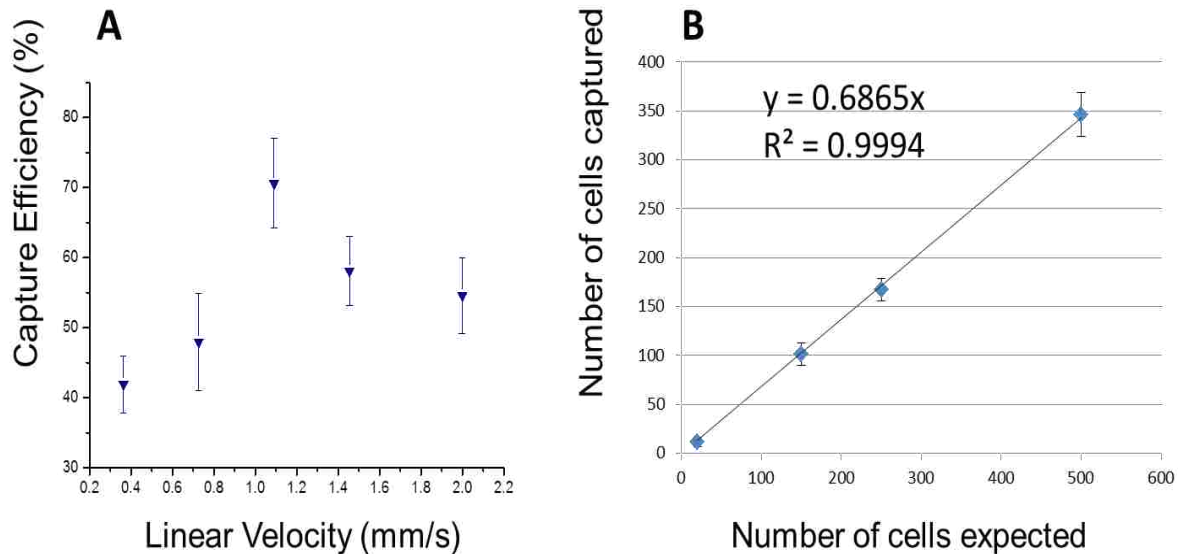


Figure 4.3 (A) Graph showing cell capture efficiency versus cell translational velocity. In these experiments an estimated 500 RPMI-8226 cells were seeded into RPMI-1640 total cell medium. The cells were prestained with a live nuclei cell dye and were introduced in the CMMC selection device at linear velocities ranging from 0.4-2 mm/s. Capture efficiency was determined by the ratio of RPMI-8226 cells captured on the CMMC selection device to the total number of RPMI-8226 cells selected on chip and collected in the effluent. Number of cells captured was determined by both brightfield and fluorescence microscopy. (B) Calibration plot of RPMI-8226 cells seeded (20-500 cells/0.5 mL) of healthy donor blood and processed through the device at the optimized linear velocity of 1.1 mm/s. Capture sensitivity for the CMMC selection assay was given by the slope ( $m = 0.6865$ ,  $r^2 = 0.9994$ ).

#### 4.3.3 On-chip Phenotype and Clonal Identification of RPMI-8226 Cells and CMMCs from Clinical Samples

Multiparametric flow cytometry (MFC) immunophenotyping has been used in clinical research studies for the differential diagnosis of MGUS, SMM and active MM.[46] There has been growing consensus on the use of a panel of antigens for the

detection of both normal and aberrant plasma cells in the bone marrow or in the peripheral blood. In particular, six-color analysis of CD138, CD38, CD45, CD56, cytoplasmic Ig  $\kappa$ , and cytoplasmic Ig  $\lambda$ , has been employed in MFC for the detection of both normal and aberrant clonal fractions of plasma cells. [1, 47] Each of these antigen markers have a functional role and are classified as: (i) Co-receptors for plasma cell signaling; (ii) molecules involved in cell-to-cell adhesion; (iii) molecules that facilitate growth of plasma cells; and (iv) proteins involved in cell survival. [32] Both CD138 and CD38 are used in combination and are found to be expressed in plasma cells. CD138 in particular is a heparin sulfate proteoglycan that promotes cell surface adhesion to collagen, fibronectin and thrombospondin. CD56 is found in some cases of active MM and has been correlated with the aggressiveness of the disease and thus, a useful marker for follow-up of minimal residual disease. [46, 47] For specific identification of clonal populations within the plasma cell population, the addition of both cytoplasmic immunoglobulin (Ig  $\kappa$ ) and (Ig  $\lambda$ ) light chain markers have been utilized. Normal plasma cell populations will have approximately equal expressions of both light chain cytoplasmic immunoglobulin markers, while pathological plasma cells will show higher expressions with  $\kappa/\lambda$  ratios  $>0.5$ . [48]

Although flow cytometry has been shown to be more clinically sensitive than morphological methods, flow cytometry does have some drawbacks for the analysis of pathological plasma cells in peripheral blood. For instance, the depletion of plasma cells in the blood resulting from RBC lysis procedures leads to sample loss, flow cytometry is

not an enrichment technique and therefore the analysis is only limited to detection and renders the plasma cells detected inaccessible for further downstream analyses such as

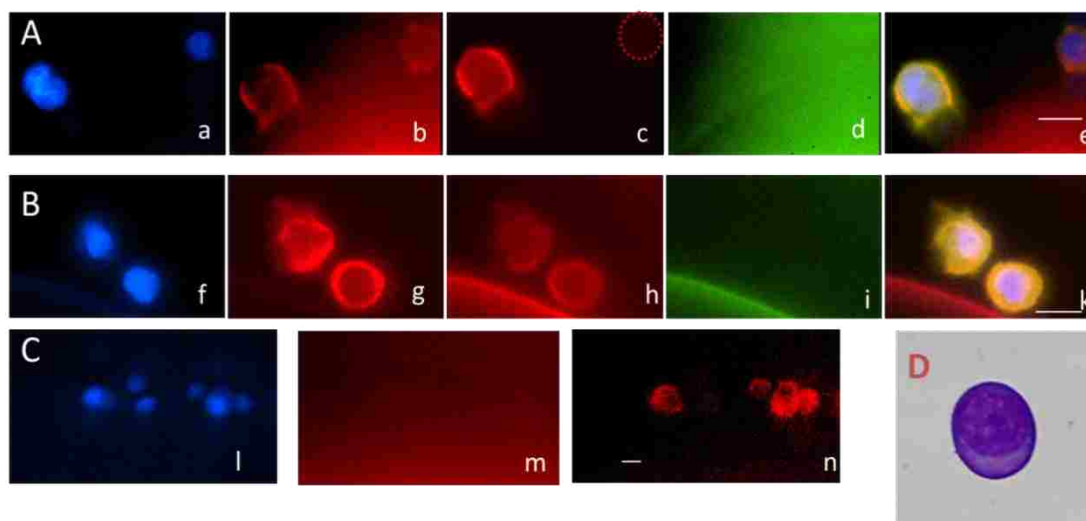


Figure 4.4 In-situ immunophenotyping and cytoplasmic staining of CMMCs. Panels (A) and (B) represent RPMI-8226 cells and CMMCs selected in a polymer microchannel via anti-human CD138/CD138, respectively. Positive CMMC surface markers are presented by micrographs: (b,g) CD56-PE; (c,h) CD38-APC; while (d,i) are negative control marker CD45-FITC for leukocyte identification. DAPI was used for nuclei identification (a,f,l). Panel (C) represents cytoplasmic staining of RPMI-8226 cells, which are the  $\lambda$  light chain expressing cells, using anti human Ig $\kappa$ -PE (m) and anti-human Ig $\lambda$ -APC (n). (D) H&E image of a released plasma cell from the CMMC selection bed using enzymatic release via trypsin. All bars represent 10  $\mu$ m.

propagation and molecular profiling. Microfluidics has, on the other hand, been shown to be more sensitive in the detection and enrichment of rare occurring cells compared to flow cytometry. [18, 22, 24, 40] The advantages of using microfluidics compared to flow cytometry include the fact that smaller samples are sufficient for the analysis, samples are contained in an enclosed device therefore minimizes sample contamination, no sample pre-processing steps are required, and finally, assay cost reduction due to the use of lower amounts of fluorescently tagged antibodies required for

immunophenotyping of the plasma cells. Studies involving the enrichment of CTCs using microfluidics have demonstrated on-chip immunophenotyping for the identification and enumeration of CTCs captured on chip. [24, 49] Following the same concept, we performed in-situ immunophenotyping of plasma cells selected by CD138 from either cell suspensions of RPMI-8226 in media as well as plasma cells selected from clinical samples. For surface staining, the following criteria was used to identify both normal and aberrant plasma cells; CD38<sup>+</sup>/CD56<sup>+</sup>/DAPI<sup>+</sup>/CD45<sup>-</sup> and/or CD38<sup>+</sup>/DAPI<sup>+</sup>/CD45<sup>-</sup> and/or CD56<sup>+</sup>/DAPI<sup>+</sup>/CD45<sup>-</sup> (see Figure 4.4 and 4.5). All other phenotypes were considered to be contaminating cells. Our results indicated that successful on-chip immunophenotyping was achieved in both RPMI-8226 model myeloma cell line (Figure 4.4A) and in CMMCs enriched from clinical samples (Figure 4.4B). Standard on-chip fluorescence imaging conditions were optimized using the RPMI-8226 cell line as a control as we already established the phenotype using flow cytometry as discussed in Section 4.1.

For cytoplasmic light chain staining, the approach we adopted used fluorescently-labeled anti-cytoplasmic Ig (κ) and anti-human Ig (λ) to identify clonal populations of CMMCs captured on-chip. In order to establish monotypic clonality using cytoplasmic light chain staining conditions, we used RPMI-8226 as a standard because it has already been established that RPMI-8226 is a lambda light chain expressing cell line (See Figures 4.4C and 4.6A).[31] Therefore, for one patient, we identified clonal populations of Kappa expressing cells, which formed a greater majority of the total number of cells captured on the CMMC selection chip (see Figure 4.6B).

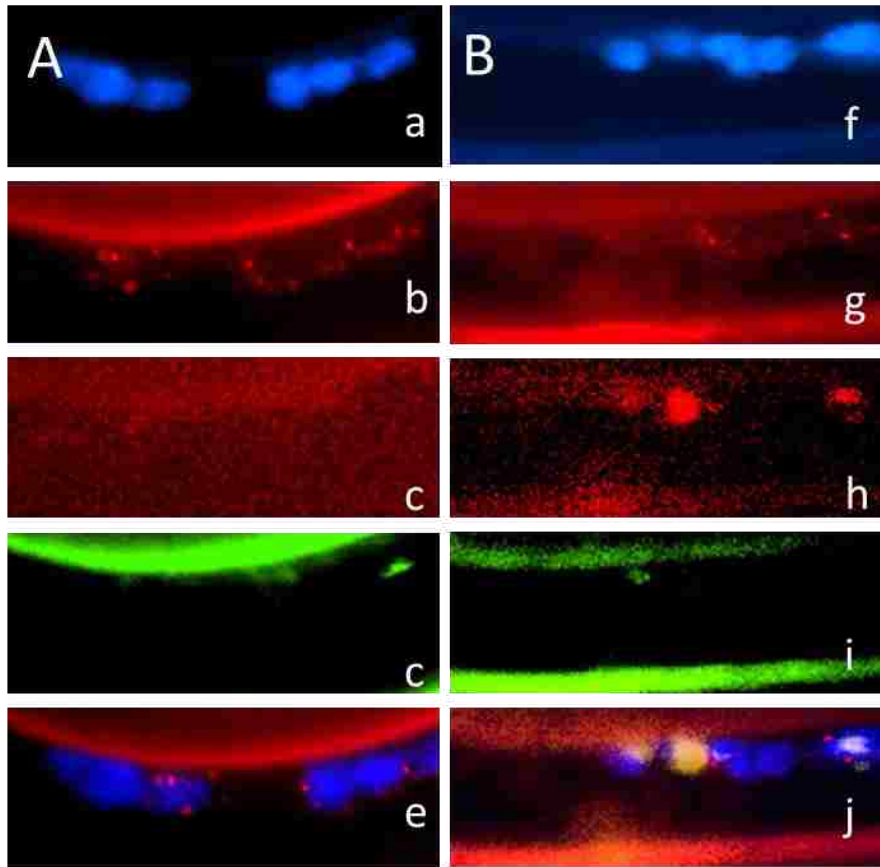


Figure 4.5 Alternative confirmatory phenotypes for CMMCs isolated from a patient sample. Panel (A) represents 6 CD138 selected cells that were found to be CD56<sup>+</sup> (b) and CD38<sup>-</sup> (c). Panel (B) shows a mix of two phenotypes side-by-side, 3 CD38<sup>+</sup>/CD56<sup>+</sup> positive cells (g,h) next to 2 CD56<sup>+</sup>/CD38<sup>-</sup> cells (h). Both panels show dim to no expression of CD45 (c,i). Nuclei were stained with DAPI (a,f). Composite images are show in e & j for both panels.



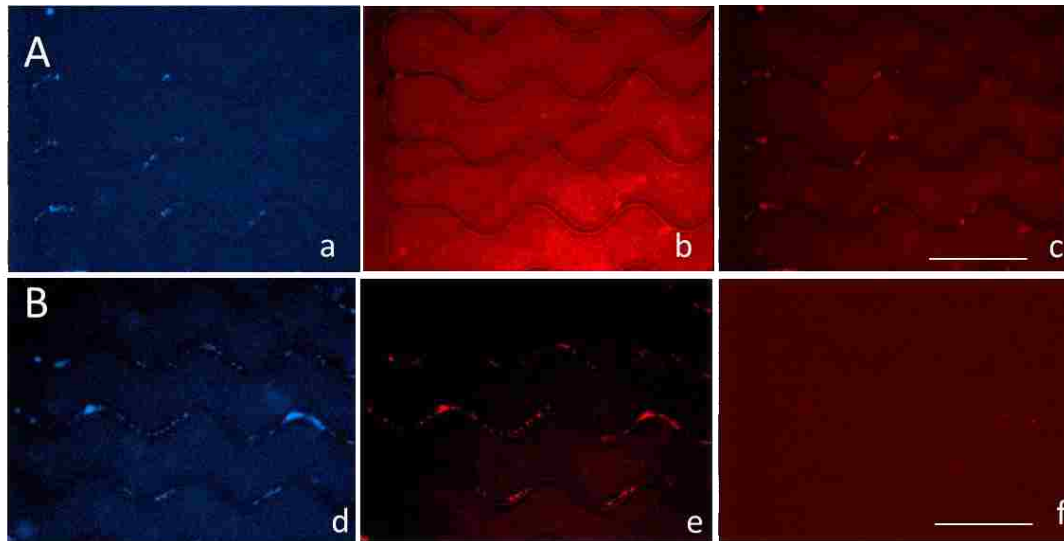


Figure 4.6 Panels A and B represent cytoplasmic staining of a clinical sample with active MM (B) using anti-human Ig  $\kappa$ -PE (b,e) and anti-human Ig  $\lambda$ -APC (c,f) and (C) cytoplasmic staining of RPMI-8226 cells as a control. Results indicated strong Kappa expression for approximately 70% of the cells enumerated and weak expression of about 10% of the total cells captured on the device for the clinical sample. Imaging conditions: 5x objective, 1.2 s exposure time for PE (Kappa) and 9 s exposure time for APC (Lambda). Bars represent 150 $\mu$ m.

#### 4.3.4 CMMCs in SMM and Active MM Clinical Samples

A total of 20 MM patient samples were analyzed in a blind study in order to determine the correlation of disease state and number of CMMCs selected. MM patients diagnosed were diagnosed with either SMM (n = 6) or active MM (n = 14). For active MM patients, we isolated an average of  $347.8 \pm 300.4$  CMMCs/mL, median = 213 CMMCs/mL with a range of 100 to 742 CMMCs/mL. CMMCs were selected in all patients with active MM. For the controls, in most cases no CMMCs were observed. We also analyzed blood from 6 patients who had been determined to have asymptomatic SMM. We found an average of  $13.2 \pm 8.9$  CMMCs/mL for this group of patients. Based

on the Kruskal-Wallis test ( $p = 0.00005$ ), there was a significant difference in the CMMCs/mL between asymptomatic SMM, and symptomatic MM, and controls. Pairwise Wilcoxon Rank-Sum tests suggested that there was a significant difference between active MM and healthy patients ( $p = 0.0006$ ). Between SMM and controls there was also a statistically significant difference in terms of CMMC numbers ( $p = 0.04$ ). Comparison between asymptomatic SMM and symptomatic MM patients also indicated a significant CMMC number difference ( $p = 0.0006$ ). This data is summarized in the box plot shown in Figure 4. 7.

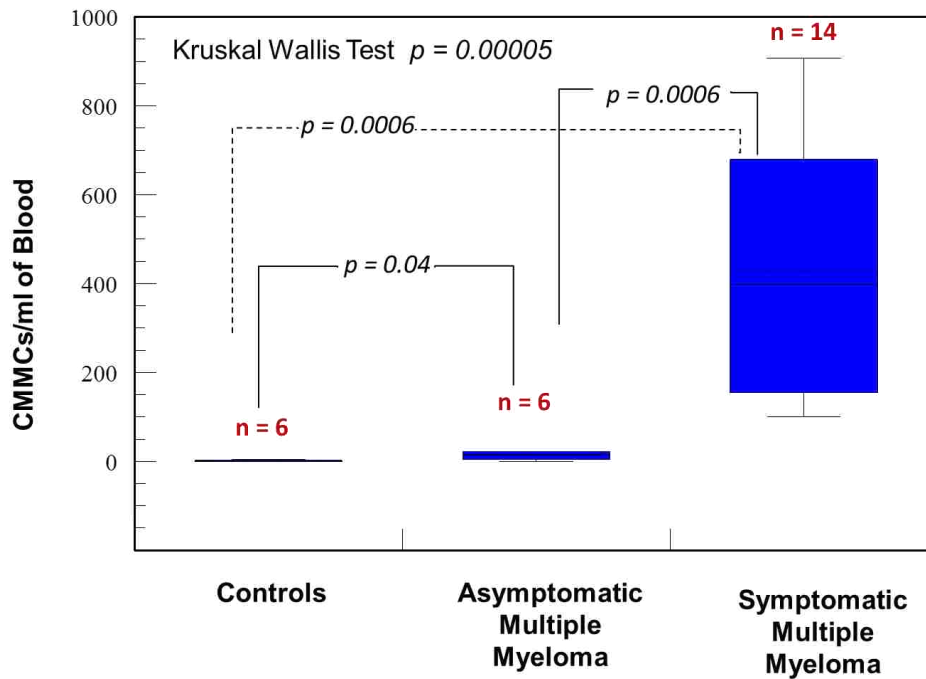


Figure 4.7 Box plots presenting count of CMMCs selected in chip from MM patient blood samples. Data are normalized to 1 mL. Lower and upper edges of box show 25th and 75th percentiles, respectively. Solid line in box represents median, and solid diamond represents mean. Error bars show maximum and minimum values.

#### 4.3.5 KRAS Mutational Analysis of Isolated CMMCs (PCR/LDR/CE)

*RAS* mutations in codons 12, 13 and 61 have been found at high frequencies in a number of cancers such as pancreatic, colorectal, lung and thyroid cancers.[50-58] The *RAS* genes encode membrane-associated guanosine triphosphates (GTPases), which are important signaling intermediates involved in the responses to a number of growth factors.[50] It therefore followed that alterations in the *RAS* gene may affect cell growth leading to cancer. *RAS* mutations have been shown to have diagnostic significance in colorectal cancer, whereby patients with mutated *KRAS* do not benefit from anti-EGFR therapy, whereas patients with wild-type *KRAS* genotypes do benefit from this therapy. [56, 58, 59]

In multiple myeloma, while the pathogenesis of the disease is not clearly known, reports have hypothesized that activating mutations of *RAS* oncogenes may contribute to interleukin 6-independent growth of myeloma cells and the suppression of apoptosis.[60] Both *NRAS* and *KRAS* mutations have been documented with a frequency of occurrence of 39% in newly diagnosed patients. It has been reported that *NRAS* mutations within codon 61 are more frequent than *NRAS* mutations found in 12, 13, and *KRAS* mutations in most MM cases. [61] The same study also indicated that *KRAS* mutations had prognostic significance with tumor burden and survival rate while *NRAS* mutations did not. Other reports also indicated that multiple mutations were found in some patients indicating heterogeneous populations of pathological plasma cells. [57]

In this study, we performed *KRAS* mutational analysis from purified genomic DNA extracted from both RPMI-8226 cells captured on the selection device and from CMMCs captured on chip from 4 clinical samples. In order to evaluate the sensitivity of our CMMC selection assay for subsequent *KRAS* mutational analysis, we seeded RPMI-8226 cells ranging from 20 to 750 cells into 0.5 mL of total cell medium and subsequently enriched them using the CMMC selection device. These cells were then released from the selection bed via trypsin, enumerated using an impedance sensor and the eluent was purified for its gDNA content with the purified material subjected to PCR. In addition, CMMCs selected from 4 clinical samples using the CMMC selection device were also released and subjected to PCR. gDNA extracted from HT-29 cells as well as RPMI-8226 cells were used as positive controls for the PCR analysis. PCR products from all 4 patient samples were submitted for Sanger sequencing for the possible detection of SNPs in the *KRAS* gene. Results seen in Figure 4.9f showed a single mutation found in patient 36 at the 37<sup>th</sup> nucleotide, where G was substituted for A; this denotes the G13S mutation, which results in a glycine substitution for serine in the resulting protein product. Although direct nucleotide sequencing is a well-established technique, the sensitivity was not adequate for the detection of low abundant mutant copies in a high background of wild type copies.

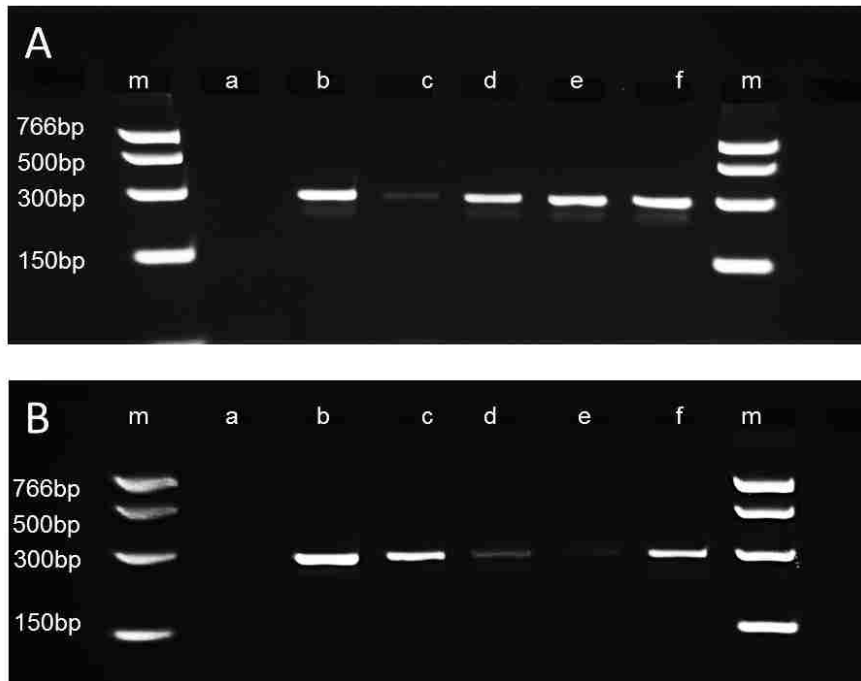


Figure 4.8 Agarose gel electrophoresis of PCR products generated from (A) RPMI-8226 cells and (B) CMMCs from 4 patient samples. PCR was run with 35 cycles with an initial denaturation step of 2 min and final extension for 7 min. Each cycle consisted of: 94°C (30 s), 59°C (30 s), 72°C (40 s). The gel was stained with ethidium bromide and run at 4.8 Vcm<sup>-1</sup>. (A) Gel electropherogram for PCR performed on RPMI-8226 cells with; (a) no gDNA template; (b) gDNA template from HT-29 directly (positive control); (c) gDNA from 20 RPMI-8226 cells; (d) gDNA from 150 RPMI-8226 cells; (e) gDNA from 500 RPMI-8226 cells; and (f) gDNA from 750 RPMI-8226 cells. Lanes a-f contain 5 µL of DNA amplicons. (B) Gel electropherogram for PCR performed on CMMCs obtained from 4 clinical samples analyzed using the CMMC selection device: (a) No gDNA and used as a negative control; (b) gDNA template from RPMI-8226 directly used as a positive control. (c) gDNA from patient 35; (d) gDNA from patient 36; (e) gDNA from patient 37; (e) gDNA from patient 38. Positive controls consisted of harvesting either HT-29 or RPMI-8226 cells from the culturing dish (~1,000 cells), lysing them, performing a solid-phase extraction of the gDNA followed by PCR of the purified sample.

LDR coupled to PCR is a method that has been shown to detect single-point mutations in DNA with sensitivities approaching 1 mutant copy in 4,000 wild type copies and is thus better equipped to detect *KRAS* mutations from heterogeneous

samples compared to Sanger sequencing.[62-64] Briefly, following PCR amplification of the gene fragment of interest, the amplicons are mixed with two LDR primers, a common and discriminating primer that flank the point mutation of interest. The discriminating primer contains a base at its 3'-end that coincides with the single base mutation site. If the 3' nucleotide of the discriminating primer is not complementary to the mutation site being interrogated, ligation of the common and discriminating primers does not occur. A perfect match between the 3'-end of the discriminating primer to the target DNA does occur, ligation of the common and discriminating primers occur and resultant LDR product length becomes the sum of nucleotides from these two primers. LDR products are then detected using CGE (capillary gel electrophoresis) based on differences in the electrophoretic mobility of ligated versus unligated primers. In our experiments, purified PCR amplicons from HT-29, RPMI-8226 and CMMCs from patients 35, 36, 37, 38 were used in the LDR assay for the detection of possible *KRAS* mutations in codons 12 and 13. Sequences used in this study for both discriminating and common primers for each possible mutation were designed from Khanna *et al.* and are listed in Table 2. [63] Genomic DNA from the HT-29 colorectal cell line was used as a negative control for these studies as it is well documented that it bears no *KRAS* mutations. gDNA from the RPMI-8226 cell line has been documented to be heterozygous, bearing both the wild type allele as well as a *KRAS* mutated allele with the G12A (c12.2C) mutation.

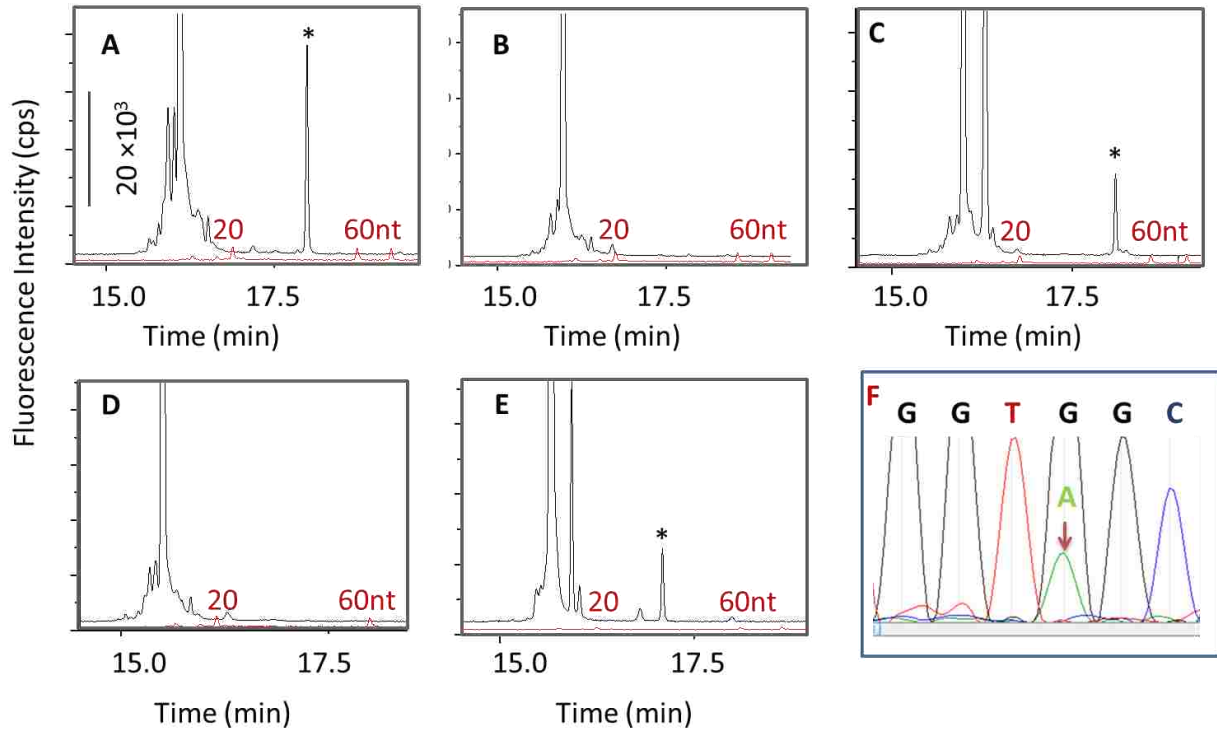


Figure 4.9 LDR and Sanger sequence analysis of sequence variations in the *KRAS* gene for codons 12 and 13 with the gDNA secured from RPMI-8226 cells, HT-29 cells, and CMMCs isolated from clinical samples. LDR consisted of 20 cycles. Initial denaturation was performed at 95°C for 2 min. Each cycle consisted of: 95°C (30 s); 60°C (2 min); and 4°C as a final hold. LDR products were analyzed using CGE performed at a capillary temperature of 60°C with an initial denaturation step prior to injection at 90°C for 3 min. CGE injection was performed at 2.0 kV for 30 s and separation was done at 6.0 kV. CGE electropherograms for various samples are shown in (A-F). LDR product peaks are represented with an asterisk \*. (A) shows the 49 nt LDR product denoting the G12A mutation found in RPMI-8226; (B) and (D) show no LDR products at the c12.2 C locus for HT-29 and patient 35, respectively; (C) shows a 54 nt LDR product denoting the G12S mutation for patient 35; and (E) shows a 42 nt product denoting the G13D mutation for patient 36. DNA size markers of 20 and 80 nt were co-electrophoresed with the LDR products. (F) Sanger sequencing trace for gDNA secured from patient 36 at codons 12 and 13 with an additional peak at c13.1A denoting the presence of mutant copies bearing the G13S mutation.

Results from the CGE electropherograms (Figure 4.9a-e) indicated the presence of a 49 nt LDR product in the RPMI-8226 analyses denoting the G12A mutation (Figure 4.9a) while no LDR products were seen in the HT-29 analysis (Figure 4.9b) for all mutant primer sets tested; these results are in agreement with reported studies.[40] A summary of the LDR products observed from the 4 patient samples analyzed are presented in Table 4.3. Multiple *KRAS* mutations were found in all of these samples indicating the heterogeneous nature of the cells captured from the respective blood samples. Patients 35 and 38, whom were known to have active MM, showed multiple LDR products as well as higher band intensities compared to patients 36 and 37 indicating higher fractions of *KRAS* mutant copies in their gDNA than patients 36 and 37, who were classified with the SMM (see Figure 4.8). These results are in agreement with early studies that indicated the frequency of these activating *RAS* mutations are associated with advanced stage MM compared to earlier stages of MM.[57, 61]

Table 4.3 *KRAS* mutational analysis on clinical samples

Patient #	No. of <i>K-ras</i> mutations via PCR/LDR/CGE assay	No. of <i>K-ras</i> mutations via Sanger Sequencing
35	5	0
36	4	1
37	2	0
38	4	0



#### 4.4 Conclusion

In this study, we have demonstrated the use of a polymer-based microfluidic device that has the capability to select CMMCs directly from whole blood as a potential diagnostic tool for MM. This device was able to isolate CMMCs, which are mesenchymal type cells, at a recovery of ~71% directly from whole blood using CD138 as the selection antigen. The CMMC selection device required no sample preprocessing, such as the lysis of RBCs, minimizing CMMC loss. We have previously demonstrated the scalability of this device and therefore, it could be reconfigured to process larger volumes of blood (7.5 mL) so as to provide higher number of cells for extensive molecular profiling studies. [24] The ability to perform on-chip immunophenotyping as well as clonal testing was demonstrated for CMMCs selected and underscores its potential use in prognostic investigational studies for MGUS, SMM and active MM disease states. Preliminary clinical data presented here on SMM and active MM demonstrates the device sensitivity to the disease state. Future studies will also include MGUS group of patients in the clinical studies and focus on patient monitoring for drug targeting studies and gene expression profiling for MM clinically relevant markers.

#### 4.5 References

1. Rawstron, A.C., *et al.*, *Circulating plasma cells in multiple myeloma: characterization and correlation with disease stage*. British Journal of Haematology, 1997. **97**(1): p. 46-55.
2. Raab, M.S., *et al.*, *Multiple myeloma*. The Lancet. **374**(9686): p. 324-339.

3. Tschumper, R.C., *et al.*, *Comprehensive Assessment of Potential Multiple Myeloma Immunoglobulin Heavy Chain V-D-J Intraclonal Variation Using Massively Parallel Pyrosequencing*. 2012. Vol. 3. 2012.
4. Hideshima, T. and K.C. Anderson, *Molecular mechanisms of novel therapeutic approaches for multiple myeloma*. *Nature Reviews Cancer*, 2002. **2**(12): p. 927-937.
5. Sirohi, B. and R. Powles, *Multiple myeloma*. *The Lancet*, 2004. **363**(9412): p. 875-887.
6. Anderson, K.C., *et al.*, *Monoclonal gammopathy of undetermined significance (MGUS) and smoldering (asymptomatic) multiple myeloma: IMWG consensus perspectives risk factors for progression and guidelines for monitoring and management*. *Leukemia*, 2010. **24**(6): p. 1121+.
7. Witzig, T.E., *et al.*, *QUANTITATION OF CIRCULATING PERIPHERAL-BLOOD PLASMA-CELLS AND THEIR RELATIONSHIP TO DISEASE-ACTIVITY IN PATIENTS WITH MULTIPLE-MYELOMA*. *Cancer*, 1993. **72**(1): p. 108-113.
8. Kumar, S., *et al.*, *Prognostic value of circulating plasma cells in monoclonal gammopathy of undetermined significance*. *Journal of Clinical Oncology*, 2005. **23**(24): p. 5668-5674.
9. Nowakowski, G.S., *et al.*, *Circulating plasma cells detected by flow cytometry as a predictor of survival in 302 patients with newly diagnosed multiple myeloma*. *Blood*, 2005. **106**(7): p. 2276-2279.
10. Witzig, T.E., *et al.*, *Detection of myeloma cells in the peripheral blood by flow cytometry*. *Cytometry*, 1996. **26**(2): p. 113-120.
11. Witzig, T.E., *et al.*, *Detection of peripheral blood plasma cells as a predictor of disease course in patients with smoldering multiple myeloma*. *British Journal of Haematology*, 1994. **87**(2): p. 266-272.
12. Witzig, T., *et al.*, *Peripheral blood monoclonal plasma cells as a predictor of survival in patients with multiple myeloma [see comments]*. *Blood*, 1996. **88**(5): p. 1780-1787.
13. San-Miguel, J.F., M.a.B. Vidriales, and A. Orfão, *Immunological evaluation of minimal residual disease (MRD) in acute myeloid leukaemia (AML)*. *Best Practice & Research Clinical Haematology*, 2002. **15**(1): p. 105-118.

14. Sezer, O., *et al.*, *Differentiation of monoclonal gammopathy of undetermined significance and multiple myeloma using flow cytometric characteristics of plasma cells*. *haematologica*, 2001. **86**(8): p. 837-843.
15. Billadeau, D., *et al.*, *Clonal circulating cells are common in plasma cell proliferative disorders: a comparison of monoclonal gammopathy of undetermined significance, smoldering multiple myeloma, and active myeloma*. *Blood*, 1996. **88**(1): p. 289-296.
16. Stott, S.L., *et al.*, *Isolation and characterization of circulating tumor cells from patients with localized and metastatic prostate cancer*. *Sci. Transl. Med.*, 2010. **2**(Copyright (C) 2010 American Chemical Society (ACS). All Rights Reserved.): p. No pp. given.
17. Maheswaran, S., *et al.*, *Detection of Mutations in EGFR in Circulating Lung-Cancer Cells*. *New England Journal of Medicine*, 2008. **359**: p. 366-377.
18. Nagrath, S., *et al.*, *Isolation of rare circulating tumour cells in cancer patients by microchip technology*. *Nature (London, U. K.)*, 2007. **450**(Copyright (C) 2010 American Chemical Society (ACS). All Rights Reserved.): p. 1235-1239.
19. Yu, M., *et al.*, *Circulating tumor cells: approaches to isolation and characterization*. *The Journal of Cell Biology*, 2011. **192**(3): p. 373-382.
20. Kirby, B.J., *et al.*, *Functional Characterization of Circulating Tumor Cells with a Prostate-Cancer-Specific Microfluidic Device*. *Plos One*, 2012. **7**(4): p. 1-10.
21. Gleghorn, J.P., *et al.*, *Capture of circulating tumor cells from whole blood of prostate cancer patients using geometrically enhanced differential immunocapture (GEDI) and a prostate-specific antibody*. *Lab on a Chip*, 2010. **10**(1): p. 27-29.
22. Jackson, J.M., *et al.*, *UV activation of polymeric high aspect ratio microstructures: ramifications in antibody surface loading for circulating tumor cell selection*. *Lab on a Chip*, 2014.
23. Dharmasiri, U., *et al.*, *High-Throughput Selection, Enumeration, Electrokinetic Manipulation, and Molecular Profiling of Low-Abundance Circulating Tumor Cells Using a Microfluidic System*. *Analytical Chemistry*, 2011. **83**(6): p. 2301-2309.
24. Kamande, J.W., *et al.*, *Modular Microsystem for the Isolation, Enumeration and Phenotyping of Circulating Tumor Cells in Patients with Pancreatic Cancer*. *Analytical Chemistry*, 2013.

25. Lin, H.K., et al., *Portable Filter-Based Microdevice for Detection and Characterization of Circulating Tumor Cells*. *Clinical Cancer Research*, 2010. **16**(20): p. 5011-5018.
26. Hupert, M., et al., *Evaluation of micromilled metal mold masters for the replication of microchip electrophoresis devices*. *Microfluidics and Nanofluidics*, 2007. **3**(1): p. 1-11.
27. Jackson, J.M., et al., *UV Modification of Polymeric High Aspect Ratio Microstructures: Ramifications in Antibody Surface Loading For Circulating Tumor Cell Selection*. *Lab Chip*, 2013, submitted for publication.
28. Wei, S.Y., et al., *Photochemically patterned poly(methyl methacrylate) surfaces used in the fabrication of microanalytical devices*. *Journal Of Physical Chemistry B*, 2005. **109**(35): p. 16988-16996.
29. McCarley, R.L., et al., *Resist-Free Patterning of Surface Architectures in Polymer-Based Microanalytical Devices*. *Journal of the American Chemical Society*, 2004. **127**(3): p. 842-843.
30. Adams, A.A., et al., *Highly efficient circulating tumor cell isolation from whole blood and label-free enumeration using polymer-based microfluidics with an integrated conductivity sensor*. *Journal of the American Chemical Society*, 2008. **130**(27): p. 8633-8641.
31. Gooding, R.P., et al., *Phenotypic and molecular analysis of six human cell lines derived from patients with plasma cell dyscrasia*. *British Journal of Haematology*, 1999. **106**(3): p. 669-681.
32. Raja, K.R.M., L. Kovarova, and R. Hajek, *Review of phenotypic markers used in flow cytometric analysis of MGUS and MM, and applicability of flow cytometry in other plasma cell disorders*. *British Journal of Haematology*, 2010. **149**(3): p. 334-351.
33. Jackson, J.M., et al., *UV Activation of Polymeric High Aspect Ratio Microstructures: Ramifications in Antibody Surface Loading For Circulating Tumor Cell Selection*. *Lab Chip*, 2013: p. Submitted for publication.
34. <http://medtextfree.wordpress.com/2012/01/12/chapter-80-morphology-of-lymphocytes-and-plasma-cells/>.
35. Dharmasiri, U., et al., *Highly efficient capture and enumeration of low abundance prostate cancer cells using prostate-specific membrane antigen aptamers immobilized to a polymeric microfluidic device*. *Electrophoresis*, 2009.

- 30**(Copyright (C) 2010 American Chemical Society (ACS). All Rights Reserved.): p. 3289-3300.
36. Chang, K.-C. and D.A. Hammer, *The Forward Rate of Binding of Surface-Tethered Reactants: Effect of Relative Motion between Two Surfaces*. Biophysical Journal, 1999. **76**(3): p. 1280-1292.
  37. Adams, A.A., et al., *Highly Efficient Circulating Tumor Cell Isolation from Whole Blood and Label-Free Enumeration Using Polymer-Based Microfluidics with an Integrated Conductivity Sensor*. J. Am. Chem. Soc., 2008. **130**(Copyright (C) 2010 American Chemical Society (ACS). All Rights Reserved.): p. 8633-8641.
  38. Dharmasiri, U., et al., *Highly efficient capture and enumeration of low abundance prostate cancer cells using prostate-specific membrane antigen aptamers immobilized to a polymeric microfluidic device*. Electrophoresis, 2009. **30**(18): p. 3289-3300.
  39. Rao, C.G., et al., *Expression of epithelial cell adhesion molecule in carcinoma cells present in blood and primary and metastatic tumors*. International Journal of Oncology, 2005. **27**(1): p. 49-57.
  40. Dharmasiri, U., et al., *High-Throughput Selection, Enumeration, Electrokinetic Manipulation, and Molecular Profiling of Low-Abundance Circulating Tumor Cells Using a Microfluidic System*. Anal. Chem. (Washington, DC, U. S.), 2011. **83**(Copyright (C) 2011 American Chemical Society (ACS). All Rights Reserved.): p. 2301-2309.
  41. Couchman, J.R., *Syndecans: Proteoglycan regulators of cell-surface microdomains?* Nature Reviews Molecular Cell Biology, 2003. **4**(12): p. 926-937.
  42. Hata, H., et al., *Multiple myeloma cells expressing low levels of CD138 have an immature phenotype and reduced sensitivity to lenalidomide*. International Journal of Oncology, 2012. **41**(3): p. 876-884.
  43. Kato, M., et al., *Loss of cell surface syndecan-1 causes epithelia to transform into anchorage-independent mesenchyme-like cells*. Molecular Biology of the Cell, 1995. **6**(5): p. 559-576.
  44. Katz, B.-Z., *Adhesion molecules—The lifelines of multiple myeloma cells*. Seminars in Cancer Biology, 2010. **20**(3): p. 186-195.
  45. O'Connell, F.P., J.L. Pinkus, and G.S. Pinkus, *CD138 (Syndecan-1), a plasma cell marker - Immunohistochemical profile in hematopoietic and nonhematopoietic neoplasms*. American Journal of Clinical Pathology, 2004. **121**(2): p. 254-263.

46. Rawstron, A.C., *et al.*, *Report of the European Myeloma Network on multiparametric flow cytometry in multiple myeloma and related disorders.* *haematologica*, 2008. **93**(3): p. 431-438.
47. Mateo Manzanera, G., J.F. San Miguel Izquierdo, and A. Orfao de Matos, *Immunophenotyping of plasma cells in multiple myeloma.* *Methods in molecular medicine*, 2005. **113**: p. 5-24.
48. Billadeau, D., *et al.*, *Detection and quantitation of malignant cells in the peripheral blood of multiple myeloma patients.* *Blood*, 1992. **80**(7): p. 1818-1824.
49. Stott, S.L., *et al.*, *Isolation of circulating tumor cells using a microvortex-generating herringbone-chip.* *Proceedings of the National Academy of Sciences*, 2010. **107**(43): p. 18392-18397.
50. Bos, J.L., *ras Oncogenes in Human Cancer: A Review.* *Cancer Research*, 1989. **49**(17): p. 4682-4689.
51. Zenonos, K. and K. Kyprianou, *RAS signaling pathways, mutations and their role in colorectal cancer.* *World journal of gastrointestinal oncology*, 2013. **5**(5): p. 97-101.
52. Riker, A., S.K. Libutti, and D.L. Bartlett, *Advances in the early detection, diagnosis, and staging of pancreatic cancer.* *Surgical Oncology*, 1997. **6**(3): p. 157-169.
53. Maheswaran, S., *et al.*, *Detection of mutations in EGFR in circulating lung-cancer cells.* *New England Journal of Medicine*, 2008. **359**(4): p. 366-377.
54. Yeh, J.J., *et al.*, *KRAS/BRAF mutation status and ERK1/2 activation as biomarkers for MEK1/2 inhibitor therapy in colorectal cancer.* *Molecular Cancer Therapeutics*, 2009. **8**: p. 834-843.
55. DeRoock, W., *et al.*, *Effects of KRAS, BRAF, NRAS, and PIK3CA mutations on the efficacy of cetuximab plus chemotherapy in chemotherapy-refractory metastatic colorectal cancer: a retrospective consortium analysis.* *Lancet*, 2010. **11**: p. 753-762.
56. Lievre, A., *et al.*, *KRAS mutations as an independent prognostic factor in patients with advanced colorectal cancer treated with cetuximab.* *J. Clin. Oncol.*, 2008. **26**(Copyright (C) 2010 American Chemical Society (ACS). All Rights Reserved.): p. 374-379.

57. Bezieau, S., *et al.*, *High incidence of N and K-Ras activating mutations in multiple myeloma and primary plasma cell leukemia at diagnosis*. *Human Mutation*, 2001. **18**(3): p. 212-224.
58. Lievre, A., *et al.*, *KRAS Mutation Status Is Predictive of Response to Cetuximab Therapy in Colorectal Cancer*. *Cancer Res.*, 2006. **66**(Copyright (C) 2010 American Chemical Society (ACS). All Rights Reserved.): p. 3992-3995.
59. Di, F.F., *et al.*, *Clinical relevance of KRAS mutation detection in metastatic colorectal cancer treated by Cetuximab plus chemotherapy*. *Br. J. Cancer*, 2007. **96**(Copyright (C) 2010 American Chemical Society (ACS). All Rights Reserved.): p. 1166-1169.
60. Billadeau, D., *et al.*, *Introduction of an Activated N-ras Oncogene Alters the Growth Characteristics of the Interleukin 6-dependent Myeloma Cell Line ANBL6*. *Cancer Res*, 1995. **55**(16): p. 3640-3646.
61. Liu, P., *et al.*, *Activating mutations of N- and K-ras in multiple myeloma show different clinical associations: analysis of the Eastern Cooperative Oncology Group Phase III Trial*. *Blood*, 1996. **88**(7): p. 2699-2706.
62. Hashimoto, M., *et al.*, *Ligase Detection Reaction/Hybridization Assays Using Three-Dimensional Microfluidic Networks for the Detection of Low-Abundant DNA Point Mutations*. *Anal. Chem.*, 2005. **77**(Copyright (C) 2010 American Chemical Society (ACS). All Rights Reserved.): p. 3243-3255.
63. Khanna, M., *et al.*, *Ligase detection reaction for identification of low abundance mutations*. *Clinical Biochemistry*, 1999. **32**(4): p. 287-290.
64. Soper, S.A., *et al.*, *Fabrication of DNA microarrays onto polymer substrates using UV modification protocols with integration into microfluidic platforms for the sensing of low-abundant DNA point mutations*. *Methods*, 2005. **37**(1): p. 103-113.

## **CHAPTER 5.FUTURE STUDIES: DEVELOPMENT OF A MODULAR WORKSTATION FOR CTC GENOTYPING**

### **5.1 Background**

Until recently, affinity based technologies focused on CTC detection and analysis have primarily targeted the EpCAM antigen for the specific capture of epithelial based CTCs in blood circulation. However, growing trends on CTC based studies have indicated the existence of tumor cells bearing other additional phenotypes. In particular, it has been suggested that CTCs expressing invasive phenotypes down-regulate and lose their epithelial antigens (including EpCAM) partly by a process called the epithelial-to-mesenchymal transition, EMT. [1-3] It has also been hypothesized that in some epithelial-based cancers, like mCRCs, CTCs consist of different sub-populations that may have a continuum of phenotypes besides the epithelial one. [1, 4, 5] Therefore, the ability to enrich different CTC sub-populations may be compromised if only EpCAM is used as the selection target. [6, 7] It is critical to consider the use of orthogonal selection agents that target, for example, invasive phenotypes, to better predict early and/or metastatic disease. Therefore, it will be necessary to use a combination of mAb for CTC selection.

We will generate CTC selection strategies that will recover with high efficiency two different CTC phenotypes. One antigen is associated with an epithelial phenotype, EpCAM(+), and the other is directed at a more invasive phenotype, seprase(+), a serine protease localized in the invadapodia. Seprase, which is an integral membrane gelatinase protein, has been shown to be involved in degradation of the ECM and



enhance tumor growth and proliferation. Seprase is differentially expressed on the invading front of human malignant tumor cells, especially localized within the invadopodia. Chen and co-workers have developed an invasion-based assay that consists of a collagen adhesion matrix (CAM) to collect CTCs by their ability to invade and ingest the CAM, which is enabled by seprase. [8-10] Seprase has been found to be overexpressed on tumor cell surfaces in >90% of human epithelial cancers; [11] it is highly expressed in CRC and PDAC tissues. [12]

The use of microfluidics for the selection and enumeration of CTCs from clinical samples has been reported. [13-18] However a system for the recovery of CTCs from whole blood, their enumeration and correlation of phenotype with genotype for particular CTC sub-populations has yet to be reported. The development of an integrated workstation that can offer these capabilities is paramount because molecular information obtained from CTCs can generate clinical information that cannot be garnered from enumeration data alone. We will use two selection targets, seprase and EpCAM, for this workstation to select CTCs that have an invasive and/or epithelial phenotype, respectively. The CTC selection units will be configured into thermoplastic modules integrated with other task-specific modules to build a fluidic bio-processor, which is an integral component to the workstation acquiring molecular and phenotype data on CTCs (Figure5.1).

The challenge with genotyping gDNA from CTCs is the low copy number of the assay's input. This is especially true for mCRC, which typically show low yields of CTCs. [19] Indeed, most studies invoking molecular profiling of CTCs have used

reverse transcription PCR with mRNA surrogates because of their higher copy number . [20, 21] [22, 23] CTC analysis of gDNA for mCRC demands minimal sample handling to reduce sample loss and contamination. The proposed workstation will target these issues. We will detect point mutations in KRAS, BRAF and PIK3CA genes isolated from CTCs of mCRC patients using the modular workstation equipped with a fluidic bio-processor that can carry out highly multiplexed assays using PCR/LDR. [24-27] Collaborative work between the Soper and Barany laboratories has demonstrated that PCR/LDR assays can be carried out in microfluidic architectures, [26, 28] but these systems have not been utilized for CTC molecular profiling. We will employ a continuous readout strategy using molecular beacon probes formed from an LDR and FRET with CCD time-delayed integration, CCD-TDI, [29] detection.

In Chapter 2, we developed a modular microfluidic system that could isolate, enumerate and phenotype CTCs. [30] To improve and build upon this system, our future objective would be to develop a modular workstation that will select circulating tumor cells (CTCs) from two orthogonal sub-populations can provide phenotypic and genotypic information about CTCs using CRC and PDAC as case examples ( see Figure 5.1). The innovative concepts in this workstation will include: (1) Serial arrangement of two CTC selection modules targeting seprase(+) and/or EpCAM(+) CTCs. To improve CTC recovery, nano-texturing of the channel walls and floors will be accomplished using 3D molding. [29] To release the CTCs from the antibody-decorated selection surface, we will investigate bifunctional oligonucleotide linkers, which will have a nucleotide that can be cleaved enzymatically or photolytically. (2) An addressable 2D

cell array composed of a multi-layered structure with valving and fluidic layers possessing excellent optical properties and a laser to eject the cells individually from specific addresses of the array. (3) Integration of molecular processing strategies of CTCs using an automated work flow in a closed architecture with continuous readout.

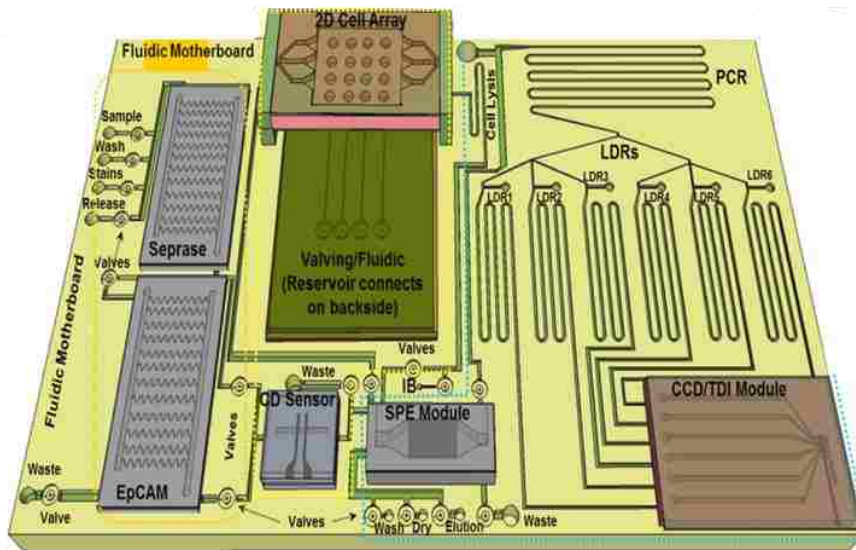


Figure 5.1 Schematic of the bio-processor, an integral component of the CTC workstation. The bio-processor is composed of modules for CTC affinity selection (Seprase and EpCAM), impedance sensor (CD), cell array with valving fluidic layer, SPE module, and imaging module for the real-time monitoring of molecular beacons via FRET produced as a result of a successful LDR. The fluidic motherboard also contains continuous flow thermal reactors for lysis, PCR and LDR. The PCR is multiplexed containing primers for the appropriate gene fragments to be interrogated. The LDRs are spatially multiplexed with each thermal reactor monitoring a specific locus. While the system shows a 6-plex LDR, this can be scaled for higher multiplexing as needed. The workstation also contains a scanning microscope for phenotyping cells in the 2D array, the imaging microscope for CCD-TDI readout, thermal control units, electronic control boards for data processing, and fluid handling hardware (syringe pumps), which are not shown.

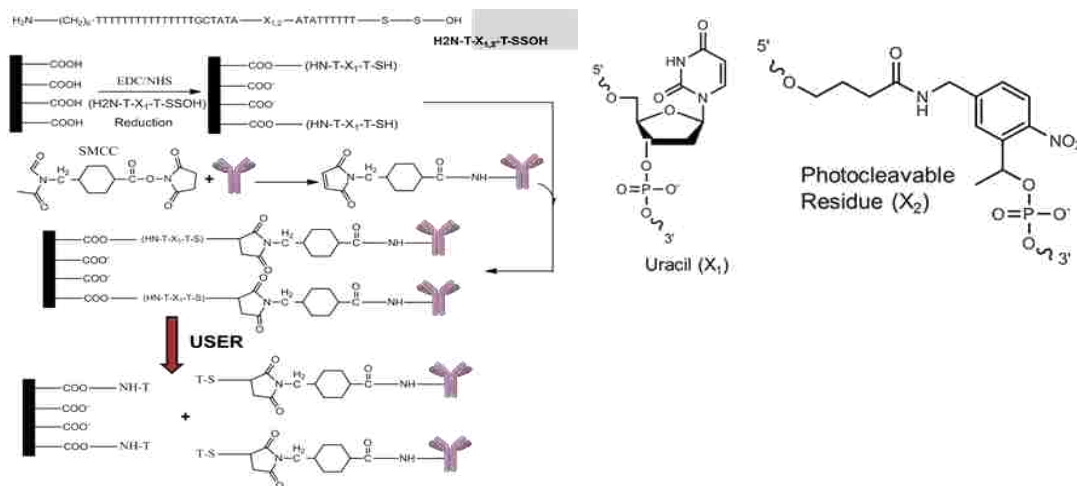
## **5.2 Enrichment of Invasive and Epithelial Phenotype CTCs from Whole Blood using Serially Arranged Modules Positioned on a Fluidic Motherboard**

One of the main aspects of CTC enrichment is to achieve maximum yields due to their rare occurrence in blood. The design, fabrication and evaluation novel CTC selection modules that contain 3D nanotextures in thermoplastic channels (PMMA or COC) decorated with antibodies targeting different CTC sub-populations will be determined. These modules will be arranged serially on a fluidic motherboard. We will also investigate the use of oligonucleotide bifunctional linkers to increase the load of mAb to the selection bed surface and provide a flexible and simple approach to release the CTCs from the selection surface.

### **5.2.1 Bi-functional Linkers**

We will incorporate, oligonucleotide bifunctional linkers with a modified nucleotide base engineered into them that can be cleaved enzymatically or photolytically to release CTCs following selection. Bifunctional linkers will consist of single-stranded oligonucleotides of varying lengths and sequence content, containing a primary amine at the 5' end and a thiol group at the 3' end. The polymer surfaces (substrate and cover plate) will be UV-activated following hot embossing. The two pieces will then be compression-sealed at room temperature and the bifunctional oligonucleotide injected into the fluidic network in the presence of EDC/NHS (Scheme 5.1). This is followed by thermal fusion bonding of the cover plate to the substrate near the T<sub>g</sub> of the substrate (~105°C for PMMA). Figure 5.2 shows a fluorescence scan of PMMA that has been UV-activated and covalently linked to an oligonucleotide through its 5' amino group using

EDC/NHS chemistry. As can be seen, both before and after thermal treatment, the amount of oligonucleotide remains constant due to the thermal stability of the oligonucleotide and its inability to be buried into the substrate when heated. Following thermal fusion bonding of the assembled cover plate, the antibody, which has been treated with succinimidyl trans-4 (maleimidymethyl) cyclohexane-1-carboxylate (SMCC), reacts with the thiol groups (Scheme 5.1).



Scheme 5.1 Single-stranded oligonucleotide bifunctional linkers used for covalently attaching mAbs to polymer surfaces bearing accessible carboxylic acids. The oligonucleotide linkers (see upper left) can contain any sequence, but is shown with a string of ~15 dT units that do not contain a primary amine so as not to be cross-linked to the surface. X<sub>1,2</sub> can be a uracil or photocleavable residue as seen in the upper right. Following device incubation with target cells, they can be released from the selection surface.

The strategy provides the ability to use different cleavable entities that are engineered into the oligonucleotide linker, such as a photocleavable or dU residue; these residues can be cleaved using light or a USER enzyme system, respectively

(Figure 5.2). For a dU residue, we can use the uracil-specific excision reagent that consists of uracil DNA glycosylase (UDG) and Endonuclease VIII to remove the dU residue

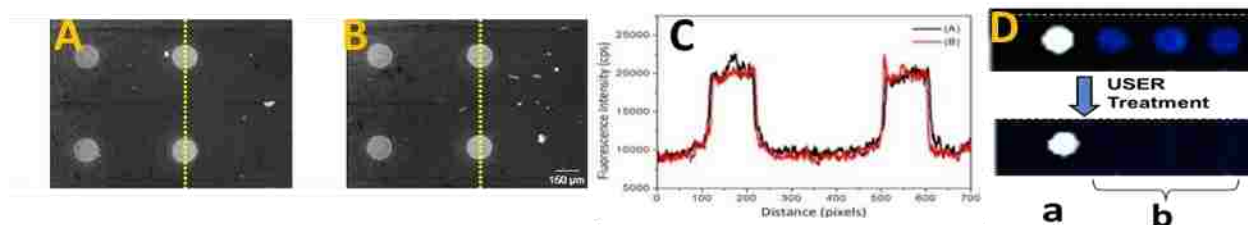


Figure 5.2 Effect of thermal fusion bonding on the stability of oligonucleotide bifunctional linkers. After modified oligonucleotide linkers were covalently attached to UV-activated PMMA, the PMMA was (A) heated to 107°C for 20 min or (B) not heated. The fluorescence intensity profiles from a vertical section of two spots (see dotted yellow line) in (A) and (B) are shown in (C). To interrogate the stability of the attached oligonucleotide linkers, solution complements to the linkers bearing a fluorescent reporter were hybridized to the linkers. As can be seen in (C), no difference in the fluorescence intensity resulted. (D) UV-activated PMMA reacted with EDC/NHS coupling reagents and a single-stranded oligonucleotide linker containing a 5' amino group and Cy3 at its 3' end. A single dU residue was added internally to the linker. After coupling, the linker was subjected to the USER system, which cleaves the linker at the dU residue. The loss of fluorescence is indicative of the cleavage. Spot (a) is a linker with no dU residue, while spot (b) contained the dU residue in the linker

## 5.2.2 Nanotextured Surfaces

Previous research has shown that nano-texturing can improve recovery of CTCs or other cell types on nanopillars, [31-35] roughened PDMS[36] or silica nanobeads. [37] Nano-texturing increases the number of anchoring points for protrusions emanating from the CTC surface. [35] However, in all reports, nano-texturing was done only to the floor of the selection devices. We have developed an innovative replication-based

technology that will allow integration of topological nanostructures into microfluidic channels in 3D. [37-39]A schematic showing the processing strategy is depicted in Figure 5.3 and is based on polymer 3D molding, which enables the rapid production of 3D patterns over large areas with high throughput and at low-cost. One of the key components for the process is the use of a flexible intermediate stamp with the desired nanostructures that can conformally mold into non-planar surfaces. PDMS was chosen as the intermediate stamp because it can stretch during the 3D fabrication process and return to its original dimensions following embossing. Figure 5.3 presents SEMs for 3D molded structures where nano-bumps (~200 nm in diameter x 100 nm height) or micro-pumps (~6  $\mu\text{m}$  in diameter x 5  $\mu\text{m}$  height) were formed on the floor and side-walls of a fluidic channel equipped with a cover plate. While the cover plate was not subjected to nano-texturing, it could also contain these structures

We will fabricate a test device for evaluating different nano-texturing modalities and operating conditions to optimize CTC recovery, especially for cells with the antigenic targets positioned on sub-cellular protrusions. The test device will consist of microchannels 150  $\mu\text{m}$  wide and 30  $\mu\text{m}$  deep. These channel dimensions are based on our previous data showing these dimensions provide high recovery of CTCs.[13] However for this test device, we will switch the depth and width from previous versions to produce low aspect ratio channels to permit interrogation of UV-activated channels for both their chemical (XPS, confocal fluorescence microscopy, water contact angle measurements) and topographical (AFM, SEM) characteristics. We will also evaluate

the ability to mold these 3D structures in high aspect ratio channels (150  $\mu\text{m}$  deep; 30  $\mu\text{m}$  wide).

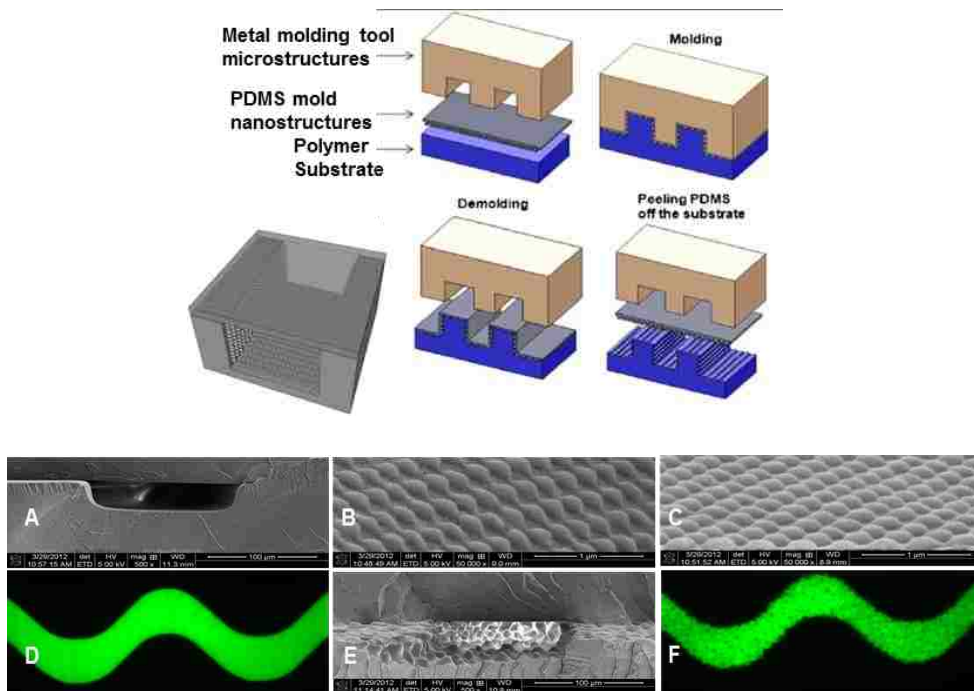


Figure 5.3 The top panel shows the process strategy for performing 3D molding using a PDMS intermediate molding tool containing nano-textures. The finished nano-textured chip is shown with ridges, but the nano-structure architecture can be altered through lithographic changes imposed on the PDMS intermediate molding tool. (A-C, E) SEM images of PMMA CTC selection channels containing nano-textures with bumps that range from 200 nm (A-D) to 5  $\mu\text{m}$  (E). (D, F) Fluorescence microscope images of nano-textured channels that were sealed with a cover plate using solvent-assisted bonding. Fluorescein was used as the dye seed in a 1X TBE buffer (pH = 8.5). These images demonstrate no leakage following cover plate bonding. For SEMs (A, E), the CTC device was sealed with a cover plate, dipped in liquid N<sub>2</sub> and fractured so as to produce a cross section of the nano-textured channel to show the integrity of the nano-features. In (A), the nano-texture structures are not visible at the magnification used but can be seen in (B), before cover plate bonding; (C), after cover plate bonding. In (E), the features are clearly visible.



### 5.2.3 Seprase and EpCAM

The ability to enrich sub-populations of CTCs using mCRC and mPDAC as models will be investigated. The sub-populations will be selected based on Seprase and EpCAM expression. Figure 5.4 shows expression differences between several selected cell lines. We will generate two CTC selection modules; the bed of one module will be decorated with mAb for Seprase (D8, D28, etc.) and the other module will contain anti-EpCAM antibodies. Both modules will be interconnected to the fluidic motherboard of the workstation in a serial arrangement (Figure 5.1). To initially evaluate the serial selection process, we will use Hs5427T (Seprase(+)) and SW620 (EpCAM(+)) cell lines seeded into a buffer to serve as positive controls. Because of the modular set-up of the system, we can investigate the selection of Seprase(+) and EpCAM(+) CTCs in each module to understand cross-reactivity. Following the positive control experiments, the cell lines will be seeded into “normal” blood to determine leukocyte infiltration during this dual-selection process. Finally, the serial selection process will be used to evaluate CTC sub-type numbers in mCRC and mPDAC patients.

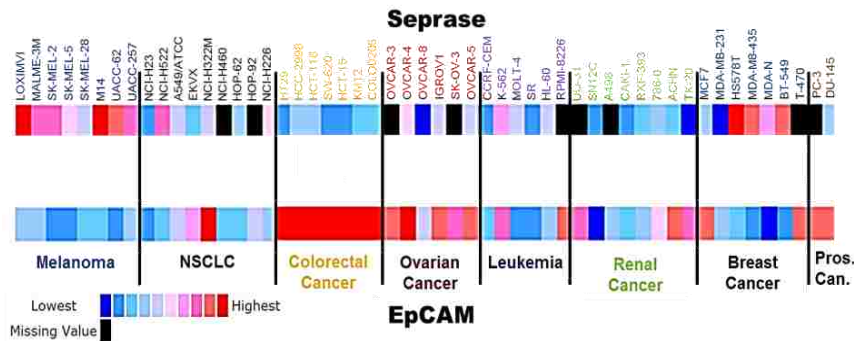


Figure 5.4 Expression differences of Seprase and EpCAM for various cancer cell lines

### **5.3 Generation of an Addressable 2-Dimensional (2D) Cell Array for Immunophenotyping via Fluorescence Imaging**

After the affinity selection of CTCs, we need to immunophenotype them using an automated workflow strategy with minimal sample handling. In addition, we may want to address groups of CTCs that have a common phenotype, or even individual CTCs to correlate phenotypes with genotypes. We should note that because of the CTC selection process from whole blood, we will have already sorted CTCs based on two divergent phenotypes, Seprase(+) and EpCAM(+).

#### **5.3.1 Dual Electrode Pair Impedance Sensor**

We have developed an impedance sensor that can detect CTCs based on size to discriminate them from interfering leukocytes and other materials. [13, 17, 40, 41] The sensing was accomplished using a resonance impedance measurement employing a 40 kHz waveform, which produced signal amplitudes dominated by the cell size. Figure 5.5 provides results for SW620 cells spiked into buffer. [13, 17, 40] Also shown are leukocytes that were isolated from a buffy coat and measured using impedance sensing. There was some overlap in the signal amplitudes between the two cell types; the misclassification frequency was ~15%. We will look to improve the discrimination between interfering cells and CTCs by adding an additional measurement channel. We will use our existing sensor and place another electrode pair in series operating at a higher frequency, which has been coined single-cell impedance cytometry. [43]

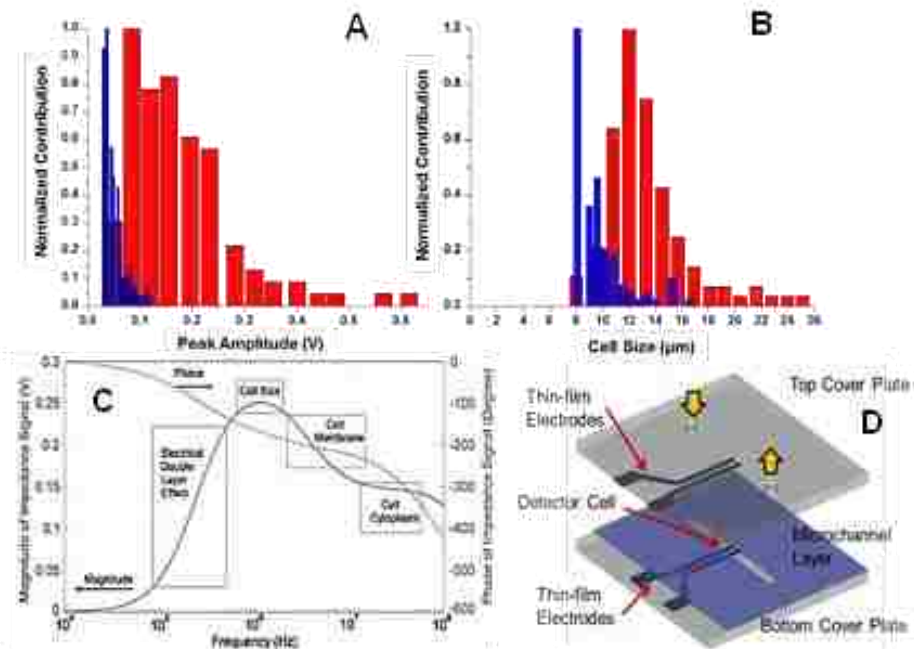


Figure 5.5 Single-cell electrical impedance detection. (A) Histograms for impedance response for leukocytes (blue bar) and SW620 cancer cells (red bar). (B) SW620 (red) and leukocyte (blue) cell size measured optically. (C) Plot of impedance response, phase and magnitude, as a function of the voltage frequency applied to the electrodes. Taken from ref.[42] with permission. (D) New electrode design in which thin films electrodes are deposited on both top and bottom plates.

The high frequency impedance measurement can provide information about the intracellular and cell membrane composition; [42, 44, 45] the low frequency measurement provides information about cell size (Figure 5.5). Scatter plots can be constructed from signal amplitudes from each sensor .[43] For example, the x-axis will consist of cell impedance amplitudes for an 100 kHz channel while the y-axis plots impedance amplitudes at >1 MHz. [46] We can also monitor electrical phase shifts, which can provide cell viability information.

### 5.3.2 2D Cell Array

In most cases, microfluidic chips for the positive selection of CTCs carry out fixation, permeabilization, staining and rinsing on the selection surface and thus need to scan the entire selection bed in three dimensions, significantly increasing processing time. [15, 47, 48] To eliminate this, our 2D cell array will define the position of a single cell within the array once it has been released from the selection bed

Several examples of cell arrays using microfluidics have been reported that consist of microwells with the cells entrapped using magnetic [49] , dielectrophoretic [50-53] ,hydrostatic [54], optical [55, 56] or confinement [57] forces. Here, we will generate a low-density 2D microwell array module for immunophenotyping CTCs with the ability to individually address each pixel of the array. We do not require high density arrays because the sample has already undergone pre-selection

In Chapter 3, we presented a 2D cell array as an imaging module where CTCs released from the HT-CTC module were collected and stained with fluorescently labeled markers for phenotype identification. [58] Collection efficiencies of 96% for fixed cells and 85 % for live cells were obtained; however, the collection efficiency for CTCs from patient samples was 72%, indicating a loss through suction, or infiltration of leukocytes with similar dimensions to CTCs. This module was interfaced to the staining and imaging module via capillaries which may account for dead volume that may lead to sample loss. For the modular workstation, the 2D cell array will adopt a different format with additional features.

The proposed cell array consists of microwells positioned in an X by Y arrangement (Figure 5.6A). Each well will be approximately 25  $\mu\text{m}$  deep with a diameter of 25  $\mu\text{m}$  because these dimensions are slightly larger than most CTCs; a well aspect ratio of 1 can typically accommodate a single cell.[59] The microwells will be laser-drilled through a suspended polymer membrane made by double-sided hot embossing. The bottom of each microwell will be sealed against a three-layer structure made from fluorinated ethylene propylene (FEP), which possesses good transmissivity at most optical wavelengths. Each row of the array will contain a microchannel underneath that is terminated with a valve, Figure 5.6B. [60] After bonding of the FEP layers to PMMA, laser ablation can be used to drill through the FEP top plate to allow hydrodynamic access to each well of the array. The microwells will be made from PMMA because of its good biocompatibility and minimal amounts of non-specific adsorption it shows. The valving and microchannels layers will use FEP because of its relatively large elongation at break value [60],and its  $T_g$ , which is close to PMMA. FEP's  $T_g$  allows it to be thermally fusion bonded to PMMA. FEP has a refractive index of 1.344, which is similar to that of water. Therefore, the holes created on the bottom of each microwell will not degrade image quality. An additional advantage of FEP is that it has a higher Young's modulus than PDMS so when applying a slight negative pressure, it will not pull the membrane onto the valve seat; these valves are normally open and a solenoid will close them.

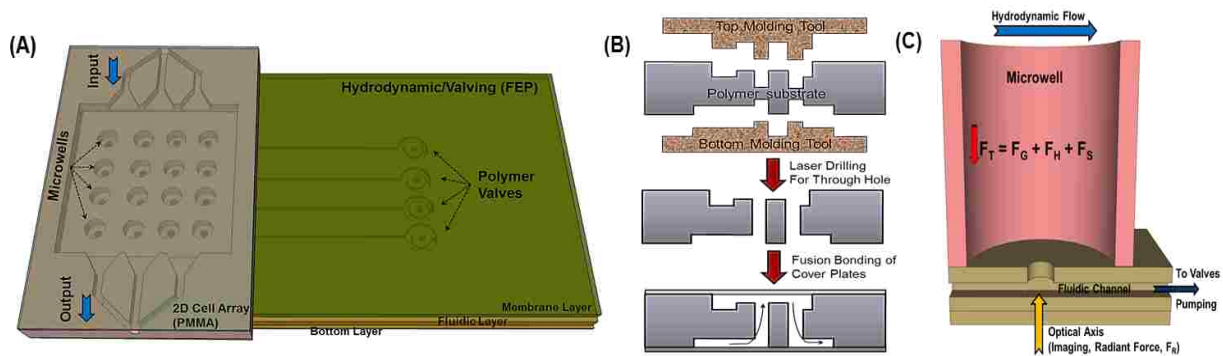


Figure 5.6 (A) Schematic of the 2D cell array. The array consists of microwells made from PMMA and a transparent FEP layer (3 layers) that serve as the fluidic, valving and through-hole units for this module. (B) Fabrication method for the polymer valves; this is accomplished using 2-sided embossing and laser drilling. The small arrows show the flow direction when the valve is open. To close the valve, a mechanical solenoid is used.[29] (C) Cross-sectional view of the microwell with the FEP layers serving as the well floor with access hole to the fluidic network. The total force ( $F_T$ ) acting on the cell to resist movement is gravity ( $F_G$ ), hydrodynamic (if applied,  $F_H$ ) and Stokes ( $F_S$ ). For a HeLa-type cell,  $F_T \approx F_G \approx 29.9$  pN. For a 1064-nm laser beam of modest intensity, a scattering force,  $F_S$ , will be able to eject the cell from this well.  $F_H$  is applied using either positive or negative operation of a syringe pump and valves, poised on the backside of this module (they are not visible in this schematic).

The module works by imposing a low flow of a cell suspension across the microwell array. Cells can be injected into the well by gravity and/or a small negative pressure applied to each well through the FEP fluidic layer. The entrapped cells within the wells have been fixed, permeabilized and stained prior to release from the selection surface and can be imaged using a 4-color microscope. The microscope we will use for phenotyping CTCs will have a mercury arc lamp, a filter cube to select the appropriate filter set and a CCD transducer. The microscope will be mounted on an XYZ motorized

translational stage. [61] We will use the standard panel to characterize CTCs including DAPI (blue), CD45 (FITC; green), and cytokeratins (phycoerythrin; red). If we require a fourth antigen in the panel to determine Seprase(+) cells expressing EpCAM or a cancer stem cell marker, we can use AlexaFluor 680. The microscope can image the array through an access port machined into the fluidic motherboard from the backside (see Figure 5.1).

To address each microwell of the 2D cell array, we will investigate the use of radiation pressure produced by a 1064-nm Nd:YAG laser fiber coupled to the scanning microscope.[62-66] For a laser beam that is not tightly focused, a scattering force will typically exceed the gradient force and thus propel the cell along the optical axis. Therefore, when the microscope is placed in line with a well, radiation forces will eject a cell from that well when this force exceeds  $F_T$  (Figure 5.6C). To assist in the ejection of cells from a well and keep the laser power low to avoid thermal effects, we can also open the valve along a row of the array to apply a slight positive  $F_H$ . To evaluate cell ejection, we can monitor the array in real time using the imaging microscope.

To test the operational metrics of this module, we will use SW620 and Hs2857T cell lines. For the initial experiments, the cells will be visualized using brightfield microscopy to determine cell entrapment efficiency. Both the cell suspension flow rate and negative pressure applied through the FEP fluidic layer will be investigated to optimize the entrapment process as well as the ejection process.

## **5.4 Integration of Fluidic Modules for Continuous Molecular Processing of CTCs even at the Single-Cell Level**

We will expand on the use of a molecular assay for detecting point mutations in gDNA using PCR/LDR with FRET readout. [67, 68] In our previous publications using this assay for CRC, only HT29 and LS180 cell lines were used and not CTCs isolated from clinical samples. Specifically, we will detect the presence/absence of point mutations in KRAS, BRAF and PIK3CA using PCR and spatial multiplexing with different primer pairs for the LDR for processing all mutations from a single input, and thus, requiring only a single color. Spatial multiplexing involves splitting the PCR products into equal volumes and feeding this into a series of LDR continuous flow thermal reactors (linear amplification). Each reactor will be seeded with LDR primers specific for the locus being interrogated. The donor/acceptor dye pair we will use is Cy5/Cy5.5 due to the relatively large Förster radius associated with this dye pair (61.7 Å) and the red emission of the acceptor, Cy5.5 ( $\lambda_{em} \sim 700$  nm), which reduces background fluorescence improving the signal-to-noise ratio in the measurement. [69, 70] In addition, the donor/acceptor dyes will be attached to the 3' and 5' ends of LDR generated molecular beacons using a 3-carbon spacer to provide optimal energy transfer efficiency. [68] This assay is attractive for mass-limited samples because of the two stages of amplification used, PCR and LDR.

### **5.4.1 PCR/LDR/FRET Assay for the Detection of *KRAS* Point Mutations**

For this task, we will integrate the modules for molecular processing of mCRC CTCs extracted from the 2D cell array either as groups or individuals based on their



phenotype. This phase of the project builds from our recent publication concerning the molecular profiling of mycobacterium tuberculosis bacterial cells as detailed in the preliminary results. [29] However, instead of using the universal array as the readout platform for the PCR/LDR, we will employ a continuous readout format using LDR formation of molecular beacons and spatial multiplexing with CCD-TDI readout . The modules that we will utilize for this phase of the processing pipeline include: (1) Continuous flow thermal reactors for CTC lysis, PCR and LDR. Polycarbonate will be used as the substrate for the motherboard due to its high Tg, minimizing microstructure deformation during thermal processing and its large elongation at break to accommodate valves [29] (2) SPE module made from polycarbonate that possesses a high density of microposts formed during the embossing step used to make the fluidic network The choice of polycarbonate here is predicated on the fact that this material, when exposed to 254 nm UV-light, generates a surface with a high propensity to let nucleic acids condense on its surface when a cell lysate is suspended in polyethylene glycol and NaCl. The attractive feature of the SPE module is that multiple cells can be sequentially lysed and immobilized to the extraction bed to analyze a group of cells.

All modules will be interconnected to the motherboard using low-dead volume interconnects laser-drilled into the module and motherboard and conformally sealed with plastic tubing.[29] This gives us the ability to disconnect any module from the motherboard and replace it with a new module. In addition, we have the flexibility in choosing which modules may be needed for the specific assay. Dummy modules

connecting input/output ports can be inserted into the motherboard to eliminate unnecessary processing steps.

## 5.5 Optical Read Out Module

In this task, we will generate an optical readout module for molecular beacon probes that are produced from the LDR continuous flow thermal cyclers. A diagram of the fluidic module for this purpose is depicted in Figure 5.7A. It consists of an embedded polymer waveguide and fluidic channels placed orthogonal to the waveguide embedded into the cover plate of this module; the evanescent field is used to excite fluorophores in the fluidic channels. We have generated a similar polymer waveguide that was made from COC and embedded into a PMMA substrate. [71] Unfortunately, the refractive index difference between the waveguide core (COC) and the cladding (PMMA) was minimal so the penetration depth of the evanescent field into the adjacent fluidic channel was small (~100 nm) when light was launched into the waveguide near the critical angle. In this application, we will use FEP as the cladding material for the core COC waveguide. The refractive index of FEP is 1.344 compared to 1.48 for PMMA and 1.53 for COC. Therefore, the penetration depth of the evanescent field using FEP should be on the order of 500 nm. With a higher penetration depth of the evanescent field, we can produce sampling channels for this optical reader that are on the order of 2  $\mu\text{m}$  wide with a depth (0.5-1.0  $\mu\text{m}$ ) that can be produced using optical lithography and generate high sampling efficiency of the LDR-generated molecular beacons. [72] Also, the channel width is sufficient to fit a series of channels within the field-of-view of a high collection efficiency microscope objective; therefore, no scanning is required improving

the duty cycle. [73] We have prepared channels in various polymers consisting of these dimensions (Figure 5.7B). In the present application, we will require the appropriate number of channels to interrogate all of the relevant mutations, with one channel serving as a positive control. The molding tool to fabricate this module will be prepared via UV-LIGA.

The COC core waveguide is situated in a guide channel hot-embossed into the FEP cover plate. A PDMS stencil containing a cavity defining the coupling prism is placed on top of the FEP cover plate reversibly sealed to the PDMS stencil. A COC melt, which utilizes a solvent for COC that does not damage FEP, is allowed to fill the cavities defined by the PDMS stencil and FEP channel. For the PMMA-embedded waveguide, we used toluene as the solvent for COC. For FEP, we will initially test toluene, but other solvents can be investigated as well. Following removal of PDMS stencil, the FEP cover plate is bonded to the FEP fluidic substrate.

For reading fluorescence generated when molecular beacons flow over the planar COC waveguide, we will use an imaging CCD camera operated in TDI mode, which provides better signal-to-noise ratio and higher duty cycle compared to a snapshot operational mode for the CCD. [72] The gain in the signal-to-noise ratio for TDI versus a snapshot scales with  $N^{1/2}$ , where  $N$  is the number of pixels along the shift axis.

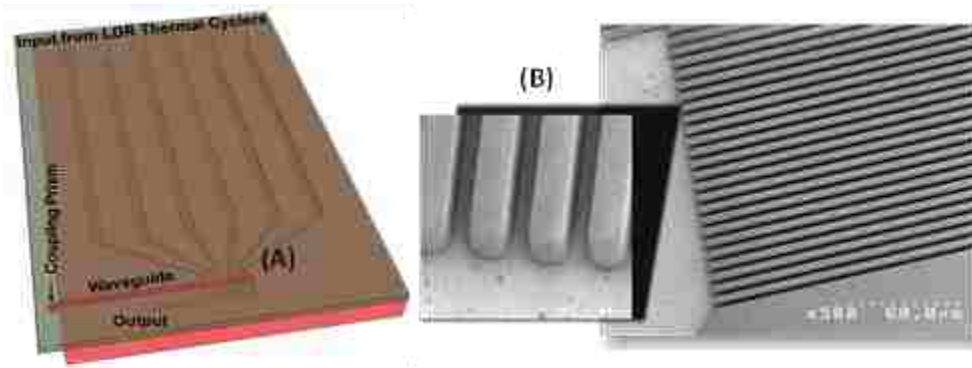


Figure 5.7 (A) Schematic of the optical readout module that consists of input connects to accept the output of each LDR thermal reactor, which are poised on the motherboard. This module consists of a cover plate with an embedded COC planar waveguide and readout channels that are approximately 2  $\mu\text{m}$  in width and 350-500 nm in depth at the detection zone (evanescent excitation of solution molecular beacons). (B) Molding tool is prepared via UV-LIGA.

In our previous work using CCD-TDI readout, double-stranded DNA stained with an intercalating dye was monitored; however, the excitation beam was launched at the side of a microchannel array instead of using a waveguide.

### 5.5.1 Characterization and Clinical Application of the Modular Work Station

One challenge in evaluating new technologies is the limited predictive value of traditional preclinical models, such as tumor cell lines. [74] Primary human tumor xenograft models have been proposed as a significant advancement over conventional xenograft models. Unlike cell lines where there is dependence on various sub-populations that are able to survive on a plastic dish, PDX tumors retain the heterogeneity from which they were derived. Recent reports suggest that patient tumors directly explanted into immunocompromised mice exhibit response rates to cytotoxic or targeted therapies similar to that seen in humans. In this phase of the project, we will

use human tumor xenografts for evaluating the ability of the workstation to select various sub-populations of CTCs to learn about CTC numbers for each selection phenotype (seprase and EpCAM) for mCRC and mPDAC

We will design PCR and LDR primer sets for codons 12 (6 loci) and 13 (1 locus) in KRAS for genotyping mCRC CTCs using PCR/LDR with FRET readout. Prof. Francis Barany will be the consultant in guiding our primer design for PCR/LDR. [26, 27, 75, 76] We will also design primer sets for the BRAF V600E mutation (1 locus) and PIK3CA mutations in the p85, C2, helical and kinase domains (2 loci; exons 9,20).[77].

We will first isolate and analyze CTCs from established PDXs using the workstation. Each mCRC PDX represents an individual patient tumor and will be expanded to 5 mice per PDX to account for variability. As our mCRC PDXs have been characterized for KRAS and BRAF mutations, we will select 5 KRAS mutant (mt) (codons 12 and 13), 5 KRAS wild-type (wt) and 2 BRAF mt mCRC PDX. We will evaluate an additional 10 KRAS wt mCRC PDX for PIK3CA mutations. As the expected frequency of mutations in PIK3CA is 30%, we anticipate the analysis of 15 KRAS wt mCRC PDX will be sufficient to detect 3-5 PIK3CA mts. All PDX blood draws (~500  $\mu$ L, left ventricle) will be analyzed for KRAS, BRAF, and PIK3CA mutations using PCR/LDR and compared to our known analysis of mutations from the human tumor tissue and correlated to the phenotype. We will also compare the KRAS, BRAF and PIK3CA mutations in EpCAM(+) and seprase(+) mCRC CTCs.

We will next evaluate the utility of the workstation prospectively in patients with mCRC. On average, 6-8 patients with mCRC undergo operations at our institution each

month. Our PDX Program will allow us to perform a prospective validation of CTCs in patients and compare our mutational analysis of driver genes with the matched de-identified tumors. We will prospectively collect matched blood and biopsies from 60 de-identified patients. We calculate this sample size will be needed to detect at least 1 patient tumor with a BRAF mutation. [77] DNA from tumor specimens will be analyzed using validated PCR/LDR assays. Comparisons between bench-top and the workstation genotyping of CTCs will be carried out throughout the course of this study. The metrics for operational performance will consist of CTC limit-of-detection to get quality genotypic data for CTC sub-populations, sample loss and potential contamination issues. For bench-top genotyping, CTC modules will be operated as stand-alone units.[78] Due to the configuration of the fluidic motherboard and the cleavable linkers we are employing, we can collect separately seprase(+) and EpCAM(+) CTCs into microfuge tubes for bench-top processing.

## 5.6 References

1. Brabletz, T., *et al.*, *Invasion and metastasis in colorectal cancer: Epithelial-mesenchymal transition, mesenchymal-epithelial transition, stem cells and Beta-catenin*. Cell Tissues Organs, 2005. **179**: p. 56-65.
2. Raimondi, C., *et al.*, *Epithelial-mesenchymal transition and stemness features in circulating tumor cells from breast cancer patients*. Breast Cancer Research, 2011. **130**: p. 449-455.
3. Dalerba, P., *et al.*, *Phenotypic characterization of human colorectal cancer stem cells*. PNAS, 2007. **104**(24): p. 10158-10163.
4. Hoshino, H., *et al.*, *Epithelial-mesenchymal transition with expression of SNAI1-induced chemoresistance in colorectal cancer*. Biochem. Biophys. Res. Commun., 2009. **390**: p. 1061-1065.

5. Vaipoulos, A.G., *et al.*, *Concise review: Colorectal cancer stem cells*. *Stem Cells*, 2012. **30**: p. 363-371.
6. Thurm, H., *et al.*, *Rare expression of epithelial cell adhesion molecule on residual micrometastatic breast cancer cells after adjuvant chemotherapy*. *Clin. Cancer Res.*, 2003. **9**(7): p. 2598-2604.
7. Pecot, C.V., *et al.*, *A novel platform for detection of CK+ and CK- CTCs*. *Cancer Discovery*, 2011: p. 580-586.
8. Paris, P.L., *et al.*, *Functional phenotyping and genotyping of circulating tumor cells from patients with castration resistant prostate cancer*. *Cancer Letters*, 2009. **277**: p. 164-173.
9. Fan, T., *et al.*, *Clinical significance of circulating tumor cells detected by an invasion assay in peripheral blood of patients with ovarian cancer*. *Gynecologic Oncology*, 2009. **112**: p. 185-191.
10. Aertgeerts, K., *et al.*, *Structural and Kinetic Analysis of the Substrate Specificity of Human Fibroblast Activation Protein  $\alpha$* . *J. Biol. Chem.*, 2005. **280**(20): p. 19441-19444.
11. Iwasa, S., *et al.*, *Increased expression of seprase, a membrane-type serine protease, is associated with lymph node metastasis in human colorectal cancer*. *Cancer Letters*, 2005. **227**: p. 229-236.
12. Coen, M.C., *et al.*, *Modification of the micro- and nanotopography of several polymers by plasma treatments*. *Applied Surface Science*, 2003. **207**: p. 276-286.
13. Adams, A.A., *et al.*, *Highly Efficient Circulating Tumor Cell Isolation from Whole Blood and Label-Free Enumeration Using Polymer-Based Microfluidics with an Integrated Conductivity Sensor*. *Journal of the American Chemical Society*, 2008. **130**(27): p. 8633-8641.
14. Nagrath, S., *et al.*, *Isolation of rare circulating tumour cells in cancer patients by microchip technology*. *Nature*, 2007. **450**(7173): p. 1235-1239.
15. Maheswaran, S., *et al.*, *Detection of Mutations in EGFR in Circulating Lung-Cancer Cells*. *New England Journal of Medicine*, 2008. **359**: p. 366-377.
16. Lin, Y.G., *et al.*, *Rare circulating tumor cells can be reliably and efficiently detected using a novel microfluidics and micro-electromechanical systems (MEMS)-based rare cell recovery platform: Preclinical and clinical data*. *Gynecologic Oncology*, 2009. **112**(2): p. 230.

17. Kuo, J.S., *et al.*, *Deformability considerations in filtration of biological cells*. Lab Chip, 2010. **10**: p. 837-842.
18. Mego, M., S.A. Mani, and M. Cristofanilli, *Molecular mechanisms of metastasis in breast cancer-clinical applications*. Nat. Rev. Clin. Oncol., 2010. **7**: p. 693-701.
19. Guo, J.M., *et al.*, *Combined use of positive and negative immunomagnetic isolation followed by real-time RT-PCR for detection of the circulating tumor cells in patients with colorectal cancers*. Journal of Molecular Medicine-Jmm, 2004. **82**(11): p. 768-774.
20. Lagoudianakis, E.E., *et al.*, *Detection of Epithelial Cells by RT-PCR Targeting CEA, CK20, and TEM-8 in Colorectal Carcinoma Patients Using OncoQuick Density Gradient Centrifugation System*. Journal of Surgical Research, 2009. **155**(2): p. 183-190.
21. Ntoulia, M., *et al.*, *Detection of Mammaglobin A-mRNA-positive circulating tumor cells in peripheral blood of patients with operable breast cancer with nested RT-PCR*. Clinical Biochemistry, 2006. **39**(9): p. 879-887.
22. Vlems, F., J. Diepstra, and I. Conelissen, *Limitations of cytokeratin 20 RT-PCR to detect disseminated tumor cells in blood and bone marrow of patients with colorectal cancer: expression in controls and downregulation in tumor tissue*. Molecular Pathology, 2002. **55**: p. 156-163.
23. Gerry, N.P., *et al.*, *Universal DNA microarray method for multiplex detection of low abundance point mutations*. Journal of Molecular Biology, 1999. **292**(2): p. 251-262.
24. Favis, R. and F. Barany, *Mutation detection in K-ras, BRCA1, BRCA2, and p53 using PCR/LDR and a universal DNA microarray*, in *Circulating Nucleic Acids in Plasma or Serum* 2000. p. 39-43.
25. Favis, R., *et al.*, *Universal DNA array detection of small insertions and deletions in BRCA1 and BRCA2*. Nature Biotechnology, 2000. **18**(5): p. 561-564.
26. Hashimoto, M., F. Barany, and S.A. Soper, *Polymerase chain reaction/ligase detection reaction/hybridization assays using flow-through microfluidic devices for the detection of low-abundant DNA point mutations*. Biosensors & Bioelectronics, 2006. **21**(10): p. 1915-1923.
27. Hashimoto, M., *et al.*, *Ligase detection reaction/hybridization assays using three-dimensional microfluidic networks for the detection of low-abundant DNA point mutations*. Analytical Chemistry, 2005. **77**(10): p. 3243-3255.



28. Wabuyele, M.B., *et al.*, *Approaching real-time molecular diagnostics: Single-pair fluorescence resonance energy transfer (spFRET) detection for the analysis of low abundant point mutations in K-ras oncogenes.* Journal of the American Chemical Society, 2003. **125**(23): p. 6937-6945.
29. Wang, H., *et al.*, *Fully Integrated Thermoplastic Genosensor for the Highly Sensitive Detection and Identification of Multi-Drug-Resistant Tuberculosis.* Angewandte Chemie-International Edition, 2012. **51**(18): p. 4349-4353.
30. Kamande, J.W., *et al.*, *Modular Microsystem for the Isolation, Enumeration and Phenotyping of Circulating Tumor Cells in Patients with Pancreatic Cancer.* Analytical Chemistry, 2013.
31. Sekine, J., *et al.*, *Functionalized Conducting Polymer Nanodots for Enhanced Cell Capturing: The Synergistic Effect of Capture Agents and Nanostructures.* Advanced Materials, 2011. **23**(41): p. 4788-+.
32. Wan, Y., *et al.*, *Nanotextured Substrates With Immobilized Aptamers for Cancer Cell Isolation and Cytology.* Cancer, 2011. **1**: p. 1-10.
33. Wang, S., *et al.*, *Highly Efficient Capture of Circulating Tumor Cells by Using Nanostructured Silicon Substrates with Integrated Chaotic Micromixers.* Angewandte Chemie, International Edition, 2010. **50**: p. 3084-3088.
34. Wang, S., *et al.*, *Three-dimensional nanostructured substrates toward efficient capture of circulating tumor cells.* Angewandte Chemie Int'l. Edition, 2009. **48**(47): p. 8970-8973.
35. Wang, S.T., *et al.*, *Capture of circulating tumor cells with a highly efficient nanostructured silicon substrates with integrated chaotic micromixers.* European Biophysics Journal with Biophysics Letters, 2011. **40**: p. 235-235.
36. Wang, B., *et al.*, *Effect of Surface Nanotopography on Immunoaffinity Cell Capture in Microfluidic Devices.* Langmuir, 2011. **27**: p. 11229-11237.
37. Farshchian, B., J. Lee, and S. Park, *Nanostructuring curved surfaces using a flexible stamp.* Proceedings of the 7th International Conference on Nanochannels, Microchannels and Minichannels (ICNMM2009), 2009: p. ICNMM2009-82173.
38. Farshchian, B., *et al.*, *3-D integration of micro-gratings into bio-analytical devices.* Proceedings of the ASME International Mechanical Engineering Congress & Exposition (IMECE 2009), 2009: p. IMECE2009-11934.

39. Sun, M.H., *et al.*, *Artificial lotus leaf by nanocasting*. *Langmuir*, 2005. **21**(19): p. 8978-8981.
40. Galloway, M., *et al.*, *Contact conductivity detection in poly(methyl methacrylate)-based microfluidic devices for analysis of mono- and polyanionic molecules*. *Analytical Chemistry*, 2002. **74**(10): p. 2407-2415.
41. Gawad, S., L. Schild, and P. Renaud, *Micromachined impedance spectroscopy flow cytometer for cell analysis and particle sizing*. *Lab Chip*, 2001. **1**: p. 76-82.
42. Sun, T. and H. Morgan, *Single-cell microfluidic impedance cytometry: a review*. *Microfluidics and Nanofluidics*, 2010. **8**: p. 423-443.
43. Hakomori, S.S., *Biochemical basis of tumor-associated carbohydrate antigens; Current trends, future perspectives, and clinical applications*. *Immunol Allergy Clin North Am*, 1990. **10**: p. 781 - 802.
44. Ayodele A. Alaiya, B.F.G.A.S.L., *Cancer proteomics: From identification of novel markers to creation of artificial learning models for tumor classification*. *Electrophoresis*, 2000. **21**(6): p. 1210-1217.
45. Cone, C.D., *The role of surface electrical transmembrane potential in normal and malignant mitogenesis*. *Ann NY Acad Sci*, 1975. **238**: p. 420 - 435.
46. Cheung, K.C., *et al.*, *Microfluidic impedance-based flow cytometry*. *Cytometry Part A*, 2010. **77A**: p. 648-666.
47. Stott, S.L., *et al.*, *Isolation of circulating tumor cells using a microvortex-generating herringbone-chip*. *Proceedings of the National Academy of Sciences of the United States of America*, 2010. **107**(43): p. 18392-18397.
48. Chalmers, J.J., *et al.*, *Theoretical analysis of cell separation based on cell surface marker density*. *Biotechnology and Bioengineering*, 1997. **59**: p. 10-20.
49. Chuang, C.H., Y.W. Huang, and Y.T. Wu, *Dielectrophoretic chip with multilayer electrodes and micro-cavity array for trapping and programmably releasing single cells*. *Biomedical Microdevices*, 2012. **14**(2): p. 271-278.
50. Di Carlo, D.D. and L.P. Lee, *Cell analysis for quantitative biology*. *Analytical Chemistry*, 2006. **78**: p. 7918-7925.
51. Gel, M., *et al.*, *Dielectrophoretic cell trapping and parallel one-to-one fusion based on field constriction created by a micro-orifice array*. *Biomicrofluidics*, 2010. **4**(2).



52. Kim, S.H., *et al.*, *An electroactive microwell array for trapping and lysing single-bacterial cells*. *Biomicrofluidics*, 2011. **5**(2).
53. Wen, L., *et al.*, *Theoretical analysis and modeling of light trapping in high efficiency GaAs nanowire array solar cells*. *Applied Physics Letters*, 2011. **99**(14).
54. Werner, M., *et al.*, *Microfluidic array cytometer based on refractive optical tweezers for parallel trapping, imaging and sorting of individual cells*. *Lab on a Chip*, 2011. **11**(14): p. 2432-2439.
55. Rettig, J.R. and A. Folch, *Large-scale single-cell trapping and imaging using microwell arrays*. *Analytical Chemistry*, 2005. **77**(17): p. 5628-5634.
56. Wang, Y.L., *et al.*, *Trapping cells on a stretchable microwell array for single-cell analysis*. *Analytical and Bioanalytical Chemistry*, 2012. **402**(3): p. 1065-1072.
57. Situma, C., *et al.*, *Fabrication of DNA microarrays onto poly(methyl methacrylate) with ultraviolet patterning and microfluidics for the detection of low-abundant point mutations*. *Analytical Biochemistry*, 2005. **340**(1): p. 123-135.
58. Kamande, J.W., *et al.*, *Modular Microsystem for the Isolation, Enumeration, and Phenotyping of Circulating Tumor Cells in Patients with Pancreatic Cancer*. *Analytical Chemistry*, 2013.
59. Svoboda, K. and S.M. Block, *Biological applications of optical forces*. *Annual Rev. Biophys. Struct.*, 1994. **23**: p. 247-285.
60. Witek, M.A., *et al.*, *Purification and Preconcentration of Genomic DNA from Whole Cell Lysates Using Photoactivated Polycarbonate (PPC) Microfluidic Chips*. *Nucleic Acids Research*, 2006. **34**: p. e74.
61. Lincoln, B., *et al.*, *Reconfigurable microfluidic integration of a dual-beam laser trap with biomedical applications*. *Biomedical Microdevices*, 2007. **9**: p. 703-710.
62. Ashkin, A., *Acceleration and trapping of particles by radiation pressure*. *Phys. Rev. Lett.*, 1970. **24**: p. 156-159.
63. Ashkin, A., *Applications of laser radiation pressure*. *Science*, 1980. **210**: p. 1081-1088.
64. Jonas, A. and P. Zemanek, *Light at work: The use of optical forces for particle manipulation, sorting and analysis*. *Electrophoresis*, 2008. **29**: p. 4813-4851.


65. Kotani, A., *et al.*, *EndoV/DNA ligase mutation scanning assay using microchip capillary electrophoresis and dual-color laser-induced fluorescence detection*. Analytical Methods, 2012. **4**(1): p. 58-64.
66. Zharov, V., T. Malinsky, and V. Alekhovich, *Photoacoustic manipulation of particles and cells*. Review of Scientific Instruments, 2003. **74**: p. 779-781.
67. Farshchian, B., *et al.*, *3D molding of hierarchical micro- and nanostructures*. Journal of Micromechanics and Microengineering, 2011. **21**(3).
68. Soper, S.A. and B.L. Legendre, *Single-molecule detection in the near-IR using continuous-wave diode laser excitation with an avalanche photon detector*. Applied Spectroscopy, 1998. **52**(1): p. 1-6.
69. Chen, P.C., *et al.*, *Limiting performance of high throughput continuous flow micro-PCR*. Proceedings of the ASME IMECE 2004, 2004: p. 62091.
70. Soper, S.A., R.L. McCarley, and M.C. Murphy, *Polymer-based microfluidic devices for PCR amplification of genomic dna*. Abstracts of Papers of the American Chemical Society, 2003. **225**: p. U199-U199.
71. Okagbare, P.I. and S.A. Soper, *Polymer-based dense fluidic networks for high throughput screening with ultrasensitive fluorescence detection*. Electrophoresis, 2010. **31**(18): p. 3074-3082.
72. Walther, A., *et al.*, *Genetic prognostic and predictive markers in colorectal cancer*. Nat Rev Cancer, 2009. **9**(7): p. 489-99.
73. Dry, J.R., *et al.*, *Transcriptional Pathway Signatures Predict MEK Addiction and Response to Selumetinib (AZD6244)*. Cancer Research, 2010. **70**(6): p. 2264-2273.
74. Fichtner, I., *et al.*, *Establishment of patient-derived non-small cell lung cancer xenografts as models for the identification of predictive biomarkers*. Clinical cancer research an official journal of the American Association for Cancer Research, 2008. **14**(20): p. 6456-68.
75. Dharmasiri, U., *et al.*, *High-Throughput Selection, Enumeration, Electrokinetic Manipulation, and Molecular Profiling of Low-Abundance Circulating Tumor Cells Using a Microfluidic System*. Analytical Chemistry, 2011. **83**(6): p. 2301-2309.
76. Khanna, M., *et al.*, *Multiplex PCR/LDR for detection of K-ras mutations in primary colon tumors*. Oncogene, 1999. **18**(1): p. 27-38.

77. Samuels, Y. and V.E. Velculescu, *Oncogenic mutations of PIK3CA in human cancers*. *Cell Cycle*, 2004. **3**(10): p. 1221-1224.
78. Dharmasiri, U., *et al.*, *High-Throughput Selection, Enumeration, Electrokinetic Manipulation, and Molecular Profiling of Low-Abundance Circulating Tumor Cells Using a Microfluidic System*. *Analytical Chemistry*, 2011. **83**: p. 2101-2109.

## APPENDIX : PERMISSIONS

11/12/13 RightsLink® by Copyright Clearance Center

  [Home](#) [Account Info](#) [Help](#)

 **ACS Publications** ADVANCING CHEMISTRY

<b>Title:</b>	Modular Microsystem for the Isolation, Enumeration, and Phenotyping of Circulating Tumor Cells in Patients with Pancreatic Cancer	Logged in as: Joyce Kamande Account #: 3000705699
<b>Author:</b>	J. W. Kamande, M. L. Hupert, M. A. Witek, H. Wang, R. J. Torphy, U. Dharmasiri, S. K. Njoroge, J. M. Jackson, R. D. Aufforth, A. Snavely, J. J. Yeh, and S. A. Soper	<a href="#">Logout</a>
<b>Publication:</b>	Analytical Chemistry	
<b>Publisher:</b>	American Chemical Society	
<b>Date:</b>	Oct 1, 2013	
<b>Copyright ©</b>	2013, American Chemical Society	

**PERMISSION/LICENSE IS GRANTED FOR YOUR ORDER AT NO CHARGE**

This type of permission/license, instead of the standard Terms & Conditions, is sent to you because no fee is being charged for your order. Please note the following:

- Permission is granted for your request in both print and electronic formats, and translations.
- If figures and/or tables were requested, they may be adapted or used in part.
- Please print this page for your records and send a copy of it to your publisher/graduate school.
- Appropriate credit for the requested material should be given as follows: "Reprinted (adapted) with permission from (COMPLETE REFERENCE CITATION). Copyright (YEAR) American Chemical Society." Insert appropriate information in place of the capitalized words.
- One-time permission is granted only for the use specified in your request. No additional uses are granted (such as derivative works or other editions). For any other uses, please submit a new request.

[BACK](#) [CLOSE WINDOW](#)

Copyright © 2013 Copyright Clearance Center, Inc. All Rights Reserved. [Privacy statement](#).  
Comments? We would like to hear from you. E-mail us at [customer-care@copyright.com](mailto:customer-care@copyright.com).

<https://s100.copyright.com/AppDispatchServlet> 1/1



RightsLink

Home

Account  
Info

Help



ACS Publications Title:

High-Throughput Selection,  
Enumeration, Electrokinetic  
Manipulation, and Molecular  
Profiling of Low-Abundance  
Circulating Tumor Cells Using a  
Microfluidic System

Lagged in as:  
Joyce Kamande  
Account #:  
3000705699

LOGOUT

Author: Udara Dharmasiri, Samuel K.  
Njoroge, Malgorzata A. Witek,  
Morayo G. Adebisi, Joyce W.  
Kamande, Mateusz L. Hupert,  
Francis Barany, and Steven A.  
Soper

Publication: Analytical Chemistry

Publisher: American Chemical Society

Date: Mar 1, 2011

Copyright © 2011, American Chemical Society

#### PERMISSION/LICENSE IS GRANTED FOR YOUR ORDER AT NO CHARGE

This type of permission/license, instead of the standard Terms & Conditions, is sent to you because no fee is being charged for your order. Please note the following:

- Permission is granted for your request in both print and electronic formats, and transitions.
- If figures and/or tables were requested, they may be adapted or used in part.
- Please print this page for your records and send a copy of it to your publisher/graduate school.
- Appropriate credit for the requested material should be given as follows: "Reprinted (adapted) with permission from (COMPLETE REFERENCE CITATION). Copyright (YEAR) American Chemical Society." Insert appropriate information in place of the capitalized words.
- One-time permission is granted only for the use specified in your request. No additional uses are granted (such as derivative works or other editions). For any other uses, please submit a new request.

BACK

CLOSE WINDOW

Copyright © 2013 Copyright Clearance Center, Inc. All Rights Reserved. [Privacy statement](#).  
Comments? We would like to hear from you. E-mail us at [customer.care@copyright.com](mailto:customer.care@copyright.com)

1  
OFFER2  
REVIEW3  
CONFIRMATION

### Step 3: Order Confirmation

**Thank you for your order!** A confirmation for your order will be sent to your account email address. If you have questions about your order, you can call us at +1.877.239.3415 Toll Free, M-F between 3:00 AM and 5:00 PM (Eastern), or write to us at [info@copyright.com](mailto:info@copyright.com). This is not an invoice.

**Confirmation Number: 11137515**  
**Order Date: 11/12/2013**

If you paid by credit card, your order will be finalized and your card will be charged within 24 hours. If you choose to be invoiced, you can change or cancel your order until the invoice is generated.

#### Payment Information

Joyce Kamande  
 jkamanda@fingers.lsu.edu  
 +1 (413)2066951  
 Payment Method: n/a

#### Order Details

##### ANNUAL REVIEW OF MEDICINE

**Order detail ID:** 64152544  
**Order License Id:** 3266760396776  
**ISSN:** 0066-4219  
**Publication Type:** Monographic Series  
**Volume:**  
**Issue:**  
**Start page:**  
**Publisher:** ANNUAL REVIEWS

**Permission Status:**  **Granted**  
**Permission type:** Republish or display content  
**Type of use:** Republish in a thesis/dissertation

**Requestor type:** Academic institution

**Format:** Print, Electronic

**Portion:** image/photo

**Number of images/photos requested:** 1

**Title or numeric reference of the portion(s):** Enrichment of circulating tumor cells (CTCs) from the peripheral blood of cancer patients is based on physical or biological properties of CTCs. Figure 2

**Title of the article or chapter the portion is from:** Circulating Tumor Cells and Circulating Tumor DNA

**Editor of portion(s):** N/A



<b>Author of portion(s)</b>	N/A
<b>Volume of serial or monograph</b>	63
<b>Page range of portion</b>	203
<b>Publication date of portion</b>	11/02/2011
<b>Rights for</b>	Main product
<b>Duration of use</b>	Life of current edition
<b>Creation of copies for the disabled</b>	no
<b>With minor editing privileges</b>	no
<b>For distribution to</b>	Worldwide
<b>In the following language(s)</b>	Original language of publication
<b>With incidental promotional use</b>	no
<b>Lifetime unit quantity of new product</b>	0 to 499
<b>Made available in the following markets</b>	Education
<b>The requesting person/organization</b>	Joyce Kamande
<b>Order reference number</b>	
<b>Author/Editor</b>	Joyce Kamande
<b>The standard identifier</b>	*23%
<b>Title</b>	Polymer Microsystems for the Enrichment of Circulating Tumor Cells and their Clinical Demonstration
<b>Publisher</b>	Louisiana State University
<b>Expected publication date</b>	Dec 2013

11/12/13

Copyright Clearance Center

Estimated size (pages) 200

Note: This item will be invoiced or charged separately through CCC's RightsLink service. More info

\$ 0.00

Total order items: 1

This is not an invoice.

Order Total: \$ 0.00

<http://www.copyright.com/jsp/confirmPurchase.do?operation=fullOperation&confirmNum=11137545&hasTCConsent=TRUE>

3/5

**Confirmation Number: 11137515**

**Special Rightsholder Terms & Conditions**

The following terms & conditions apply to the specific publication under which they are listed

**ANNUAL REVIEW OF MEDICINE**

**Permission type:** Republish or display content

**Type of use:** Republish in a thesis/dissertation

**TERMS AND CONDITIONS**The following terms are individual to this publisher:

None:

**Other Terms and Conditions:** None  
**STANDARD TERMS AND CONDITIONS**  
 1. Description of Service; Defined Terms. This Republication License enables the User to obtain licenses for republication of one or more copyrighted works as described in detail on the relevant Order Confirmation (the "Work(s)"). Copyright Clearance Center, Inc. ("CCC") grants licenses through the Service on behalf of the rightsholder identified on the Order Confirmation (the "Rightsholder"). "Republication", as used herein, generally means the inclusion of a Work, in whole or in part, in a new work or works, also as described on the Order Confirmation. "User", as used herein, means the person or entity making such republication.  
 2. The terms set forth in the relevant Order Confirmation, and any terms set by the Rightsholder with respect to a particular Work, govern the terms of use of Works in connection with the Service. By using the Service, the person transacting for a republication license on behalf of the User represents and warrants that he/she/it (a) has been duly authorized by the User to accept, and hereby does accept, all such terms and conditions on behalf of User, and (b) shall inform User of all such terms and conditions. In the event such person is a "freelancer" or other third party independent of User and CCC, such party shall be deemed jointly a "User" for purposes of these terms and conditions. In any event, User shall be deemed to have accepted and agreed to all such terms and conditions if User republishes the Work in any fashion.  
 3. Scope of License; Limitations and Obligations.  
 3.1 All Works and all rights therein, including copyright rights, remain the sole and exclusive property of the Rightsholder. The license created by the exchange of an Order Confirmation (and/or any invoice) and payment by User of the full amount set forth on that document includes only those rights expressly set forth in the Order Confirmation and in these terms and conditions, and conveys no other rights in the Work(s) to User. All rights not expressly granted are hereby reserved.  
 3.2 General Payment Terms: You may pay by credit card or through an account with us payable at the end of the month. If you and we agree that you may establish a standing account with CCC, then the following terms apply: Remit Payment to: Copyright Clearance Center, Dept 001, P.O. Box 643006, Boston, MA 02264-3006. Payments Due: Invoices are payable upon their delivery to you (or upon our notice to you that they are available to you for downloading). After 30 days, outstanding amounts will be subject to a service charge of 1-1/2% per month or, if less, the maximum rate allowed by applicable law. Unless otherwise specifically set forth in the Order Confirmation or in a separate written agreement signed by CCC, invoices are due and payable on "net 30" terms. While User may exercise the rights licensed immediately upon issuance of the Order Confirmation, the license is automatically revoked and is null and void, as if it had never been issued, if complete payment for the license is not received on a timely basis either from User directly or through a payment agent, such as a credit card company.  
 3.3 Unless otherwise provided in the Order Confirmation, any grant of rights to User (i) is "one-time" (including the editions and product family specified in the license), (ii) is non-exclusive and non-transferable and (iii) is subject to any and all limitations and restrictions (such as, but not limited to, limitations on duration of use or circulation) included in the Order Confirmation or invoice and/or in these terms and conditions. Upon completion of the licensed use, User shall either secure a new permission for further use of the Work(s) or immediately cease any new use of the Work(s) and shall render inaccessible (such as by deleting or by removing or covering links or other locators) any further copies of the Work (except for copies printed on paper in accordance with this license and still in User's stock at the end of such period).  
 3.4 In the event that the material for which a republication license is sought includes third party materials (such as photographs, illustrations, graphs, inserts and similar materials) which are identified in such material as having been used by permission, User is responsible for identifying, and seeking separate licenses (under this Service or otherwise) for, any of such third party materials; without a separate license, such third party materials may not be used.  
 3.5 Use of proper copyright notice for a Work is required as a condition of any license granted under the Service. Unless otherwise provided in the Order Confirmation, a proper copyright notice will read substantially as follows: "Republished with permission of [Rightsholder's name], from [Work's title, author, volume, edition number and year of copyright]; permission conveyed through Copyright Clearance Center, Inc." Such notice must be provided in a reasonably legible font size and must be placed either immediately adjacent to the Work as used (for example, as part of a by-line or footnote but not as a separate electronic link) or in the place where substantially all other credits or notices for the new work containing the republished Work are located. Failure to include the required notice results in loss to the Rightsholder and CCC, and the User shall be liable to pay liquidated damages for each such failure equal to twice the use fee specified in the Order Confirmation, in addition to the use fee itself and any other fees and charges specified.  
 3.6 User may only make alterations to the Work if and as expressly set forth in the Order Confirmation. No Work may be used in any way that is defamatory, violates the rights of third parties (including such third parties' rights of copyright, privacy, publicity, or other tangible or intangible property), or is otherwise illegal, sexually explicit or obscene. In addition, User may not conjoin a Work with any other material that may result in damage to the reputation of the Rightsholder. User agrees to inform CCC if it becomes aware of any infringement of any rights in a Work and to cooperate with any reasonable request of CCC or the Rightsholder in connection therewith.  
 4. Indemnity. User hereby indemnifies and agrees to defend the Rightsholder and CCC, and their respective employees and directors, against all claims, liability, damages, costs and expenses, including legal fees and expenses, arising out of any use of a Work beyond the scope of the rights granted herein, or any use of a Work which has been altered in any unauthorized way by User, including claims of defamation or infringement of

rights of copyright, publicity, privacy or other tangible or intangible property.5. Limitation of Liability. UNDER NO CIRCUMSTANCES WILL CCC OR THE RIGHTSHOLDER BE LIABLE FOR ANY DIRECT, INDIRECT, CONSEQUENTIAL OR INCIDENTAL DAMAGES (INCLUDING WITHOUT LIMITATION DAMAGES FOR LOSS OF BUSINESS PROFITS OR INFORMATION, OR FOR BUSINESS INTERRUPTION) ARISING OUT OF THE USE OR INABILITY TO USE A WORK, EVEN IF ONE OF THEM HAS BEEN ADVISED OF THE POSSIBILITY OF SUCH DAMAGES. In any event, the total liability of the Rightsholder and CCC (including their respective employees and directors) shall not exceed the total amount actually paid by User for this license. User assumes full liability for the actions and omissions of its principals, employees, agents, affiliates, successors and assigns.6. Limited Warranties. THE WORK(S) AND RIGHT(S) ARE PROVIDED "AS IS". CCC HAS THE RIGHT TO GRANT TO USER THE RIGHTS GRANTED IN THE ORDER CONFIRMATION DOCUMENT. CCC AND THE RIGHTSHOLDER DISCLAIM ALL OTHER WARRANTIES RELATING TO THE WORK(S) AND RIGHT(S), EITHER EXPRESS OR IMPLIED, INCLUDING WITHOUT LIMITATION IMPLIED WARRANTIES OF MERCHANTABILITY OR FITNESS FOR A PARTICULAR PURPOSE. ADDITIONAL RIGHTS MAY BE REQUIRED TO USE ILLUSTRATIONS, GRAPHS, PHOTOGRAPHS, ABSTRACTS, INSERTS OR OTHER PORTIONS OF THE WORK (AS OPPOSED TO THE ENTIRE WORK) IN A MANNER CONTEMPLATED BY USER; USER UNDERSTANDS AND AGREES THAT NEITHER CCC NOR THE RIGHTSHOLDER MAY HAVE SUCH ADDITIONAL RIGHTS TO GRANT.7. Effect of Breach. Any failure by User to pay any amount when due, or any use by User of a Work beyond the scope of the license set forth in the Order Confirmation and/or these terms and conditions, shall be a material breach of the license created by the Order Confirmation and these terms and conditions. Any breach not cured within 30 days of written notice thereof shall result in immediate termination of such license without further notice. Any unauthorized (but licensable) use of a Work that is terminated immediately upon notice thereof may be liquidated by payment of the Rightsholder's ordinary license price therefor; any unauthorized (and unlicensable) use that is not terminated immediately for any reason (including, for example, because materials containing the Work cannot reasonably be recalled) will be subject to all remedies available at law or in equity, but in no event to a payment of less than three times the Rightsholder's ordinary license price for the most closely analogous licensable use plus Rightsholder's and/or CCC's costs and expenses incurred in collecting such payment.8. Miscellaneous.8.1 User acknowledges that CCC may, from time to time, make changes or additions to the Service or to these terms and conditions, and CCC reserves the right to send notice to the User by electronic mail or otherwise for the purposes of notifying User of such changes or additions; provided that any such changes or additions shall not apply to permissions already secured and paid for.8.2 Use of User-related information collected through the Service is governed by CCC's privacy policy, available online here: <http://www.copyright.com/content/cc3/en/footer/footer/privacypolicy.html>.8.3 The licensing transaction described in the Order Confirmation is personal to User. Therefore, User may not assign or transfer to any other person (whether a natural person or an organization of any kind) the license created by the Order Confirmation and these terms and conditions or any rights granted hereunder; provided, however, that User may assign such license in its entirety on written notice to CCC in the event of a transfer of all or substantially all of User's rights in the new material which includes the Work(s) licensed under this Service.8.4 No amendment or waiver of any terms is binding unless set forth in writing and signed by the parties. The Rightsholder and CCC hereby object to any terms contained in any writing prepared by the User or its principals, employees, agents or affiliates and purporting to govern or otherwise relate to the licensing transaction described in the Order Confirmation, which terms are in any way inconsistent with any terms set forth in the Order Confirmation and/or in these terms and conditions or CCC's standard operating procedures, whether such writing is prepared prior to, simultaneously with or subsequent to the Order Confirmation, and whether such writing appears on a copy of the Order Confirmation or in a separate instrument.8.5 The licensing transaction described in the Order Confirmation document shall be governed by and construed under the law of the State of New York, USA, without regard to the principles thereof of conflicts of law. Any case, controversy, suit, action, or proceeding arising out of, in connection with, or related to such licensing transaction shall be brought, at CCC's sole discretion, in any federal or state court located in the County of New York, State of New York, USA, or in any federal or state court whose geographical jurisdiction covers the location of the Rightsholder set forth in the Order Confirmation. The parties expressly submit to the personal jurisdiction and venue of each such federal or state court. If you have any comments or questions about the Service or Copyright Clearance Center, please contact us at 978-750-8400 or send an e-mail to [info@copyright.com](mailto:info@copyright.com).v. 1.1

Close



Joyce Kamande <jkaman1@tigers.lsu.edu>

---

## Permission to use figure for a Dissertation

2 messages

---

**Joyce Kamande** <jkaman1@tigers.lsu.edu>  
To: bk88@cornell.edu

Fri, Oct 18, 2013 at 1:05 PM

Dear Sir,

I would like to use 2 figures from your publication that appeared in the Plos one journal for a thesis. I am a graduate student from Louisiana State University and will be graduating this year. The Title of my thesis is "Polymer Microsystems for the Enrichment of Circulating Tumor Cells and their Clinical demonstration.

The article I am referring to is found here <http://www.plosone.org/article/info%3Adoi%2F10.1371%2Fjournal.pone.0035976>

Kindly grant me permission to use the GEDI figures for my thesis

Thank you

Joyce

-

**Joyce W. Kamande**  
Ph.D. Candidate  
Department of Chemistry LSU  
Bio-medical and Engineering Dept. UNC  
email: [jkamande@med.unc.edu](mailto:jkamande@med.unc.edu) or [jkaman1@tigers.lsu.edu](mailto:jkaman1@tigers.lsu.edu)  
phone: 410-206 6951

*"In the confrontation between the stream and the rock, the stream wins. Not by strength but by perseverance!"*

---

**Brian Kirby** <bk88@cornell.edu>  
To: Joyce Kamande <jkaman1@tigers.lsu.edu>

Tue, Oct 22, 2013 at 9:30 PM

sure, as long as the paper is cited. best wishes with your thesis and defense cheers BK

[Quoted text hidden]

--

\*\*\*\*\*

Dr. Brian J. Kirby  
Associate Professor  
Associate Director for Graduate Affairs

Sibley School of Mechanical and Aerospace Engineering  
Director of Graduate Studies  
Graduate Field of Mechanical Engineering  
238 Upson Hall, Cornell University  
Ithaca, NY 14853  
Associate Professor of Engineering in Medicine  
Division of Hematology and Oncology  
Weill Cornell Medical College  
1300 York Ave  
New York, NY 10065  
[607-255-4379](tel:607-255-4379)  
[607-255-1222](tel:607-255-1222) FAX  
[kirby@cornell.edu](mailto:kirby@cornell.edu)  
<http://www.kirbyresearch.com>

Case: 02798484 "Request to use figures for reuse [ ref:\_00DU0lfis.\_500U09Ni7h:ref

]Inbox



**plosone** via [hstubi8osxqv.u-ifismac.na12.bnc.salesforce.com](mailto:hstubi8osxqv.u-ifismac.na12.bnc.salesforce.com)

to me

Dear Joyce Kamande,

Thank you for contacting PLOS ONE.

All PLOS content is open access. You can read about our open access license at <http://www.plos.org/journals/license.html>. This license allows you to download, reuse, reprint, modify, distribute, and/or copy articles or images in PLOS journals, so long as proper attribution is given to the original source (which you can easily do by including the article's citation and/or the image credit).

There are many ways to access our content, including HTML, XML, and PDF versions of each article. Higher resolution versions of figures can be downloaded directly from the article. Additionally, our articles are archived at PubMed Central (<http://www.pubmedcentral.gov/>), which offers a public FTP service from which you can download a complete site of files for each of our articles.

See <http://www.pubmedcentral.gov/about/openftlist.html> for links to the FTP site, file list, and organizational directory.

Kind Regards,  
Anna O'Shea  
PLOS ONE  
Staff EO

Case Number: 02798484

ref:\_00DU0lfis.\_500U09Ni7h:ref

----- Original Message -----

From: Joyce Kamande [[jkaman1@tigers.lsu.edu](mailto:jkaman1@tigers.lsu.edu)]

Sent: 20/10/2013

To: [plosone@plos.org](mailto:plosone@plos.org)

Subject: Request to use figures for reuse in a Thesis dissertation

To whom it may concern,

I wish to request permission for the use of 2 figures from the following article that appeared in your journal for my dissertations entitled " Polymer microsystems for the enrichment of Circulating Tumor Cells and their Clinical Demonstration"

Here is the link to the article

<http://www.plosone.org/article/info%3Adoi%2F10.1371%2Fjournal.pone.0035976>

Regards,

Joyce Kamande

--

Joyce W. Kamande  
Ph.D. Candidate  
Department of Chemistry LSU  
Bio-medical and Engineering Dept. UNC  
email: [jkamande@med.unc.edu](mailto:jkamande@med.unc.edu)<mailto:[jkamande@med.unc.edu](mailto:jkamande@med.unc.edu)>  
or [jkaman1@tigers.lsu.edu](mailto:jkaman1@tigers.lsu.edu)<mailto:[jkaman1@tigers.lsu.edu](mailto:jkaman1@tigers.lsu.edu)>  
phone: [410-206 6951](tel:410-206-6951)

"In the confrontation between the stream and the rock, the stream wins. Not by strength but by perseverance!"

---

Confidentiality Notice: This email and any attachments are solely for the use of the intended recipient, contain confidential and proprietary information, and may be privileged. If you are not the intended recipient (or authorized to receive messages for, or deliver them to, the intended recipient), you may not use, copy, disclose or distribute this email and any attachments. If you think you received this email in error, please notify the sender by return email or by telephone, and delete this email and any attachments from your system.

Disclaimer/Virus Notice: The views or opinions expressed in this email are those of the sender and do not necessarily represent those of Public Library of Science unless otherwise specifically stated. Neither PLOS nor any of its agents accept any responsibility for any viruses that may be contained in this email or any attachments, and it is your responsibility to scan the email and any attachments.

With kind regards  
Anna O'Shea  
Staff EO  
PLOS ONE

**AIP PUBLISHING LLC LICENSE  
TERMS AND CONDITIONS**

Nov 12, 2013

**All payments must be made in full to CCC. For payment instructions, please see information listed at the bottom of this form.**

License Number	3251680598046
Order Date	Oct 17, 2013
Publisher	AIP Publishing LLC
Publication	Biomechanics
Article Title	ApoStream™, a new dielectrophoretic device for antibody independent isolation and recovery of viable cancer cells from blood
Author	Vishal Gupta, Insiya Jafferji, Miguel Garza, et al.
Online Publication Date	Jun 27, 2012
Volume number	6
Issue number	2
Type of Use	Thesis/Dissertation
Requestor type	Student
Format	Print and electronic
Portion	Figure/Table
Number of figures/tables	1
Title of your thesis / dissertation	Polymer Microsystems for the Enrichment of Circulating Tumor Cells and their Clinical Demonstration
Expected completion date	Dec 2013
Estimated size (number of pages)	200
Total	0.00 USD

**Terms and Conditions**

AIP Publishing LLC -- Terms and Conditions: Permissions Uses

AIP Publishing LLC ("AIPP") hereby grants to you the non-exclusive right and license to use and/or distribute the Material according to the use specified in your order, on a one-time basis, for the specified term, with a maximum distribution equal to the number that you have ordered. Any links or other content accompanying the Material are not the subject of this license.



1. You agree to include the following copyright and permission notice with the reproduction of the Material: "Reprinted with permission from [FULL CITATION]. Copyright [PUBLICATION YEAR], AIP Publishing LLC." For an article, the copyright and permission notice must be printed on the first page of the article or book chapter. For photographs, covers, or tables, the copyright and permission notice may appear with the Material, in a footnote, or in the reference list.
2. If you have licensed reuse of a figure, photograph, cover, or table, it is your responsibility to ensure that the material is original to AIPP and does not contain the copyright of another entity, and that the copyright notice of the figure, photograph, cover, or table does not indicate that it was reprinted by AIPP, with permission, from another source. Under no circumstances does AIPP, purport or intend to grant permission to reuse material to which it does not hold copyright.
3. You may not alter or modify the Material in any manner. You may translate the Material into another language only if you have licensed translation rights. You may not use the Material for promotional purposes. AIPP reserves all rights not specifically granted herein.
4. The foregoing license shall not take effect unless and until AIPP or its agent, Copyright Clearance Center, receives the Payment in accordance with Copyright Clearance Center Billing and Payment Terms and Conditions, which are incorporated herein by reference.
5. AIPP or the Copyright Clearance Center may, within two business days of granting this license, revoke the license for any reason whatsoever, with a full refund payable to you. Should you violate the terms of this license at any time, AIPP, AIP Publishing LLC, or Copyright Clearance Center may revoke the license with no refund to you. Notice of such revocation will be made using the contact information provided by you. Failure to receive such notice will not nullify the revocation.
6. AIPP makes no representations or warranties with respect to the Material. You agree to indemnify and hold harmless AIPP, AIP Publishing LLC, and their officers, directors, employees or agents from and against any and all claims arising out of your use of the Material other than as specifically authorized herein.
7. The permission granted herein is personal to you and is not transferable or assignable without the prior written permission of AIPP. This license may not be amended except in a writing signed by the party to be charged.
8. If purchase orders, acknowledgments or check endorsements are issued on any forms containing terms and conditions which are inconsistent with these provisions, such inconsistent terms and conditions shall be of no force and effect. This document, including the CCC Billing and Payment Terms and Conditions, shall be the entire agreement between the parties relating to the subject matter hereof.

This Agreement shall be governed by and construed in accordance with the laws of the State of New York. Both parties hereby submit to the jurisdiction of the courts of New York County for purposes of resolving any disputes that may arise hereunder.

**WOLTERS KLUWER HEALTH LICENSE  
TERMS AND CONDITIONS**

Nov 12, 2013

**All payments must be made in full to CCC. For payment instructions, please see information listed at the bottom of this form.**

License Number	3253391020148
License date	Oct 20, 2013
Licensed content publisher	Wolters Kluwer Health
Licensed content publication	Diagnostic Molecular Pathology
Licensed content title	The Clinical Significance of Circulating Tumor Cells in the Peripheral Blood
Licensed content author	Yahya Elshimali and Wayne Grody
Licensed content date	Jan 1, 2006
Volume Number	15
Issue Number	4
Type of Use	Dissertation/Thesis
Requestor type	Individual
Author of this Wolters Kluwer article	No
Title of your thesis / dissertation	Polymer Microsystems for the Enrichment of Circulating Tumor Cells and their Clinical Demonstration
Expected completion date	Dec 2013
Estimated size(pages)	200
Billing Type	Invoice
Billing address	960 cinnamon dr. DURHAM, NC 27713 United States
Total	0.00 USD

**JOHN WILEY AND SONS LICENSE  
TERMS AND CONDITIONS**

Nov 12, 2013

---

This is a License Agreement between Joyce W Kamande ("You") and John Wiley and Sons ("John Wiley and Sons") provided by Copyright Clearance Center ("CCC"). The license consists of your order details, the terms and conditions provided by John Wiley and Sons, and the payment terms and conditions.

**All payments must be made in full to CCC. For payment instructions, please see information listed at the bottom of this form.**

License Number	3253380753272
License date	Oct 20, 2013
Licensed content publisher	John Wiley and Sons
Licensed content publication	International Journal of Cancer
Licensed content title	Isolation of circulating epithelial and tumor progenitor cells with an invasive phenotype from breast cancer patients
Licensed copyright line	Copyright © 2009 UICC
Licensed content author	Janice Lu,Tina Fan,Qiang Zhao,Wei Zeng,Eva Zaslavsky,John J. Chen,Michael A. Frohman,Marc G. Golightly,Stefan Madajewicz,Wen-Tien Chen
Licensed content date	Aug 6, 2009
Start page	669
End page	683
Type of use	Dissertation/Thesis
Requestor type	University/Academic
Format	Print and electronic
Portion	Figure/table
Number of figures/tables	1
Original Wiley figure/table number(s)	Figure 5
Will you be translating?	No
Total	0.00 USD

**ROYAL SOCIETY OF CHEMISTRY LICENSE  
TERMS AND CONDITIONS**

Nov 12, 2013

---

This is a License Agreement between Joyce W Kamande ("You") and Royal Society of Chemistry ("Royal Society of Chemistry") provided by Copyright Clearance Center ("CCC"). The license consists of your order details, the terms and conditions provided by Royal Society of Chemistry, and the payment terms and conditions.

**All payments must be made in full to CCC. For payment instructions, please see information listed at the bottom of this form.**

License Number	3252780390351
License date	Oct 19, 2013
Licensed content publisher	Royal Society of Chemistry
Licensed content publication	Lab on a Chip
Licensed content title	Microsieve lab-chip device for rapid enumeration and fluorescence in situ hybridization of circulating tumor cells
Licensed content author	Li Shi Lim,Min Hu,Mo Chao Huang,Wai Chye Cheong,Alfred Tau Liang Gan,Xing Lun Looi,Sai Mun Leong,Evelyn Siew -Chuan Koay,Mo-Huang Li
Licensed content date	Aug 28, 2012
Volume number	12
Issue number	21
Type of Use	Thesis/Dissertation
Requestor type	academic/educational
Portion	figures/tables/images
Number of figures/tables/images	2
Format	print and electronic
Distribution quantity	500
Will you be translating?	no
Order reference number	
Title of the thesis/dissertation	Polymer Microsystems for the Enrichment of Circulating Tumor Cells and their Clinical Demonstration
Expected completion date	Dec 2013
Estimated size	200
Total	0.00 USD

**JOHN WILEY AND SONS LICENSE  
TERMS AND CONDITIONS**

Nov 12, 2013

---

This is a License Agreement between Joyce W Kamande ("You") and John Wiley and Sons ("John Wiley and Sons") provided by Copyright Clearance Center ("CCC"). The license consists of your order details, the terms and conditions provided by John Wiley and Sons, and the payment terms and conditions.

**All payments must be made in full to CCC. For payment instructions, please see information listed at the bottom of this form.**

License Number	3266740023536
License date	Nov 12, 2013
Licensed content publisher	John Wiley and Sons
Licensed content publication	Advanced Materials
Licensed content title	Electrospun TiO <sub>2</sub> Nanofiber-Based Cell Capture Assay for Detecting Circulating Tumor Cells from Colorectal and Gastric Cancer Patients
Licensed copyright line	Copyright © 2012 WILEY-VCH Verlag GmbH & Co. KGaA, Weinheim
Licensed content author	Nangang Zhang, Yuliang Deng, Qidong Tai, Boran Cheng, Libo Zhao, Qinglin Shen, Rongxiang He, Longye Hong, Wei Liu, Shishang Guo, Kan Liu, Hisan-Rong Tseng, Bin Xiong, Xing-Zhong Zhao
Licensed content date	Apr 23, 2012
Start page	2756
End page	2760
Type of use	Dissertation/Thesis
Requestor type	University/Academic
Format	Print and electronic
Portion	Figure/table
Number of figures/tables	1
Original Wiley figure/table number(s)	Figure 1
Will you be translating?	No
Total	0.00 USD



Joyce Kamande <jkaman1@tigers.lsu.edu>

---

## Permission to use figure for Dissertation

1 message

---

**Joyce Kamande** <jkaman1@tigers.lsu.edu>

Thu, Oct 17, 2013 at 9:30 PM

To: ijo@spandidos-publications.com, contact@spandidos-publications.com

To whom it may concern,

I am graduate student about to complete my dissertation on Circulating Tumor Cells (CTCs). As part of my literature review I would like to use a figure of the Gilupi device from an article that was published in your journal.

This is the link to the article <http://www.spandidos-publications.com/10.3892/ijo.2012.1557>

--Kindly let me know if I could get permission to use the figure.

thank you

Joyce

**Joyce W. Kamande**  
**Ph.D. Candidate**  
**Department of Chemistry LSU**  
**Bio-medical and Engineering Dept. UNC**  
email: [jkamande@med.unc.edu](mailto:jkamande@med.unc.edu) or [jkaman1@tigers.lsu.edu](mailto:jkaman1@tigers.lsu.edu)  
phone: [410-206 6951](tel:410-206-6951)

*"In the confrontation between the stream and the rock, the stream wins. Not by strength but by perseverance!"*



Joyce Kamande <jkaman1@tigers.lsu.edu>

**D.A. Spandidos** 1 message

**International Journal Of Oncology-Spandidos Publications** <ijo@spandidos-publications.com> Fri, Oct 18, 2013 at 7:23 AM

To: Joyce Kamande <jkaman1@tigers.lsu.edu>

[contact@spandidos-publications.com](mailto:contact@spandidos-publications.com) [www.spandidos-publications.com](http://www.spandidos-publications.com)

International Journal of Oncology  
10, Vriaxidos Street, Athens 116 35, Greece  
Joyce W. Kamande

October 18, 2013

International Journal of Oncology, 2012

Use of figure

Thank you for your message received October 18, 2013. Permission is hereby granted for reproduction of the above for the purpose of Thesis presentation, as outlined in your message.

Yours sincerely,

Demetrios A. Spandidos

-----  
Professor D.A. Spandidos  
10 Vriaxidos Street  
116 35 Greece  
Fax: [+30 \(210\) 725-2922](tel:+302107252922)  
Tel: [+30 \(210\) 7517117](tel:+302107517117)  
E-mail: [ijo@spandidos-publications.com](mailto:ijo@spandidos-publications.com)  
Website: [www.spandidos-publications.com](http://www.spandidos-publications.com)  
-----

**SPRINGER LICENSE  
TERMS AND CONDITIONS**

Nov 13, 2013

---

---

This is a License Agreement between Joyce W Kamande ("You") and Springer ("Springer") provided by Copyright Clearance Center ("CCC"). The license consists of your order details, the terms and conditions provided by Springer, and the payment terms and conditions.

**All payments must be made in full to CCC. For payment instructions, please see information listed at the bottom of this form.**

License Number	3267410574700
License date	Nov 13, 2013
Licensed content publisher	Springer
Licensed content publication	Microfluids and Nanofluids
Licensed content title	Single-cell microfluidic impedance cytometry: a review
Licensed content author	Tao Sun
Licensed content date	Jan 1, 2010
Volume number	8
Issue number	4
Type of Use	Thesis/Dissertation
Portion	Figures
Author of this Springer article	No
Order reference number	
Title of your thesis / dissertation	Polymer Microsystems for the Enrichment of Circulating Tumor Cells and their Clinical Demonstration
Expected completion date	Dec 2013
Estimated size(pages)	200
Total	0.00 USD



LINDBERGER COMPREHENSIVE CANCER CENTER  
CLINICAL ONCOLOGY RESEARCH PROGRAM  
UNIVERSITY OF NORTH CAROLINA AT CHAPEL HILL

**LCCC-1121: Quantification and Characterization of Circulating Tumor Cells in  
Solid Tumors**

**Principal Investigator**

Jen Jen Yeh, MD  
Assistant Professor  
Departments of Surgery and Pharmacology  
Campus Box 7213  
170 Manning Dr. 1150 POB  
Chapel Hill, NC 27599  
919-966-5223 (PHONE)  
919-966-8806 (FAX)  
Email: [Jen\\_Jen\\_Yeh@med.unc.edu](mailto:Jen_Jen_Yeh@med.unc.edu)

**Co-Principal Investigator**

Rachel Aufforth, MD  
Fellow, Division of Surgical Oncology  
Department of Surgery  
Email: [aufforth@med.unc.edu](mailto:aufforth@med.unc.edu)

**Co-Principal Investigator**

William Y. Kim, MD  
Assistant Professor  
Departments of Medicine and Genetics  
Email: [wwkim@med.unc.edu](mailto:wwkim@med.unc.edu)

**Co-Investigator(s)**

Steven A. Soper, Ph.D.  
Professor  
Departments of Biomedical Engineering and Chemistry  
Email: [chsoper@lsu.edu](mailto:chsoper@lsu.edu)

Nancy Allbritton, MD, PhD  
Professor and Chair  
Department of Biomedical Engineering  
Professor, Departments of Chemistry and Pharmacology  
Email: [nallbri@unc.edu](mailto:nallbri@unc.edu)

Christopher E. Sims, MD  
Professor  
Departments of Chemistry and Medicine  
Email: [cesims@unc.edu](mailto:cesims@unc.edu)

**Biostatistician**

Allison Deal, MS

LINEBERGER COMPREHENSIVE CANCER CENTER  
CLINICAL ONCOLOGY RESEARCH PROGRAM  
UNIVERSITY OF NORTH CAROLINA AT CHAPEL HILL

919-966-1387

Allison\_Deal@med.unc.edu

**Study Coordinator:**

Rachel Aufforth, MD

919-966-5221 (PHONE)

919-966-8806 (FAX)

Email: [Aufforth@med.unc.edu](mailto:Aufforth@med.unc.edu)

**Study Coordinator:**

Sarah Gallagher

Department of Urologic Oncology

919-966-2326 (PHONE)

**Sponsor:** Lineberger Comprehensive Cancer Center

**Funding Source:** institutional start-up, TRD

**Version Date:** April 12, 2012

LINBERGER COMPREHENSIVE CANCER CENTER  
CLINICAL ONCOLOGY RESEARCH PROGRAM  
UNIVERSITY OF NORTH CAROLINA AT CHAPEL HILL

**LCCC 1121: Quantification and Characterization of Circulating Tumor Cells in  
Solid Tumors.**

**Principal Investigator**

Jen Jen Yeh, MD  
Campus Box 7213  
170 Manning Dr. 1150 POB  
Chapel Hill, NC 27599  
919-966-5221 (PHONE)  
919-966-8806 (FAX)  
Email: Jen\_Jen\_Yeh@med.unc.edu

**Signature Page**

The signature below constitutes the approval of this protocol and the attachments, and provides the necessary assurances that this trial will be conducted according to all stipulations of the protocol, including all statements regarding confidentiality, and according to local legal and regulatory requirements and applicable U.S. federal regulations and ICH guidelines.

**Principal Investigator (PI) Name:** Jen Jen Yeh



**PI Signature:**

**Date:** April 12, 2012

**Version Date:** April 12, 2012

University of North Carolina at Chapel Hill  
Consent for Storing Biological Specimens With Identifying Information

---

IRB Study # 11-1924  
Consent Form Version Date: 8-2-2012

**Title of Study: LCCC 1121: Quantification and Characterization of Circulating  
Tumor Cells in Solid Tumors.**

**Principal Investigator:** Jen Jen Yeh, MD  
**UNC-Chapel Hill Department:** Surgery, Division of Surgical Oncology  
**UNC-Chapel Hill Phone number:** 919-966-5221  
**Co-Principal Investigator:** Rachel Aufforth, MD  
**Co-Principal Investigator:** William Kim, MD

**Sponsor:** Linberger Comprehensive Cancer Center  
**Funding Source:** NC-TraCS, Society of Surgical Oncology

**Study Contact telephone number:** 919-966-5221  
**Study Contact email:** Aufforth@med.unc.edu

---

**What are some general things you should know about research?**

Research is designed to gain scientific information that may help other people in the future. You may not receive any direct benefit from participating. There also may be risks.

You may refuse to take part in research. If you are a patient with an illness, you do not have to be in research in order to receive treatment.

Details are discussed below. It is important that you understand this information so that you can make an informed choice. You will be given a copy of this consent form. You should ask the researchers named above, or staff members who may assist them, any questions you have about this study at any time.

**What is the purpose of this study?**

Research with blood, tissue or body fluids (specimens) can help researchers understand how the human body works. Research can also answer other questions by using specimens.

The purpose of this particular research is to determine the importance of circulating tumor cells (CTCs) in patients with solid tumors by determining how many CTCs circulate in the blood, and what their characteristics are. In the future we hope to study whether the number and/or characteristics of CTCs in a particular cancer type can help researchers predict how that cancer will respond to

treatment, how likely it will come back after response, etc. The specimens that will be collected will be blood drawn from you at different times during your care. The blood will be analyzed for the number of CTCs as well as molecular markers that may be important in your disease. No unprocessed blood samples will be stored. All materials will be discarded after the analysis is complete.

If you are identified as a healthy control participant in this study than your blood will be used to help establish the baseline of "normal" CTCs. This will allow researchers to understand the significance of CTC levels in patients with solid tumors. The specimen that will be collected will be blood. The blood will be analyzed for the number of CTCs as well as possible molecular markers. No unprocessed blood samples will be stored. All materials will be discarded after the analysis is complete.

**How will the specimens be collected?**

The specimens will be collected during a venous blood draw at various times during your care. A total of 7.5ml of blood will be drawn at each blood draw. This is equivalent to 1½ teaspoons. All specimens will be taken in standard venous blood sampling technique by a trained technician. All specimens will be drawn at your clinic visits and no special visits will need to be made. Every effort will be made to coordinate this blood draw with a scheduled blood draw but this may not be possible. The study coordinator and/or protocol assistant will meet with you prior to each blood draw to answer questions and remind you of the study and its purpose.

**What will happen to the specimens?**

The specimens will be stored in blood sample tubes prior to the investigation. Once the investigation is complete the specimens will be destroyed. The specimens must be processed within three days time, so will be destroyed in a timely fashion. The specimens will be labeled with your study number. Only the researchers associated with this study will have access to the link between the study number and your identifiable data. This data will be kept in a secure file cabinet in a secure room in a secure building. Under no conditions will your specimens or data be released to other investigators.

**What are the possible benefits to you?**

Benefits to you are unlikely. Results from this study may provide additional information that will be helpful in understanding of disease treatment and follow up care.

**What are the possible risks or discomforts involved with the use of your specimens?**

The known risks are associated with the venous blood draw and are minimal. These include but are not limited to bruising, blood clots, injury to surrounding structures such as arteries, pain, nerve damage, bleeding, allergy, vaso-vagal

reaction, anxiety/fear. There are no long-term risks to the venous blood sampling. There is the possibility however small that there are unknown risks for this study.

There is a small risk of breach of confidentiality in this study. We will code all specimens and remove all identifiers from the data forms that are filled out, however in order to follow long term we will need to know who is in the study. The list of patients enrolled in the study and the link between the uncoded data and the coded data will be kept in a secure file cabinet in a secure room in a secure building. Only the researchers associated with this study will have access to this data. If there was a breach of confidentiality there would be a chance that people you did not want to know about your disease would find out.

For tumor genetic research, we will look at certain changes in the genes (DNA) from a sample of your tumor cells to see if these changes are related to your cancer, and/or how well you respond(ed) to your cancer treatment. Almost always, the changes in the genes from tumor samples are not found in normal cells, as the genetic changes from your tumor most likely occurred after you were born.

**Will there be any cost to you for the study?**

There will be no cost to you for the study and use of the specimens for research purposes.

**Will you receive anything for the use of your specimens?**

You will not receive anything for taking part in this research.

**Who owns the specimens?**

Any blood, body fluids, or tissue specimens obtained for this purpose become the exclusive property of the University of North Carolina at Chapel. This organization may retain, preserve or dispose of these specimens and may use these specimens for research that may result in commercial applications. There are no plans to compensate you for any future commercial use of these specimens.

**How will your privacy be protected?**

Your privacy will be protected by coding all specimens and data where possible, by using a unique study ID for each person instead. This makes sure that only certain people will have access to the link of your identifying data to your study ID. These people include the researchers associated with this study. The link will be kept in a secure file cabinet, in a secure room, in a secure building. All computer files will be password protected kept on a computer that is password protected, kept in a secure room in a secure building.

Information from your medical records may be stored along with your specimens(s). You will be asked to sign a separate form ("HIPAA authorization") to allow researchers to review your medical records.

You will not be identified in any report or publication about research using your specimens. Although every effort will be made to keep research records private, there may be times when federal or state law requires the disclosure of such records, including personal information. This is very unlikely, but if disclosure is ever required, UNC-Chapel Hill will take steps allowable by law to protect the privacy of personal information. In some cases, your information in this research could be reviewed by representatives of the University, research sponsors, or government agencies for purposes such as quality control or safety.

A Federal law called the Genetic Information Nondiscrimination Act (GINA) generally makes it illegal for health insurance companies, group health plans, and most employers to discriminate against you based on your genetic information. GINA does not protect you against genetic discrimination by companies that sell life insurance, disability insurance, or long-term care insurance. GINA also does not protect you against discrimination based on an already-diagnosed genetic condition or disease.

**Will researchers seek approval from you to do future studies involving the specimens?**

By signing this consent form, you are giving your permission for researchers to use your specimens as described above. Current and future research is overseen by a committee called the Institutional Review Board (IRB). The role of the IRB is to protect the rights and welfare of research participants. In some cases, the IRB may require that you be re-contacted and asked for your consent to use your data in a specific research study. You have the right, at that future time, not to participate in any research study for which your consent is sought. Refusal to participate will not affect your medical care or result in loss of benefits to which you are entitled.

**Will you receive results from research involving your specimens?**

Most research with your specimens is not expected to yield new information that would be meaningful to share with you personally. There are no plans to re-contact you or other subjects with information about research results.

**Can you withdraw from the research study?**

If you decide that you no longer wish to participate in the study, you should contact the researchers on the front page of this form.

Any analysis in progress at the time of your request or already performed prior to your request being received by the researcher will continue to be used as part of the research study. Once the researchers have been notified, all remaining specimens would be destroyed.

**What will happen if you are injured by this research?**

All research involves a chance that something bad might happen to you. This may include the risk of personal injury. In spite of all safety measures, you might develop a reaction or injury from having your specimen collected. If such problems occur, the researchers will help you get medical care, but any costs for the medical care will be billed to you and/or your insurance company. The University of North Carolina at Chapel Hill has not set aside funds to pay you for any such reactions or injuries, or for the related medical care. However, by signing this form, you do not give up any of your legal rights.

**Who is sponsoring this research?**

This research is funded by the University of North Carolina at Chapel Hill and the Society of Surgical Oncology. This means that the research team is being paid by the sponsors for doing the study. A company called Biofluidica Microtechnologies is involved in this study because it owns or makes a device being used in this study. Dr. Soper, a co-investigator on this study, has a financial interest in a technology that is being used with your blood sample. Dr. Soper is currently part owner of a device and Biofluidica Microtechnologies, to whom the device has been licensed. If either the patent or approach is successful at some point in the future, Dr. Soper may receive financial benefits. In addition, Dr. Allbritton, a co-investigator on this study, is part owner of a technology that may be used with your blood sample. If either the patent or approach is successful at some point in the future, Dr. Allbritton may receive financial benefits. Committees at the University of North Carolina at Chapel Hill have reviewed these arrangements. They concluded that the possible benefit to the persons listed above is not likely to affect your safety or the scientific quality of the study. If you would like more information, please ask the researchers listed in the first page of this form.

**What if you have questions about this research?**

You have the right to ask, and have answered, any questions you may have about this research. If you have questions, you should contact the researchers listed on the first page of this form.

**What if you have questions about your rights as a research subject?**

All research on human volunteers is reviewed by a committee that works to protect your rights and welfare. If you have questions or concerns about your rights as a research subject you may contact, anonymously if you wish, the Institutional Review Board at 919-966-3113 or by e-mail to IRB\_subjects@unc.edu.



**Subject's Agreement:**

I have read the information provided above. I have asked all the questions I have at this time. I voluntarily agree to participate. I agree to my specimen(s) being stored with the identifying code(s).

\_\_\_\_\_  
Signature of Research Subject

\_\_\_\_\_  
Date

\_\_\_\_\_  
Printed Name of Research Subject

\_\_\_\_\_  
Signature of Research Team Member Obtaining Consent

\_\_\_\_\_  
Date

\_\_\_\_\_  
Printed Name of Research Team Member Obtaining Consent



THE UNIVERSITY  
of NORTH CAROLINA  
at CHAPEL HILL

OFFICE OF HUMAN RESEARCH ETHICS  
Medical School Building 52  
Mason Farm Road  
CB #7097  
Chapel Hill, NC 27599-7097  
(919) 986-3113  
Web site: [ohre.unc.edu](http://ohre.unc.edu)  
Federalwide Assurance (FWA) #4801

To: Kristy Richards  
Medicine

From: Biomedical IRB

Approval Date: 4/08/2013  
Expiration Date of Approval: 4/07/2014

RE: Notice of IRB Approval by Expedited Review (under 45 CFR 46.110)  
Submission Type: Renewal  
Expedited Category: 9 Continuing rev, min risk by full IRB  
Study #: 09-0768

Study Title: LCCC 0824: Tissue Procurement for Hematolymphoid Conditions  
Sponsors: Lineberger Cancer Center Core Grant and University Cancer Research Fund  
Lineberger Comprehensive Cancer Center  
University of North Carolina at Chapel Hill

This submission has been approved by the IRB for the period indicated.

#### Study Description:

**Purpose:** Support and enhance translational, clinical and basic research for Lineberger Comprehensive Cancer Center members (and non-members who have an LCCC member as sponsor and collaborator) with IRB approved studies, by providing a centralized, quality controlled, quality assured facility for the procurement, processing, storage and distribution of normal and malignant tissue specimens and corresponding blood specimens.

**Participants:** This tissue procurement protocol will allow for participation by all individuals age 18 or older who are seen in evaluation or consultation at the hematology oncology clinics of the University of North Carolina Hospitals, at the stem cell transplant clinic or in the hospital itself.

**Procedures (methods):** The protocol will allow for the collection of tissue, including lymph node biopsies, bone marrow aspirate and/or core, and blood and serum from patients at the time of diagnosis, completion of treatment and at relapse. All patient specimens will be deidentified by the UNC Tissue Procurement Facility (TPF). Identifying information will be kept separately by the TPF, and will only be available to researchers who have IRB approved protocol that have received permission for the use of this information by the hematology tissue procurement committee.

#### Submission Description:

Addition of Jennifer Strother, Cheryl Carlson, Katarzyna Jamieson, Megan Fuchs

Removal of Ranju Singh, Reynaldo Garcia, Robert IRons, Payal Desai, Christine Lin, Ryan Raddin

Page 1 of 2

**Change of status of:**

Miesha Mooberry, Marshall Mazepa, Benjamin Vincent and Amber Esselmacher to Co-investigators; Wasiuddin Khan from Project Manager to Regulatory Associate.

**Adult Consent, Prisoner Consent, and Skin Punch Biopsy Forms:**

Cherie Dunphy, Payal Desai, Christine Lin, Ryan Raddin, Robert Irons were removed as co-investigators.

Cheryl Carlson, Megan Fuchs, Amber Esselmacher, George Fedoriv, Katarzyna Jamieson were added as co-investigators.

**Regulatory and other findings:**

This research, which involves pregnant women, meets criteria set forth in section 45 CFR 46.204. In accordance with 46.204(d), maternal consent is sufficient since the research holds prospect of direct benefit to the pregnant woman, the prospect of direct benefit to the pregnant woman and the fetus, or no prospect of benefit for the woman nor the fetus but the risk to the fetus is not greater than minimal and the purpose of the research is the development of important biomedical knowledge which cannot be obtained by any other means.

In accordance with 45 CFR 46.304, the convened IRB committee included a board member who is a prisoner representative. This research, which involves prisoners, meets criteria set forth in section 45 CFR 46.305(a)(1-7) and is permitted according to 45 CFR 46.306, (Category 5: waiver for certain epidemiologic research to study potential risk factor associations for a disease).

This approval includes a limited waiver of HIPAA authorization to identify potential subjects for recruitment into this research study, as allowed under 45 CFR 164.512. This temporary waiver provides access to protected health information (PHI) to confirm eligibility and facilitate initial contact, after which consent and HIPAA authorization will be sought. Access and use is limited to the minimum amount of PHI necessary to review eligibility criteria and to contact potential subjects.

The Board agreed that this research, which consists of storage, in a specimen repository that has an approved honest broker system, of tumor specimens collected at the time of clinically indicated surgery involves no more than minimal risk and future reviews may be done on an expedited basis, under Expedited Review, Category 9. The Prisoner representative will continue to be involved in the review of the study.

The IRB has determined that decisionally impaired subjects may be enrolled in this research with the consent of a legally authorized representative (LAR). The following individuals may give surrogate consent for another to participate, in order of priority: (1) a court appointed guardian, or (2) an agent pursuant to a health care power of attorney, or (3) in some circumstances, a person appointed under a durable general power of attorney. If one of these three LARs is used, the PI should obtain a copy of documentation granting this authority. If the first three LARS do not exist, and as long as there is no evidence to the contrary, the following members of the immediate family may give surrogate consent, again in order of priority: (4) spouse, (5) adult child, (6) parent.

This research, which was originally approved by the Full Board, is being renewed by the IRB under Expedited Review, Category 9.

**Investigator's Responsibilities:**

Federal regulations require that all research be reviewed at least annually. It is the Principal

16/2/20

Investigator's responsibility to submit for renewal and obtain approval before the expiration date. You may not continue any research activity beyond the expiration date without IRB approval. Failure to receive approval for continuation before the expiration date will result in automatic termination of the approval for this study on the expiration date.

Your approved consent forms and other documents are available online at [http://apps.research.unc.edu/irb/irb\\_event.cfm?actn\\_info&irbid\\_09-0768](http://apps.research.unc.edu/irb/irb_event.cfm?actn_info&irbid_09-0768)

You are required to obtain IRB approval for any changes to any aspect of this study before they can be implemented. Any unanticipated problem involving risks to subjects or others (including adverse events reportable under UNC-Chapel Hill policy) should be reported to the IRB using the web portal at <http://irbis.unc.edu>.

This study was reviewed in accordance with federal regulations governing human subjects research, including those found at 45 CFR 46 (Common Rule), 45 CFR 164 (HIPAA), 21 CFR 50 & 56 (FDA), and 40CFR 26 (EPA), where applicable.

CC:  
Stefanie Sarantopoulos, Medicine  
Prasanna Bhende, Lineberger Comprehensive Cancer Center  
Ashton Madison, Lineberger Comprehensive Cancer Center  
Wasiuddin Khan, Lineberger Comprehensive Cancer Center

06/20/19

## VITA

Joyce Wanjiru Kamande was born in Nairobi, Kenya, to Mr. Peter N. Kamande and Mrs. Winny W. Kamande. She attended Makini Academy, in Kenya for her high school, from 1998–2001. Shortly after graduation Joyce enrolled at the University of Nairobi, Kenya for a Bachelors in Science (2003). While still at the University, Joyce also enrolled at Strathmore College for a Certified Public Accounting certification and completed CPA part III section 5 in 2004. In June 2007, she graduated with a first class honors in chemistry from the University of Nairobi (Kenya).

In the Fall 2008, Joyce was accepted to the Graduate School doctoral program at Louisiana State University (LSU) in the Department of Chemistry. In the Fall of 2011 she relocated to the University of North Carolina (Chapel Hill), department of Bio-Medical Engineering as a Research Assistant for the analysis of clinical blood samples from pancreatic, melanoma, colorectal and myeloma patients as part of her major dissertation project. During her graduate school career, she received the James W. Robinson Award for outstanding research in analytical sciences. She has been a member the American Chemical Society (ACS), the National Organization for the Professional Advancement of Black Chemists and Chemical Engineers (NOBCChE), and the Chemistry Graduate Council, LSU Chapter. Joyce Kamande is currently a candidate for the Doctor of Philosophy in Analytical chemistry, which will be awarded to her at the December 2013 Commencement at LSU, Baton Rouge